

Structural and functional studies of the alternating access mechanism of secondary active transporters

Dissertation

zur Erlangung des Doctorgrades

an der Fakultät für Mathematik, Informatik und Naturwissenschaften

Fachbereich Chemie

der Universität Hamburg

vorgelegt von

Maria C. Kokkinidou

aus Thessaloniki, Griechenland

Hamburg

2019

Thesis evaluators

Prof Dr. Arwen R. Pearson

Institute for Nanostructure and Solid State Physics, University of Hamburg

Prof Dr. Henning Tidow

Group Leader at the Institute of Biochemistry and Molecular Biology, University of Hamburg

Defence committee

Prof Dr. Arwen R. Pearson

Institute for Nanostructure and Solid State Physics, University of Hamburg

Prof. Dr. Andrew Torda

Head of Research Group Biomolecular Modeling, University of Hamburg

Dr. Christian Löw

Group leader at the European Molecular Biology Laboratory (EMBL) and the Centre of of Structural and Systems Biology (CSSB)

Tag der Disputation: 26.07.2019

This thesis describes work performed under the joint supervision of Prof. Dr. Arwen R. Pearson Institute of Nanostructure and Solid State Physics at the Universität Hamburg and Prof. Dr. Christian Betzel at the Department of Chemistry at the Universität Hamburg. This work was supported and funded by the Joachim Herz Stiftung. The work described in this dissertation was performed between December 2014 and December 2018 in the group of Prof. Dr. Arwen R. Pearson in the Centre for Free Electron Laser Science (CFEL) at the Bahrenfeld Campus of the Universität Hamburg.

Maria C. Kokkinidou

July 2019

List of publications

1. Jackson, SM, Ivanova, E, Calabrese, AN, Polyakova, A, Sharples, DJ, Shimamura, T, Brueckner, F, Simmons, KJ, Sahai, M, Majd, H, Kunji, E, Ahmad, I, Weyand, S, Suzuki, S, Ashcroft, AE, Kokkinidou, M, Pearson, A, Beckstein, O, Baldwin, SA, Iwata, S, Cameron, AD and Henderson, PJF (2018) Structure, Substrate Recognition, and Mechanism of the Na⁺-Hydantoin Membrane Transport Protein, Mhp1. in G Roberts and A Watts (eds), *Encyclopedia of Biophysics.*, Chapter 10091-1, Springer, pp. 1-12.
2. Calabrese A.N., Jackson, S.M., Jones, L.N., Beckstein, O., Heinkel, F., Gsponer, J., Sharples, D., Sans, M., Kokkinidou, M., Pearson, A.R., Radford, S.E., Ashcroft, A.E., Henderson, P.J.F. (2017) Topological dissection of the membrane transport protein Mhp1 derived from cysteine accessibility and mass spectrometry. *Analytical Chemistry* 89 8844- 8852.

Abstract

This project aimed to provide functional and structural insights into the alternating access transport mechanism of the secondary active transporter Mhp1, the membrane hydantoin permease-1, from *Microbacterium liquefaciens* of the nucleobase-cation symporter family (NCS-1). Mhp1 has already been observed in three conformational states along the putative reaction coordinate (Shimamura et al. 2010). In an attempt to capture Mhp1 in additional conformations several mutants were produced, where key residues of the sodium and binding cavities of Mhp1 were altered.

Initially mutants were produced and characterised, followed by crystallographic analysis. As Mhp1's mechanism of transport is a highly dynamic process, this mechanism was further investigated in solution, to avoid the crystal packing limitations. Size-exclusion chromatography coupled small angle X ray scattering was employed to probe the conformational homogeneity of Mhp1. A second membrane transporter, LeuT from *Aquifex aeolicus*, was also studied. The production and crystallisation of wild-type LeuT as well as the first studies of a new triple mutant were performed to enable time-resolved studies.

Zusammenfassung

Ziel dieses Projects ist es funktionale und strukturelle Einsichten in den abwechselnden Zugriffs-transportmechanismus des sekundären aktiven Transporters Mhp1, die Membran Hydantoin Permease-1 aus *Microbacterium liquefaciens*, der Nucleobasen-cation symporter Familie (NCS-1), zu erlangen. Bisher konnte Mhp1 in drei Konformationen entlang der vermuteten Reaktionskoordinate beobachtet werden (Shimamura et al. 2010). In einem Versuch Mhp1 in zusätzlichen Konformationen einzufangen, wurden verschiedene Mutanten produziert, bei denen Schlüsselaminosäuren der Natrium- und Substrat Bindungstellen verändert wurden.

Zunächst wurden Mutanten produziert und charakterisiert, gefolgt von kristallographischen Analysen. Da Mhp1's Transportmechanismus ein sehr dynamischer Prozess ist, wurden die Einschränkungen eines Kristallgitters umgangen, indem der Mechanismus weiter in Lösung untersucht wurde. Größenausschlusschromatographie in Verbindung mit Kleinwinkelröntgenstreuung wurde verwendet um die konformationelle Homogenität von Mhp1 zu untersuchen. Außerdem wurde ein zweiter Membrantransporter, LeuT aus *Aquifex aeolicus*, studiert. Die Produktion und Charakterisierung von wild-type LeuT, sowie erste Untersuchungen eines Dreifach-Mutanten für zeitaufgelösten Studien wurden durchgeführt.

Acknowledgements

First and foremost I would like to thank my supervisor Prof. Arwen Pearson. I am grateful to her for inspiring me and teaching me how to pursue my ideas in research in a scientifically sound way. I really appreciate her ability to motivate me to try always one step further. Her advices and support these years have been essential elements for the completion of this thesis.

My sincere thanks to the Joachim Herz Stiftung for supporting me through a PhD scholarship for my studies. I would like especially to thank Dr. Eva Äckermann for her support and understanding. I would like to thank also the PIER graduate school for the nice moments and the interchange of scientific knowledge from different disciples. I am especially thankful to Mrs Stefanie Tepass and Max Rose for their support and continuous interest during my time in Hamburg.

I would also like to thank Prof. Christian Betzel my second supervisor for supporting my new enrolment to the Chemistry department and Mrs Wallenius to make this difficult procedure goes smoothly. I am indebted to thank Dr. Christo Savva and Dr. Alice Clark for their continued interest on my studies and for their always valuable advices!

I would like to express my gratitude to Prof. Peter Henderson for giving me the chance to work on this exciting and challenging project of secondary active transporters. Dr. Anna Polyakova for teaching me all Mhp1 "tricks" at the beginning of my Ph.D. studies, and being always there to reply on my random questions during my studies. Mr David Sharples for the important cell fermentations at the university of Leeds. Special thanks to Sohail Azmat, Jawad A. Khan, Sonja Sucic and Prof. Thomas Stockner from the Medical University of Vienna for our collaboration for the LeuT project.

I would like to thank also the ESRF (France) beamline scientists for being very helpful and supportive during numerous beamtimes especially Dr. David Von Stetten and Dr. Martha Brennich. As well as Tsutomu Matsui BL4-2 SAXS beamline from SSRL (USA). The SPC

members from EMBL outstation Hamburg: Ioanna Maria Nemtanu, Janina Hinrichs, Dr. Maria -Garcia Alai, and Dr. Melissa Ann Graewert EMBL from P12 BioSAXS beamline.

I am grateful to all the Pearson-Lab members for the great time working together and especially Marta Sans for her guidance regarding the organic chemistry work and for being a great friend, Dr. Briony Yorke for her initial guidance in crystallographic studies, Dr. Sam Horrel for useful discussions, and for making valuable comments on the first draft of this thesis, Dr. Helen Ginn for extensive reading of my thesis and being a unique friend, Yunyun Gao for sharing many SAXS beamtimes and for analysing of the SAXS data of Mhp1. Marta, Brandon, Henry and Joe love working in the lab with you! This written thesis wouldn't be possible without the technical support of Georgia, Dr. Romain Letrun and Giwrgis (a great photographer). LaTeX is easy when you have the correct people next to you: Helen, Henry and especially Georgia.

I am very thankful to all of my friends for the great time we spent together in and around Hamburg: Aline, Antonia, Camilla, Cedric, Giorgos, Daria, Dana, Josi, Iris and Ioli, Kimonas, Krystian (Sonia and Aline), Lia, Masha, Maria, Ritsa, Romain (alphabetically). Madiha Fayyaz, Nedaa Alexandra Asbah and Σωκράτη Ξενίδη for their patient support. Marie, Kirsten, Theresa, Andreas and Franzi for the first interesting nine months. Also Tonia, Maria P. and Andreas for introducing me to a "new", beautiful this time, Hamburg. Alexandra, Lia, Jasone, Helen for inspiring breaks during writing. Jasone μου or Jasonetxu muchas gracias por todo! My uni friends from Greece Aleka, Alexandros, Giorgina, Maria, Vasoula, Renou, and Thalia for our great friendship all those years and more are yet to come. Last but not least I would like to thank Alexandra, Eleni and Giwrgis who have been standing next to me as family from the very first month!

I dedicate this work to my beloved Ειρήνη, Μαριγώ, Χαράλαμπο, Χρύσα and Περικλή for their continued encouragement, support and love.

This journey wouldn't be the same without all of you!

Thank you all,

Maria

ὡς οὐδὲν γλύκιον ἦς πατρίδος οὐδὲ τοκῆων γίνεται,
εἶ περ καὶ τις ἀπόπροθι πίονα οἶκο
γαίῃ ἐν ἀλλοδαπῇ ναίει ἀπάνευθε τοκῆων.
εἰ δ' ἄγε τοι καὶ νόστον ἐμὸν πολυκηδέ' ἐνίσπω,
ὄν μοι Ζεὺς ἐφέηκεν ἀπὸ Τροίηθεν ἰόντι.

Ὅμηρου Ὀδύσσεια (ι' 34-38)

Contents

Abstract	i
Zusammenfassung	ii
Acknowledgements	iii
Table of contents	vi
List of Figures	xi
List of Tables	xvi
1 Introduction	1
1.1 Transport through biological membranes	2
1.2 Secondary active membrane transporters	3
1.3 LeuT, the Leucine transporter	5
1.4 Mhp1 a sodium-hydantoin symport transporter	7
1.4.1 Binding sites of Mhp1	10
1.4.2 The alternating access mechanism in Mhp1 and its conformational states	13
1.4.3 Conformational changes during transport or states and switching NEM labelling	16
1.4.4 Mhp1 hydantoin ligands	19
1.4.5 Mhp1 solved structures	22

1.5	Techniques for structural studies to probe the mechanism of membrane transport proteins	23
1.5.1	Challenges of structural studies of membrane proteins	23
1.5.2	Crystallisation of integrate membrane proteins (IMPs)	25
1.5.3	Crystal lattice organisation of membrane proteins	29
1.5.4	Circular dichroism to assess structural integrity of Mhp1	31
1.5.5	Spectrophotofluorimetry to probe ligand binding behaviour to membrane transport protein Mhp1	32
1.5.6	Small angle X-ray scattering (SAXS)	34
1.5.7	Macromolecular crystallography	36
1.6	Project aims	37
2	Materials and Methods	38
2.1	Source of Materials	38
2.2	Mhp1 protein purification and crystallisation of wild-type and mutants	42
2.2.1	Expression and inner membrane preparations for Mhp1	42
2.2.2	Protein purification of Mhp1	42
2.2.3	Protein purification of Mhp1 in absence of sodium	43
2.2.4	Initial crystallisation of Mhp1	44
2.2.5	Co-crystallisation of Mhp1 with hydantoin ligands	44
2.2.6	High-throughput crystallisation techniques	44
2.3	Protein production and crystallisation of wild-type LeuT from <i>Aquifex aerolicus</i>	45
2.3.1	Protein expression of wild-type LeuT	45
2.3.2	Membrane preparations of wild-type LeuT	45
2.3.3	Immobilised metal affinity chromatography (IMAC) protein purification of wild-type LeuT	46
2.3.4	His ₈ -tag removal and further purification of wild-type LeuT	47
2.3.5	Size-exclusion chromatography purification (SEC)	47
2.3.6	Crystallisation of wild-type LeuT	47

2.4	Protein production of triple-mutant LeuT	48
2.4.1	Site-directed mutagenesis and plasmid constructs	48
2.4.2	Protein expression and purification of triple-mutant LeuT-SS	48
2.4.3	Cross-linking of Cys320 and Cys400 for disulphide bond formation	49
2.4.4	Monitoring of oxidation state of disulphide-bond formation	49
2.5	Protein analysis and quantification	51
2.5.1	Protein quantification applying the Schaffner-Weissmann assay	51
2.5.2	Protein analysis by SDS-PAGE	51
2.5.3	Western Blotting	52
2.6	Biophysical characterisation	53
2.6.1	Circular Dichroism	53
2.6.2	Steady-state tryptophan fluorescence spectrophotofluorimetry assay for Mhp1	54
2.7	Structural Characterisation	55
2.7.1	MX data collection and structure solution	55
2.7.2	Small-angle X-ray scattering studies coupled with size exclusion chromatography (SEC-SAXS)	55
2.8	Synthesis of Mhp1 hydantoin ligands	57
2.8.1	Experimental procedures	57
3	Searching for intermediate states of Mhp1 by applying single-point mutations of sodium and ligand binding sites	62
3.1	Purification of Mhp1 variants for structural studies	64
3.1.1	Purification of Mhp1 variants	64
3.1.2	Monitoring Mhp1 variant purity during purification	65
3.2	Biophysical characterisation of Mhp1 variants for structural studies	73
3.2.1	Assessing the secondary structure and thermal stability of Mhp1 variants using circular dichroism	73

3.2.2	Assessing ligand-binding behaviour of Mhp1 variants by steady-state tryptophan fluorescence quenching	81
3.2.3	Assessing ligand-binding behaviour of wild-type Mhp1 in presence and absence of sodium	87
3.2.4	Spectroscopic data of Mhp1 mutants towards observing an inward-open conformation	89
3.3	Crystallisation of Mhp1 variants	91
3.3.1	Reproduction and optimisation of previously published crystallisation conditions for outward form	93
3.3.2	Reproduction and optimisation of previously published crystallisation conditions towards an inward-form	96
3.4	Mhp1 mutant structural studies by X-ray crystallography	102
3.4.1	X-ray crystal structure of Mhp1 Ala38Gly mutant	102
3.4.2	X-ray crystal structure of the Mhp1 mutant Met39Cys in complex with L-BH	111
3.4.3	X-ray crystal structures of Mhp1 mutant Ala222Ser	117
3.4.4	Data processing of Ala309Asn	123
3.5	Discussion	123
4	Mhp1 variants in complex with detergent, a solution based study	128
4.1	Structural studies of wild type Mhp1 in solution	129
4.1.1	SEC-SAXS studies of wild-type Mhp1 in complex with NM detergent .	130
4.1.2	Oligomerisation of Mhp1 in crystal packing based on reported Mhp1 structures	133
4.1.3	SEC-SAXS studies of wild-type Mhp1 in complex with DDM detergent	135
4.2	Structural studies of Mhp1 mutants in solution	138
4.2.1	SEC-SAXS of Mhp1 mutants adopting an outward conformation in crystals	138
4.2.2	SEC-SAXS of Mhp1 mutants proposed to occupy an inward conformation	140

4.3	Discussion	145
5	LeuT	147
5.1	Protein Purification of wild-type LeuT (LeuT-WT)	148
5.1.1	Purification wild-type LeuT	148
5.1.2	Crystallisation of wild-type LeuT and initial crystallographic data	151
5.2	Triple-mutant LeuT (LeuT-SS) purification and cross-linking attempts	154
5.2.1	Expression and membrane preparation of the triple-mutant LeuT (LeuT-SS)	154
5.2.2	Disulphide bond formation on LeuT transporter	155
5.2.3	Cysteine cross-linking on membranes	157
5.2.4	Small-scale purification of wild-type LeuT and triple-mutant LeuT after cross-linking on membranes	159
5.3	Discussion	160
6	Conclusions and future outlook	161
	Appendix A Mhp1 and LeuT buffers	183
	Appendix B NMR spectra	190
	Appendix C List of hazardous substances	195

List of Figures

1.1	Crystal structure of the LeuT transporter	5
1.2	The secondary active transporters of the LeuT superfamily.	6
1.3	The common structure fold among the members of the LeuT superfamily	7
1.4	Schematic representation of the conversion of hydantoin compounds to optically pure amino acids	8
1.5	Crystal structure of the Mhp1 hydantoin transport protein from <i>Microbacterium liquefaciens</i>	9
1.6	Mhp1 topological diagram and crystal structure in inward-open conformation	10
1.7	Sodium binding site of Mhp1	11
1.8	The ligand-binding site of Mhp1	12
1.9	The alternating access mechanism of the Na ⁺ Hydantoin membrane transport protein, Mhp1	14
1.10	The three conformational states of Mhp1 of the alternating access mechanism	16
1.11	Locations of the Mhp1 cysteine residues in the crystal structures of the different conformations	17
1.12	Mass spectrometry of wild-type Mhp1 unlabelled and labelled with NEM	18
1.13	Mass spectrometry of wild-type Mhp1-DDM after labeling with NEM under the addition of L-BH and/or sodium in different conditions	19
1.14	Solubilisation of membrane proteins using detergent	24
1.15	Schematic representation of the phase diagram for the crystallisation of macromolecules based on two of the most commonly varied parameters based on two of the most commonly varied parameters protein and precipitant concentrations	27
1.16	Crystal lattice packing of membrane proteins	30

1.17	Demonstration of shifts observed in membrane protein circular dichroism spectra with respect to the soluble protein spectra.	32
1.18	Superimposition of the wild-type Mhp1 ligand binding sites in the outward-facing and outward-occluded crystal structures	33
1.19	Schematic representation of a size-exclusion chromatography run coupled with light scattering	36
2.1	Scheme of synthetic route of <i>L</i> -BH 3.	58
2.2	Scheme of synthetic route of <i>L</i> -IMH 6.	59
2.3	Scheme of synthetic route of <i>L</i> -NMH 9.	60
2.4	Scheme of synthetic route of BVH 12.	60
3.1	Location of Mhp1 residues coordinating the sodium and ligand in their binding sites.	63
3.2	SDS-PAGE gel (a) and Western blot (b) of wild-type Mhp1 purified in NM detergent for crystallisation trials.	66
3.3	SDS-PAGE gel and Western Blot of the Mhp1 Ala38Gly in the sodium binding site	67
3.4	SDS-PAGE gel and Western Blot of the Mhp1 Met39Cys in the sodium binding site	68
3.5	SDS-PAGE gel and Western Blot of the Mhp1 Ile41Phe in the sodium binding site	68
3.6	SDS-PAGE gel and Western Blot of Mhp1 Ala309Asn purified in NM in the presence of Na	69
3.7	SDS-PAGE gel and Western blotting of Mhp1 Ala309Asn purified in NM in the absence of Na	70
3.8	SDS-PAGE gel and Western Blot of Mhp1 Thr313Ala purified in NM in the presence of Na	70
3.9	SDS-PAGE gel and western blotting of Mhp1 Thr313Ala purified in NM in absence of Na.	71

3.10	SDS-PAGE gel and Western Blot of the Mhp1 Gln42Asn in the ligand binding site.	71
3.11	SDS-PAGE gel and Western Blot of the Mhp1 Gly219Ser in the ligand-binding site	72
3.12	SDS-PAGE gel and Western Blot of Mhp1 Ala222Ser of the ligand-binding site	72
3.13	Far-UV CD single spectra of the purified wild-type Mhp1 in NM detergent. . .	74
3.14	CD analysis to monitor the thermal stability of freshly purified wild-type Mhp1 purified in NM	75
3.15	Comparison of CD thermal melts from wild-type Mhp1 purified in DDM and NM detergents	75
3.16	CD spectrum from thermal melt experiments from 20° C to 90° for the sodium-binding site mutations	76
3.17	CD spectra and thermal melts of Ala309Asn and Thr313Ala in presence and absence of Na.	78
3.18	CD spectrum from thermal melt experiments from 20° C to 90° for the ligand-binding site mutations	79
3.19	Tryptophan fluorescence quenching by <i>L</i> -benzyl-hydantoin.	82
3.20	Mhp1 mutation Ile41Phe	84
3.21	Fluorescence quench curves for binding of <i>L</i> -BH to Mhp1 containing mutations in the binding sites	85
3.22	Binding of <i>L</i> -BH in wild-type Mhp1 purified in NM in presence and absence of sodium	88
3.23	The fluorescence change upon the addition of <i>L</i> -BH to the Ala309Asn-DDM and Thr313Ala-DDM mutants	90
3.24	Wild-type Mhp1 crystals forming after applying the streaking method	92
3.25	Crystals from Mhp1 mutants a) Ala38Gly, b) Met39Cys, c) Ile41Phe, d) Ala222Ser	94
3.26	Crystallisation of Ala309Asn in orthorhombic conditions.	94
3.27	Mhp1 mutant Ala309Asn crystals obtained under hexagonal conditions. . . .	98

3.28	Additional crystal morphologies appeared in crystallisation drops of Ala309Asn under hexagonal conditions	99
3.29	Needle shape crystals from Ala38Gly-apo and the corresponding diffraction pattern	103
3.30	Anisotropic diffraction data of Ala38Gly-apo	103
3.31	Crystal packing of Ala38Gly-apo structure	105
3.32	Cross-refinement to confirm the conformation the Ala38Gly-apo based on a segment of the external thin gate TMH 10	108
3.33	The structure of Ala38Gly in apo state.	109
3.34	NEM-Mass spectrometry measurements in Mhp1 variants in DDM.	110
3.35	Crystal packing of Met39C-LBH structure	114
3.36	The ligand-binding site of the crystal structure of the Met39Cys in complex with <i>L</i> -BH	115
3.37	Cross refinement of the Met39Cys, Crystal 2 to confirm its conformation in the absence of ligand.	116
3.38	Electron density map of the crystal structure Ala222Ser in the apo state	119
3.39	The electron density map of ligand binding site in the crystal structure Ala222Ser in complex with <i>L</i> -BH	120
3.40	The electron density map of ligand-binding site from the Ala222Ser in complex with <i>L</i> -IMH	122
4.1	Calculated scattering curve of Mhp1 in absence and presence of NM detergent	131
4.2	Elution profiles from the SEC-SAXS runs of wild-type Mhp1 in NM detergent.	132
4.3	Crystal packing of Mhp1 crystallised in outward-facing conformation (P2 ₁ 2 ₁ 2 ₁)	134
4.4	Crystal packing of Mhp1 crystallised in inward-facing conformation (P6). . . .	135
4.5	Elution profiles from the SEC-SAXS runs of wild-type Mhp1 in DDM	136
4.6	Elution profiles from the SEC-SAXS runs of the wild-type Mhp1 in various salt concentrations	138

4.7	Elution profiles from the SEC-SAXS runs of the Mhp1 mutants Met39Cys and Ala222Ser in NM detergent.	139
4.8	Elution profiles from the SEC-SAXS runs of the Mhp1 mutant Ala309Asn in NM detergent.	142
4.9	Elution profiles from the SEC-SAXS runs of the Mhp1 mutant Thr313Ala in NM detergent.	143
4.10	Comparison of the elution profiles from the SEC-SAXS runs of the Mhp1 mutant Ala309Asn in NM detergent in orthogonal (Tris buffer, pH 7) and hexagonal (Bicine buffer, pH 9) conditions with the elution profiles of the wild-type Mhp1 in NM and DDM detergent.	144
5.1	SDS-PAGE of wild-type LeuT purification steps in DDM.	150
5.2	Size exclusion chromatography profile of wild-type LeuT in β -OG detergent. .	151
5.3	SDS-PAGE gel of wild-type LeuT size exclusion chromatography in β -OG detergent.	151
5.4	Crystallisation and diffraction of wild-type LeuT.	152
5.5	Graphical representation of triple mutant LeuT S-S with the mutated cysteine residues	154
5.6	Scheme of cross-linking disulphide bond formation using the catalyst copper-phenanthroline	156
5.7	Scheme of DNTB reaction with thiol compound	156
5.8	Comparing triple-mutant LeuT mobility in SDS-PAGE under reducing and non reducing conditions after cross-linking treatment on membranes	158
5.9	SDS-PAGE gel of the wild-type LeuT and triple-mutant LeuT after cross-linking treatment on membranes	159

List of Tables

1.1	Synthesised hydantoin compounds	20
1.2	Reported crystal structures for Mhp1	22
2.1	Source of materials for Mhp1 and LeuT.	41
2.2	Detergent concentrations during the Mhp1 purification.	43
3.1	List of purified Mhp1 mutants of sodium and ligand-binding pockets	64
3.2	Apparent K _d and B _{max} values for wild-type Mhp1 purified in DDM and NM in comparison to previous reference values.	82
3.3	L-BH binding in Mhp1 mutants purified in NM and in DDM.	86
3.4	L-BH binding in Mhp1 mutants purified in NM in presence and absence of NaCl.	89
3.5	Crystallisation conditions of wild-type Mhp1 reported structures in three different conformational states.	91
3.6	Summary of crystals obtained for Mhp1 variants in outward crystal conditions.	95
3.7	Crystallisation of Ala309Asn Mhp1 mutant in hexagonal conditions	98
3.8	Crystals of Thr313Ala in hexagonal conditions	101
3.9	Data collection and refinement statistics for the structure of Ala38Gly-apo Mhp1 variant. For each appropriate column, the number in brackets represents the information for the outer shell only.	107
3.10	Data collection and refinement statistics for the structure of Met39Cys in complex with L-BH Mhp1 variant. For each appropriate column, the number in brackets represents the information for the outer shell only.	113

3.11	Data collection and refinement statistics for the structure of Ala222Ser Mhp1 variant. For each appropriate column, the number in brackets represents the information for the outer shell only.	118
3.12	Summary of Mhp1 mutant crystal structures obtained	125
3.13	List of estimated melting points (T _m) obtained from CD thermal melts of the Mhp1 mutants purified in NM.	127
4.1	Summary of SEC-SAXS parameters of the wild-type Mhp1 purified in NM detergent	132
4.2	Summary of SEC-SAXS parameters of the wild-type Mhp1 purified in DDM detergent	137
4.3	Summary of SEC-SAXS parameters of the Mhp1 mutants Met39Cys and Ala222Ser purified in NM.	139
4.4	Ala309Asn in NM detergent in Tris and Bicine buffers.	142
4.5	Thr313Ala in NM detergent in Tris and Bicine buffers.	143
4.6	Comparison of Mhp1 wild-type in NM and DDM detergents (Tris buffer) with the Mhp1 mutant Ala309Asn in NM detergent in Tris and Bicine buffers. . .	145
5.1	Data collection Statistics for the structure of wild-type LeuT. For each appropriate column, the number in brackets represents the information for the outer shell only	153
A.1	Detergent concentrations during Mhp1 purification steps and desired exchange.	185
A.2	Detergent used in the current thesis.	185
A.3	Characteristics of detergents used for Mhp1 and LeuT purifications.	186
A.4	SDS-PAGE stacking and running gels	186
C.1	List of hazardous substances	196

List of Abbreviations

Å	Ångström
A280	UV absorbance at specified wavelength (in this example, 280 nanometers)
APS	Ammonium persulfate
BSA	Bovine serum albumin
CD	Circular dichroism
CMC	Critical micellar concentration
CNS	Central neuron system
DMSO	Dimethylsulfoxide
Dmax	Maximum particle dimension
<i>E. coli</i>	<i>Escherichia coli</i>
EDTA	Ethylenediaminetetraacetic acid (chelating agent) or Ethylenediaminetetraacetate
EAAT	Excitatory amino acid transporters
EtOH	Ethanol
ESRF	European Synchrotron Radiation Facility
HEPES	4-(2-hydroxyethyl)-1-piperazineethanesulfonic acid
5HIR	5-helix inverted repeat

HPLC	High-performance liquid chromatography
IPTG	Isopropyl β -D-thiogalactopyranoside
LB medium	Luria-Bertani medium
Leu	Leucine
LeuT	Leucine transporter
MALLS	Multi angle laser light scattering
MES	2-(N-morpholino)ethanesulfonic acid
MFS	Major facilitator superfamily
Mhp1	Membrane hydantoin permease 1
MeOH	Methanol
β -ME	β -mercaptoethanol
MW	Molecular weight
MWCO	Molecular weight cutoff
MR	Molecular replacement
NCS-1	Nucleobase-cation symporter-1
Ni-NTA	Nickel-nitrilotriacetic acid
NMR	Nuclear magnetic resonance
NSS	Neurotransmitter sodium symporter
OD	Optical Density
PDB	Protein Data Bank
PDC	Protein-detergent complex
PEG ₄₀₀	Poly(ethylene glycol) 400

PEG ₅₅₀ MME	Poly(ethylene glycol) 500 Methyl ether
PMSF	Phenylmethanesulfonyl fluoride
R _g	Radius of gyration
SDS-PAGE	Sodium dodecyl sulphate- polyacrylamide gel electrophoresis
SAXS	Small-angle X-ray scattering
SEC	Size-exclusion chromatography
SSRL	Stanford Synchrotron Radiation Lightsource
TCA	Trichloroacetic acid
T _m	Transition midpoint, apparent melting temperature
TMH	Transmembrane helix
TMD	Transmembrane domain
TFA	Trifluoroacetic acid
Tris	2-amino-2-hydroxymethyl-1,3-propanediol
WB	Western blotting

Abbreviations of the detergents

DDM	n-Dodecyl- β -D-maltopyranoside
NM	n-Nonyl- β -D-maltopyranoside
β -OG	n-octyl- β -D-glucopyranoside

Abbreviations of Mhp1 variants

WT-DDM	Wild-type Mhp1 solubilised and purified in DDM detergent
WT-NM	Wild-type Mhp1 solubilised in DDM, purified in NM detergent

Abbreviations of LeuT variants

LeuT-WT	Wild-type LeuT
LeuT-SS	Triple-mutant LeuT

Abbreviations of hydantoin synthesis

All	Allantoin = 5-ureidohydantoin = (2,5-dioxo-4-imidazolidinyl) urea
Boc	tert-Butyloxycarbonyl protecting group
BVH	5-bromovinylhydantoin = (5E)-5-[(3-bromophenyl)methylidene]imidazolidine-2,4-dione
Hyd	Hydantoin = imidazolidine-2,4-dione
L-BH	5-benzyl-L-hydantoin = (5S)-5-benzylimidazolidine-2,4-dione
L-IMH	5-indolylmethyl-L-hydantoin = (5S)-5-(1H-indol-3-ylmethyl)imidazolidine-2,4-dione
L-NMH	5-(2-naphthylmethyl)-L-hydantoin = (5S)-5-(naphthalen-2-ylmethyl)imidazolidine-2,4-dione

Abbreviations

The abbreviations used in the current thesis have been proposed by the International Union of Biochemistry (IUB) and the International Union of Pure and Applied Chemistry (IUPAC) according to IUPAC- IUB Joint Commission on Biochemical Nomenclature (JCBN), Nomenclature and Symbolism for Amino Acids and Peptides, Recommendations, Eur. J. Biochem., 138 (1984) 9, J. Biol. Chem., 264(1989) 663 and the Abbreviations and Symbols in peptide science: a revised guide and commentary, J Peptide Sci., 12 (2006),1.

Nomenclature

The numbering of the chemical molecules is established according to their order of appearance

Chapter 1

Introduction

At the synapses allowing the transfer of signals between neurons, chemical neurotransmitters bridge the gap between electrical signals upstream and downstream. At the synaptic cleft, the concentration of the extracellular neurotransmitters produced is regulated by sodium-coupled secondary active transporters or neurotransmitter transporters. These transporters are responsible for removing the excess of released neurotransmitters and transporting them back into the neuron or surrounding glial cells, and thereby recycling them. The malfunction or improper regulation of the secondary active transporters contributes to neurological and neuropsychiatric disorders in humans (Gether et al. 2006). As a result, these transporters are important targets for drugs in the treatment of psychotic states, schizophrenia, clinical depression, diabetes, and obesity (Gether et al. 2006, Bröer & Palacin 2011, Wright 2013).

However, the molecular mechanism of the transporters underlying sodium-coupled neurotransmitter uptake has not yet been fully understood. Homologues of neurotransmitter transporters have been studied computationally and experimentally, elucidating important structural and functional information revealing molecular details of the transport mechanism, binding of the sodium and substrate, and conformational dynamics (Wong et al. 2012, Kazmier et al. 2017). Studies of the homologues have also given valuable insights into the understanding of the architecture and mechanism of mammalian neurotransmitter transporters. Bacterial ho-

mologues are often studied when the eukaryotic homologues are not available. These provide an experimental platform on which clinically significant eukaryotic members can eventually be pursued and accelerate the discovery of therapeutic agents. Furthermore, several bacterial analogues have been found to have a similar structural fold. These have been found to have both similar structure and mechanism, providing insights into the those of structurally similar transporters also of therapeutic importance.

Secondary active transporters that are of particular interest in this current thesis are the Mhp1 protein from the nucleobase cation symporter-1 family (NCS-1) and the LeuT from the neurotransmitter sodium symporters (NSS). They are related to each other structurally, but not in sequence.

1.1 Transport through biological membranes

The passage of ions, nutrients, small molecules in and out of the cell is regulated by the cell membrane and its components. Membranes are lipid bilayers and due to their interior hydrophobicity, they are permeable only to certain solutes. They allow small, hydrophobic or neutral molecules such as O_2 , CO_2 , N_2 , NH_3 , HCO_2H or benzene, glycerol, ethanol by passive diffusion (or simple diffusion), without the participation of any transporter or channel. For bigger, polar or charged molecules (amino acids, nucleotides, glucose) or ions (H^+ , Na^+ , HCO_3^- , K^+ , Ca^{2+} , Cl^- , Mg^{2+}) the membrane is not intrinsically permeable. In this case, there are integrate membrane proteins (IMPs) that mediate the transportation across the cell membrane of those molecules. These proteins are divided into passive transporters which do not require assistance from a free energy source, and active transporters which do.

In passive transport (or facilitated diffusion), the hydrophilic or large molecules bind to the IMPs and pass across the membrane based solely on their concentration gradient without the

use of extra energy. Passive transporters (uniporters) transport the molecule by undergoing a series of structural conformational changes and they transport one molecule at a time at a slow rate (Gadsby 2009). On the other hand, channel proteins create a hydrophilic pore through the membrane allowing the flow of the molecules freely down their concentration gradient. Channels can be regulated either by the chemical gradient of the molecule (ligand-gated channel), by the membrane potential (voltage-gated channels) or by a mechanical force (stress-activated channel).

Active transport involves the use of energy, in contrast to passive transport, and is used by primary and secondary active transporters. The primary active transporters use light, hydrolysis of ATP or redox reactions as energy sources to transport the substrate, often ions. This extra energy means that they can also be transported against their chemical gradient (primary active transporters). These may therefore produce electrochemical gradients of ions that the secondary active transporters may then exploit in order to power the "uphill" translocation of specific substrates across the membrane. This co-transport can be in the same direction (symporter) or in opposite directions (antiporters). Active transport is important for maximising absorption of a nutrient source.

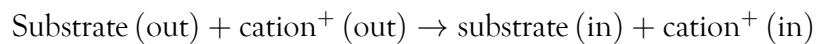
1.2 Secondary active membrane transporters

Secondary active transporters have been found in all species (Shimamura et al. 2010). They have a wide variety of substrates including neurotransmitters, vitamins, amino acids and purines. Crystal structures of several sodium-coupled transporters from functionally different families and with little sequence identity have been shown repeatedly to exhibit a remarkable structural similarity (Abramson & Wright 2009, Forrest & Rudnick 2009, Forrest et al. 2011). Well-studied structural folds include the MFS-fold, the LeuT-fold and the NhaA-fold (Shi 2013), of which the LeuT-fold will be the subject of discussion in this thesis.

- **NCS-1 family (nucleobase-cation symporter-1)**

The nucleobase cation symporter-1 (NCS-1) family, designated A.2.39 (Saier Jr et al. 2006, 2008) consists of over 2000 currently sequenced proteins derived from Gram-negative and Gram-positive bacteria, archaea, yeast, fungi, and some plants (Pantazopoulou & Diallinas 2007, Ren et al. 2006, Ren & Paulsen 2007). The NCS-1 family exhibits diverse substrate selectivity, transporting compounds such as hydantoins, allantoin, cytosine, nicotinamide riboside and thiamine. These substrates act as either energy sources or supplies of cofactors or biosynthetic precursors (Weyand et al. 2010).

The NCS-1 family is part of a transporter superfamily that has since been termed the amino acid-polyamine-organocation (APC) superfamily (Vastermark et al. 2014). NCS-1 proteins are structurally related by a 5-helix/5-helix internal pseudosymmetry to other families in the APC superfamily. Therefore the APC superfamily is also called the 5-helix inverted repeat (5HIRT) or LeuT superfamily of ion-coupled transporters in the literature . The generalised transport reaction for the NCS-1 family of transporters has been reported as follows (Jackson et al. 2013).



1.3 LeuT, the Leucine transporter

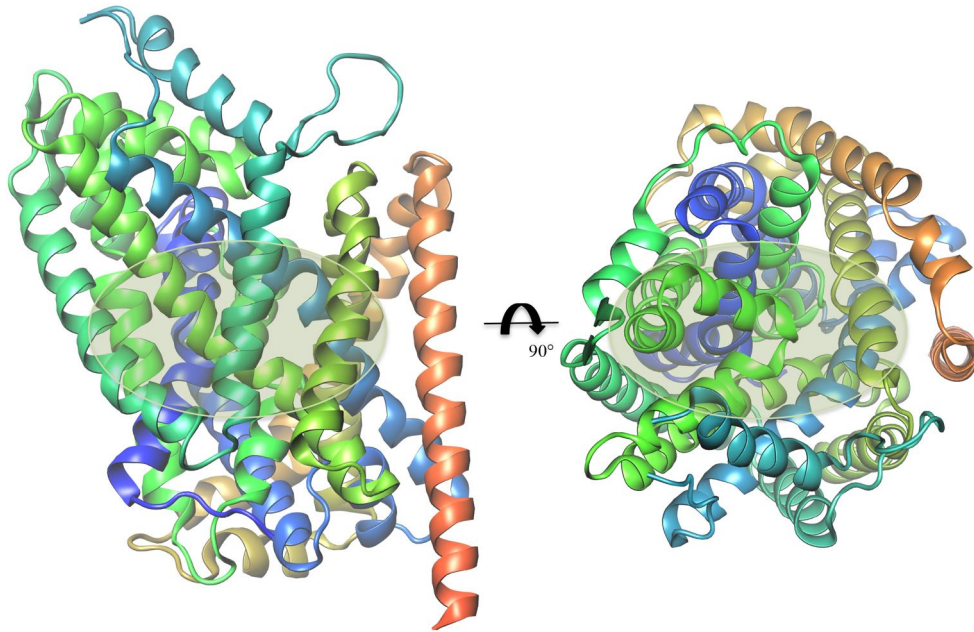


Figure 1.1: Crystal structure of the LeuT transporter. Crystal structure of the LeuT transporter (PDB code 2A65) in cartoon representation from N- to C-terminus in rainbow colouring. The ligand and sodium binding site are highlighted in the green ellipse. Picture was prepared by VMD (Humphrey et al. 1996) and rendered using Tachyon (Stone 1998).

The LeuT transporter from *Aquifex aeolicus* is a membrane protein of 519 amino acids with a molecular weight of 58 kDa that transverses the membrane 12 times. The structure of LeuT consists of 12 transmembrane helices (TMHs). The first ten helices constitute the core transport domain, and the two remaining helices in the C-terminus have a role in the dimerisation of the transporter. The core TMHs 1-5 and 6-10 form the pseudosymmetry of the LeuT-fold representing an inverted repeat (Yamashita et al. 2005). The first two helices of each repeat come together to form a four-helix bundle. The first reported crystallographic structure of LeuT (Figure 1.1) was determined at 1.65 Å resolution in complex with its ligand, leucine, and two sodium ions in an outward-occluded state (Yamashita et al. 2005). Since then, LeuT has been crystallised in different conditions (Krishnamurthy & Gouaux 2012, Wang et al. 2012, Krishnamurthy & Gouaux 2012, Malinauskaite et al. 2016) and in various conformations including a substrate-free state, inward-open state (Krishnamurthy & Gouaux 2012), competitive and non-competitive inhibitor-bound states (Singh et al. 2008, Zhou et al. 2007, 2009).

An important group of secondary active transporters have been observed to have a structural fold similar to that of the LeuT protein (Yamashita et al. 2005). These proteins were originally classified in separate families due to the extreme dissimilarity of their sequences (Saier Jr et al. 2006), but after solving the structures they were all brought under the umbrella of the LeuT transporter superfamily.

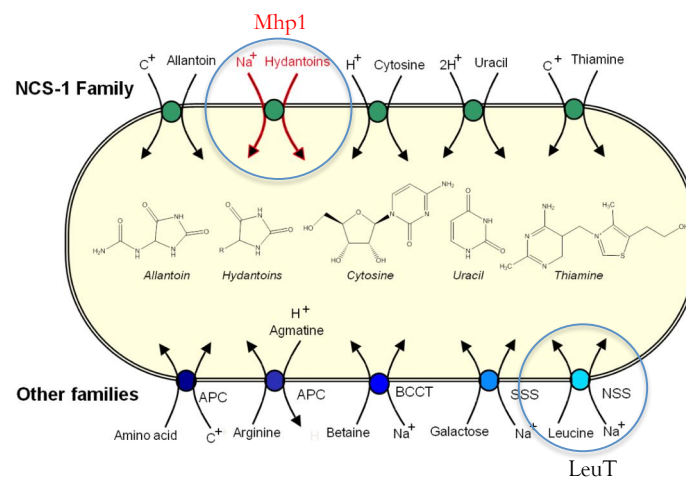


Figure 1.2: The secondary active transporters of the LeuT superfamily. Schematic representation of the cytoplasmic membrane of a bacterial cell (yellow oval). Members of the NCS-1 family are depicted by green circles. Their transporting chemical compound are drawn inside the cell. Other families having the LeuT fold are represented in blue. Figure kindly provided by Prof Peter Henderson.

These are the benzyl-hydantoin transporter Mhp1 from the nucleobase-cation symporter family (NCS-1) (Weyand et al. 2008, 2010, 2011), the sodium-galactose symporter vSGLT (Faham et al. 2008) from the sodium-solute symporter (SSS) family, the sodium-betaine symporter BetP (Ressler et al. 2009) and the L-carnitine/ γ -butyrobetaine antiporter CaiT (Tang et al. 2010, Schulze et al. 2010) both members of the betaine-choline-carnitine transporter (BCCT) family, the H^scoupled amino acid transporter ApcT (Shaffer et al. 2009) as well as in the arginine/agmatine antiporter AdiC (Fang et al. 2009, Gao et al. 2009, Kowalczyk et al. 2011) both of which are members of the amino acid-polyamine-organocation (APC) transporter family (Vastermark et al. 2014). This thesis focuses on two families of these secondary active transporters: the NCS-1 family and the NSS family. Both families belong to the LeuT superfamily (Krishnamurthy et al. 2009), also called 5-helix inverted repeat transporter (5HIRT) superfamily (Adelman et al. 2011).

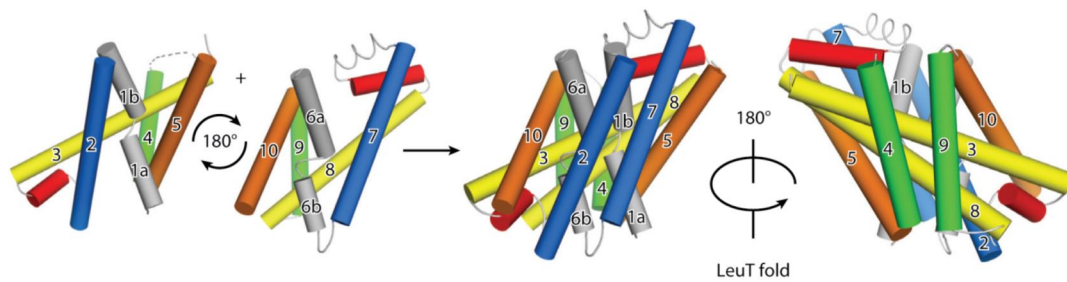


Figure 1.3: The common structure fold among the members of the LeuT superfamily. Cartoon representation of the LeuT fold illustrating the pseudo-two-fold repeat unit. This is the common structure fold among the members of the LeuT superfamily. Helices are represented by cylinders. Adapted from Shi (2013).

The LeuT fold comprises two copies of a 5 TMH structural motif (TMHs 1-5 and TMHs 6-10). The two repeats are related to each other by a two-fold pseudo-symmetry axis to form the core of LeuT, parallel to the membrane plane. Helices 1 and 6 are broken where the substrate binding site is accommodated.

1.4 Mhp1 a sodium-hydantoin symport transporter

Membrane hydantoin permease-1 (Mhp1), from *Microbacterium liquefaciens* is a bacterial sodium-coupled secondary active symporter member of the NCS-1 family (Saier Jr et al. 2006, 2008, Ren & Paulsen 2007). It is encoded in the gene cluster *hyu* which consists of enzymes associated with the production of amino acids. Mhp1 facilitates the co-transport across the cell membrane of hydantoin compounds (hydantoin compounds with a substitution at the 5-position of the aromatic ring with a hydrophobic group). Mhp1 has a moderate preference for L-hydantoin, but transports both enantiomers across the membrane. It uses the energy derived from the sodium ion gradient to drive the transport process. Inside the cell, the hydantoin compounds are hydrolysed and converted into L-phenylalanine and L-tryptophan amino acids by other members of *hyu* gene cluster as depicted in Figure 1.4 (Suzuki & Henderson 2006).

In biotechnology, these are important intermediates in the production of optically pure antibiotics, pesticides, pharmaceuticals and food additives (Syldatk et al. 1990, Suzuki & Henderson 2006, Clemente-Jiménez et al. 2008, Las Heras-Vázquez et al. 2008).

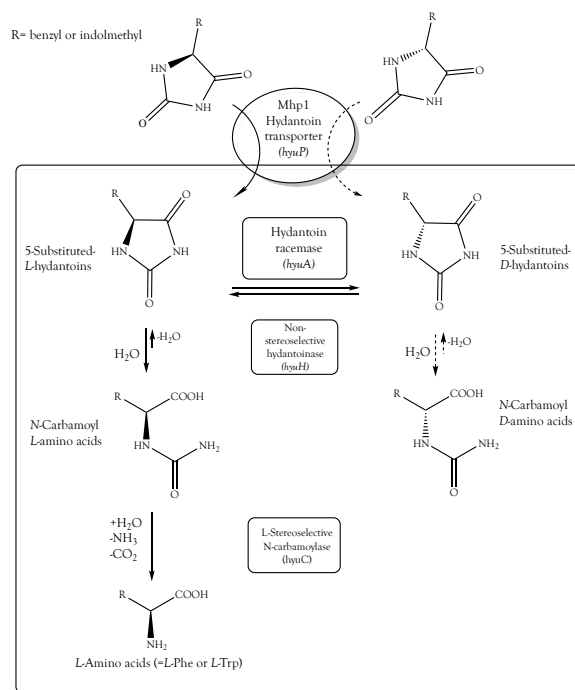


Figure 1.4: Schematic representation of the conversion of hydantoin compounds to optically pure amino acids. The predicted functions of the encoded proteins by the *hyu* gene cluster (Mhp1 hydantoin transporter (*hyuP*), hydantoin racemase (*hyuA*), hydantoinase (*hyuH*), and N-carbamoylase (*hyuC*)) process in *Microbacterium liquefaciens* (AJ 3912). Picture prepared using ChemDraw and based on a similar figure from Suzuki & Henderson (2006).

Crystal structure of Mhp1

The first crystal structure of Mhp1 was solved in 2008 and was the first structure determined of any NCS-1 family member. It was found to have a similar protein fold to that of the LeuT protein from the NSS family (Yamashita et al. 2005). Mhp1 was also the first of the LeuT-fold superfamily to be characterised crystallographically in outward-facing, inward-facing and outward-facing/occluded conformations of an alternating access cycle (Weyand et al. 2008, Shimamura et al. 2010).

The Mhp1 transporter is an integral membrane protein consisting of 12 TMHs (Figure 1.5), with ten core TMHs and two additional C-terminal helices (Weyand et al. 2008). The ten core helices form a structural fold which is conserved in the LeuT superfamily members and is called the LeuT fold or 5HIRT fold (Figure 1.3) (Weyand et al. 2008, 2011, Abramson & Wright 2009, Krishnamurthy et al. 2009, Shimamura et al. 2010).

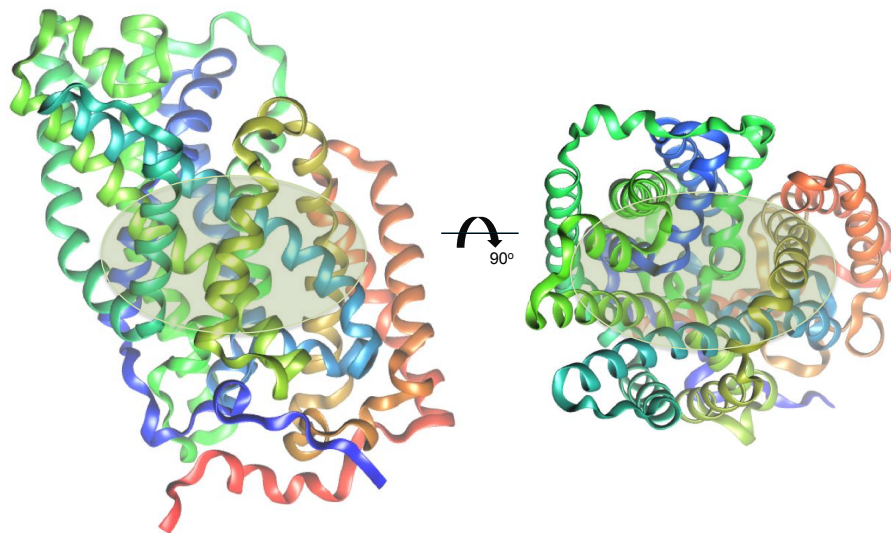


Figure 1.5: Crystal structure of the Mhp1 hydantoin transport protein from *Microbacterium liquefaciens*. **Left:** The Mhp1 structure viewed in the plane of the membrane. The figure is based on the high-resolution structure outward-open form of the Mhp1 protein (PDB code 2JLN). The position of the substrate in the Mhp1- benzyl-hydantoin complex structure is shown as green ellipse. **Right:** Top-down view of the same Mhp1 molecule. Picture was prepared by VMD (Humphrey et al. 1996) and rendered using Tachyon (Stone 1998).

The 12 transmembrane helices are generally grouped into three segments, which are referred to as the *bundle motif*, the *hash motif* and the two C-terminal TMHs. The *bundle motif* consists of four helices: TMH 1, TMH 2 and their symmetry partners TMH 6 and TMH 7. The *hash motif*, named after its similarity to the appearance of a hash sign (#), comprises another four helices: TMH 3, TMH 4 and their symmetry partners TMH 8 and TMH 9. The two C-terminal transmembrane helices (TMH 11 and TMH 12) (Shimamura et al. 2010, Weyand et al. 2011) sit on the outside of the protein. TMH 5 sits between one of the links between the bundle and hash motifs, facing the membrane. TMH 10 links the hash motif with the C-terminal helices TMH 11 and TMH 12. TMH5 and the bundle motif together make one of the 5HIRT repeats, and likewise for TMH 10 and the hash motif (Figure 1.6). One additional intracellular helix

(IN 2-3) is found between TMH 2 and TMH 3, and one extracellular helix (OUT 7-8) between TMH 7 and TMH 8.

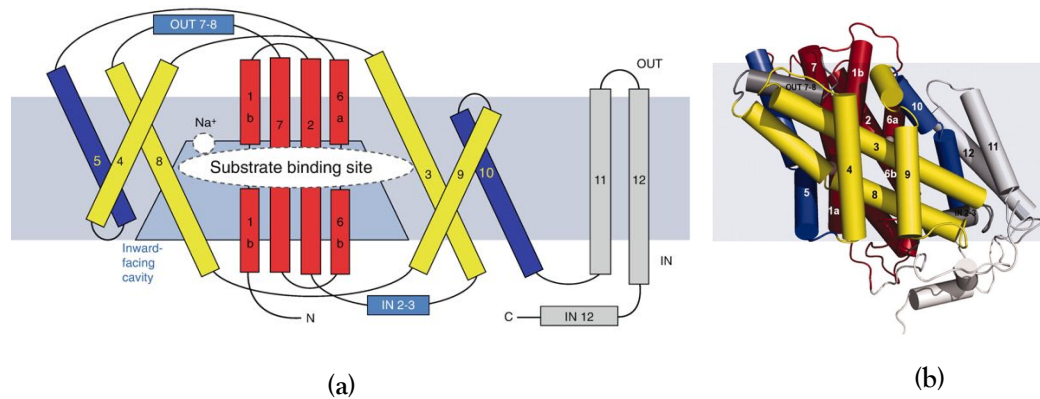


Figure 1.6: Mhp1 topological diagram and crystal structure in inward-open conformation. (a) **Topological diagram of Mhp1.** The membrane is shown in grey and the inward-facing cavity observed in the structure is highlighted in light blue. The positions of the substrate and the sodium binding sites are depicted as a white ellipsoid and white circle, respectively. TMHs 3 and 8 pack onto each other in three dimensional space to form the protein depicted in (b). Picture adapted from Weyand et al. (2008). (b) **Mhp1 structure of the inward-open conformational state in cartoon representation.** The bundle motif helices (TMHs 1a, 1b, 2, 6a, 6b, and 7) are coloured red, the hash motif helices (TMHs 3, 4, 8, and 9) are coloured yellow, the flexible helices (TMHs 5 and 10) are coloured in blue, the C-terminal helices (TMHs 11 and 12) are coloured light grey, and the non-membrane helices surface extracellular (OUT 7-8) and the cytoplasmic surface helices (IN 2-3,) are coloured darker gray. The longer helices (TMHs 5, 8-10) that show a distinct curvature are shown here as two shorter helices broken in the middle. Adapted from Calabrese et al. (2017).

1.4.1 Binding sites of Mhp1

The binding of sodium and benzyl-hydantoin are tightly coupled in Mhp1. The sodium and the ligand binding sites are located between the hash and bundle motifs and the involved residues to the binding procedure are located in TMHs 1 and 6 where the helices break. Sodium binding stabilises the outward-facing conformation of the protein, which in the absence of sodium should only occur transiently. In the inward-open structure both binding sites are disrupted, particularly the sodium binding site where the residues interacting with the sodium move approximately 4.5 Å further apart (Shimamura et al. 2010).

The sodium binding site in Mhp1

The sodium binding site in Mhp1 is located between TMH 1a, TMH 1b and TMH 8, in a conserved binding site also found in LeuT and vSGLT members of the LeuT superfamily. (Figure 1.7) (Weyand et al. 2008, 2011, Shimamura et al. 2010). The sodium interacts with the main chain carbonyl-oxygen atoms of residues Ala 38 (TMH 1), Ile 41 (TMH 1), and Ala 309 (TMH 8) as well as with the hydroxyl-oxygen-atom side chains of Ser 312 (TMH 8) and Thr 313 (TMH 8).

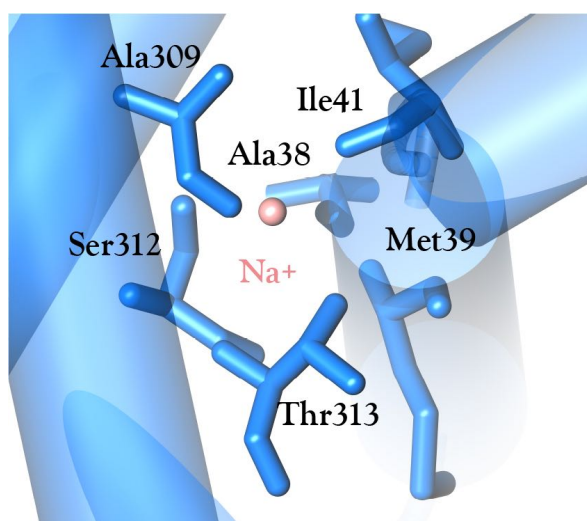


Figure 1.7: The sodium-binding site of Mhp1. The key interacting residues in the sodium binding cavity and the sodium are shown in ball and stick representation. Picture was prepared by VMD (Humphrey et al. 1996) using the wild-type apo structure of Mhp1 PDB code 2JLN and rendered using Tachyon (Stone 1998).

The unwound segment of TMH 1 has been identified as an important region for coordinating the sodium and the ligand binding sites (Watanabe et al. 2010). The sodium binding site in Mhp1 is approximately 8 Å away from the substrate binding site, supporting a sodium linkage to the ligand binding mechanism (Abramson & Wright 2009, Krishnamurthy et al. 2009). On the other hand, in the inward-open conformation the crystal structure (Shimamura et al. 2010, Weyand et al. 2011) revealed that TMH 8 has moved 4.5 Å further away, thus, the sodium binding site is no longer intact, resulting in only three contacts of the sodium with the protein. As a result, the position of the sodium binding site suggests a possible important role for the sodium in the mechanism.

The ligand binding site in Mhp1

The location of the ligand binding site of Mhp1 as well as the molecular basis of its specificity to hydantoin substrates have been established previously (Weyand et al. 2008, Simmons et al. 2014, Polyakova 2015). The substrate binding site is located approximately halfway across the membrane bilayer in the centre of the core domain of the protein at the breaks in the discontinuous helices TMHs 1 and 6, and facing TMHs 3 and 8 (Figure 1.8).

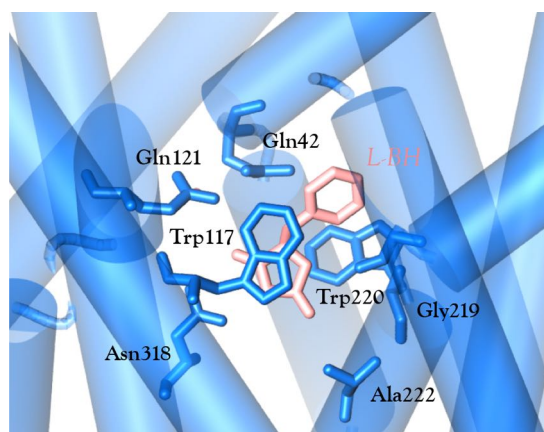


Figure 1.8: The ligand-binding site of Mhp1. The key interacting residues of the ligand binding cavity are shown in ball and sticks representation. The ligand L-BH is displayed in the cavity in light pink colour ball and stick representation. 4D1B Mhp1 structure was used with the L-BH bound. Picture was prepared by VMD (Humphrey et al. 1996) and rendered using Tachyon (Stone 1998).

The crystal structures of Mhp1 bound to L-BH and L-IMH revealed that the hydantoin moiety of the ligands is bound in an aromatic “cage” provided by two tryptophan residues Trp 117 (TMH 3) and Trp 220 (TMH 6) with possible hydrogen bonds to neighbouring protein Gln/Asn residues. More specifically, the indole ring of Trp117 forms π -stacking interactions (face-to-face/sandwich) with the hydantoin moiety of L-BH (4D1B.pdb, (Weyand et al. 2008)) and L-IMH (PDB code 4D1A, (Simmons et al. 2014)). Trp220 reorients its indole ring to form π -stacking (edge-to-face) interactions with the benzyl-ring of the L-BH (PDB code 4D1B (Weyand et al. 2008)) and in the case of L-IMH, with the indole ring (PDB code 4D1A (Simmons et al. 2014)). Thus, explicit changes in the tryptophan environment occur during the binding allowing the use of tryptophan fluorescence to monitor both the structural and kinetic changes.

Important residues for the ligand binding apart from the Trp 117 and Trp 220 have been proposed to be the Gln 42, Gln 121, Gly 219, Ala 222, Asn 314, Ala 317 and Asn 318 (Jackson 2012). These are depicted in Figure 1.8. The side chains of Gln 121 and Asn 318 are proposed to interact with the hydantoin moiety of the ligand and to form one hydrogen bond and two hydrogen bonds respectively. Gly 219 also forms a backbone hydrogen bond with the hydantoin moiety, while Ala 44 forms a backbone hydrogen bond with the benzyl-ring.

1.4.2 The alternating access mechanism in Mhp1 and its conformational states

The alternating access mechanism was initially proposed by Jardetzky (1966). This mechanism is preserved among the family members of the LeuT superfamily. Mhp1 was the first transporter protein from the LeuT superfamily and from the secondary active transporter NCS-1 family (Diallinas 2008) for which crystal structures of all three key conformations relevant to the proposed alternating access mechanism have been captured, substrate-free outward-open (Weyand et al. 2008), substrate-bound occluded (Weyand et al. 2011, Simmons et al. 2014), and substrate-free inward-open (Weyand et al. 2011).

The secondary active transporters transport the potential solutes across the membrane utilising the free energy of the electrochemical potential. The substrate binding site is exposed to one side or the other of the membrane during the transport process. In order for this to be possible a substantial conformational change of the transporter is required.

Figure 1.9 represents the proposed alternating access mechanism of Mhp1 displaying the intermediate states of the mechanism among the three conformational states obtained from the crystals structures: outward-open (III) (PDB code JLN), outward-occluded (V) (PDB code 4D1B), inward-open (IX) (PDB code 2X79). The bundle helices 1, 2, 6, 7 are in red. The hash motif helices 3, 4, 8, 9 forming the internal thick gate are in yellow; the external thin gate containing part of helix 10 is in blue. The internal thin gate containing part of helix 5

is also in blue. The rotation axis of the thick gate, running approximately parallel to TMH 3, is shown as a filled black circle on TMH 3. The process of transport from outside to inside follows the steps from 1 to 10.

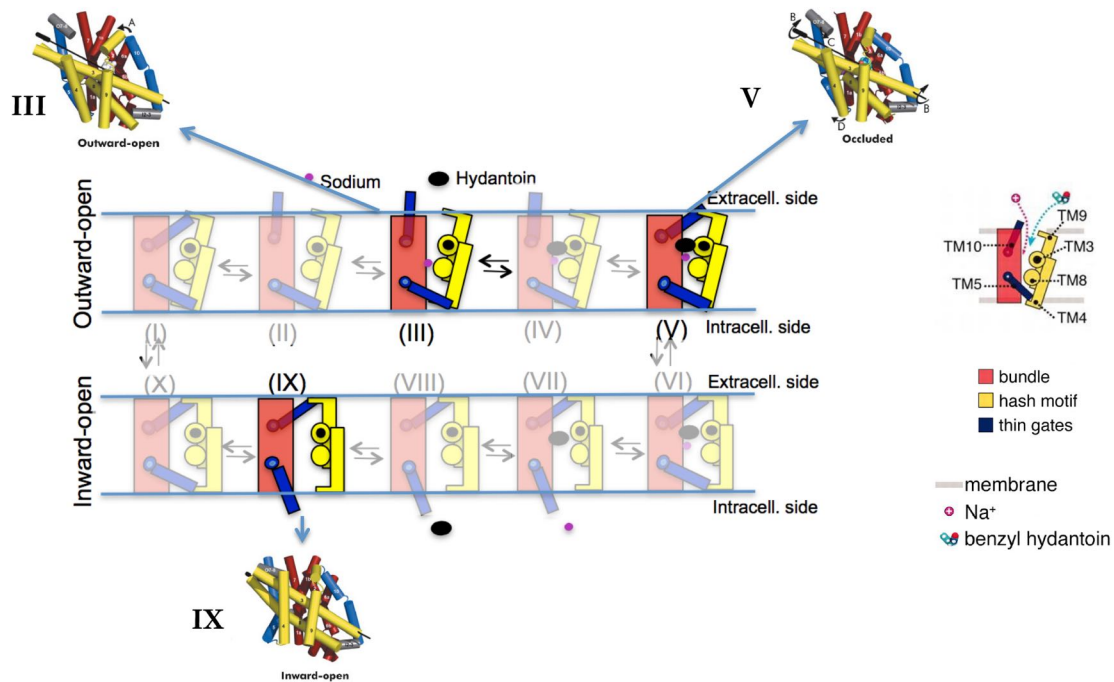


Figure 1.9: The alternating access mechanism of the Na⁺ Hydantoin membrane transport protein, Mhp1. A schematic illustration/representation of the possible conformations highlighting the thick (yellow) and thin (dark blue) gates. The three diagrams coloured as in Figure 1.6b represent the outward-open(III), occluded (V) and inward-open (IX) crystal structures. The diagrams in transparent colours show possible intermediate states. The bundle helices 1, 2, 6, 7 are in red. The hash motif helices 3, 4, 8, 9 forming the internal thick gate are in yellow; the external thin gate containing part of helix 10 is in blue and the internal thin gate containing part of helix 5 also in blue. Upon sodium and substrate binding the extracellular thin gate (TMH 10) closes to form the occluded state. The internal thick gate then opens with a rigid body rotation relative to the bundle motif. Either independently or concomitantly with this the intracellular thin gate (TMH 5) also opens to allow the substrates to exit towards the cytoplasm. The process of transport from outside to inside follows the steps from 1 to 10 supported by MD simulations. Original figure provided by Peter Henderson.

The transition between the conformational states can be described as the interplay of the buried thick gate (hash motif), and the two thin gates (the external (TMH 10) and the internal (TMH 5)). The thick gate regulates the big conformational change from the outward-open and occluded states to the inward-open state which is the rigid body rotation of the hash motif relevant to the bundle motif. As a result the ligand binding site faces towards the intracellular

space. The thin gates comprises only some residues in the respective helices and they are responsible for smaller changes. More specifically the extracellular thin gate TMH 10 opens and closes the binding sites of sodium and substrate in the outward-open and occluded states, while the intracellular/internal TMH 5 allows the opening and release of substrate and sodium toward the inside of the cell when the thick gate and the external thin gate are closed to the outside. The sequence of events presented in the schematic illustration (Figure 1.9) has been found in MD simulations (Shimamura et al. 2010, Adelman et al. 2011) and is fully compatible with the alternating access mechanism of transmembrane transport (Jardetzky 1966).

More detailed study of the different conformational states (Figure 1.10) reveals that the outward-open and the occluded conformations show very high similarity but neither of them superimposes well with the inward-open state, arising the question whether or not there is only one occluded state. Molecular dynamic simulations suggest an additional hypothesised conformation in the membrane: the inward-facing-occluded state (Beckstein, unpublished data; Adelman et al. 2011). Upon substrate binding to the outward-open conformation the TMH 10 (N-terminal half) rearranges so as to close to the occluded state. A significant overall rigid-body rotation of the hash motif relative to the bundle motif (approximately 30°) around an axis in line with TMH 3, the pseudo-symmetrical structural element of the protein (Forrest & Rudnick 2009, Boudker & Verdon 2010) leads to inward-open state. This rotation is accompanied by two other main changes to the protein. TMH 5 (the N-terminal equivalent of TMH 10) opens the cavity further to the exterior. Secondly, a small extracellular helix moves to seal the extracellular face of the protein completely. The C-terminus (helices 11, 12) moves relatively little in comparison to the other Mhp1 segments. During the conformational changes, the occluded state of the protein always prevents net movement of either cation or substrate without the other – their movement becomes “coupled”.

Molecular dynamics simulations show evidence (Shimamura et al. 2010, Adelman et al. 2011) for the sequence of events presented above which is compatible with the alternating access mechanism of the transmembrane transport. In the outward-open and occluded conformational states of Mhp1 the sodium in its binding cavity is coordinated by five hydrogen bonds.

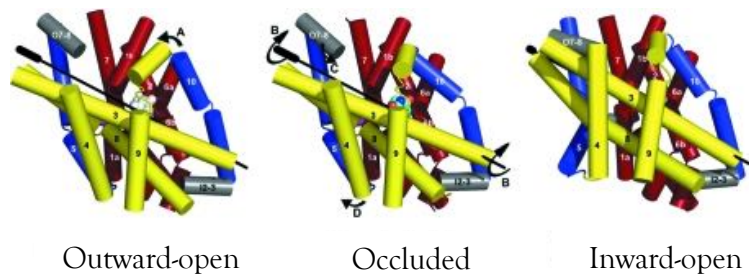


Figure 1.10: The three conformational states of Mhp1 of the alternating access mechanism. The three conformational states of Mhp1 and the movements of their helices which are delineated by arrows. A: TMH 10 bends over the substrate. B: The hash motif rotates by 30 ° around the rotation axis shown as a black line. C: The small extracellular helix (OUT 7-8) moves to seal completely the extracellular side of the protein. D: The flexible TMH 5 bends to open the cavity on the intracellular side in a reciprocal manner to TMH 10. Adapted from Shimamura et al. (2010).

1.4.3 Conformational changes during transport or states and switching NEM labelling

Mhp1 has been crystallised in three different conformations (outward-open, outward occluded with substrate bound, and inward-open), but what is Mhp1's dominant conformation in solution? Are the inward and outward forms in equilibrium in solution? What is the influence of hydantoin and sodium binding in this conformation equilibrium? How can this equilibrium be switched?

Calabrese et al. (2017) used a combination of cysteine accessibility and mass spectrometry to address the topological transitions of Mhp1. Mhp1 has three natural cysteines (Figure 1.11). Cys 327, out of the three, is the most accessible cysteine residue in all three conformations and has an enhanced solvent accessibility only in the inward-facing (relative to the outward-

facing) conformation. The other two cysteines Cys 69 (TMH 2) and Cys 234 (TMH 6) are not solvent accessible. Thus, Cys 327 (TMH 8) can be modified by reactions with the thiol-reactive *N*-ethylmaleimide (NEM) only when Mhp1 adopts an inward-facing conformation. Thus, the accessibility of Cys 327 is a useful probe for discrimination between the inward-facing and outward-facing conformational states of Mhp1.

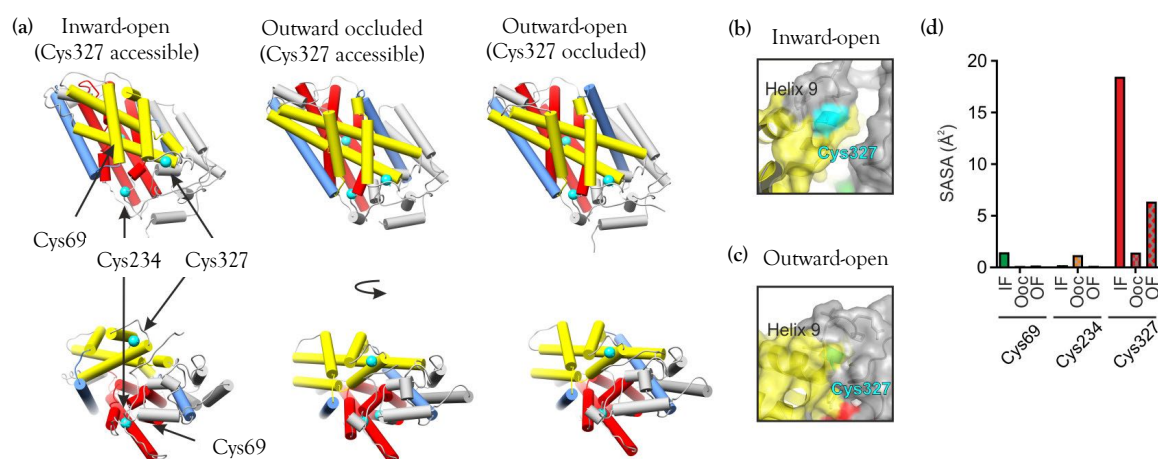


Figure 1.11: Locations of the Mhp1 cysteine residues in the crystal structures of the different conformations. (a) Mhp1 different conformations inward-open (PDB code 2X79), outward-occluded (PDB 4D1B), and outward-open (PDB 2JLN). Helices are represented as cylinders and coloured as in figure above (Figure 1.6). The Cys residues are shown in cyan as ball and stick representation. (b, c) Location of Cys 327 (cyan) in inward-open (b) and outward-open (c), showing that TMH 9 protects Cys 327 from solvent in the outward-open conformation, (d) Average side-chain solvent-accessible surface area (SASA) values of the three Cys residues of Mhp1 in 20 ns MD simulations started from the inward-open (IF), outward-occluded (OOc), and outward-open (OF) crystal structures. Adapted from Calabrese et al. (2017).

Mass spectrometry experiments of wild-type Mhp1 unlabelled and labelled with NEM have shown that in the absence of sodium and hydantoin ligand the predominant species observed corresponds to Mhp1+1NEM (red) with minimal unlabelled Mhp1 (blue) and negligible Mhp1+2NEM (yellow) and Mhp1+3NEM (green) detected (Figure 1.12).

These experiments have shown that wild-type Mhp1 purified in DDM detergent in the absence of sodium or L-BH substrate, adopts an inward-facing conformation and it maintains this conformation after the addition of sodium or L-BH substrate. However, only the simultaneously

addition of sodium and *L*-BH substrate in a concentration dependent manner altered the conformation equilibrium from the inward-facing to the outward-facing state as Figure 1.13 depicts (Kazmier et al. 2014, Calabrese et al. 2017). This makes the understanding of individual steps (intermediate states) of the transport cycle more difficult.

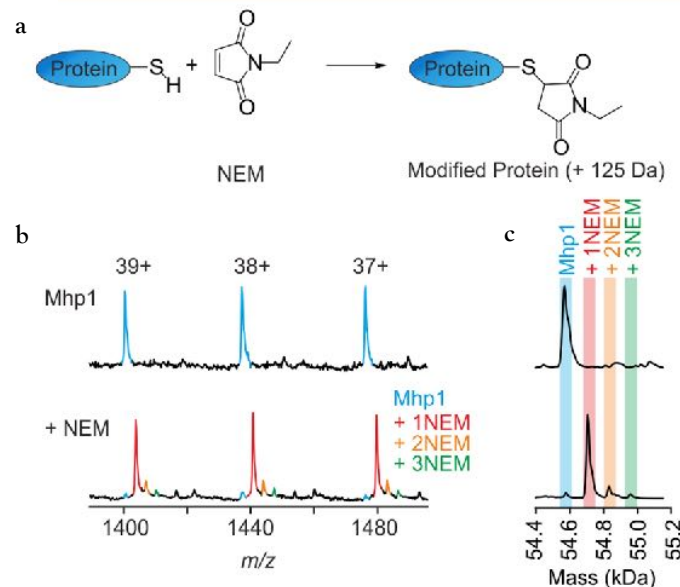


Figure 1.12: Mass spectrometry on wild-type Mhp1 unlabelled and labelled with NEM. (a) Reaction of a Cys residue of Mhp1 with NEM, (b), Part of unprocessed mass spectrum of unlabelled Mhp1 (upper) and labelled with NEM (lower), only three charge states are shown for clarity, (c) Deconvoluted mass distributions of unlabelled and labelled Mhp1. The shading indicates the expected masses of Mhp1 respectively. Adapted from Calabrese et al. (2017).

By the co-addition of 140 mM NaCl and *L*-BH substrate (Figure 1.13ai) mass distributions were obtained consistent with the presence of both unlabelled-Mhp1 (outward-facing conformation) and labelled-Mhp1 +1NEM (inward-facing conformation), indicating that the combination of both sodium and *L*-BH leads to an equilibrium of both outward-facing (unlabelled mass distribution, blue shade) and inward facing conformations (labelled-Mhp1+1NEM, red shade). Increasing the NaCl concentration from 140 mM to 1 M (1.13bi and bii) gives a similar pattern, but amount of the labelled-Mhp1+1NEM was reduced significantly suggesting that a shift in population towards unmodified-Mhp1 has occurred and indicating the outward-facing conformation is now occurred. The co-addition of 1 M sodium and 2 mM *L*-BH led to a significant diminution in NEM labelling and the proportion of labelled Mhp1 (inward-facing) was

reduced to a much higher extent compare to 140 mM NaCl. To sum up, both 1 M sodium and 2 mM L-BH are required to obtain a significant shift of the conformational equilibrium of Mhp1 in DDM towards the outward-facing conformation.

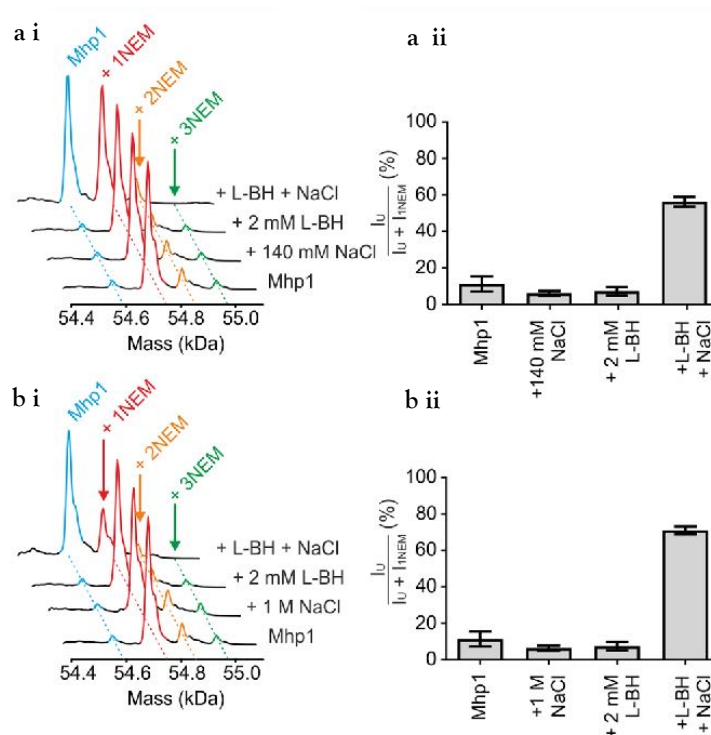


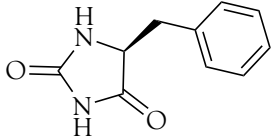
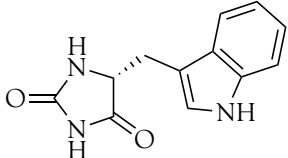
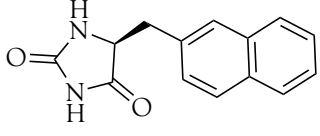
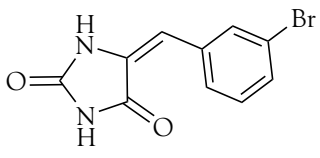
Figure 1.13: Mass spectrometry of wild-type Mhp1-DDM after labeling with NEM under the addition of L-BH and/or sodium in different conditions. (a) 140 mM NaCl and (b) 1 M NaCl. (i) Deconvoluted mass distributions of Mhp1 after NEM labeling under varied solution conditions. (ii) Relative abundances of unlabeled Mhp1 (I_U) relative to Mhp1 with 1 NEM label (I_{1NEM}) in the mass spectra. Data are shown as mean \pm SEM of three independent experiments. Adapted from Calabrese et al. (2017).

1.4.4 Mhp1 hydantoin ligands

The transport protein Mhp1 from *Microbacterium liquefaciens* transports 5-substituted hydantoins in a sodium-coupled mechanism across the cell membrane (Suzuki & Henderson 2006, Shimamura et al. 2010). Suzuki & Henderson (2006) have found that Mhp1 mediates primarily the uptake of 5-indolyl-methyl-L-hydantoin (L-IMH) and 5-benzyl-L-hydantoin (L-BH) into *Microbacterium liquefaciens* as part of a metabolic salvage pathway for their conversion to amino acids. Studies of various hydantoin compounds have identified that both the hydantoin-

toin moiety and a 5-substituent group (hydrophobic and aromatic moiety) are necessary for hydantoin-ligand to have an effective binding to Mhp1 with reasonable affinity and uptake (Simmons et al. 2014). This was supported as when either moiety is removed the ligand binding is abolished. Compounds such as purines, allantoin, or cytosine are not recognised by Mhp1 (Suzuki & Henderson 2006, Simmons et al. 2014, Calabrese et al. 2017). This specificity for the more hydrophobic-hydantoin ligands of Mhp1 may be explained by the increased number of favourable hydrogen bonding interactions between the hydantoin moiety and the residues of the ligand binding cavity which is located in the bundle region between the TMH1 and TMH 6 as previously discussed (Figure 1.8).

Table 1.1: Synthesised hydantoin compounds

Hydantoin compounds	Structure
5-benzyl- <i>L</i> -hydantoin (<i>L</i> -BH)	 3
5-indolylmethyl- <i>L</i> -hydantoin (<i>L</i> -IMH)	 6
5-(2-naphthylmethyl)- <i>L</i> -hydantoin (<i>L</i> -NMH)	 9
5-Bromovinylhydantoin (BVH)	 12

Radiolabelled compound uptake assays have identified five hydantoin ligands that bind to Mhp1 with a higher apparent affinity than the *D/L*-IMH (the highest affinity hydantoin com-

pound previously known), while *L*-IMH is the ligand with the highest level of uptake (Jackson 2012, Simmons et al. 2014). The hydantoin compounds that were synthesized in our chemistry laboratory for the purposes of this thesis are the 5-benzyl-*L*-hydantoin (*L*-BH) **3**, and 5-indolylmethyl-*L*-hydantoin (*L*-IMH) **6**, the 5-(2-naphthylmethyl)-*L*-hydantoin (*L*-NMH) **9** and 5-bromovinylhydantoin (BVH) **12** (Section 2.8). These hydantoin ligands were successfully used in co-crystallisation of wild-type Mhp1 (Table 1.2) (Simmons et al. 2014, Polyakova 2015). Crystal structures were solved by X-ray crystallography, giving insights into the Mhp1 ligand binding mechanism. Interestingly, the ligand *L*-NMH bound to Mhp1 in a way that revealed the importance of the thin gate TMH 10 since it works more as inhibitor. The thin gate remain opened after the addition of *L*-NMH, revealing an outward-open conformation with bound ligand, probably due to steric clashes.

1.4.5 Mhp1 solved structures

As it mentioned earlier Mhp1 has been crystallised in three different conformations. Mutations in the key residues for the ligand binding and the sodium binding were also crystallised in complex with various hydantoin compounds (Polyakova 2015). Table 1.2 lists the 3D structures of wild-type Mhp1 and its variants. Most of them were determined at moderate resolutions (3.5 Å) from crystals grown by vapour diffusion.

Table 1.2: Reported crystal structures for Mhp1

Mhp1 variants	Conformational state	Ligand bound	Publication
Wild-type Mhp1			
2JLN	Outward-facing		Weyand et al. (2008)
4D1A	Occluded	<i>L</i> -IMH	Simmons et al. (2014)
4D1B	Occluded	<i>L</i> -BH	Simmons et al. (2014)
4D1C	Occluded	BVH	Simmons et al. (2014)
4D1D	Occluded	<i>L</i> -NMH	Simmons et al. (2014)
2X79	Inward-facing		Shimamura et al. (2010)
Mhp1 mutants			
Gln42Asn	Occluded	<i>L</i> -BH	Polyakova (2015), PhD Thesis
Gln42Asn	Occluded	<i>L</i> -IMH	Polyakova (2015), PhD Thesis
Gln42Asn*	Occluded	<i>L</i> -BH	Polyakova (2015), PhD Thesis
Ser312Ala	Outward-open **	<i>L</i> -NMH	Polyakova (2015), PhD Thesis
Lys110Leu	Occluded	<i>L</i> -BH	Polyakova (2015), PhD Thesis
Lys110Leu	Occluded	<i>L</i> -IMH	Polyakova (2015), PhD Thesis

*Low sodium conditions

** Ser312Ala bound to *L*-NMH has an outward-open form and is not occluded due to the bulky nature of the 5-(2-naphthylmethyl) substituent of the ligand that prevents the occlusion of the TMH 10. *L*-NMH in to Ser312Ala in the same way as it inhibits the wild-type Mhp1 (Simmons et al. 2014). Mhp1 mutant crystal structures have not yet been deposited to the PDB.

1.5 Techniques for structural studies to probe the mechanism of membrane transport proteins

Membrane proteins, and especially membrane transporters, play an important role in biological systems since they are involved in communication and transfers between the inside of living cells and their immediate environment. Various biochemical and biophysical techniques need to be combined with X-ray crystallography and small-angle X-ray scattering in order to study the structure-function relationships and understand their mechanism.

1.5.1 Challenges of structural studies of membrane proteins

The study of membrane proteins is still one of the most challenging targets in structural biology. Structural information of membrane proteins has been difficult to achieve mainly due to their partially hydrophobic surface areas, flexibility and lack of stability. Membrane proteins are embedded in a hydrophobic lipid bilayer in the cell but biochemical and biophysical experiments are carried out in aqueous solution. Membrane proteins need to be extracted from the cell membrane to study them *in vitro*. Thus, a number of difficulties related to membrane protein expression, solubilisation, purification, crystallisation, data collection and structure solution need to be overcome (Carpenter et al. 2008).

Despite the improvements in many of the experimental steps, there are still major bottlenecks in the process. Firstly, is the production of the membrane protein of interest in sufficient quantity. Usually they exist in very low levels in their native hosts thus their overexpression in heterologous systems is required. Many problems can occur, from aggregation (of the protein in the cytoplasm (Drew et al. 2003)) to protein malfunction because of missing important post-translational modifications (Junge et al. 2008) due to the lack of specific machineries in the heterologous hosts (mostly in eukaryotic membrane proteins (Eshaghi et al. 2005, Wagner et al. 2006)). In this case, membrane proteins have to be targeted to the host cell membrane

before they can fold correctly. Specific systems are required in the host cell such as the SRP-Sec61 system that inserts membrane proteins into the endoplasmic reticulum of eukaryotic cells (Schnell & Hebert 2003). Besides this, the design of multiple constructs, test of different expression systems and culture conditions is also required to find the appropriate condition for each membrane protein.

As it mentioned before, integral membrane proteins are not soluble in aqueous buffer due to their hydrophobic surfaces. Therefore, they require an amphipathic molecule, such as a detergent, to mimic the lipid bilayer/membrane and maintain their structural integrity (Privé 2007) and possibly their native states in solution. Membrane proteins are extracted from the host cell membrane using detergents which are surfactants that solubilise membrane lipids and make possible the handling of membrane proteins in a hydrophobic environment. They cover the hydrophobic surface of the protein, allowing solubilisation. Detergents consist of a hydrophilic head group (typically polar, sometimes charged) and a hydrophobic (apolar) tail, which inserts into the membrane. The membrane-embedded proteins are extracted from the membrane when the detergent concentration is above its critical micelle concentration (CMC) and water soluble, spherical micelles can be formed (Lee 2005, Privé 2007).

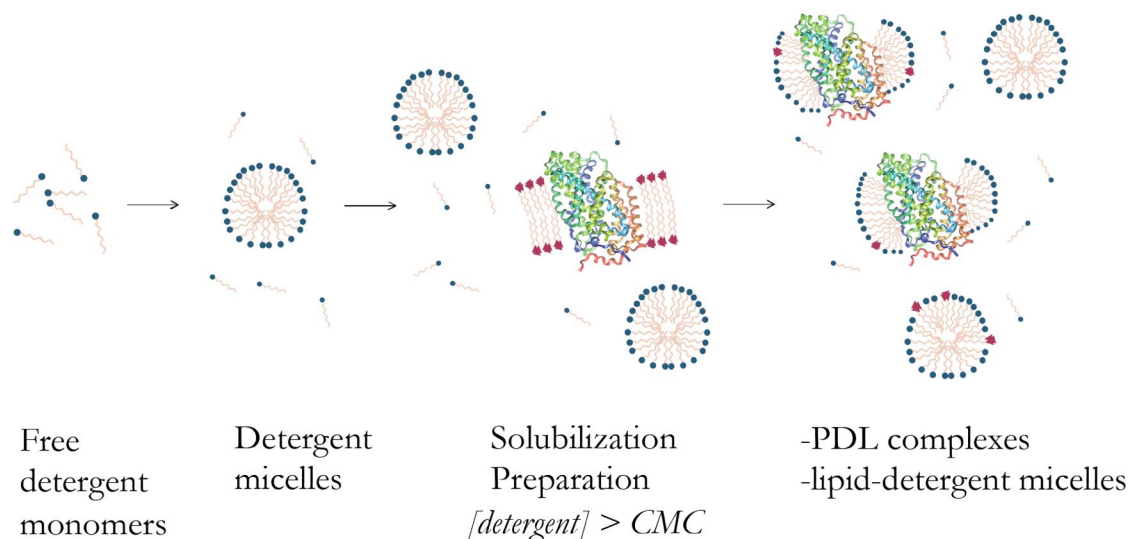


Figure 1.14: Solubilisation of membrane proteins using detergent. CMC is the critical micelle concentration where detergent monomers selfassociate to form micelles. Adapted from Newby et al. (2009).

This results in the formation of a protein detergent complex (PDC) and the protein's hydrophobic surface, which is normally buried within the core of the membrane bilayer, is coated by the detergents and protected (le Maire et al. 2000, Lee 2005, Garavito & Ferguson-Miller 2001). The choice of detergent is a crucial part of the purification process (Lee 2005). Series of detergents are tested to examine the one that extracts the largest quantity of soluble, active, homogeneous, stable protein (Iwata 2003). The stability of the protein-detergent complex is vital for functional studies, spectroscopic analysis and crystallisation trials of the membrane proteins (Rosenbusch 2001).

Subsequently, purified protein can be exchanged into a variety of different detergents for crystallisation trials (Iwata 2003). Detergent exchange can be done with various methods in order to remove the excess detergent once proteins are solubilised, or to transfer the membrane protein into a different detergent more suitable for crystallisation (Seddon et al. 2004). For detergents with high CMC and small molecular weight micelles dialysis or size-exclusion chromatography are efficient ways of detergent removal or exchange in detergent concentrations less than their CMC concentration due to their small molecular weight. Dialysis and size exclusion chromatography are effective when the detergent concentration used is less than the CMC, so micelles are not likely to form but instead the detergent remains monomeric. Size-exclusion chromatography also provides a polishing purification step due to separation of protein-detergent complex, detergent-lipids and micelles due to their different size. However, dialysis is less suited for non-ionic detergents due to the long time needed for the removal and size-exclusion chromatography is limited by sample volume.

1.5.2 Crystallisation of integrate membrane proteins (IMPs)

Protein crystallisation still remains the main bottleneck in the process of obtaining structural information near atomic resolution by X-ray crystallography. The growing of 3D crystals suitable for X-ray crystallography is a highly demanding technique in terms of protein preparation and protein quality prior to any crystallisation attempt. Critical requirements of the protein

preparation are the high purity (free from contaminants) protein, a homogenous protein sample (avoiding aggregates) and a protein thermally stable in solution (Bergfors 1999, McPherson 1999).

Crystallisation of membrane proteins is especially challenging due their hydrophobic nature. Protein crystallisation is a phase transition phenomenon where a protein solution is brought to a supersaturation state (Ataka 1993, McPherson 1999, Ducruix & Giegé 1999) where the protein reaches a concentration that exceeds its solubility limit while still remaining in solution. There are different methods to crystallise integrated membrane proteins which can be divided in two categories: *in surfo* methods and *in meso* methods.

- **Membrane protein crystallisation using in surfo methods**

The crystallisation *in surfo* method is a common and quite successful method for crystallisation of membrane proteins. In this case, the detergent-solubilised membrane protein is manipulated as a soluble protein and is crystallised using the more traditional protein crystallisation methods of vapour diffusion (Sutton & Sohi 1994, Delmar et al. 2015), microbatch (Chayen 1998, Loll et al. 2003), dialysis (Iwata 2003) and counter diffusion or free-interface diffusion (Segelke 2005).

The protein crystallisation process can be illustrated using a phase diagram (Figure 1.15). This diagram is divided sharply into the undersaturation, and supersaturation regions by the solubility curve (line denoting maximum solubility at specific protein and precipitant concentrations), which represents the equilibrium between the solid phase and the free-molecule (liquid) phase. The undersaturation zone is below the solubility curve where the protein is fully dissolved and will never crystallise. The supersaturation region is further divided into: metastable, nucleation (or labile), and precipitation zones. In the metastable zone nuclei, that have been formed in the nucleation zone, will grow to crystals but no further nucleation takes place (García-Ruiz 2003). In the nucleation (or labile) zone spontaneous nucleation will take

place and crystals start forming. At very high supersaturation, the precipitation zone, protein amorphously precipitates. In the phase diagram (Figure 1.15) the arrows display how the protein and precipitant concentrations are varying in each of the crystallisation methods. By varying the concentration of precipitant, protein, additives and manipulating various parameters that include temperature, pH and ionic strength protein association is facilitated and eventually crystals are obtained (McPherson et al. 2011).

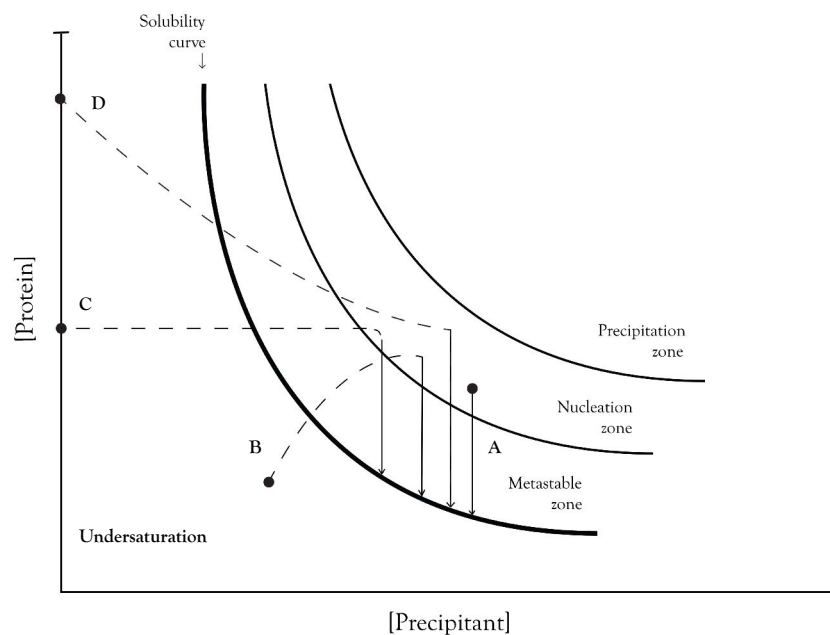


Figure 1.15: Schematic representation of phase diagram for the crystallisation of macromolecules based on two of the most commonly varied parameters protein and precipitant concentrations. The solubility curve is depicted by a solid line dividing the undersaturation and saturation regions. The four major crystallisation methods are highlighted on the picture showing that in order to produce crystals, all the systems need to reach the nucleation zone, after which they make their way through the metastable zone and eventually arrive at the solubility curve. Each method achieves this journey via a different route. \circ represents the starting conditions. In the case of dialysis and free-interface diffusion two alternative starting points are shown since the undersaturated protein solution can contain solely protein or alternatively, protein with a low concentration of the precipitating agents. (A) Batch crystallisation. (B) Vapor diffusion. (C) Dialysis. (D) Free-interface diffusion (also known as liquid/liquid diffusion) (Adapted from Chayen (1998), Bergfors (2003)).

The most widely used method is the *vapour-diffusion* technique. Protein solution is mixed with reservoir solution in a droplet, in a hanging-drop or sitting-drop configuration. This droplet is suspended over the reservoir solution in a sealed chamber for equilibration. The droplet con-

tains a lower concentration of precipitant than the reservoir solution, so water vapour diffuses out of the drop until the osmolarity of the drop and precipitant are equal (until equal vapour pressures are obtained). This dehydration of the droplet causes a slow concentration of both the protein and precipitant leading to supersaturation of the protein solution and leading the protein ideally to nucleate. Droplet-to-reservoir distance affects the equilibrium rate and crystallisation process.

The *dialysis* technique involves dialysing the protein solution against crystallisation-precipitant solution using a semi-permeable membrane. The protein concentration remains constant in the dialysis vessel, while the semi-permeable membrane allows small molecules and crystallisation reagents to pass. Protein crystallisation takes place due to this diffusion of the precipitant solution out of, or into the sample. However, formed crystals are difficult to assess once they grow.

In the *micro-batch* technique the protein solution and the precipitant solution are mixed at their final concentration, bringing the system into the supersaturation region at a fixed rate, and sealed under a layer of parafilm oil to prevent evaporation. It is an easy set up where many conditions and a wide range of ratios can be used. The equilibration rate and the crystallisation process are also affected by the droplet:reservoir volume ratios, temperature and precipitating agents (Forsythe et al. 2002).

Convection-free crystallisation or counter diffusion, is a crystallisation technique that has been shown to promote the growth of well-ordered crystals (Vergara et al. 2005) since it minimises supersaturation and impurity levels (Ng et al. 2003). The protein and the precipitant solution are placed at opposite ends of a convection-free environment (capillaries, gels or viscous materials and/or under microgravity). Solutions are allowed to diffuse one against each other (Garcia-Ruiz 2003, Ng et al. 2003) creating a supersaturation gradient.

- **Membrane protein crystallisation in meso methods**

An alternative method of membrane protein crystallisation, the *in meso* method, can be used to obtain crystals by reconstituting the detergent-solubilised-protein into a lipidic environment, mimicking the protein's native environment. This can be achieved using lipidic cubic phase, LCP, (Cherezov et al. 2006, Caffrey 2009), lipidic sponge phases, LSP, (Landau & Rosenbusch 1996, Wöhri et al. 2008, Wadsten et al. 2006) or bicelles (Faham & Bowie 2002), instead of detergent micelles as a medium for crystal growth (Katona et al. 2003, Cherezov et al. 2006). This bicontinuous lipidic mesophase is a stabilising and organizing lipid bilayer reservoir that works as a prelude to crystallogenesis (Caffrey 2008, Caffrey & Porter 2010, Caffrey 2009).

In both LCP and LSP phases the membrane proteins can freely diffuse in the lipid bilayer and concentrate to form nuclei instead of being enclosed in detergent micelles. More specifically, lipidic cubic phase (LCP) is a complex 3D- network of bicontinuous lipid bilayer and two separated water channels. It is formed by continuous/vigorous mixing of specific lipid-like molecules and the detergent-solubilised protein (in aqueous buffer) at a certain ratio and temperature prior to crystallisation trials. LCP provides the advantage that protein-protein interactions are not only through soluble protein domains and loops but also through the trans-membrane segments. This method produces crystals with high diffraction quality but the main drawback still remains the harvesting step. The crystals often diffract to a higher resolution compare to the crystals produced by the *in surfo* methods due to different crystal packing (Figure 1.16). The drawback of this crystallisation technique is the ratio of lipids-proteins, the lipid mixture handling and the crystal harvesting.

1.5.3 Crystal lattice organisation of membrane proteins

Membrane protein crystals can be classified into three types according to how they are formed: 2D crystals, 3D crystals type I and 3D crystals type II (Michel 1983). 2D crystals are mainly used in electron microscopy and are not suitable for X-ray crystallography studies. They are

considered to be formed from reconstitution of biomembranes where hydrophobic interactions are formed between detergents and lipids. All the membrane protein X-ray structures that have been solved up to date are from 3D crystals in Type I or II crystal lattices.

Crystal lattice Type I 3D membrane protein crystals are mainly created during crystallisation *in meso* (in lipidic cubic phase (LCP) or related systems) (Qutub et al. 2004, Caffrey et al. 2012). The crystal contacts are create mostly by polar interactions and hydrophobic interactions. Membrane proteins and lipids are self-assembled in a way similar to the lipid bilayer (Figure 1.16 a) and protein–detergent–lipid hydrophobic interactions are formed.

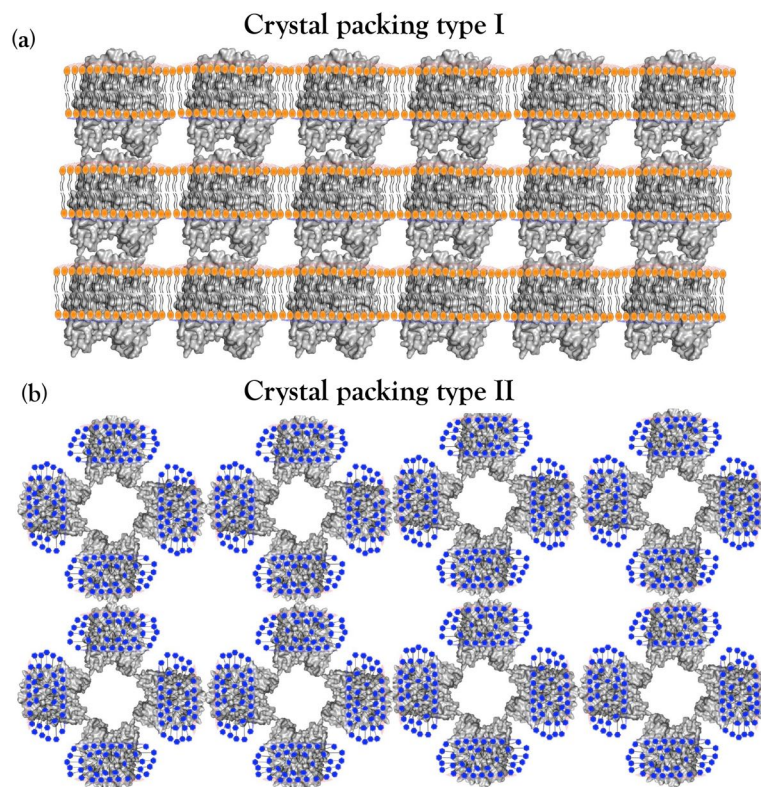


Figure 1.16: Crystal lattice packing of membrane proteins. (a) **Crystal packing Type I:** (*in meso*) The membrane protein molecules and lipid molecules are assembled as in a biological membrane. Lipid-protein and protein–protein interactions are formed to make the crystals. (b) **Crystal packing Type II:** (*in surf*) Crystals are formed by polar protein-protein interactions of the hydrophilic protein regions while their hydrophobic surface is covered by the detergent micelle (represented here by blue dots). Large solvent channels are usually created in this type of packing. Adapted from Birch et al. (2018).

Crystallisation *in surf* usually generates crystal lattice Type II (Figure 1.16) (Michel 1983, Qutub et al. 2004). The crystal contacts are made only by the extracellular, polar regions of the

proteins (Michel 2018), while the the hydrophobic surface of the membrane proteins is covered by the detergent micelle. In this crystal packing type, the detergent or other surfactant belt surrounds the membrane protein and the exposed regions of the protein are rather limited therefore the intermolecular protein-protein contacts are reduced. This results in extremely fragile crystals with large solvent content (Carpenter et al. 2008). Therefore, when crystallising *in surfo*, the choice of detergent is particularly important as the shape and size of the detergent micelle play a vital role in crystal formation since detergents with small micelles hardly cover the hydrophobic surface of the protein leading to protein aggregation, and with large micelles usually tend to cover the entire protein.

1.5.4 Circular dichroism to assess structural integrity of Mhp1

Circular dichroism (CD) spectroscopy is a well-established biophysical tool for the structural characterisation of biopolymers such as proteins and nucleic acids in the Far-UV region from 180-260 nm. Circular dichroism is the difference between the absorption of left- and right-handed circularly polarised light by chiral molecules. It can be used to study the different secondary structural elements/types (alpha helix, parallel and antiparallel beta sheet, turn, and other) of soluble as well as membrane proteins (Wallace et al. 2003, Miles & Wallace 2016, Kelly et al. 2005) as it produces characteristic spectra.

Soluble proteins with predominantly α -helical structures have maximum peaks around 193 nm and minima at 208 nm and 222 nm. However, for membrane proteins the maxima and minima are shifted (Wallace & Janes 2003, Miles & Wallace 2016). This shifted maxima is a typical behaviour of membrane proteins since they do not form uniform isotropic solutions in aqueous environments as soluble proteins do because the protein-detergent complexes are large hydrophobic, anisotropic particles (Bulheller et al. 2007) (Figure 1.17).

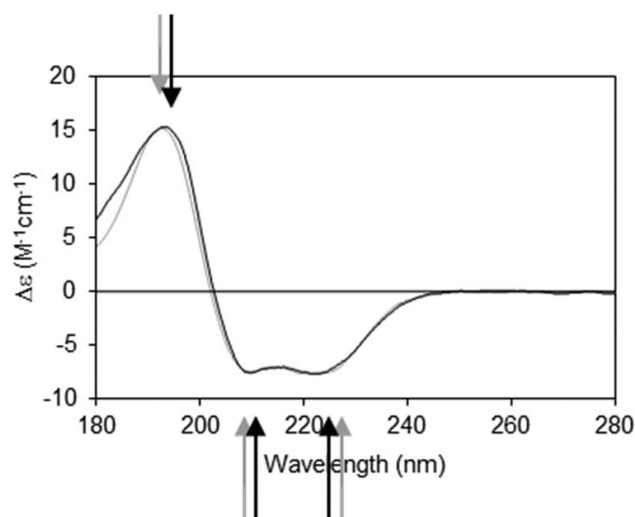


Figure 1.17: Demonstration of shifts observed in membrane protein circular dichroism spectra with respect to the soluble protein spectra. Demonstration of spectra shifts observed in membrane protein spectra relevant to the soluble protein spectra of predominately α helical proteins. Membrane proteins black line and soluble in grey line. Adapted from Miles & Wallace (2016).

The CD spectrum is a good indicator for the folded status of the protein, but the magnitude of the CD signal does not correlate with the stability. To assess this, the changes in the ellipticity of the signal when the secondary structures are denatured, for instance by heating, changing the pH or adding denaturation agents such as urea, must be monitored. The changes in CD as a function of temperature, at characteristic wavelengths, can be used to determine the thermodynamics of unfolding (or more precisely change of state), the midpoint of the unfolding transition (T_m), and the free energy (ΔG) of folding. In addition, analysis of CD spectra obtained as a function of temperature may also be useful in determining whether a protein has unfolding or folding intermediates (Greenfield 2006).

1.5.5 Spectrophotofluorimetry to probe ligand binding behaviour to membrane transport protein Mhp1

Tryptophan residues have an intrinsic fluorescence that is highly sensitive to the environment (Chen & Barkley 1998). As a natural fluorophore tryptophan can be excited at 280-300 nm

and emits light maximally at 330-345 nm. To avoid simultaneous excitation of tyrosine residues at 280 nm, it is preferable to excite tryptophan specifically at 295 nm. When tryptophan residues are located in the ligand binding cavity and are proposed to be involved in the ligand binding, a convenient way to assess ligand binding is by monitoring the change in tryptophan fluorescence upon the binding. The interaction of the ligand with the tryptophan residue in the binding cavity results in a decrease of the fluorescence intensity signal at 330-345 nm known as "quenching". By titrating the ligand against the fluorescence signal an apparent dissociation constant (K_d) is obtained and the fluorescence change can be observed on a millisecond timescale (Ivanova et al., 2012, Walmsley, 2000).

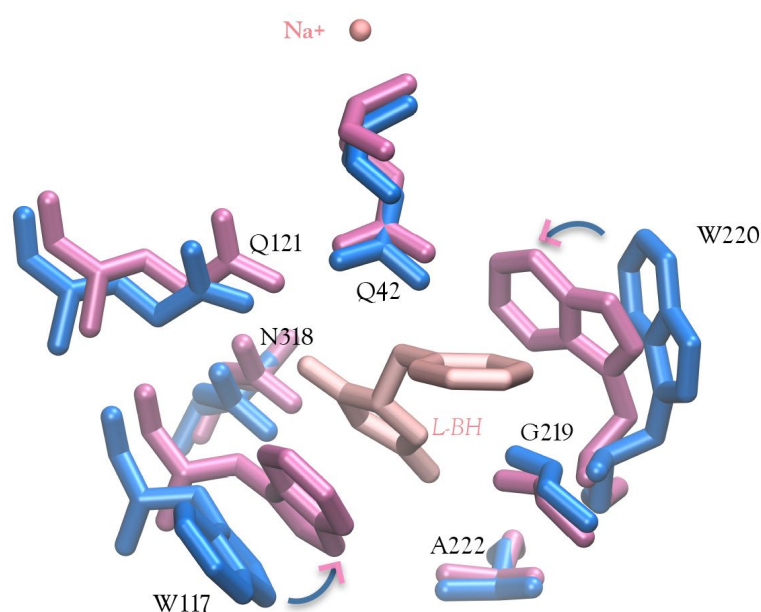


Figure 1.18: Superimposition of the wild-type Mhp1 ligand binding sites in the outward-facing (blue, PDB code 2JLN) and outward-occluded (magenta, PDB code 4D1B) crystal structures in the ligand binding site. Re-orientation and structural rearrangements of the residues involved in ligand binding. Residues are displayed as sticks representations while L-BH ligand and Na⁺ are in ball and stick representation (coloured light pink). The Trp117 and Trp220 specifically are moving towards the ligand. Picture was prepared by VMD (Humphrey et al. 1996) and rendered using Tachyon (Stone 1998).

In the ligand binding site of Mhp1 two tryptophan residues are involved in the ligand binding site according to previously published structures. The transition of Mhp1 from the outward-open to the occluded structure demands the re-orientation of Trp117 and Trp220 (Figure 1.18) that form π -stacking interactions with different moieties of the bound ligand.

More specifically, according to the crystal structures previously solved the indole ring of Trp117 forms π -stacking interactions with the hydantoin moiety of *L*-BH PDB code 4D1B, (Weyand et al. 2008) and face-to-face π -stacking interactions with the hydantoin moiety of the *L*-IMH PDB code 4D1A (Simmons et al. 2014), while the indole ring of Trp220 forms π -stacking interactions with the benzyl ring of the *L*-BH PDB code 4D1B, (Weyand et al. 2008) and π -stacking interactions with the indole ring of *L*-IMH PDB code 4D1A (Simmons et al. 2014). Thus, explicit changes in the tryptophan environment are involved in the binding, allowing to monitor the structural and kinetic changes.

Quenching of tryptophan fluorescence techniques has been already used for analysis of ligand binding kinetics in other transporter membrane protein members of the LeuT superfamily such as vSGLT (Veenstra et al. 2002), CaiT (Jung et al. 2002, Schulze et al. 2010), BetP (Ge et al., 2011), Mhp1 (Weyand et al. 2008, Simmons et al. 2014), as well as in members of the MFS superfamily such as GalP (Walmsley et al. 1994, Martin et al. 1995, Sukumar 2012), LacY (Smirnova et al. 2008, 2012) and GlpT (Auer et al. 2001). *L*-BH was selected among the four hydantoin substrates (Section 2.8) because of its low absorbance or fluorescence at wavelengths used (Jackson 2012) .

It is of great importance to distinguish ligand binding from ligand transport in the membrane transport protein analysis. (Smirnova et al. 2008), (Ivanova unpublished) have shown that ligand binding to membrane proteins (fluorescence spectroscopy experiments) occurs on the millisecond time scale. However, the ligand accumulation into cells (cell uptake assays) or proteoliposomes needs approximately five minutes to reach a plateau (Singh et al. 2008, Fang et al. 2009, Ma et al. 2012).

1.5.6 Small angle X-ray scattering (SAXS)

Small angle X-ray scattering (SAXS) has been used to gain structural information of the dynamics and to characterise the Mhp1 in solution without any restrictions imposed by the crystal

lattice. SAXS is a powerful biophysical method to study the overall shape, size of a biomolecule and oligomeric state (Kikhney & Svergun 2015). In the case of membrane proteins SAXS experiments have been used to obtain structural information about the overall shape of the protein-detergent complex (PDC) and the detergent organization around the purified protein. The basic parameters that SAXS can reveal are the radius of gyration, R_g , (measure for the overall size of the macromolecule), and the maximum intra-particle distance, D_{max} , (represents the maximum size of a particle).

The main challenge in SAXS experiments of membrane proteins is an accurate buffer subtraction due to the high concentration of detergent crucial for protein solubilisation. The protein-detergent solution consists of the protein-detergent complex (PDC), empty micelles, and free detergent monomers. A size-exclusion chromatography column prior to the SAXS collection (SEC-SAXS) (Berthaud et al. 2012) has been used to overcome the problem of inaccurate buffer subtraction, where during the run the PDC complex is separated from the detergent monomers and free-micelles (Figure 1.19), which produce strong and characteristic scattering patterns (Lipfert et al. 2007, Oliver et al. 2013).

At the beginning of a SEC-SAXS run the first buffer scans are averaged and can be used as buffer blank for the PDC peak later in the same run. The combination of size exclusion chromatography (SEC) with SAXS and with static light scattering (SLS) is an accurate and reliable methods, to determine molar mass, characterise the protein-detergent complex (PDC), and monitor oligomerisation/aggregation state in solution prior to crystallisation experiments as well as to evaluate protein integrity and stability.

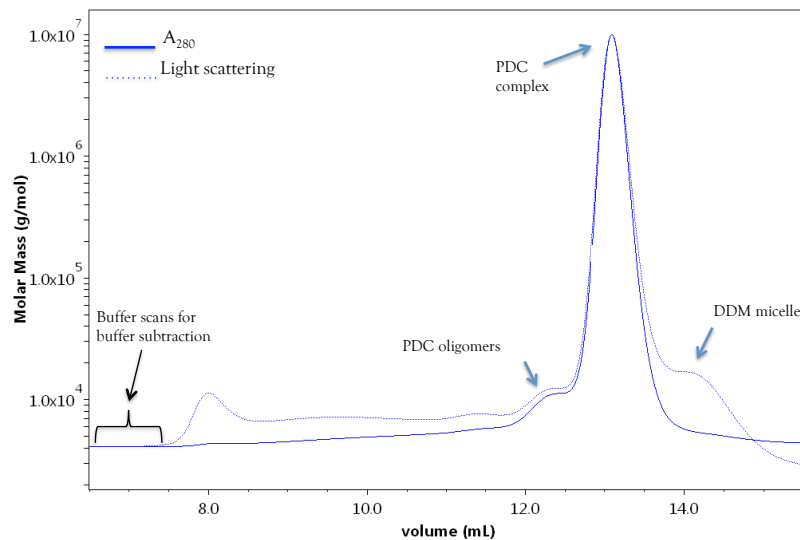


Figure 1.19: Schematic representation of a size-exclusion chromatography run coupled with light scattering. Size-exclusion profile of the wild-type Mhp1 in DDM (WT-DDM) prior to SEC-SAXS experiments. The absorbance (blue line) is combined with the static light scattering (blue dash line) indicating that by SEC run the PDC complex is separated from excess free micelles.

1.5.7 Macromolecular crystallography

X-ray protein crystallography is the ultimate experiment to elucidate the 3D structural information of the biological systems in near atomic resolution. However, there are many challenges to overcome for a successful determination of a protein structure and even more for a membrane protein structure.

The first challenge to overcome is the production of a well-diffracting protein crystal. The native environment of protein is in a solution (cytosol, extracellular environment) or a fluid assembly (cell membrane) and not an ordered solid crystal. In case of membrane proteins (MP), the MP must order itself into a periodically repeating arrangement (3D crystal) despite the detergent molecules that are bound around its hydrophobic regions (1.5.2). In addition, crystals need to survive the radiation damage caused by X-rays (Garman 2003). Cryo-cooling conditions can be used to prevent decay of the crystals but it is difficult to predict or identify the best.

Regarding the fact that crystalline phase is not the native environment of the protein, in case of conformational changes questions are arising. Does the protein adopt the same structure conformation in solution as in crystal, or it is an effect of the crystal packing? While structures can give a very informative snapshot of the dynamic process in combination with functional assays and complimentary studies is needed to fully characterise the system.

1.6 Project aims

The current doctoral work aims to provide functional and structural insights into the transportation alternating access mechanism of the secondary active membrane transporter Mhp1, the membrane hydantoin permease-1, from *Microbacterium liquefaciens* of the nucleobase-cation symporter family (NCS-1). The initial aim was the production and the functional and structural characterisation of single point mutations of key residues ready for crystallographic studies following functional studies (Chapter 3). In addition, size-exclusion coupled small-angle X-ray scattering was employed to probe conformational homogeneity of Mhp1 to study the different functional behaviour and crystallisability in various detergents as well as to understand the ligand binding in presence and absence of sodium for wild-type Mhp1 and its mutants (Chapter 4). A second membrane transporter LeuT from *Aquifex aeolicus* will also studied in Chapter 5. Production and crystallisation attempts of the wild-type LeuT and of a new triple mutant are described.

Chapter 2

Materials and Methods

2.1 Source of Materials

Antibiotics	
Ampicillin	Sigma-Aldrich, DE
Bacterial growth media	
Glycerol	ROTH
CaCl ₂ ·2H ₂ O	Sigma-Aldrich
MgSO ₄	Sigma-Aldrich, DE
MgCl ₂	Sigma-Aldrich, DE
IPTG (Isopropyl- β -D-1-thiogalactopyranoside)	Melford laboratories
Microagar	Melford laboratories
Tryptone	Melford laboratories
Yeast extract	Melford laboratories
Filters and membranes	
Cellulose nitrate membrane filters (0.22 μ m)	Whatman International Ltd
Nitrocellulose membrane filters type GTSF (0.22 μ m)	Millipore Ltd., UK
Millex GP filter unit PES membrane (0.22 μ m)	Millipore Ltd., UK
Protein molecular weight standards	
Sigma Marker TM low range, mol wt 6.5-66 kDa, (M3913)	Sigma-Aldrich, DE
Amersham Rainbow High range marker 12-225 kDa, (RPN756E)	Healthcare, GE

Color prestained protein standard, Broad range 11-245 kDa, (NEB No.P7712)	New England Biolabs
PageRuler prestained Protein ladder	Thermoscientific
BenchMark His-tagged Protein Standard	ThermoFischer Scientific
Recombinant DNA technology	
1kb DNA ladder	Invitrogen Ltd, UK
dNTPs	Invitrogen Ltd, UK
Lambda DNA EcoRI and HindIII markers	Promega Ltd., UK
DNA SYBR safe (Invitrogen, USA)	EMD Biosciences, Inc. Novagen Brand, USA
<i>E. coli</i> BL21 (DE3) cells	EMD Biosciences, Inc. Novagen Brand, USA
XL10-Gold ultracompetent cells	Stratagene, USA
Oligonucleotide primers	Eurofins MWG Ltd, UK
DpnI restriction enzyme and buffer 4	New England Biolabs Ltd, U
QIAprep spin miniprep kit	QIAGEN Ltd., UK
Protein Purification Mhp1	
Nickel-nitriloacetic acid (Ni-NTA) resin	QIAGEN Ltd., UK.
HisTrap, FF histidine-tagged, 5 ml (Ni-NTA) affinity column	Healthcare, GE
n-dodecyl-beta-D-maltoside (DDM)	Anatrace
Econo-pac 10DG desalting column	BioRad laboratories, UK
HiTrap TM 5 ml, desalting column	GE Healthcare
Vivaspin 20 and Vivaspin 6 100,000 MWCO tubes	Amicon, GE Healthcare
Protein Purification LeuT	
TALON metal affinity resin (cobalt)	Clontech
Econo-Pac empty chromatography columns 1.5x12 cm 14 cm	Bio-Rad
Chemically competent bacterial cells C41 (DE3)	Lucigen
HiTrap TALON crude column (1 ml)	Healthcare GE
Amicon Ultra-15 centrifugal devices 50kDa MWCO	Millipore
Zeba TM Spin Desalting Columns, 40K MWCO, 10 mL Thermo	Fischer Scientific
Membrane dialysis tubing 7000 cutoff	SERVA
C-Crown-15	ROTH
SDS-PAGE immunoblotting chemiluminiscence	
2% bis-acrylamide, 40% acrylamide	BioRad laboratories, UK
Acetic acid	Fisher Scientific, DE

Ammonium persulphate	Sigma-Aldrich, DE
Bovine serum albumin (BSA)	Sigma-Aldrich, DE
Brilliant blue R	Sigma-Aldrich, DE
Bromophenol blue	Sigma-Aldrich, DE
Glycine	ROTH
Potassium chloride (KCl)	ROTH
β -mercaptoethanol	Sigma-Aldrich, DE
Methanol	Sigma-Aldrich, DE
TEMED	Sigma-Aldrich, DE
TRIS	ROTH
Triton-X-100	Sigma-Aldrich, DE
Tween 20	Sigma-Aldrich, DE
Sodium dodecyl sulphate (SDS)	ROTH
SuperSignal west Pico chemiluminescent substrate	Fisher Thermo Science Pierce Ltd., DE
HisProbe HRP	Fisher Thermo Science Pierce Ltd., DE
Immobilion Transfer Membrane: PVDF membrane 0.45 μ m	Immobilon Millipore

Protein concentration assay

Bovine serum albumin (BSA)	Life Science
Sodium hydroxide (NaOH)	Acros Organics
Naphthol blue black	Sigma-Aldrich, DE
Trichloroacetate (TCA)	Sigma-Aldrich, DE
Tris base ultrapure (TRIS base)	ROTH
Ethanol	Fisher Scientific Ltd., UK
Methanol	Fisher Scientific Ltd., UK
Glacial acetic acid	Fisher Scientific Ltd., UK

Spectrophotofluorimetry

Choline chloride	Sigma-Aldrich, DE
Dimethyl sulfoxide (DMSO)	Fischer Scientific

Cross-linking for LeuT

N-Ethylmaleimide	Sigma-Aldrich, DE
1,10 phenanthroline	Alfa-Aesar
Copper (II) Sulfate	ROTH
Copper Chloride	Alfa-Aesar
1,4-Dithiothreitol (DTT)	ROTH
Sodium Chloride (NaCl)	Fisher Scientific
n-dodecyl-beta-D-maltoside (DDM)	Anatrace

Crystallisation and crystal handling	
Na ₂ HPO ₄	Fisher Scientific
NaH ₂ PO ₄	Fisher Scientific
K ₂ HPO ₄	Fisher Scientific
KH ₂ PO ₄	Fisher Scientific
PEG ₄₀₀	Fluka Analytical
MES monohydrate	ROTH
18-crown-6	Sigma-Aldich, DE
PEG ₅₅₀ MME	JBS Screen single stock, Jena Biosciences
24 well crystallisation plates, hanging drop	CELLSTAR Greiner-Bio-One
96 well crystallisation plates, sitting x 2 drops	Swissci, TTPLabtech (4150-05823)
Cover slips 18 mm	ROTH
Mounted LithoLoops	Molecular Dimensions Limited
GE Bayer Silicone Grease	Jena Biosciences
Size exclusion chromatography	
Superdex 200 Increase 3.2/300 2.4 ml	GE
BioSEC-3 100 Å	Agilent technologies
Synthesis of hydantoin compounds/Mhp1 ligands	
Hydantoin	TCI
3-Bromobenzaldehyde	TCI
Ethanolamine	TCI
N-(tert-Butoxycarbonyl)3-(2-naphthyl)-L-alanine	TCI
Trifluoroacetic acid (TFA)	TCI
Dichloromethane (DCM)	TCI
Potassium cyanate (KOCN)	TCI
Phosphorus pentoxide P ₂ O ₅	TCI
TLC plates	Macherey-Nagel
UV irradiation	A.Krüss Optronik
L-tryptophan	TCI
L-phenylalanine	TCI
Ethyl acetate	TCI

Table 2.1: Source of materials for Mhp1 and LeuT.

2.2 Mhp1 protein purification and crystallisation of wild-type and mutants

2.2.1 Expression and inner membrane preparations for Mhp1

Wild-type Mhp1 and its mutants, both His₆-tagged, were over-expressed in 30 or 100 L fermentations of BL21 (DE3) *Escherichia coli* cells (NovagenTM). Inner membrane preparations were made and stored at -80° C, by our collaborator Mr David Sharples (University of Leeds) as previously described (Jackson 2012). The cell stocks were previously prepared by Dr. Scott Jackson (Jackson 2012).

2.2.2 Protein purification of Mhp1

Frozen aliquots of inner membrane preparations were thawed and resuspended to a final protein concentration of 1-3 mg/ml (Protein concentration assay Section 2.5.1) in a DDM solubilisation buffer (20 mM Tris-HCl pH 8.0, 20 mM imidazole pH 8.0, 300 mM NaCl, 20% (v/v) glycerol, 1% (w/v) n-dodecyl- β -D-maltopyranoside (DDM) detergent) and mixed on a rotatory mixer for 4 hours at 4° C. Soluble membranes fractions were separated from insoluble membranes by centrifugation at 100,000 \times g for 1 hour using a Ti-75 rotor (Beckman Coulter) in an Optima XPN-90 ultracentrifuge (Beckman Coulter) at 4° C.

The supernatant was loaded onto a Ni-NTA affinity column (HisTrap, FF histidine-tagged, 5 ml, GE) pre-equilibrated in DDM wash buffer (10 mM Tris-HCl pH 8.0, 20 mM imidazole pH 8.0, 10% (v/v) glycerol, 0.1% (w/v) DDM detergent) for 16 hours at 4° C, using a peristaltic pump at low speed to achieve gentle binding. The column was washed with 10 column volumes (CV) of the DDM wash buffer to remove any unbound contaminants. A second extensive, and crucial for crystallisation, washing step using 20 CV NM wash buffer (10 mM Tris-HCl pH 8.0, 20 mM imidazole pH 8.0, 10% (v/v) glycerol, 0.7% (w/v) n-nonyl- β -D-maltopyranoside (NM)

detergent) was performed to exchange the DDM detergent. The bound His₆-tagged Mhp1 protein was eluted using 5 CVs of NM elution buffer (10 mM Tris-HCl pH 8.0, 300 mM imidazole pH 8.0, 5% (v/v) glycerol, 0.7% (w/v) NM detergent). The eluted fractions were collected and concentrated up to 1.5 ml using a Vivaspin 20 spin concentrator with a molecular weight cut off (MWCO) of 100 kDa at 3000×g for 40 minutes to 120 minutes.

The concentrated protein was applied to a desalting column (HiTrapTM 5 ml, GE) pre-equilibrated with NM desalting buffer (10 mM Tris-HCl pH 8.0, 2.5% (v/v) glycerol, 0.5% (w/v) NM) to remove the excess imidazole. Protein was eluted using 2 ml of NM desalting buffer and concentrated to 10 mg/ml in a Viva Spin 6 MWCO 100 kDa concentrator. Concentrated protein was separated into 25 µl aliquots and flash-cooled in liquid nitrogen for storage at -80° C. All purification steps were performed at 4° C.

Table 2.2: Detergent concentrations during the Mhp1 purification.

Detergent Name	Solubilisation	Wash buffer 1*	Wash buffer 2**	Elution buffer	Desalting buffer
DDM	1% w/v	0.1% w/v	0.05% w/v	0.05% w/v	0.05% w/v
	19 mM	1.9 mM	0.95 mM	0.95 mM	0.425 mM
NM			0.7% w/v	0.7% w/v	0.5% w/v
			14 mM	14 mM	10 mM
	10xCMC	2.5 x CMC	2.5 x CMC	2.5 x CMC	1.8 x CMC

* Wash buffer 1 used the same detergent as the solubilisation

**Wash buffer 2 for exchange to NM detergent

During this thesis solubilisation happened only on DDM

2.2.3 Protein purification of Mhp1 in absence of sodium

Mhp1 variants were also purified in complete absence of sodium. Sodium was substituted with potassium from the first step of solubilisation the membrane preparations all the way

to desalting step and following crystallisation trials. Buffers were prepared and their pH was adjusting potassium bases instead of sodium (Buffer Tris-KOH pH8, KCl).

2.2.4 Initial crystallisation of Mhp1

Freshly purified wild-type Mhp1 in NM desalting buffer, (Section 2.2.2), was equilibrated against 100 mM sodium phosphate pH 7.0, 27-35% PEG₃₀₀ and 50 - 200 mM NaCl in a 1:1 ratio using the vapour diffusion hanging drop crystallisation technique. Needle-shaped crystals appeared over-night and continued to grow for at least three months. Crystal formation benefited from the use of a streaking method developed by Dr. Anna Polyakova (Polyakova 2015) to gradually mix mother liquor into the protein drop (further described in 4.4.3).

2.2.5 Co-crystallisation of Mhp1 with hydantoin ligands

Mhp1 hydantoin ligands (*L*-BH, *L*-IMH, *L*-NMH and BVH) were synthesised (Section 2.8) for co-crystallisation (Simmons et al. 2014). The ligands *L*-BH, *L*-IMH and *L*-NMH were dissolved in 100% PEG₃₀₀ and combined with mother liquor to a final concentration of 2-5 mM. For co-crystallisation of Mhp1 with BVH, a stock solution of BVH in 100% PEG₃₀₀ was prepared. 5 mM of stock BVH was added to the protein solution prior to the mixture with the mother liquor.

2.2.6 High-throughput crystallisation techniques

Crystallisation trials using a membrane commercial screen were carried out with freshly prepared protein at the EMBL-SPC facility. Sitting drops were set with the nanolitre dispensing robot TTPLabtech (4150-05823) MOSQUITO on Swissci crystallisation trays.

2.3 Protein production and crystallisation of wild-type LeuT from *Aquifex aerolicus*

2.3.1 Protein expression of wild-type LeuT

Wild-type LeuT and mutant (His₈-tagged LeuT) were produced in *E. coli* C41 cells and over-expressed by collaborators Dr Azmat Sohail and Jawad Khan at the Medical University of Vienna as previously described (Sohail et al. 2016). For each batch of protein purification, a pET16b plasmid harbouring LeuT cDNA was freshly transformed into chemically competent *E. coli* C41 (DE3) cells from Lucigen. The wild-type LeuT gene was cloned into a pET16b vector, to give wild-type LeuT with a thrombin cleavable C-terminal His₈-tag. The transformed cells were inoculated in Luria-Bertani (LB) medium (10% (w/v) NaCl, 5% (w/v) yeast extract, 10% (w/v) peptone) supplemented with 0.1 mg/ml ampicillin. Once the inoculum reached an optical density at 600 nm (OD 600) of 0.6, cells were induced with 0.2 mM IPTG for 20 hours at 20° C.

2.3.2 Membrane preparations of wild-type LeuT

Overexpressed cells were re-suspended in lysis buffer (20 mM Hepes pH 7.5, 200 mM NaCl, 1 mM EDTA, 5 mM MgCl₂, 20 µg/ml DNase-1 supplemented with 1 mM PMSF and 0.4 mg/ml Lysozyme) and were incubated for 90 minutes at 4° C. Cell lysis was then performed twice on ice using an Avestin EmulsiFlex-05 under a pressure of 15,000-12,000 psi. Unlysed cells were pelleted by centrifugation at 5000×g for 15 minutes at 4° C using a Sorvall RC6+ and F14-6x rotor (Thermo-Scientific). Crude membrane fractions were pelleted by high-speed centrifugation at 120000×g for two hours using an Avast Optima L80 Ultracentrifuge (Beckman Coulter). Cell membrane pellets were resuspended in 20 mM Hepes pH 7.5, 200 mM NaCl, 30% (v/v) glycerol and aliquoted prior to being flash cooled in liquid nitrogen and stored at -80° C. Samples were then shipped to Hamburg on dry ice.

2.3.3 Immobilised metal affinity chromatography (IMAC) protein purification of wild-type LeuT

The crude frozen membranes from Vienna were thawed and homogenized in buffer (20 mM Hepes pH 7.5, 200 mM NaCl, 2.5% (v/v) glycerol supplemented with 1 mM PMSF (Phenylmethylsulfonyl protease inhibitors)). Homogenized membranes were solubilised for 90 minutes on a rotatory mixer at 4° C in solubilisation buffer (20 mM Hepes pH 7.5, 200 mM NaCl, 2.5% (v/v) glycerol and 1% (w/v) DDM detergent) with stirring. For reasonable solubilisation 1% (w/v) DDM detergent was used for 5-10 mg/ml total protein concentration in membranes. The insoluble membranes were pelleted by ultracentrifugation at a speed of 120,000×g at 4° C for 20 minutes using a Ti-75 rotor (Beckman Coulter) in an Optima XPN-90 ultracentrifuge (Beckman Coulter). The supernatant was incubated overnight on a rotatory mixer (16 hrs) at 4° C with cobalt metal affinity resin (TALON, Clontech) pre-equilibrated in binding buffer (20 mM Hepes pH 7.5, 200 mM NaCl, 5 mM imidazole, 2.5% (v/v) glycerol and 0.05% (w/v) DDM). IMAC was performed the next day by batch purification using a table-top centrifuge for 1 min at 1000×g. TALON resin was washed with 0, 5, 10, 10 and 20 mM imidazole before being loaded into a gravity flow column (Econo-Pac -Column® Bio-rad). LeuT was eluted from the TALON resin with three CVs of elution buffer (20 mM Hepes pH 7.5, 200 mM NaCl, 250 mM imidazole, 2.5% (v/v) glycerol, 0.5% (w/v) DDM). The eluted protein was concentrated using a 50 kDa MWCO Amicon Ultra-15 spin concentrator at 3000×g, to a volume of approximately 1.5 ml. To remove the excess imidazole the concentrated protein was passed through a ZebaSpin desalting column (Thermo-Scientific) with 40 kD MWCO. The ZebaSpin desalting column was pre-washed and pre-equilibrated with the desalting buffer (20 mM Hepes pH 7.5, 20 mM NaCl, 2.5% (v/v) glycerol, 0.05% (w/v) DDM) following the suggested procedure by the company. Protein was eluted from the column after centrifugation at 1000×g for 4 mins on a table-top centrifuge. All purification steps were performed at 4° C. The total protein concentration before solubilisation (membrane preparation) and after purification was determined with the Schaffner-Weissmann assay, described in Section 2.5.1, an assay that can be performed with lipid-containing samples without interference (Kaplan & Pedersen 1985).

2.3.4 His₈-tag removal and further purification of wild-type LeuT

The His₈-tag was removed by proteolytic cleavage using a trypsin-like serine protease, thrombin, (Sigma Aldrich). Cleavage was performed over 3 hrs at 4° C using 10 units of thrombin for every 2.5 mg of protein, as per the manufacturer's instructions. Thrombin protease was removed using a Benzamidine affinity column (HiTrapTM BenzamidineFF, 1 ml, GE), which binds thrombin with high affinity while cleaved LeuT can be collected in the flow through. Following thrombin digestion the protein/His₈-tag mixture was incubated overnight with TALON resin at 4° C. An additional step of affinity chromatography with cobalt resin was performed the next day to remove the cleaved tag and uncleaved protein. Pure wild-type LeuT was concentrated to 7.5 mg/ml using a spin concentrator (Amicon) with a MWCO of 50 kDa, and spun down, ready for size-exclusion chromatography.

2.3.5 Size-exclusion chromatography purification (SEC)

A Superdex 200 column (S200 16/600, 120 ml prep grade column, Amersham Biosciences) was equilibrated with β -OG exchange buffer (20 mM Hepes pH 8.0, 190 mM NaCl, 10 mM KCl, and 40 mM n-octyl- β -D-glucopyranoside (β -OG) (2 \times CMC; Anagrade, Anatrace) to exchange the DDM detergent. The LeuT solution was loaded onto the Superdex column at a flow rate of 1 ml/min at 0.5 mPa for 1.5 CV. LeuT was collected and concentrated to a final concentration of 5 mg/ml. Wild-type LeuT purification for crystallisation in Hepes conditions was performed with 7 mg/ml LeuT.

2.3.6 Crystallisation of wild-type LeuT

Initial crystallisation trials were performed at Prof. Djinovic's lab in the Vienna Biocenter, Max F. Perutz laboratories. Crystallisation trials were carried out with freshly purified LeuT in β -OG detergent in sitting drops by vapour diffusion. The mother liquor was based on published conditions containing 100 mM Tris-MES pH 5.0-7.4, 50-200 mM NaCl, 20-24% (v/v) PEG₅₅₀MME, 10% (v/v) glycerol (Malinauskaite et al. 2016) and 100 mM Hepes-NaOH pH 7.0,

200 mM NaCl, 18-28% (v/v) PEG₅₅₀MME (Yamashita et al. 2005). Stock buffers were filtered using the 0.22 µl Millipore syringe filter units and combined using the Rigaku Desktop Alchemist, which mixes the stock solutions to an appropriate pH. TTP's Mosquito Robot was used for automated crystallisation plate set up. Crystals were obtained only in Hepes conditions (Yamashita et al. 2005) and were cryo-protected with a reservoir solution containing 35% (v/v) PEG₅₅₀MME and 40 mM β-OG and then flash-cooled in liquid nitrogen. Wild-type LeuT crystals were reproduced successfully in our laboratories in Hamburg performing only hanging drop vapour diffusion crystallisation techniques and yielding bigger crystals.

2.4 Protein production of triple-mutant LeuT

2.4.1 Site-directed mutagenesis and plasmid constructs

A triple-mutant LeuT (LeuT-SS) was designed and produced by our collaborator in the Medical University of Vienna Dr. Azmat Sohail using the QuickChange Lightning Site-directed mutagenesis kit (Agilent Technologies). Single cysteines were introduced within the wild-type LeuT open reading frame template that had been ligated into the EcoRI site of the episomal expression vector. For each single and paired double cysteine mutant, two independent clones were isolated in parallel. The presence of the mutations was verified by DNA sequencing at the Gene Sequencing Facility of Vienna (Eurofins Genomics).

2.4.2 Protein expression and purification of triple-mutant LeuT-SS

Protein expression and membrane preparations for the LeuT-SS were carried out with our collaborator in the Medical University of Vienna, Mr. Jawad Khan as previously described in Section 2.3.1 and 2.3.2 for the wild-type LeuT. Protein purification was performed in Hamburg using the membranes kindly provided by Mr. Khan. Purification of LeuT-SS was performed as previously described for wild-type LeuT purification at 4° C (Sections 2.3.3, 2.3.4, 2.3.5) with

a pre-packed cobalt resin column (HiTrap TALON crude, 1 ml GE) instead of cobalt resin (TALON, Clonetech). Triple-mutant LeuT (LeuT-SS) was purified under potassium conditions instead of sodium to obtain the inward conformation and in presence of C-Crown-15 to absorb the residual sodium.

2.4.3 Cross-linking of Cys320 and Cys400 for disulphide bond formation

The disulphide bond of the triple-mutant LeuT (LeuT-SS, Leu400Cys-Phe320Cys-Lys288Ala) between cysteines 400 and 320 was formed prior to crystallisation trials. Wild-type LeuT (LeuT-WT) was treated under the same conditions as the LeuT-SS, in parallel, to be used as a negative control. Purification of the LeuT-SS was also carried out without cross-linking treatment as a positive control. The oxidation level of this pair of cysteines was examined on cells, on native membranes and on purified protein. Cross-linking reactions in membrane preparations and purified protein was initiated by ambient oxygen and the addition of Cu(II)-1,10-Phenanthroline (Copper-phenanthroline, CuP) which acts as a oxidant catalyst. The CuP was prepared using Cu_2SO_4 and 1,10-phenanthroline in a ratio of 1:2.5 dissolved in pre-cooled K buffer (20 mM Hepes pH 7.5 and 200 mM KCl). For cross-linking in cells, resuspended cells in K-buffer were mixed with 1 mM:2.5 mM catalyst. Oxidation reactions were performed over 30 minutes on ice. For cross-linking in membranes, the 1 mM:2.5 mM oxidant was mixed with 10 mg/ml of protein (total concentration, quantified with SW assay 2.5.1). Cross-linking was performed at different incubation times at room temperature and at 4° C to investigate the optimal conditions. For cross-linking of purified protein in detergent, 10 μM protein was incubated with 10 μM :100 μM or 100 μM : 250 μM or 200 μM :400 μM Copper-phenanthroline (CuP) catalyst.

2.4.4 Monitoring of oxidation state of disulphide-bond formation

The oxidation state of cross-linked LeuT-SS (Leu400Cys-Phe320Cys-Lys288Ala) was followed by non-reducing SDS-PAGE analysis (electrophoretic mobility shift) and by the sulfhydryl assay reagent, DNTB also known as Ellman's reagent (Ellman 1959).

Quenching the reaction prior to monitoring of oxidation with Non-reducing SDS-PAGE

Non-reducing SDS-PAGE electrophoretic analysis was performed to check any shift in the mobility of cross-linked proteins. Reactions were quenched with 10 mM N-ethyl-maleimide (NEM) for 30 minutes at 24° C to quench the free sulfhydryl (-SH) groups. A 10-fold molar excess of Na-EDTA pH 8.0 (to chelate the Cu) relative to CuP was also used to terminate the cross-linking reaction. Additionally, samples were treated with 10 mM DDT to reverse the cross-linking as a control. Notably, cysteines can cross-linked during denaturation and boiling steps, therefore an adequate NEM concentration should be used to block the free sulfhydryl groups. A parallel control can test the artifactual crosslinking during the denaturation step.

Quantifying Sulfhydryl groups using the DNTB thiol assay

The DNTB-Thiol assay (5,5'-Dithio-bis-(2-nitrobenzoic acid) was performed only on LeuT purified in detergent protein solution. DNTB reacts with the free sulfhydryl group of the mutated cysteine residues 400 and 320, yielding a mixture of the disulphide and the TNB (2-nitro-5-thiobenzoic acid) product, which can be followed by UV-VIS at 412 nm. For each unknown sample to be tested a tube containing 50 µl of Ellman's reagent solution (4 mg Ellman's reagent in 1 ml reaction buffer), 2.5 ml reaction buffer (100 mM Sodium phosphate pH 8.0, containing 1 mM EDTA) and 250 µl sample was prepared. 50 µl of Ellman's reagent solution and 2.75 ml reaction buffer was used as a blank. The mixture was incubated for 15 minutes at room temperature. To quantify the concentration of the free thiol groups, the absorbance of the product TNB at 412 nm was measured using an UV-VIS spectrophotometer. The fresh stock of Ellman's reagent in reaction buffer (0.1 M sodium phosphate, 1 mM EDTA, pH 8.0) at 10 mM concentration can be stored in the dark at RT for only a day.

2.5 Protein analysis and quantification

2.5.1 Protein quantification applying the Schaffner-Weissmann assay

For accurate determination of protein in the presence of high levels of lipids the Schaffner-Weissmann protein concentration assay (SW assay) was used (Schaffner & Weissmann 1973). 2 and 4 μ l aliquots of protein sample were diluted in 270 μ l deionised water prior to the addition of 30 μ l buffer (1 M Tris-HCl pH 7.5, 10% (w/v) SDS) and 60 μ l of 60% (v/v) Trichloroacetic acid (TCA). A circular 0.45/0.22 μ m HWAP/MF Millipore membrane filter was marked into quarters in pencil and soaked in deionised water. The 2 and 4 μ l protein samples were vortexed and the precipitated protein was transferred drop-wise onto one quarter of the membrane filter under a vacuum manifold. Any remaining protein in the Eppendorf tube was rinsed out with 300 μ l 6% (v/v) TCA and transferred to the membrane filter on the same spot. The remaining two quarters were used as a control. The membrane filter was washed with 3 ml 6% (v/v) TCA and placed on a Petri dish containing a staining solution (0.1% (w/v) naphthol-blue black in a solution with a methanol:glacial acetic acid:water ratio of 45:10:45 (v/v)) for 3 minutes with stirring. The membrane filter was washed in four steps: deionized water for 30 seconds, twice in destaining solution (methanol:glacial acetic acid:water ratio of 90:2:8 (v/v)) for 1 minute and deionized water for 2 minutes. Each quarter was cut out and transferred into a new Eppendorf tube containing 1 ml of elution buffer (25 mM NaOH, 0.05 mM EDTA, 50% (v/v) ethanol). After incubation at 37° C for 10 minutes the stained protein was eluted from the paper and its OD 630 was measured using a WPA Biowave II UV/Visible spectrophotometer (Biochrom Ltd.) and the concentrations calculated using a BSA standard graph as reference.

2.5.2 Protein analysis by SDS-PAGE

SDS-PAGE electrophoresis was carried out as described by Laemmli (Laemmli, 1970) using a discontinuous gel consisting of a 4% (v/v) stacking and a 15% (v/v) resolving gel. For all proteins (Mhp1 and LeuT variants: wild-type and mutants) samples from IMAC purification

were diluted to contain 10 µg final protein for SDS-PAGE analysis. These aliquots were diluted to a total volume of 15 µl with distilled water. Samples were prepared for electrophoresis by mixing with 5µl of sample buffer (4× buffer: 60 mM Tris-HCl pH 7.2, 10% (v/v) glycerol, 2% (w/v) SDS, 0.005% (w/v) bromophenol blue, 3% (v/v) β-mercaptoethanol) (SDS solution). Samples were incubated for 15 minutes at room temperature, not 95° C, to prevent sample aggregation (Sagney et al., 1996). Electrophoresis was performed for approximately 90 minutes at 130 V in 1x SDS running buffer (1 g/L SDS, 3.03 g/L Tris base, 14.41 g/L glycine pH 8.3) until the dye front had reached the bottom of the gel using a Thermo-Scientific apparatus. Gels were stained for 30 minutes with Coomassie blue in staining solution (methanol:glacial acetic acid:water in a ratio of 50:10:40 (v/v), containing 0.2% (w/v) Coomassie Brilliant Blue R) with gentle stirring. This was washed with destaining solution (methanol:glacial acetic acid:water in a ratio of 8:10:82 (v/v) for 60-120 minutes until the protein bands were visible enough to compare them with the standard molecular weight ladder (SigmaMarker low range mol wt. 6.5-66 kDa).

2.5.3 Western Blotting

For western blotting analysis a PVDF membrane was soaked in methanol for 15 minutes before being transferred to SDS-PAGE running buffer at 50% dilution with distilled water. This membrane was cut to a size a bit bigger than the gel. The gel and filter papers were soaked in transfer buffer (2.9 g glycine, 5.8 g Tris-base, 0.37 g SDS, 200 ml methanol to a final volume of 1 L) (Towbin et al. 1979). A sandwich was prepared comprising layers of sponge, filter paper, PVDF membrane, the polyacrylamide gel from the SDS-PAGE, filter paper and sponge. The protein samples were transferred from the polyacrylamide gel to the membrane by the application of 15 V for 3 hours in a WB WetTransfer-cell Blot SD WET transfer cell (Bio-Rad Laboratories Inc.). After transfer, the PVDF membrane was removed from the sandwich and incubated with 10 ml TBST buffer (25 mM Tris-HCl pH 7.8, 150 mM NaCl, 0.05% (v/v) Tween-20) containing 3% (w/v) BSA for 1 hour. The membrane was washed twice at room temperature with 15 ml TBST buffer for 10 minutes with stirring. The membrane was then

incubated with 5 μ l HIS probe-HRP solution in 10 ml TBST buffer for 1 hour, followed by four identical washing steps as described previously. The membrane was incubated for 5 minutes in 10 ml of SuperSignal West Pico chemiluminescent working solution (5 ml West Pico stable peroxide solution and 5 ml West Pico luminol/enhancer solution). The Gel-doc machine (Bio-Rad) and GeneSnap program at the EMBL-Hamburg laboratories were used to image the Western blots. For earlier Western blots a high-range rainbow marker was used, in which case these blots were scanned and superimposed with the Gel-doc images. For later Western blots, BenchMark His-tagged Protein Standard (ThermoFischer Scientific) was used which required no special treatment.

2.6 Biophysical characterisation

2.6.1 Circular Dichroism

The secondary structure of wild-type Mhp1 and its mutants were analysed by Far-UV (180-260 nm) spectrum circular dichroism in order to assess the structural integrity of protein. Data were collected on two ChirascanTM CD spectrometers (Applied Photophysics), one funded by the Wellcome Trust grant code 094232 at the University of Leeds and the second belonging to the SPC facility at EMBL-Hamburg. Analysis of the secondary structure was performed using the ChirascanTM software provided by Applied Photophysics. Concentrated protein was diluted in storage buffer to approximately 0.1-0.2 mg/ml in a quartz cuvette with 1 mm path length. Spectra were recorded at 20° C over 190-260 nm with 1 nm step resolution, 0.5 s/step scan rate, 4.3 nm bandwidth. Scans were performed on air, protein and buffer solutions to allow for background and buffer subtraction to be performed. The thermal stability was analysed by thermal melts using the same parameters by ramping the temperature over the range of 20-90° C with 1° C increment steps. 30 seconds additional time were allowed between steps to stabilise the temperature before the next scan.

2.6.2 Steady-state tryptophan fluorescence spectrophotofluorimetry assay for Mhp1

For the analysis of hydantoin ligand binding to wild-type Mhp1 and its various mutants, a steady-state spectrophotofluorimetry technique was carried out using a Photon Technology International spectrophotofluorimeter (Applied Photophysics) PTI equipped with a temperature-controlled cell (thermostated cell) set to 18° C (University of Leeds, Astbury centre). Purified Mhp1 was diluted to a final protein concentration of 140 µg/ml (2.57 µM) in the fluorimetry buffer. The hydantoin ligand tested in the steady-state fluorescence assay was the D/L-BH 100 mM stock solution dissolved in 100% DMSO. To investigate whether the presence of sodium was the driving force of the binding mechanism in Mhp1, the fluorescence quench caused by titration of ligand to the Mhp1 was analysed in the presence and absence of NaCl. Therefore, three fluorimeter buffers were prepared with different NaCl concentrations (0 mM, 15 mM and 140 mM). In order to keep the anionic strength constant (maintain the same ionic compositions) at 140 mM among the solutions (to achieve total osmolarity equivalent to 140 mM salt) as indicated in the Section 1.5.5, choline chloride was used in equivalent concentrations (in compensating concentrations) where NaCl was lacking (140 mM, 125 mM and 0 mM, Appendix B: buffers). Protein solution was incubated for 4.5 minutes with stirring inside the sample cell of the fluorimeter at 18° C using a 1 cm length quartz cuvette. L-BH ligand was titrated into the protein solution to a final concentration of 0-2 mM range using a 10 µl Hamilton syringe. The ligand was mixed with the protein for 1.5 minutes to equilibrate before the fluorescence spectra were obtained. The samples were excited at 280 nm and the emitted fluorescence of the sample was recorded over 310-360 nm. The ligand does not fluoresce in the absence of protein. The experiments were repeated in triplicate. Control measurements demonstrated that the buffer and DMSO solvent at the concentrations used did not influence the fluorescence of the protein or the hydantoin-promoted quenching. Data were analysed using the Michaelis-Menten tool in Graph Pad Prism6 software to obtain the apparent dissociation constant (K_d , µM) and the maximal binding (B_{max} , %).

2.7 Structural Characterisation

2.7.1 MX data collection and structure solution

X-ray diffraction data for Mhp1 and LeuT were collected at various beamlines of Diamond Light Source (DLS) (UK) and the European Synchrotron Radiation Source (ESRF). Data were collected under nitrogen stream. Specific details are summarised in the Tables of Chapter ??.

The data were indexed, integrated and scaled using the XDS package (Kabsch 2010). Initial phases were obtained by molecular replacement (MR) using MOLREP (Vaguine et al. 1999) in the CCP4 interface with Protein Data Bank PDB codes 2A65 for wild-type LeuT and 2JLN for wild-type Mhp1 as molecular replacement models. Manual real space refinement was performed in Coot (Emsley & Cowtan 2004) and automated refinement in reciprocal space using REFMAC5 (Murshudov et al. 2011) In REFMAC5, refinement was performed at first with rigid body, then with jelly body refinement, followed by TLS refinement.

2.7.2 Small-angle X-ray scattering studies coupled with size exclusion chromatography (SEC-SAXS)

SEC-SAXS experiments were performed at the biological small-angle X-ray scattering beamline BL4-2 at Stanford Synchrotron Radiation facility-SSRL (CA, USA) and at the BM29 beamline (Pernot et al. 2013) at the European Synchrotron Radiation Facility-ESRF (Grenoble, France). Mhp1 was run through an analytical size-exclusion chromatography (SEC) column and the eluted protein was analysed by small-angle X-ray scattering. Using this procedure, the PDC is diluted into the column running buffer to obtain a monodisperse sample and separate the excess of detergent micelles. Accurate buffer correction can be achieved by subtracting an average of a number of buffer scans at the beginning of the run from the main PDC peak (Section 1.5.6).

Sample preparation

Purified protein samples in 25 μl volumes were shipped on dry ice to the synchrotrons and stored at -80°C . The protein samples were dissolved in the respective SEC buffers conditions at the desired concentrations (approximately 5 mg/ml) and incubated for 1 hour. For experiments conducted in ESRF double protein concentration (approximately 10 mg/ml) was used for better SAXS signal. Protein concentration was carefully measured using the Schaffner and Weissmann assay (Section 2.5.1). All samples were spun down at high speed for 10 minutes prior to the injection. The SEC columns used were the Supedex200 Increase 3.2/300 (GE). SEC experiments and column pre-equilibration were performed at a flow rates of 0.05 ml/min at room temperature. The column was equilibrated for 3 column volumes of the corresponding buffer at 0.05 and 0.1 ml/min flow rate, 50 μl and 5 μl of protein was injected into the S200 increase and SEC-3 columns respectively. For SEC experiments a full run was carried out for 1.5 CV. All buffers were filtered through 0.22 μm filter and degassed. To avoid the use of sodium azide buffers were changed daily.

SEC-SAXS buffers: Appendix A.2 Mhp1 size-exclusion chromatography buffers for scattering studies.

SEC-SAXS data collection at BL4-2, SSRL

SEC-SAXS experiments were carried out at beamline BL4-2 at the Stanford Synchrotron Radiation Laboratory (SSRL) at room temperature for the WT-NM and its mutants Ala222Ser and Met39Cys. Protein samples were filtered through 0.2 μm centrifugal filter units (Millipore) prior to loading on to the respective SEC column. The solution flow was controlled by an FPLC Äcta purifier system, X-ray wavelength $\lambda=1\text{ \AA}$ and sample-to-detector distance $D=1.7\text{ m}$. Scattering data were collected using a CCD detector or Pilatus 300 K. Sample was injected manually with a Hamilton syringe. The flow rate was set to 150 $\mu\text{L}/\text{min}$, and 20 μL of the Mhp1 solution was injected onto the column.

SEC-SAXS data collection at BM29, ESRF

SEC-SAXS data were collected using the high-performance liquid chromatography (HPLC) system installed at BM29 (Malvern HPLC), directly attached to the flow-through capillary of the SAXS exposure unit (Round et al. 2015) at room temperature for the WT-DDM, Ala309Asn, and Thre313Ala Mhp1 variants. The detector (Pilatus 1M) was at 2867 mm distance from the sample. The elution profile was monitored by UV absorption at 280 nm. Data were collected at the beginning of the each run for accurate buffer subtraction. The first 50 frames, corresponding to the SEC buffer, were averaged to provide a low noise buffer signal. The exposure time was 1 sec and a total of 1200 frames were collected across the protein elution peak of the protein-detergent complex and the signal from the protein-detergent complex was obtained. In this thesis only the basic SEC-SAXS analysis is presented. The extensive analysis of SEC-SAXS data was performed by Yunyun Gao, Ph.D. student, as part of his doctoral thesis.

2.8 Synthesis of Mhp1 hydantoin ligands

For the synthesis of compounds 5-benzyl-*L*-hydantoin (*L*-BH) **3**, 5-indolylmethyl-*L*-hydantoin (*L*-IMH) **6** and 5-(2-naphthylmethyl)-*L*-hydantoin (*L*-NMH) **9** the procedure of Patching was used (Patching 2011). Synthesis of 5-bromovinyl-hydantoin (BVH) **12** was based on the procedure of Thenmozhiyal et al. (2004). The chemical compounds are numbered based on their order of appearance.

2.8.1 Experimental procedures

The Mhp1 ligands, hydantoin-5 substituted compounds used during this thesis, were synthesised under the guidance of Dr. Marta Sans. All reagents and solvents obtained from commercial suppliers were used without further purification due to their high quality. Solvents were removed under reduced pressure using a rotary evaporator Büchi R-100 at diaphragm pump pressure. Samples were freed of remaining traces of solvent under high vacuum. NMR data

were recorded at the NMR Service in the Chemistry Department of the University of Hamburg using a Bruker AV3400.

Chromatography: Progress of the reaction was monitored by thin layer chromatography (TLC), which was performed using ALUGRAM® SIL G/ UV254 pre-coated aluminium sheets (plates) (Macherey-Nagel) and visualised using UV irradiation with a VILBER LOURMAT® lamp and standard staining agents.

- **Synthesis of 5-benzyl-L-hydantoin, L-BH (3)**

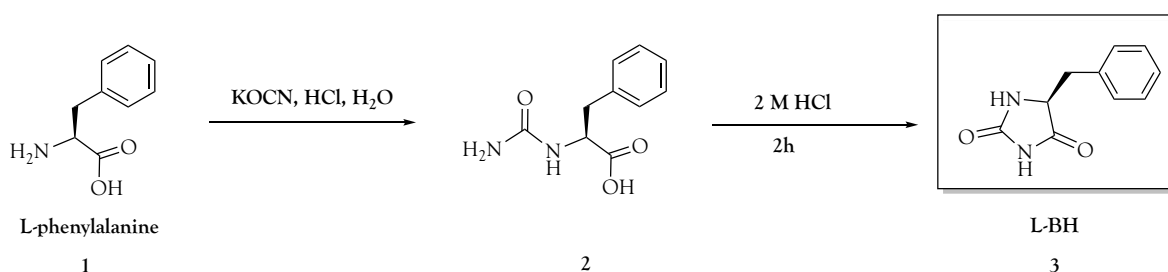


Figure 2.1: Scheme of synthetic route of L-BH 3.

L-phenylalanine (200 mg, 1.21 mmol) **1** was dissolved in 60 ml of distilled water and potassium cyanate (200 mg, 2.406 mmol) was added. The mixture was stirred under reflux for 20 h. The solution was cooled to room temperature and the total volume was reduced to 10 ml under reduced pressure. Concentrated HCl was then added drop wise until pH 1 was reached. The solution was filtered under suction, washed with cold water, dried on a filter and under high vacuum overnight. This produced 240 mg of a white solid **2** which was transferred to a round-bottomed flask and used in the next step without further purification. Then, 137 ml of concentrated HCl were added and the reaction was left stirring under reflux overnight. The volume of the reaction was reduced to 8 ml affording a white needle-shaped solid. The solid was filtered under suction, washed with cold water and dried under vacuum overnight. L-BH (150 mg, 0.630 mmol) **3** was obtained in a 46% yield over two steps. NMR data indicate the formation of the product (Appendix B.1a).

- Synthesis of 5-indolylmethyl-L-hydantoin, L-IMH (6)

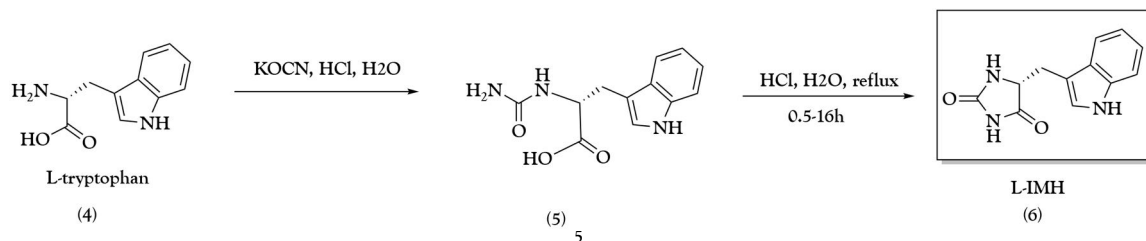


Figure 2.2: Scheme of synthetic route of L-IMH 6.

The synthesis of 5-indolylmethyl-L-hydantoin was attempted with a similar synthetic route as in L-BH, based on a two-step reaction with L-tryptophan as a starting material. L-tryptophan (200 mg, 1 mmol) 4 and potassium cyanate (160 mg, 1.972 mmol) were dissolved in 50 ml distilled water and stirred at 65-70° C overnight under reflux. The solution was cooled to room temperature and the total volume was reduced to 8 ml under reduced pressure. Concentrated HCl was added until a white precipitate appeared which was assumed to be N-carbamoyl-L-tryptophan 5. The solid was filtered under suction, washed with cold water and dried under reduced pressure for two hours. 200 mg of this solid were transferred into a round bottom flask for the second reaction and 114.2 ml of 2 M HCl were added. The reaction was stirred under reflux overnight. The volume was reduced to 8 ml and the mixture was kept in an ice-water bath until the formation of white crystals was observed. Finally, the crystals were filtered under suction, washed with 40 ml of cold water and dried under reduced pressure overnight affording L-IMH (200 mg, 0.872 mmol) 6 with 89% yield. NMR data indicate the formation of the product (Appendix B.1c).

- Synthesis of 5-(2-naphthylmethyl)-L-hydantoin, L-NMH (9)

Commercially available N-(tert-Butoxycarbonyl)-3-(2-naphthyl)-L-alanine (200 mg, 0.634 mmol) 7 was dissolved in 10 ml of anhydrous dichloromethane, and freshly distilled TFA (5 ml) was added slowly to the mixture. The reaction was stirred under a N₂ atmosphere at room temperature and the progression of the reaction was followed by TLC. After completion, the solvent was evaporated under reduced pressure to afford 140 mg of the free amino compound as a

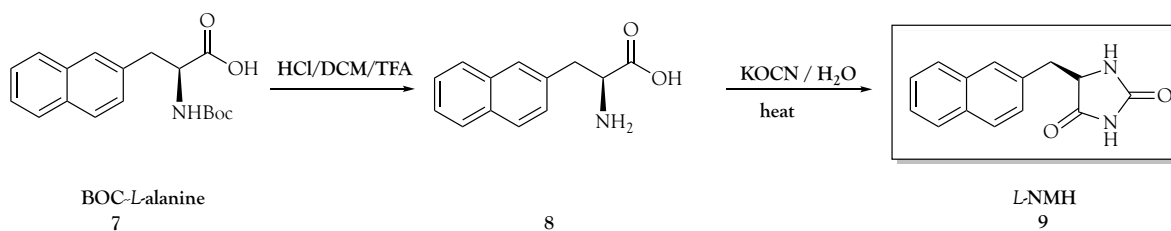


Figure 2.3: Scheme of synthetic route of *L*-NMH 9.

yellow oil with a quantitative yield.

Intermediate 8 (140 mg, 0.650 mmol) was then mixed with potassium cyanate (105.56 mg, 1.301 mmol) in water (33 ml) and stirred at 70° overnight. The solution was cooled to room temperature and the total volume was reduced to 8 ml. 1 M HCl solution (20 ml) was added and the solution was kept at room temperature for 2-4 hours until a white precipitate was observed. The solid was collected by filtration, washed with 50 ml of cold water and dried under vacuum for 4 hours. The product was then transferred into a 250 ml round bottom flask where 30 ml of 2 M HCl were added and the reaction was left stirring under reflux overnight. The volume was reduced to 8 ml and mixture kept in an ice-water bath until the formation of white crystals was observed. Finally, the crystals were filtered under suction, washed with 40 ml of cold water and dried under reduced pressure overnight affording *L*-NMH (74.75 mg, 0.315 mmol) 9 with 48% yield. NMR data indicate the formation of the product (Appendix B.1e)

• **Synthesis of 5-bromovinyl-hydantoin, BVH (12)**

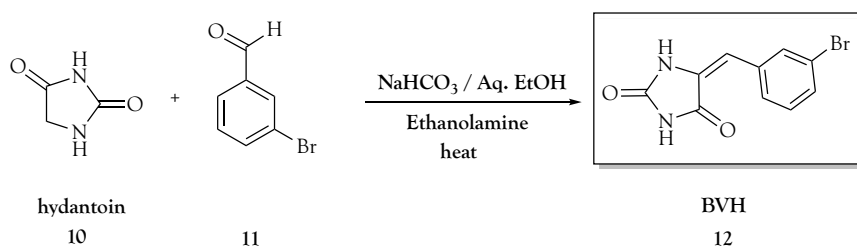


Figure 2.4: Scheme of synthetic route of BVH 12.

BVH was prepared using a modified procedure previously described by Thenmozhiyal et al. (2004). Hydantoin (500 mg, 5.00 mmol) **10** was dissolved in water (10 ml) at 70° C with stirring. The pH of the mixture was adjusted to 7.0 by the addition of a saturated solution of NaHCO₃. Ethanolamine (0.45 ml) was added to the reaction mixture and the temperature raised to 120° C. To this, an equimolar quantity of 3-bromo-benzylaldehyde (0.6 ml, 5 mmol) **11** dissolved in 10 ml EtOH was added drop wise with continuous stirring. The temperature was raised to 140° C and kept under reflux for 16 hours until the formation of a precipitate was observed. This precipitate was filtered and washed with 40 ml of a mixture EtOH/water (1:5) to give the desired compound BVH (340 mg, 1.273 mmol) **12** in a 26% yield. NMR data indicate the formation of the product (Appendix B.1g).

Chapter 3

Searching for intermediate states of Mhp1 by applying single-point mutations of sodium and ligand binding sites

Several biochemical and functional studies have previously been performed for Mhp1 aiming at understanding the mechanism of alternating access transport (Jackson 2012, Simmons et al. 2014, Kazmier et al. 2014). This highly dynamic process requires structural rearrangements of the protein in order to facilitate the binding and the transportation of the hydantoin ligands. Previous mutagenesis of key positions in the binding pockets and subsequent functional studies have identified several mutants of Mhp1 that display altered ligand binding and transport behaviour. These can lead to mutants where hydantoin ligands bind with comparatively very low affinity, or where the sodium-dependent binding is abolished or perturbed (Simmons et al. 2014), or both. These mutants are ideal candidates for structural analysis in order to further probe the transport mechanism by solving yet unknown intermediate states of Mhp1 using X-ray crystallography. Several Mhp1 variants were purified and examined for their structural integrity and thermal stability by circular dichroism to assess their suitability for crystallisation and structural studies. Several mutants could be carried forward to data collection and further analysis. Steady-state tryptophan fluorescence quenching assays were used to compare the

wild-type and some of the mutants to examine the effect of the mutations on their binding ability.

Mhp1 mutants in both sodium and ligand-binding sites presented here are listed in Table 3.1 according to their location in either the sodium (Ala38Gly, Met39Cys, Ile41Phe, Ala309Asn, Thr313Asp) or the ligand-binding sites (Ala222Ser, Gln42Asn, Gly219Ser) (Figure 3.1).

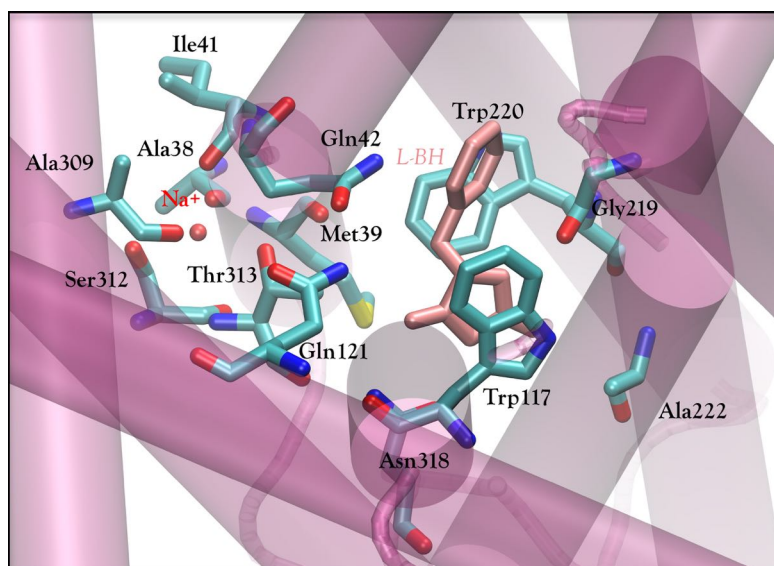


Figure 3.1: Location of Mhp1 residues coordinating the sodium and ligand in their binding sites. Helices are depicted as cylinders, residues in the binding site cavities are in ball and stick representation coloured as C=cyan, N=blue, O=red, S=yellow. Sodium and ligand are also in ball and stick representation coloured red and light pink respectively. The reported Mhp1 structure bound *L*-BH (PDB code 4D1B) has been used here. Picture was prepared by VMD (Humphrey et al. 1996) and rendered using Tachyon (Stone 1998).

Table 3.1: List of purified Mhp1 mutants of sodium and ligand-binding pockets

Mutation	Binding site	Position	Motif
Ala38Gly	Sodium	Helix 1	Bundle
Met39Phe	Sodium	Helix 1	Bundle
Ile41Cys	Sodium	Helix 1	Bundle
Ala309Asn	Sodium	Helix 8	Hash
Thr313Ala	Sodium	Helix 8	Hash
Gln42Asn	Ligand	Helix 1	Bundle
Gly219Ser	Ligand	Helix 6	Bundle
Ala222Ser	Ligand	Helix 6	Bundle

3.1 Purification of Mhp1 variants for structural studies

3.1.1 Purification of Mhp1 variants

For biophysical characterisation and structural determination of wild-type Mhp1 and its mutants (hereby referred to collectively as Mhp1 variants), proteins were initially expressed in the University of Leeds by our collaborator Mr David Sharples as described in Section 2.2.1 and purified (by the author) *via* affinity chromatography as described in Section 2.2.2 based on previously established protocols (Shimamura et al. 2008), for which results are presented.

Mhp1 variants were solubilised using the most typically used detergent for membrane proteins, the 12-carbon chain n-dodecyl- β -D-maltoside (DDM) leading to successfully purified and functionally active Mhp1 protein (Section 2.2.2) (Suzuki & Henderson 2006, Weyand et al. 2008). However, protein crystals from Mhp1 purified in DDM detergent were not obtained. An extensive extra second wash of NM buffer was required to exchange the DDM detergent to a shorter 9-carbon chain nonyl- β -D-maltopyranoside (NM) detergent (Section 2.2.2). This detergent has been previously shown to be required to promote Mhp1 crystal formation (Weyand

et al. 2008). All Mhp1 variants were treated with identical purification protocols and detergent exchange.

The locations of each mutant are illustrated in Figure 3.1. The purity and existence of the purified Mhp1 mutants were assessed with SDS-PAGE gels and anti-His-tag Western blotting. CD spectra confirmed the secondary structure of Mhp1 variants, while steady-state spectrophotofluorimetry was used to investigate the effects on the ligand-binding ability of Mhp1 variants.

3.1.2 Monitoring Mhp1 variant purity during purification

Mhp1 protein mutants had to be sufficiently pure and in sufficient quantity for biophysical analysis and crystallisation. The protein purity was determined by SDS-PAGE gel electrophoresis under denaturing conditions. Immunoblotting was performed to confirm that the purified protein was indeed the N-His₆tagged Mhp1 of interest and to see whether the additional bands shown in the SDS-PAGE gel could be a result of differentially folded/cleaved Mhp1 or simply contaminating proteins from the cell membrane. Membrane transport proteins have been shown to migrate on an SDS-PAGE gel typically at 65-75% of their actual molecular mass (Ward 2000, Saidijam et al. 2003, 2005). Membrane proteins do not fully unfold in SDS sample buffer due to the presence of other detergents and the stable hydrophobic contacts, causing the protein to have a more compact size (Rath et al. 2009). Wild-type Mhp1 protein with a N-His₆tag has a theoretical mass of 54581 Da, while mass spectrometry measurements showed 54582.3 Da (Jones 2010, PhD). The SDS-PAGE gel from the stages of purification of wild-type Mhp1 showed a strong band at approximately 36 kDa at the final desalting step (Figure 3.2a, lane 9). The Western blot confirms this band is the final purified Mhp1 product (Figure 3.2b, lane 8).

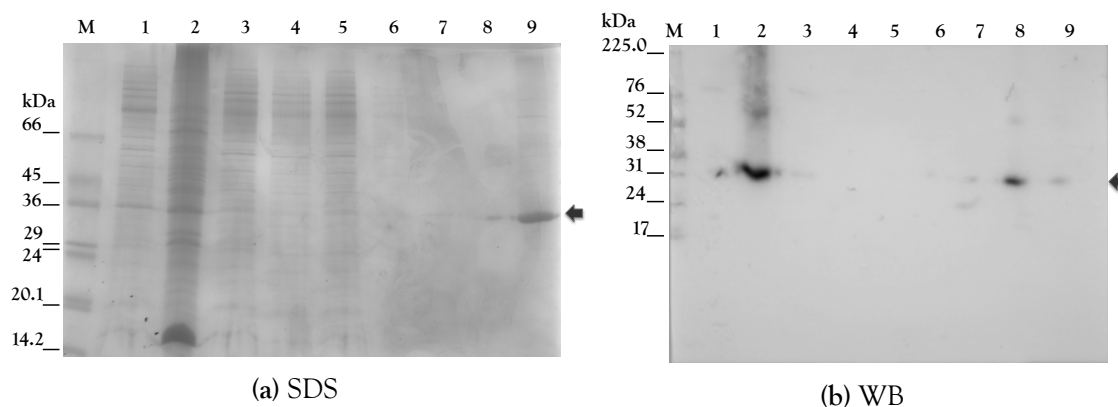


Figure 3.2: (a) SDS-PAGE gel and (b) Western blot of wild-type Mhp1 purified in NM detergent for crystallisation trials. The samples in both the gel and blot are the same, with the blot samples being diluted 1:14 times. **(a) SDS-PAGE:** (M) molecular weight marker, (1) supernatant after ultracentrifugation, (2) insoluble pellet after ultracentrifugation, (3) after incubation O/N with nickel beads, (4) unbound flowthrough, (5) loaded as in (3), (6) after wash in DDM, (7) after wash in NM, (8) after elution in NM, (9) after desalting step, **(b) Western blotting:** (M) molecular weight marker, (1) supernatant after ultracentrifugation, (2) insoluble pellet after ultracentrifugation, (3) after incubation O/N with nickel beads (4) unbound flowthrough, (5) after wash in DDM, (6) after wash in NM, (7) after elution in NM, (8) after desalting step, (9) residual on Ni-NTA resin beads. The arrows indicate the position of Mhp1.

A second fainter band is also observed migrating at approximately double the molecular mass of the main protein band. Since this second band is also visible on the Western blot, it is unlikely to be a contaminant. It could be either protein that has fully unfolded in SDS and hence migrates closer to the actual molecular mass of the protein, or alternatively a separated protein dimer as it runs approximately at double the mass of the primary band. This is often observed in membrane transport proteins.

All Mhp1 mutants also migrated at approximately 36 kDa, similar to wild-type Mhp1 (Figure 3.2). However, generally a higher level of contamination in the Mhp1 mutant samples was observed. Particularly in the cases of Ile41Phe (Figure 3.5), Gln42Asn (Figure 3.10), Gly219Ser (Figure 3.11) and Ala222Ser (Figure 3.12) there were significantly more bands unrelated to Mhp1. For Ala309Asn (Figure 3.6) and Thr313Ala (Figure 3.8), extra bands at approximately 60-80 kDa were observed and Western blotting suggests that these may be Mhp1 protein

in higher oligomer states. Met39Cys (Figure 3.4) mutant showed a single clean band, and Ala38Gly (Figure 3.3) showed a single, albeit weak band.

Sodium binding site Mhp1 mutations

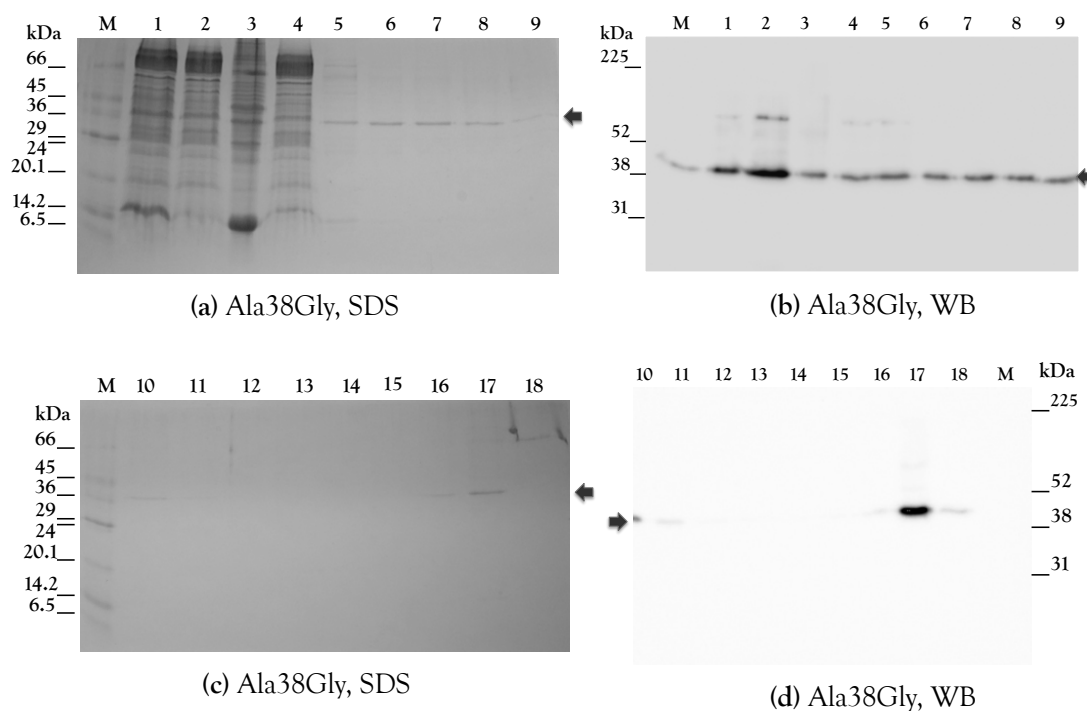


Figure 3.3: SDS-PAGE gel and Western Blot of Mhp1 Ala38Gly. SDS-PAGE (a and c): (M) molecular weight marker, (1) solubilisation for 4 hrs, (2) supernatant after ultracentrifugation, (3) insoluble pellet after ultracentrifugation, (4) unbound flowthrough O/N, (5) after wash in DDM F1, (6) after wash in DDM F2, (7) after wash in DDM F3, (8) after wash in DDM F4, (9) after wash in NM F11, (M) molecular weight marker, (10) after elution in NM F21, (11) after Elution in NM F26, (12) flowthrough after elution F29, (13) flowthrough after elution F30 (14) flowthrough after elution F31, (15) flowthrough after elution F38, (16) desalting sample application (17) after desalting step, (18) flowthrough after desalting, **Western blot (b and d):** (M) molecular weight marker and a bit of the 2nd sample (wrong loading), (1) solubilisation for 4 hrs, (2) supernatant after ultracentrifugation, (3) insoluble pellet after ultracentrifugation, (4) unbound flowthrough, (5) unbound flowthrough as in (4), (6) after wash in DDM F1, (7) after wash in DDM (12) flowthrough after elution F29, (13) flowthrough after elution F30, (14) flowthrough after elution F31, (15) flowthrough after elution F38, (16) desalting sample application, (17) after desalting step, (18) flowthrough after desalting, (M) molecular weight marker. F: Fraction. The arrows indicate the position of Mhp1.

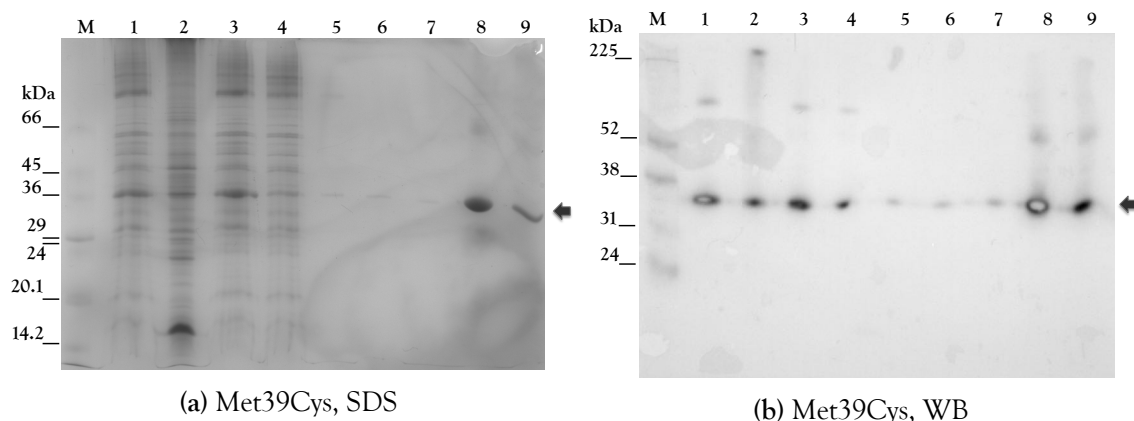


Figure 3.4: SDS-PAGE gel and Western Blot of Mhp1 Ile41Phe in the sodium binding site (a) **SDS-PAGE:** (M) molecular weight marker, (1) supernatant after ultracentrifugation, (2) insoluble pellet after ultracentrifugation, (3) after incubation O/N with nickel beads, (4) unbound flowthrough, (5) after wash in DDM, (6) after wash in NM, (7) after elution in NM, (8) after desalting step and concentrated protein, (9) residual on Ni-NTA resin beads, (b) **Western Blot:** (M) molecular weight marker, (1) supernatant after ultracentrifugation, (2) insoluble pellet after ultracentrifugation, (3) after incubation O/N with nickel beads, (4) unbound flowthrough, (5) after wash in DDM, (6) after wash in NM, (7) after Elution in NM, (8) after desalting step and concentrated protein, (9) residual on Ni-NTA resin beads. The arrows indicate the position of Mhp1. The arrows indicate the position of Mhp1.

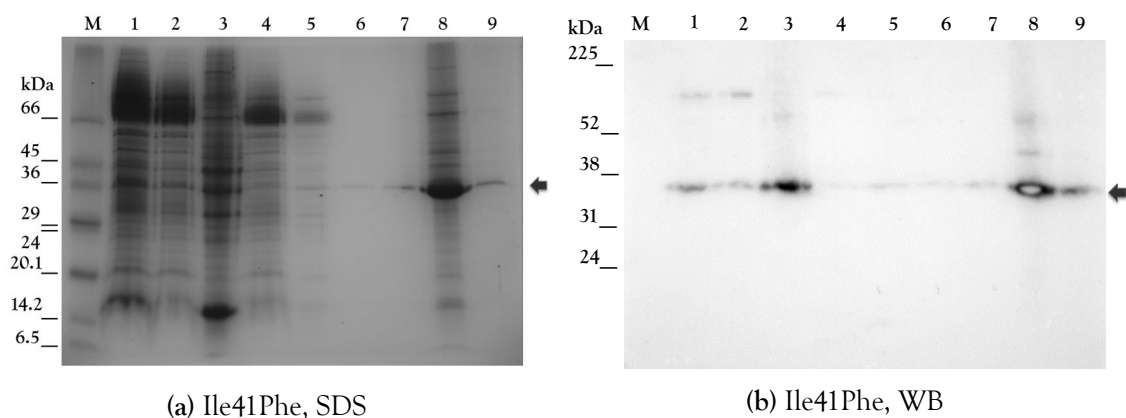


Figure 3.5: SDS-PAGE gel and Western Blot of Mhp1 Ile41Phe of the sodium binding site (a) **SDS-PAGE:** 15 μ g samples loaded as follows: (M) molecular weight marker, (1) solubilisation for 4hrs, (2) supernatant after ultracentrifugation, (3) insoluble pellet after ultracentrifugation, (4) unbound flowthrough, (5) after wash in DDM, (6) after wash in NM, (7) after elution in NM, (8) concentrated after desalting, (9) residual on Ni-NTA resin beads, (b) **Western Blot:** (M) molecular weight marker, (1) solubilisation for 4hrs, (2) supernatant after ultracentrifugation, (3) insoluble pellet after ultracentrifugation, (4) unbound flowthrough, (5) after wash in DDM, (6) after wash in NM (7) after elution in NM, (8) concentrated after desalting, (9) residual on Ni-NTA resin beads. The arrows indicate the position of Mhp1.

The production of Mhp1 mutants Ala309Asn and Thr313Ala in final detergent NM instead of DDM was carried out with the final goal of crystallisation trials to investigate whether these mutants adopt an alternative conformation (Jackson 2012). Because of this, those mutants were purified following the protocol described previously (Section 2.2.2) in the presence and in the absence of sodium to investigate also whether the sodium drives the equilibrium between the conformations towards an outward-open conformation (Section 3.2.4). For this purpose sodium chloride was substituted with potassium chloride and the buffers were adjusted with the appropriate base (potassium hydroxide) whenever it was needed.

The purification of Mhp1 mutants Ala309Asn and Thr313Ala in the presence (Figures 3.6, 3.8) and absence of sodium (Figures 3.7, 3.9) was successful. The presence of potassium chloride instead of sodium did not lower the protein yield. SDS-PAGE gels confirmed that the mutants Ala309Asn and Thr313Ala migrated at 35-37 kDa similarly to wild-type Mhp1 (Figure 3.2) were successfully obtained. Western blots of the mutants confirmed the existence of the His₆-tagged mutants. Oligomers are also visible in the two gels.

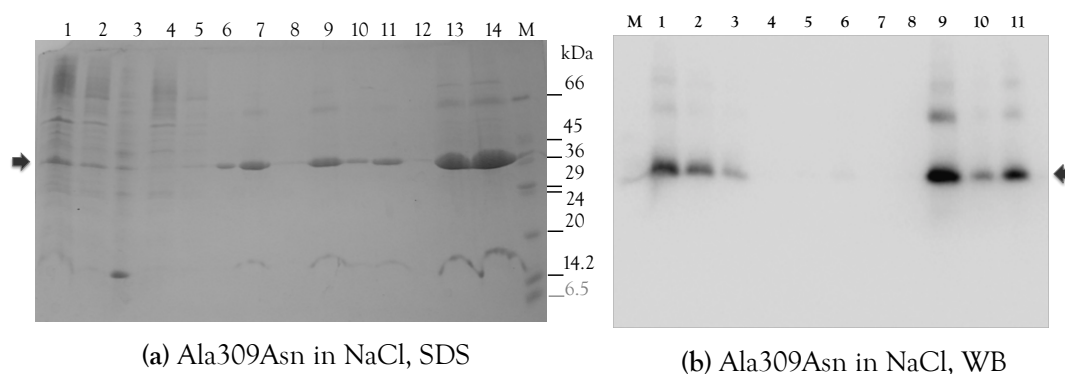


Figure 3.6: SDS-PAGE gel and Western Blot of Mhp1 Ala309Asn purified in NM in the presence of Na. (a) **SDS-PAGE:** (1) solubilisation, (2) supernatant and (3) insoluble pellet after ultracentrifugation, (4) unbound flowthrough, (5) after wash in DDM, (6) after elution in NM, (7) after elution concentrated protein, (8) desalting sample application, (9) after desalting step, (10) desalting flowthrough, (11) after desalting concentrated, (12)-, (13) protein concentrated to 5 mg/ml for SAXS (14) to 8 mg/ml for MX, (15) molecular weight marker, (b) **Western blotting:** (M) molecular weight marker, (1) membrane prep pre solubilisation, (2) solubilisation, (3) supernatant and (4) insoluble pellet after ultracentrifugation, (5) unbound flowthrough (6) after wash in DDM, (7) after wash in NM, (8) after elution in NM, (9) after elution concentrated, (10) protein concentrated to 5 mg/ml for SAXS, (11) to 8 mg/ml for MX.

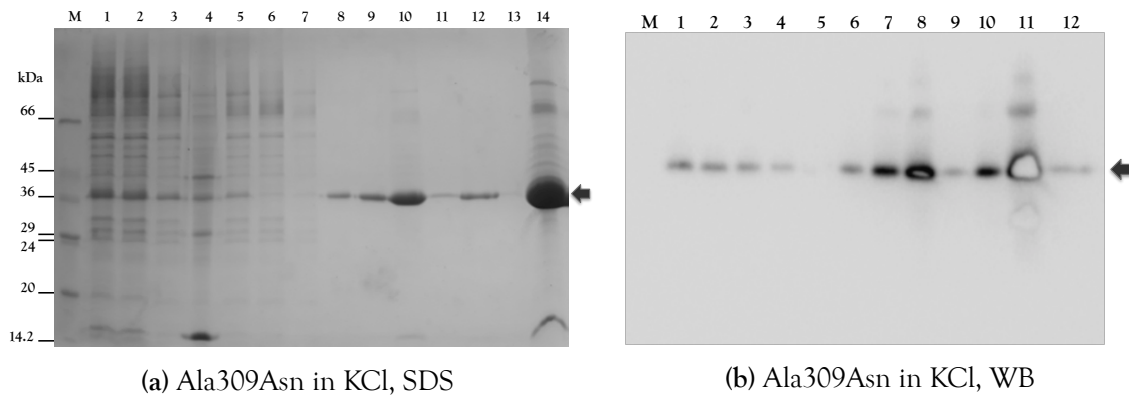


Figure 3.7: SDS-PAGE gel and Western blotting of Mhp1 Ala309Asn purified in NM in the absence of Na. (a) **SDS-PAGE:** (1) molecular weight marker, (2) solubilisation 1, (3) solubilisation 2, (4) supernatant and (5) insoluble pellet after ultracentrifugation, (6) flowthrough after single manual load, (7) unbound flowthrough, (8) after wash in DDM, (9) after wash in NM, (10) after elution in NM, (11) concentration after elution, (12) desalting sample application, (13) after desalting step, (14) desalting flowthrough, (15) concentration after desalting, (b) **Western blot:** (M) molecular weight marker, (1) solubilisation 2, (2) supernatant and (3) insoluble pellet after ultracentrifugation, (4) unbound flowthrough, (5) after wash in DDM, (6) after wash in NM, (7) after elution in NM, (8) concentrated after elution in NM, (9) desalting sample application, (10) desalted protein, (11) concentrated after desalting, (12) desalting flowthrough.

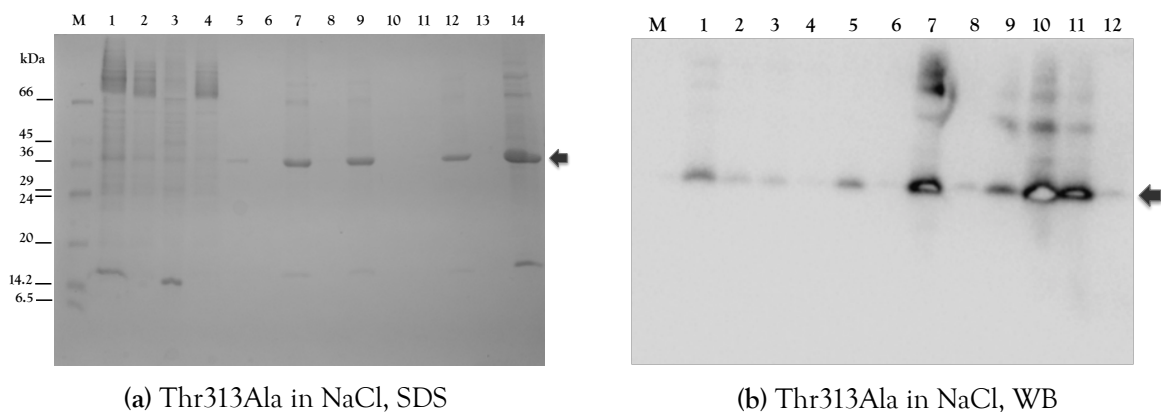


Figure 3.8: SDS-PAGE gel and western blotting of Mhp1 Thr313Ala purified in NM in the presence of Na. (a) **SDS-PAGE:** (1) molecular weight marker, (2) solubilisation, (3) supernatant and (4) insoluble pellet after ultracentrifugation, (5) unbound flowthrough, (6) after wash in DDM, (7) after wash in NM, (8) concentrated after elution in NM, (9) desalting sample application s1, (10) after desalting s1, (11) desalting flowthrough s1, (12) desalting sample application s2, (13) after desalting s2, (14) desalting flowthrough s2 (15) concentrated after desalting s1, (b) **Western blot:** (M) molecular weight marker, (1) Incubation, (2) supernatant and (3) insoluble pellet after ultracentrifugation, (4) unbound flowthrough, (5) after wash in DDM, (6) after wash in NM, (7) concentrated after elution in NM, (8) desalting sample application s1, (9) after desalting s1, (10) concentrated after desalting s1, (11) after desalting s2, (12) desalting flowthrough s2. (s1: sample 1, s2: sample 2).

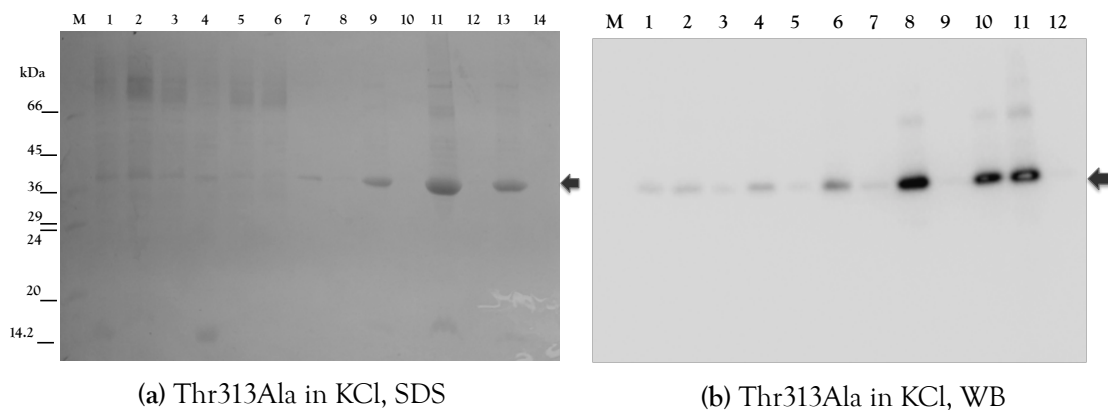


Figure 3.9: SDS-PAGE gel and western blotting of Mhp1 Thr313Ala purified in NM in absence of Na. (a) **SDS-PAGE:** (M) molecule weight marker, (1) membrane pre pre-solubilisation, (2) solubilisation, (3) supernatant and (4) insoluble pellet after centrifugation, (5) unbound flowthrough, (6) unbound flowthrough, (7) after wash in DDM, (8) after wash in NM, (9) concentrated after elution in NM, (10) flowthrough of of concentrator tube from (9), (11) concentrated after desalting, (12) flowthrough of concentration after desalting, (13) after desalting step, (14) empty, (b) **Western blot:** (M) molecular weight marker, (1) solubilisation, (2) supernatant and (3) insoluble pellet after ultracentrifugation, (4) after wash in DDM, (5) after wash in NM, (6) after elution in NM, (7) unbound flowthrough, (8) concentrated after elution, (9) flowthrough after concentration (8), (10) desalting sample application, (11) concentrated after desalting, (12) flowthrough after desalting.

Ligand-binding site Mhp1 mutations

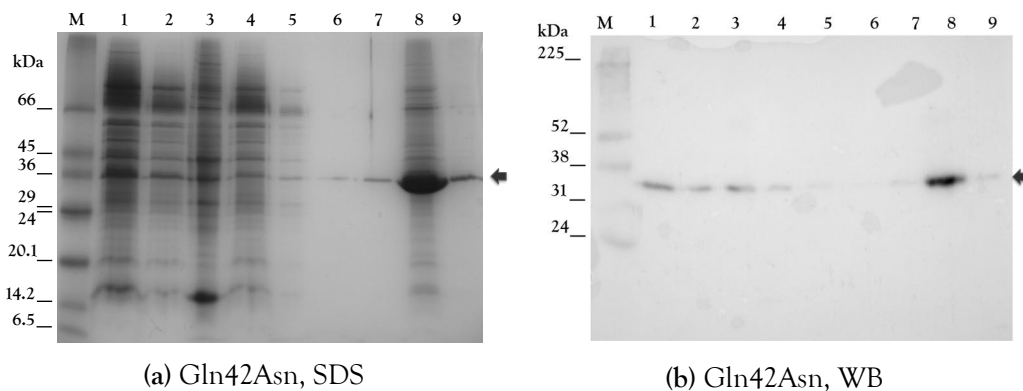


Figure 3.10: SDS-PAGE gel and Western Blot of the Mhp1 Gln42Asn in the ligand-binding site (a) **SDS-PAGE:** 15 μ g samples loaded as follows: (M) molecular weight marker, (1) solubilisation, (2) supernatant and (3) insoluble pellet after ultracentrifugation, (4) unbound flowthrough, (5) after wash in DDM, (6) after wash in NM, (7) after elution in NM, (8) concentrated after desalting, (9) residual on Ni-NTA resin beads, (b) **Western Blot:** (M) molecular weight marker, (1) solubilisation, (2) supernatant and (3) insoluble pellet after ultracentrifugation, (4) unbound flowthrough, (5) after wash in DDM, (6) after wash in NM, (7) after elution in NM, (8) concentrated after desalting, (9) residual on Ni-NTA resin beads.

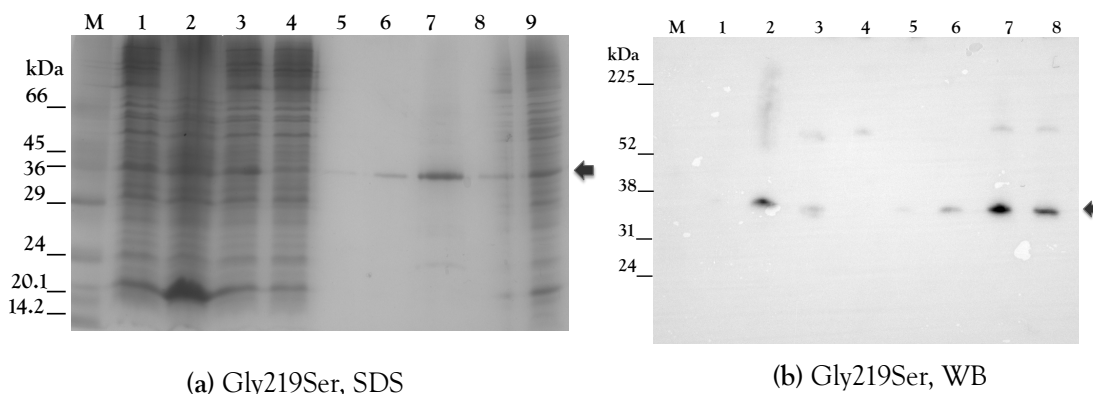


Figure 3.11: SDS-PAGE gel and Western Blot of the Mhp1 Gly219Ser in the ligand-binding site. (a) SDS-PAGE: (M) molecular weight marker, (1) supernatant and (2) insoluble pellet after ultracentrifugation, (3) incubation O/N, (4) flowthrough, (5) wash in NM, (6) elution in NM, (7) membranes prep of Gly219Ser-1, (8) membranes prep of Gly219Ser-2, **(b) Western Blot:** (M) molecular weight marker, (1) supernatant, and (2) insoluble pellet after ultracentrifugation, (3) incubation O/N, (4) Flowthrough, (5) after wash in NM, (6) after elution in NM, (7) membranes prep of Gly219Ser-2, (8) membranes prep of Gly219Ser-2.

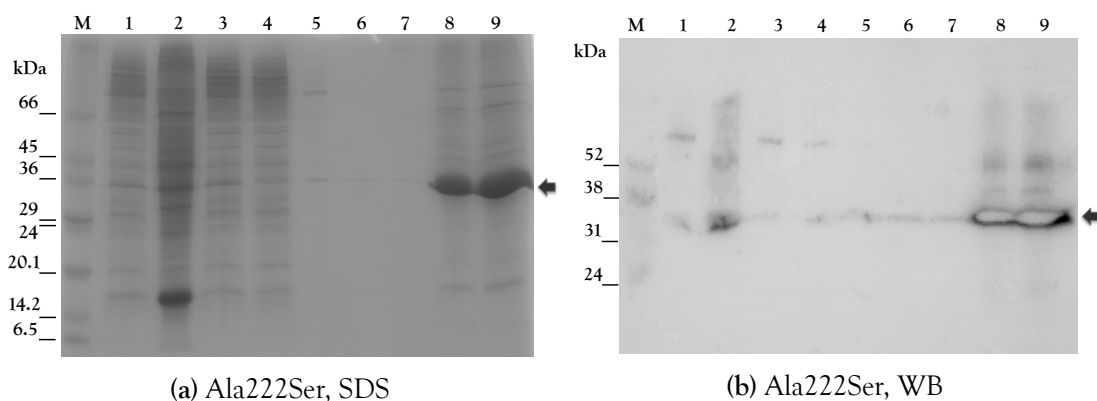


Figure 3.12: SDS-PAGE gel and Western Blot of Mhp1 Ile41Phe of the ligand-binding site. (a) SDS-PAGE: 15 μ g samples loaded as follows: (M) molecular weight marker, (1) supernatant and (3) insoluble pellet after ultracentrifugation, (3) incubation O/N, (4) flowthrough, (5) wash in DDM, (6) wash in NM, (7) elution in NM, (8) concentrated after desalting at 8 mg/ml, (9) concentrated after desalting at 10 mg/ml, **(b) Western Blot:** (M) molecular weight marker, (1) supernatant and (2) insoluble pellet after ultracentrifugation, (3) incubation O/N, (4) flowthrough, (5) wash in DDM, (6) wash in NM, (7) elution in NM, (8) concentrated after desalting at 8 mg/ml, (9) at 10 mg/ml.

The SDS-PAGE gels of the purified Mhp1 mutants show that the final step of the purification protocol produces more than one clear band, suggesting the protein is not highly pure. An extra step of size-exclusion chromatography did increase the purity and yield a monodisperse sample. However, no crystals formed from these samples, leading to the hypothesis that

these impurities might help the crystallisation process (personal communication, Prof. Peter Henderson, Dr. Anna Polyakova). Therefore, for the purpose of crystallisation and related biochemical experiments, no additional size exclusion chromatography was carried out.

3.2 Biophysical characterisation of Mhp1 variants for structural studies

3.2.1 Assessing the secondary structure and thermal stability of Mhp1 variants using circular dichroism

The structural integrity of freshly purified Mhp1 variants, and their thermal stabilities, were examined by circular dichroism using the Applied Photophysics Chirascan CD spectrometer (Section 2.6.1) from 190-260 nm prior to crystallisation trials.

Wild-type Mhp1 purified in NM

The CD spectra (Figure 3.13) indicate that freshly purified wild-type Mhp1 in NM is correctly folded. CD spectra produced characteristic spectra with predominantly alpha-helical structure as expected given the Mhp1 crystal structure (PDB code 2JLN). The characteristic spectrum has minima at 209 and 222 nm, but the maximum was a bit shifted to higher wavelengths within the range of 192 - 197 nm (Wallace & Janes 2003) as it is normal for membrane proteins (Section 1.5.4).

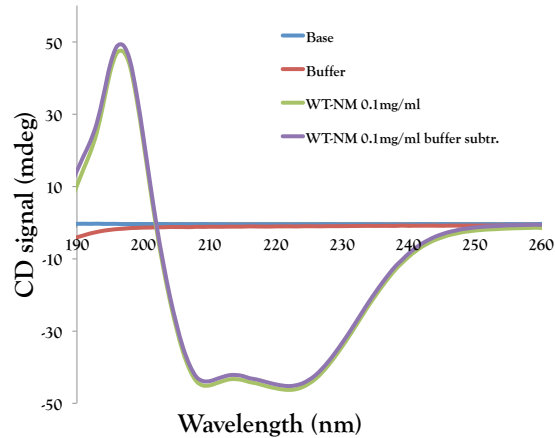


Figure 3.13: (a) Far-UV CD single spectrum of the purified wild-type Mhp1 in NM detergent. The CD scans were carried out at 20° C.

Thermal melts were also carried out between 20° C to 90° C as described in Section 2.6.1. Figure 3.14a shows the decay in elliptical signal while increasing the temperature due to loss of secondary structure. The thermal stability of the protein was assessed using the decrease in CD signal at 208 nm (Figure 3.14b) by measuring the temperature at which the protein is 50% unfolded (T_m or melting temperature) and/or determining the equilibrium constant for the folding-unfolding reaction. Figure 3.14b displays changes in ellipticity shape for the two minima at 208 nm and 222 nm. In this case there is not a single sigmoidal curve which indicates one transition from the folded to unfolded state. Instead there appear to be two stages to the unfolding process. The fact that the melting curve does not tail off at 90° C shows also that the protein is not completely unfolded at this temperature. The exact melting temperatures (T_m) could not be determined because the fully unfolded state is never reached. This is necessary, based on the equation for calculating the T_m (Greenfield 2006).

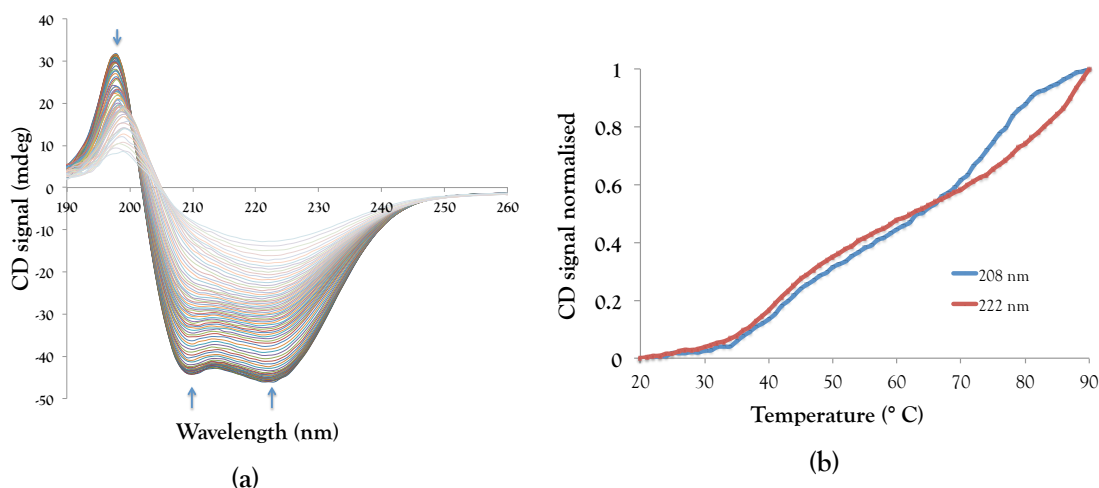


Figure 3.14: CD analysis to monitor the thermal stability of freshly purified wild-type Mhp1 purified in NM. (a) CD thermal scans from 190-260 nm completed from 20° C to 90° C, (b) The change in the CD signal for the two minima plotted against the temperature.

CD spectra for wild-type Mhp1 purified in DDM were also recorded, to understand whether the detergent potentially induces some sort of structural change. Interestingly, the CD signal at 208 nm indicates that wild-type Mhp1 purified in DDM is more stable than in NM (Figure 3.15). The graph shows only one transition stage due to the midpoint of the sigmoidal curve at around 55° C. At 90° C it is still not fully unfolded, so maybe a second transition would come if it were possible to reach higher temperatures compared to protein in NM.

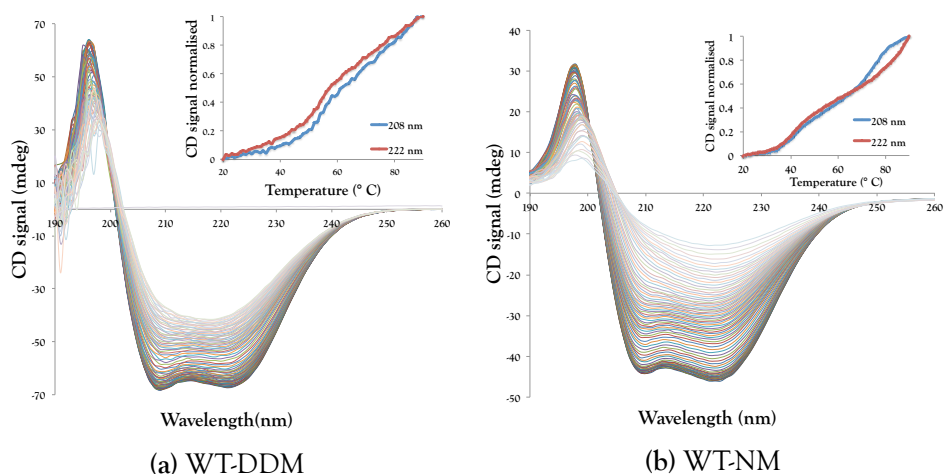


Figure 3.15: Comparison of CD thermal melts from wild-type Mhp1 purified in (a) DDM and in (b) NM detergent.

Mhp1 mutants purified in NM

CD spectra were collected for the Mhp1 mutants to determine the effects of single-point mutations in the sodium (Figure 3.16) and ligand (Figure 3.18) binding sites. Mhp1 mutants produced the characteristic spectra for α -helical proteins. Shifts of the maxima were also observed as in the wild-type Mhp1 in NM. A continuous ramping CD scan was also carried out on the Mhp1 mutants to determine whether the point mutations have any effect on the melting temperature, thermal stability and unfolding pattern of the proteins compared to the wild-type Mhp1. To compare the CD curves, the ellipticity data (θ) in millidegrees (mdeg) were normalised.

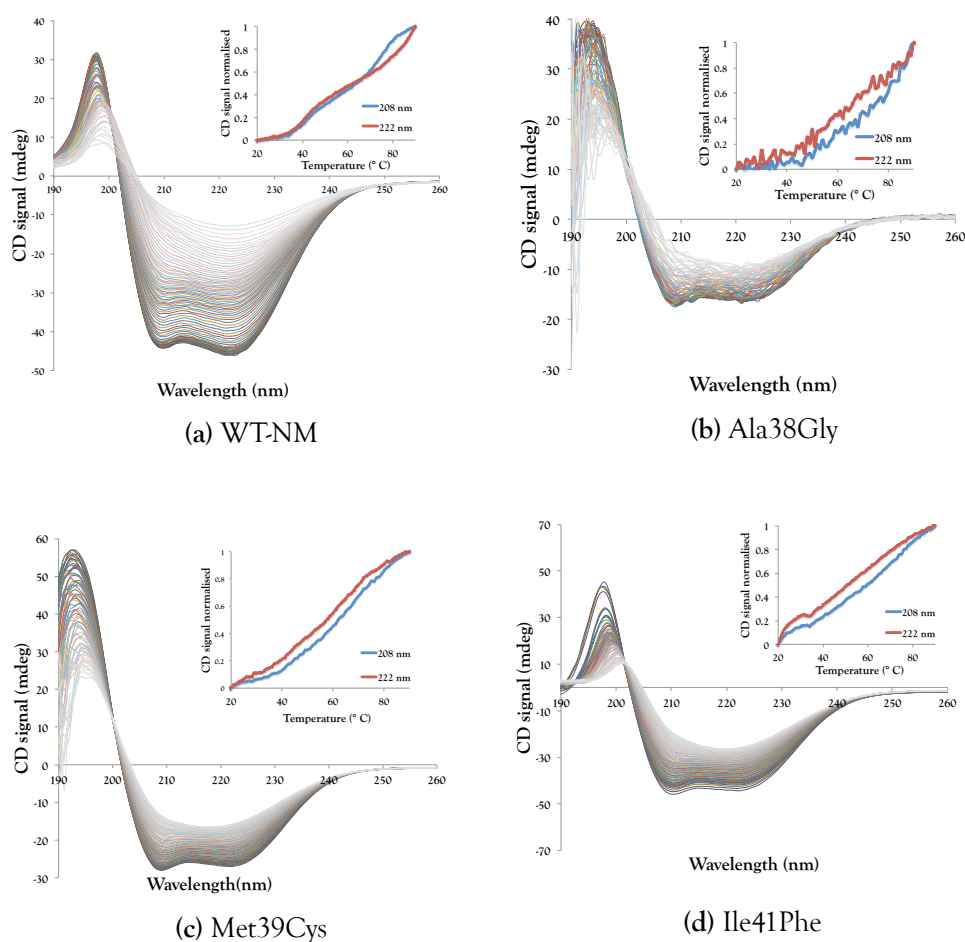
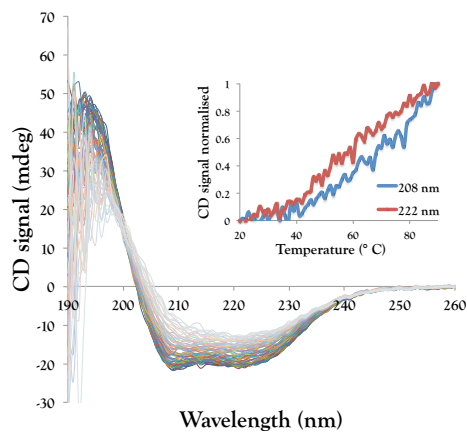


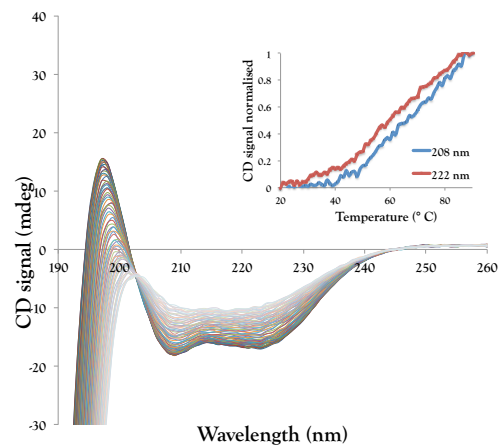
Figure 3.16: CD spectrum from thermal melt experiments from 20° C to 90° for the sodium-binding site mutations. CD signal plotted against temperature for Mhp1 wild-type and the sodium binding site mutations: (a) wild-type Mhp1, (b) Ala38Gly, (c) Met39Cys, (d) Ile41Phe.

The T_m of the mutants could not be obtained because proteins were stable enough not to unfold completely at the final 90° C temperature of the experiment. However, the graphs can qualitatively show relative stability as the two minima become indistinguishable at different temperatures. The data suggest the thermal stability of some of the Mhp1 mutations were increased, and these mutants have made Mhp1 more rigid. In contrast, Gly219Ser showed much lower stability. Mutant Gly219Ser reaches a fully unfolded state, and therefore the T_m can be calculated to 53.94° C.

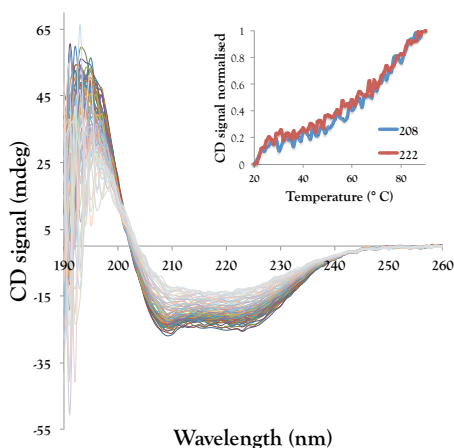
CD experiments were carried out for the mutants Ala309Asn and Thr313Ala in both presence and complete absence of sodium (Figure 3.17) producing the expected CD spectra indicating folded protein independent of the sodium presence/absence. The thermal stability of the protein was assessed using the decrease in CD signal at 208 nm as previously described. In the thermal melt graph the grey curves indicate unfolding states. T_m can be calculated for the mutants purified in absence of sodium up to 60.1 ° C for Ala309Asn and 62.9 ° C for Thr313Ala and an estimated can be made for those purified in presence of sodium (Table 3.13).



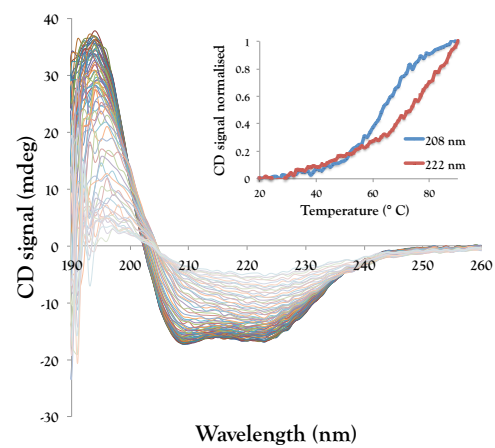
(a) Ala309Asn in NaCl



(b) Ala309Asn in KCl



(c) Thr313Ala in NaCl



(d) Thr313Ala in KCl

Figure 3.17: CD spectra and thermal melts of Ala309Asn and Thr313Ala in presence and absence of Na. CD signal plotted against temperature for Mhp1 wild-type Ala309Asn and Thr313Ala in (a) and (c) in presence of sodium and (b) and (d) in absence of sodium, respectively.

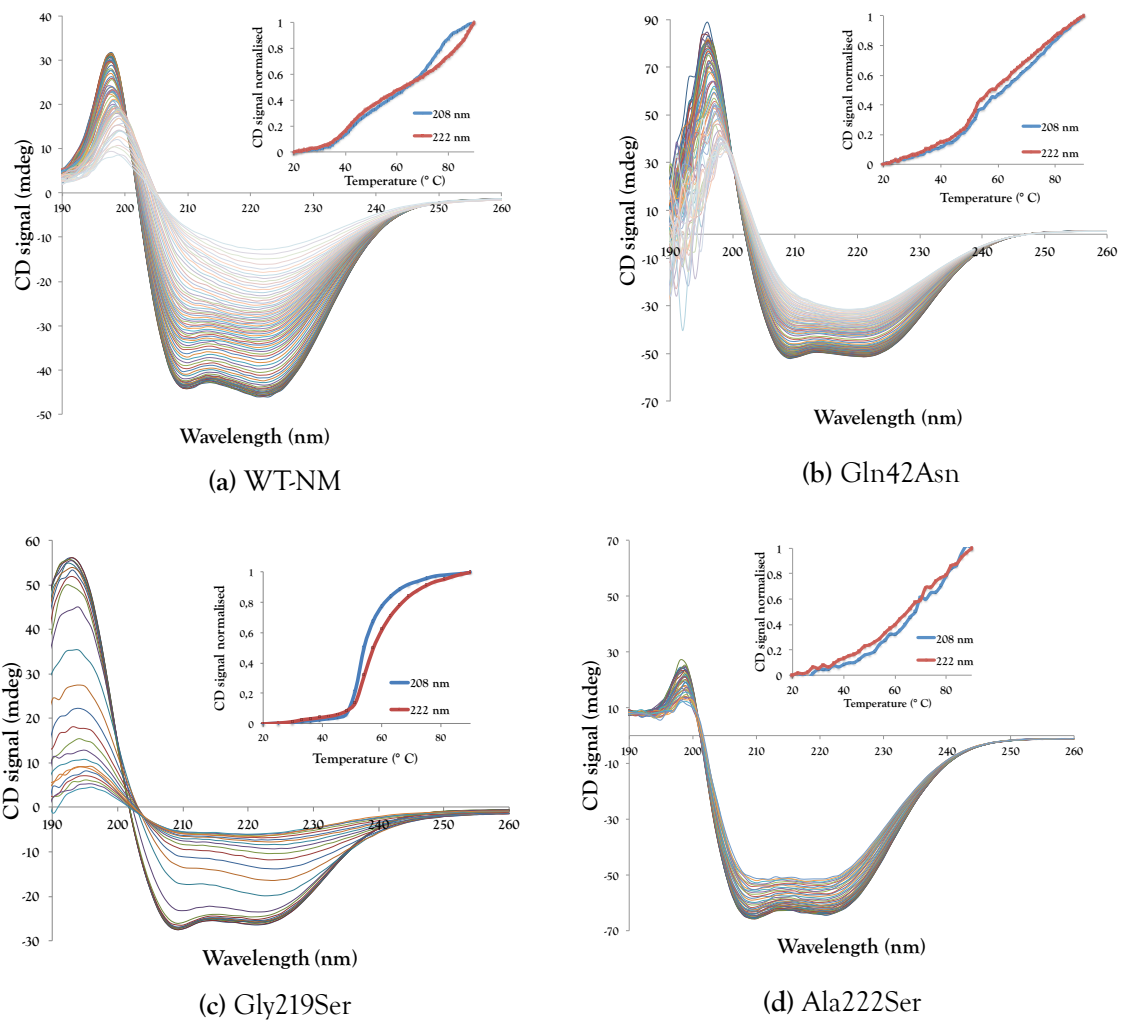


Figure 3.18: CD spectrum from thermal melt experiments from 20° C to 90° for the ligand-binding site mutations. CD signals plotted against temperature for the ligand-binding site mutations: (a) wild-type Mhp1, (b) Gln42Asn, (c) Gly219Ser (for which a larger increment of 3° C was used), (d) Ala222Ser.

In conclusion, CD spectra for the wild-type Mhp1 in NM and its mutants of both the sodium- and the ligand-binding sites indicated folded Mhp1 mutants with correct secondary structure. The single point mutations in the sodium- or ligand-binding sites did not lead to any major secondary structural changes in the protein according to their CD spectra. Thermostability studies showed the mutants were stable at higher temperature values for most of the Mhp1 mutants which might be an indication of an improved ability to form crystals.

3.2.2 Assessing ligand-binding behaviour of Mhp1 variants by steady-state tryptophan fluorescence quenching

Suzuki and Henderson (2006) suggested that the ligand binding ability of Mhp1 could be studied using a steady-state spectrophotofluorimetry assay as described in Sections 1.5.5 and 2.6.2. The ligand-binding ability of Mhp1 as well as its molecular specificity for hydantoin substrates had been previously demonstrated, and revealed that Mhp1 binds *L*-BH in a sodium-dependent manner (Weyand et al. 2008, Simmons et al. 2014).

Wild-type Mhp1 purified in NM

The *L*-BH ligand was added to the fresh wild-type Mhp1 protein purified in NM and fluorescence spectra were obtained as described in Section 2.6.2. The fluorescence quenching upon the addition of *L*-BH to the wild-type Mhp1 was measured in the presence and absence of sodium chloride at various concentrations. Figure 3.19 shows representative titration curves for preparations of wild-type Mhp1 and shows that the purified protein was functional in accordance with previous studies (Jackson 2012, Polyakova 2015), Table 3.2. The titrations confirmed that the binding of *L*-BH ligand to wild-type Mhp1 purified in NM was sodium-dependent as seen in previous studies, with the affinity of Mhp1 for *L*-BH alone (apparent K_d of 0.918 mM) increasing in the presence of 15 mM sodium chloride (apparent K_d of 0.1184 mM) (Weyand et al. 2008, Simmons et al. 2014).

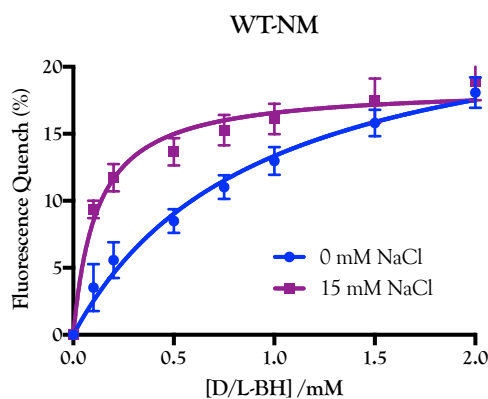


Figure 3.19: The tryptophan fluorescence quenching by L-BH in the wild-type Mhp1 purified in NM. Wild-type Mhp1 purified in NM was titrated with L-BH (0-2 mM) in the absence (blue line) and presence (purple line) of 15 mM NaCl at 18° C. Each data set displays the average of three repeats of each titration with error bars showing the standard error of the mean. Reference values are listed in Table 3.2.

The steady-state fluorescence L-BH ligand-binding studies reported here (Figure 3.19) indicate that L-BH can bind to purified wild-type Mhp1 in the absence of added sodium yet with lower affinity. By the addition of sodium the binding affinity of L-BH was increased dramatically. This lower affinity binding of L-BH in the absence of sodium indicates that some of the residues in the Mhp1 ligand-binding site may still be able to interact with the ligand even when sodium is apparently absent.

Table 3.2: Apparent Kd and Bmax values for wild-type Mhp1 purified in DDM and NM in comparison to previous reference values.

WT Mhp1	[Na ⁺] (mM)	Apparent Kd (mM)	Bmax (%)
DDM *	0	0.74±0.06	18.90±0.7
	15	0.04±0.001	21.80±0.1
DDM **	0	1.27±0.2	26.01±2.4
	15	0.04±0.01	23.64±0.3
NM **	0	3.66±0.8	22.93±3.7
	15	0.27±0.02	18.95±0.3

*Reference values from Jackson (2012); **Reference values from Polyakova (2015)

Wild-type Mhp1 purified in NM (WT-NM), for crystallisation purposes, exhibits lower ligand-binding affinity compared to wild-type Mhp1 purified DDM (WT-DDM) (Polyakova 2015). An explanation could be that the shorter detergent creates a smaller, tighter detergent corona surrounding the hydrophobic belt of the protein and the Mhp1-NM complex is more rigid than the Mhp1-DDM complex. Also, this smaller detergent corona could potentially leave a slightly larger part of the protein exposed to the solvent and, as a result, transient protein-protein interactions might occur and hamper the ligand binding. Yet, in high ligand concentrations binding still saturates. SEC-SAXS measurements on the two complexes has been carried out as described below (Section 4.1.1 4.1.3), a useful tool to assess transient oligomerisation, as well as to give more information on the shape and characteristics of the Mhp1 in complex with each detergent.

Mhp1 mutants purified in NM

The impact of the single point mutations on the ligand-binding ability of Mhp1 was studied by spectrophotofluorimetry (Sections 1.5.5 and 2.6.2) which provides a convenient means of assessing the sodium-dependent *L*-BH ligand binding to the Mhp1 variants. Previous studies have been conducted on the Mhp1 variants in DDM detergent (Jackson 2012). Here, the ligand binding to Mhp1 purified proteins in NM was investigated in order to examine their behaviour under the conditions that lead to crystallisation.

Ile 41 was proposed to play a key role in the binding of sodium in the outward and occluded states, and is mutated to phenylalanine in this position in the NCS-1 family members. The tryptophan fluorescence quenching assay for the sodium-binding site mutant Ile41Phe-NM showed that the binding of *L*-BH is clearly perturbed by the mutation to a larger aromatic side chain (Figure 3.21c, Table 3.3). The reduced ligand-binding activity appears to be restored to that of wild-type by inclusion of 140 mM NaCl. In order for the protein to accommodate the Phe 41 residue in the place of isoleucine, the protein will be forced to change conformation due to this unwieldy side chain. Figure 3.20 illustrates the neighbouring phenylalanine residues

Phe 267 (TMH 7) and Phe 305 (TMH 8) next to the Phe 41 (TMH 1) where potential steric interactions might occur. As a result of these unfavourable interactions the sodium-binding site might be disturbed by a movement of discontinuous TMH 1 in relation to TMH 8 and consequently the *L*-BH ligand-binding may be impaired at low sodium but overcome by higher sodium concentrations.

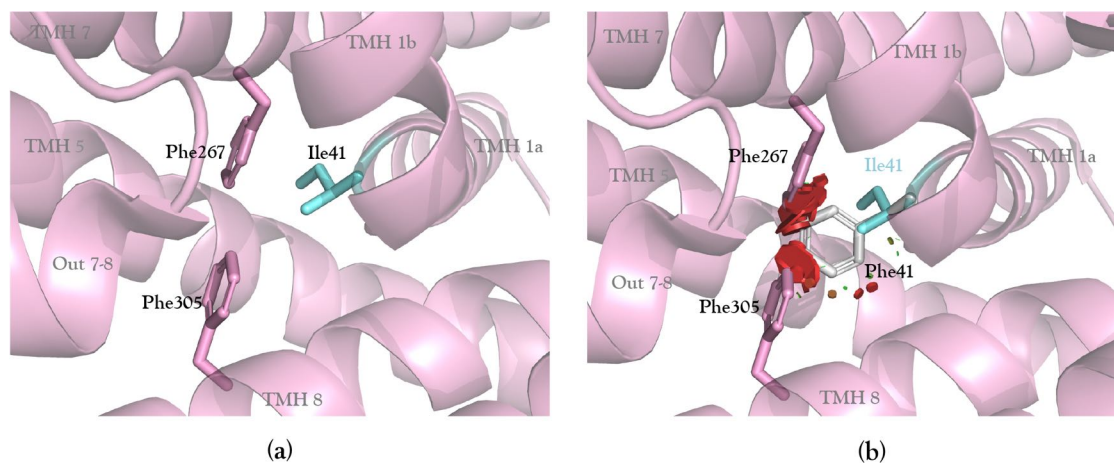


Figure 3.20: Mhp1 mutation Ile41Phe. (a) Helices are depicted as cartoon representation (pink) and the residues Phe 267 (pink) and Phe 305 (pink) that are in close proximity to Ile 41 (cyan) are in stick representation, (b) The possible steric interactions (red) after the mutation of Ile41Phe (coloured in white) with neighbouring Phe 267, and Phe 305. The reported Mhp1 structure bound *L*-BH (PDB code 4D1B) has been used here for preparation of this picture using PyMOL Molecular Graphics System, Schrödinger, LLC.

In contrast, the Met39Cys-NM mutant bound *L*-BH in a much less sodium-dependent manner than the wild-type Mhp1 or the rest of the mutants. As seen in Table 3.3, the binding affinity is significantly hindered by the mutation but is not as successfully restored by adding sodium. Although Met 39 does not directly coordinate the sodium or the ligand-binding site, its side chain is exposed on the surface of the ligand-binding cavity (Figure 3.1). The disruption of ligand binding as a result of the shorter amino acid, Cys 39, implies that Met 39 may interact with the hydantoin ligand while it approaches the cavity or somehow stabilises the binding site.

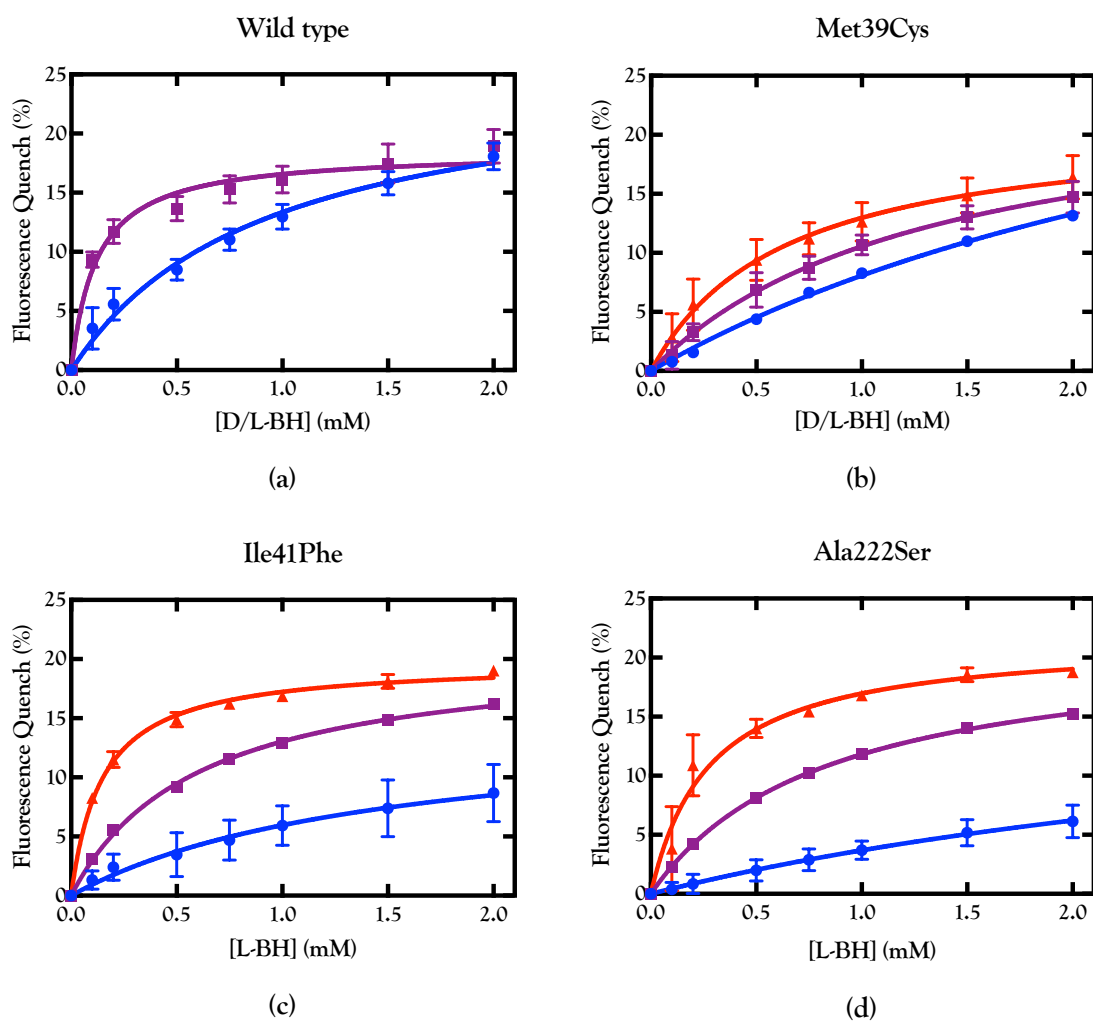


Figure 3.21: Fluorescence quench curves for binding of L-BH to Mhp1 containing mutations in the binding sites. Sodium binding site: (b) Met39Cys-NM, (c) Ile41Phe-NM, ligand-binding site: (d) Ala222Ser-NM. Sodium chloride at 0 mM (blue), 15 mM purple, and 140 mM (red).

Previous reports for both Ile41Phe-DDM and Met39Cys-DDM mutations purified in DDM showed a restored activity with 15 mM NaCl (Jackson 2012). However, the results here show that in NM the mutants Ile41Phe and Met39Cys need the addition of 140 mM sodium to reach a similar binding affinity to that in DDM.

The ligand-binding site was probed by studying the mutant Ala222Ser. Of all the mutations, this reduced L-BH binding the most (Figure 3.21d, Table 3.3). The presence of 15 mM sodium could partially restore the sodium-dependent binding of L-BH but in 140 mM sodium the bind-

ing affinity has not reached that of the wild-type Mhp1 on 15 mM sodium. The L-BH binding in the Ala222Ser mutant purified in NM was significantly impaired compared to the mutant purified in DDM (Jackson 2012), but after the addition of 15 mM sodium, similar behaviour was observed for both Ala222Ser purified in DDM and in NM. Changes in the binding affinity are more surprising for this mutation, as it is not clear why the mutation of Ala 222 to serine should have any such consequence, given its position in the binding site. Therefore it was important to bring this mutant forward to structural studies.

Table 3.3: L-BH binding in Mhp1 mutants purified in NM and in DDM.

Mhp1 variant	[Na ⁺] (mM)	Apparent Kd (mM)	Bmax (%)	Apparent Kd (mM)	Bmax (%)
purified in		NM		DDM*	
Wild type Mhp1	0	0.92 ± 0.17	25.57 ± 2.2	0.74 ± 0.063	18.90 ± 0.70
	15	0.12 ± 0.02	18.53 ± 0.64	0.03 ± 0.01	21.80 ± 0.10
Met39Cys	0	3.66 ± 0.72	37.68 ± 5.32	0.84 ± 0.11	14.4 ± 0.9
	15	1.32 ± 0.25	24.53 ± 2.46	0.12 ± 0.02	16.9 ± 0.2
	140	0.63 ± 0.15	21.15 ± 1.88	-	-
Ile41Phe	0	1.49 ± 0.85	14.84 ± 4.6	1.6 ± 0.86	10.7 ± 3.2
	15	0.6 ± 0.02	20.86 ± 0.23	0.29 ± 0.004	19.9 ± 0.7
	140	0.15 ± 0.01	19.78 ± 0.28	-	-
Ala222Ser	0	4.4 ± 3.2	19.8 ± 10.8	2.8 ± 0.7	22.3 ± 3.9
	15	0.8 ± 0.02	21.6 ± 0.2	0.18 ± 0.02	17.3 ± 0.4
	140	0.28 ± 0.06	21.66 ± 1.4	-	-

*Values for Mhp1 variants purified in DDM obtained previously by Jackson, Ph.D. 2012

3.2.3 Assessing ligand-binding behaviour of wild-type Mhp1 in presence and absence of sodium

The binding of hydantoin-ligands to the purified wild-type Mhp1 has been shown, by spectrophotofluorimetry, to be in sodium-dependent manner (Weyand et al. 2008, Simmons et al. 2014). Studies of cations (K^+ , Li^+ , Rb^+ , Cs^+) and anions (Cl^- , CO_3^{2-} , SO_4^{2-} , PO_4^{2-}) do not promote the binding of *L*-BH to purified wild-type Mhp1 (Ma, 2010), supporting the idea of a sodium-linked ligand-binding transport mechanism. The question arises of how the sodium promotes ligand binding. It has been proposed that Mhp1 in solution is in an equilibrium between outward-open and inward-open forms (Calabrese et al. 2017, Kazmier et al. 2014). The sodium binding stabilises the outward-facing open conformation of Mhp1 in which there is an intact sodium and substrate binding site and hence promotes the ligand binding (Weyand et al. 2011). Calabrese et al. (2017) suggests that the binding of sodium may cause conformational changes and the side chains responsible for the ligand-binding reorient so they can interact with the ligand and create a higher affinity ligand-binding site.

In order to study the binding activity of the wild-type Mhp1 without having sodium as the driving force, the tryptophan fluorescence quenching assay was repeated but with potassium chloride instead of sodium chloride. In order to achieve the complete absence of sodium, the purification of wild-type Mhp1 in NM was also performed in potassium chloride prior to spectrophotofluorimetry.

Figure 3.22 demonstrates that in case of purified wild-type Mhp1-NM in presence of potassium, the *L*-BH bound to a much lower extent at 0 mM potassium chloride (Figure 3.22b) compared to 0 mM sodium chloride (Figure 3.22b). The titration curves also show that the *L*-BH binding is unaffected by adding higher potassium chloride concentrations in the wild-type Mhp1-NM purified in potassium, unlike the same experiments performed with sodium chloride. Therefore the synergistic enhancement of the ligand binding seen with increasing

sodium was abolished in the case of potassium. Therefore, the assay suggests wild-type Mhp1 in presence of potassium remains in a state of low ligand binding affinity as there is no response to the addition of potassium. In the presence of the potassium the curves of different concentrations (Figure 3.22b) seem almost imposed. However the K_d and B_{max} values do not agree. Mhp1 protein in the presence of 140 mM KCl was precipitated at the end of the measurements and this could explain the high values of K_d and B_{max} . The CD of Mhp1 mutants purified in potassium also altered lower T_m compare to the same mutants purified in the presence of sodium (Figure 3.17). Thus suggests that the presence of potassium has an effect on Mhp1. But further work is needed to better understand this.

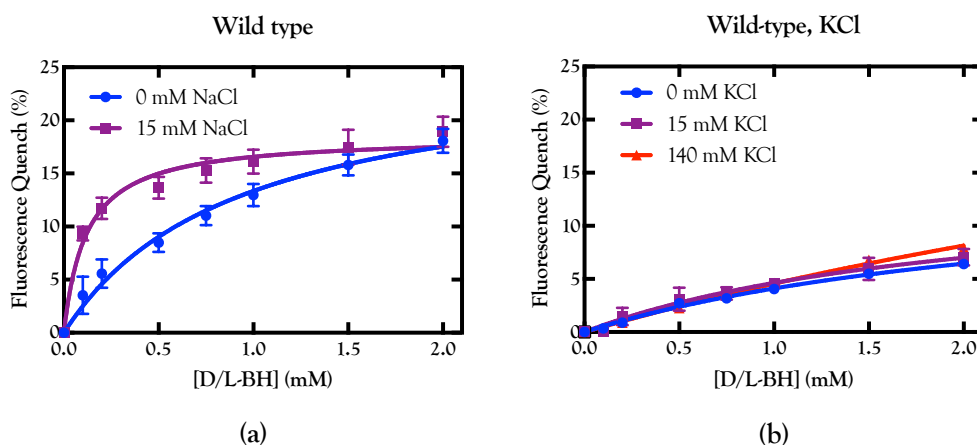


Figure 3.22: Binding of L-BH in wild-type Mhp1 purified in NM and either sodium or potassium. The figure shows the fluorescence quenching during addition of L-BH in the presence of an increasing sodium chloride concentration (a) and in absence of sodium but in the presence of an increasing potassium chloride concentration (b). Buffer compositions were the same apart from the sodium chloride was replaced by the same concentrations of potassium. Titrations were performed in the presence of 0 mM (blue), 15 mM (purple), 140 mM (red) sodium chloride (a) or potassium chloride (b). The error bars display the the standard error of the mean from three replicates of each titration.

Table 3.4: *L*-BH binding in Mhp1 mutants purified in NM in presence and absence of NaCl.

wild-type Mhp1, NM	(mM)	Apparent Kd (mM)	Bmax (%)
NaCl	0	0.91±0.2	25.57±2.2
	15	0.12±0.02	18.53±0.7
KCl	0	2.63±0.6	14.92±2.2
	15	2.10±0.8	14.36±3.3
	140	7.23±2.6	37.59±11.1

3.2.4 Spectroscopic data of Mhp1 mutants towards observing an inward-open conformation

The three conformational states of Mhp1 observed crystallographically are proposed to represent different conformations along the alternating access mechanism (Section 1.4.2). Multiple structures have been solved by X-ray crystallography in the outward open form, and in the occluded state bound to various hydantoin ligands. However, only one crystal structure has been obtained to be in the inward-open, where a seleno-L-methionine derivatised Mhp1 was prepared and crystallised under more basic conditions compared to the outward-open structures (Table 3.5). The inward-open or inward-closed states or intermediate states were and still are the most difficult structures to obtain and the reasons for this vary.

The only reported Mhp1 structure in an inward-open conformation shows that the sodium-binding site is disrupted, which was also supported with MD simulations on the inward-facing-occluded state (Section 1.4.2). Could the mechanistic disruption of the sodium binding site by single-point mutations stabilise the Mhp1 in an inward-open conformation?

Surprisingly, two mutations in the sodium-binding site that coordinate the sodium directly have shown different behaviour to the rest of the sodium-binding mutations. Biochemical and functional studies by our collaborators in the University of Leeds (Henderson Lab) indicate specifically that the Ala309Asn and Thr313Ala mutations purified in DDM detergent have *L*-BH binding almost completely independent of the sodium concentration (Jackson 2012)

(Figure 3.23), and also that they adopt an inward-facing conformation (Ivanova et al unpublished data).

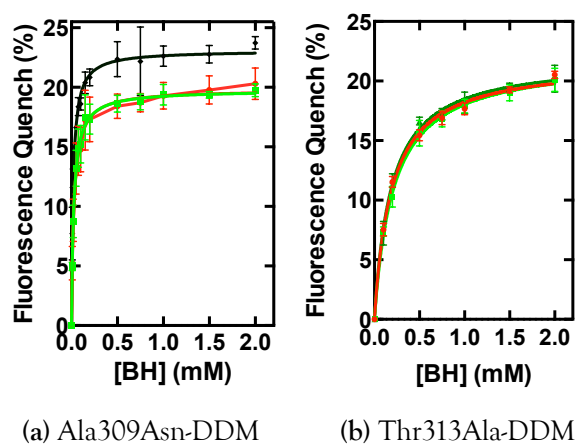


Figure 3.23: The fluorescence change upon the addition of L-BH to the Ala309Asn-DDM and Thr313Ala-DDM mutants obtained by collaborators (Jackson 2012) and reproduced here with their permission. L-BH was titrated 0-2 mM in 0 mM (red), 15 mM (light green) and 140 mM (dark green) NaCl.

A more detailed look into the sodium-binding site reveals that the residues Ala309 and Thr313 participate directly in coordinating the sodium. Mutating those residues would be useful to probe the effect on the conformation of Mhp1 of a potentially disrupted sodium-binding site.

Thus, it would be useful to obtain crystal structures in order to see the alteration to the sodium-binding site in the absence of sodium (Section 3.3.2). These mutants were purified in presence of sodium (Figures 3.6 and 3.8) and in presence of potassium (Figures 3.7, 3.9). CD analysis of the secondary structure and thermal stability of the mutants (Figure 3.17) were performed to assess the structural integrity and melting point of these mutants. Unfortunately, the functional analysis of the mutants Ala309Asn and Thr313Ala purified in NM was not performed that would assess the influence of potassium chloride as well as the new NM detergent on ligand binding. The structural studies of those mutants purified in NM detergent in both sodium and potassium conditions are presenting later in this thesis (Sections 3.3 and 4.2.2).

3.3 Crystallisation of Mhp1 variants

For the crystallisation of wild-type Mhp1 and its mutants, the previously published conditions were used as described in Sections 2.2.4 and 2.2.5. These published crystallisation conditions of Mhp1 provide an excellent starting point for crystallisation trials. However, further optimisation was still required to obtain well diffracting crystals from pure and stable protein since the purification and crystallisation procedures were to be carried out under different environmental conditions in the University of Hamburg.

The previously obtained three different conformations of Mhp1 based on crystal structures were obtained under two different crystallisation conditions presented in Table 3.5 giving rise to two different crystal forms in which protein adopts different conformations.

Table 3.5: Crystallisation conditions of wild-type Mhp1 reported structures in three different conformational states.

Mhp1 conformations	Outward-open	Occluded	Inward-open
PDB code	2JLN	4D1A, 4D1B 4D1C, 4D1D	2X79
Detergent	NM	NM	NM
Buffer	100 mM NaPO ₄ pH 7	100 mM NaPO ₄ pH 7	100 mM Bicine pH 9
NaCl (mM)	100	100	100
PEG ₃₀₀ (v/v %)	27-35	27-35	24-28
Reservoir solution	300µl	300µl	400µl
Ratio	1µl:1µl	1µl:1µl	1.5µl:1.5µl
Temperature (° C)	18	18	4
Crystal morphology	Needle-shaped	Needle-shaped	Hexagonal
Space group	P2 ₁ 2 ₁ 2 ₁	P2 ₁ 2 ₁ 2 ₁	P6 ₁
Crystal form	Orthorhombic	Orthorhombic	Hexagonal
Unit cell dimensions (Å, °)	a=79.7, b=109.1 c=113.8, α=β=γ=90	a=95.6, b=106.7, c=107.8 α=β=γ=90	a=b=173.9, c=74.5 α=β=90, γ=120

The majority of the previous reported structures adopt outward-facing (substrate-free) and outward-occluded (substrate-bound) conformations were from needle-shaped crystals, crystallised in an orthorhombic space group $P2_12_12_1$ (Weyand et al. 2008, Simmons et al. 2014). By contrast, the only Mhp1 structure in the inward-open (substrate-free) conformation was crystallised in a hexagonal crystal lattice, space group $P6_1$ under more basic conditions, with a visible hexagonal morphology (Shimamura et al. 2010).

A new crystallisation protocol for Mhp1 developed by Polyakova (2015), using a streaking method to mix the mother liquor into the protein droplet was used for all Mhp1 variants (wild-type and mutants) in order to improve crystal size and to obtain better diffracting crystals. This crystallisation of Mhp1 is based on a counter diffusion technique (Section 1.5.2), mimicking that performed by the commercial kits (e.g. CrystalHarpTM, CrystalFormerTM). The mother liquor droplet was pipetted next to the protein droplet while applying a streaking motion with the pipette tip dispensing it through the protein droplet, forming a temporary gradient which then lets the protein and the mother liquor slowly diffuse into each other. This gradient also generates a crystal size gradient from showers of smaller crystals at the one end of the elongated droplet to fewer, thicker and well-separated needle-shaped crystals at the other end.

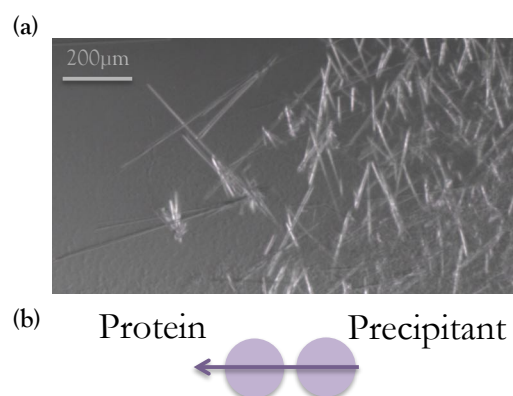


Figure 3.24: Wild-type Mhp1 crystals forming after applying the streaking method. A gradient in crystal sizes (a) is formed by applying the streaking method (b).

Crystals of freshly purified wild-type Mhp1 in NM were successfully reproduced in the orthorhombic form using the published crystallisation conditions, after applying the streaking method, typically yielding 100-1000 μm long needle-shaped crystals (Figure 3.24). The conditions were set up in 24-well plates sealed with vacuum grease and the crystals appeared overnight and were then allowed to grow for 2-3 weeks. The crystals obtained from the initial crystallisation trials were harvested in-house at the crystallisation room with a controlled temperature of 24° C for screening at the synchrotron. Sample mounts were nylon loops, MiTeGen MicroMeshes™ and elongated MiTeGen MicroLoops™ which are designed to support long rod-shaped crystals. The crystals were flash-cooled by directly plunging them into liquid nitrogen and no additional cryo-protection was used, following the published conditions (Weyand et al. 2008, Shimamura et al. 2008, 2010, Simmons et al. 2014).

3.3.1 Reproduction and optimisation of previously published crystallisation conditions for outward form

The Mhp1 mutants were also crystallised using the same conditions as the wild-type Mhp1 (Table 3.5). Co-crystallisation was also carried out with the four hydantoin ligands synthesised for the purposes of this project (Sections 2.2.5 and 2.8). Crystals were obtained for all Mhp1 mutants (Figure 3.25 and 3.26) in the sodium-binding (Ala38Gly, Met39Cys, Ile41Phe, Ala309Asn, Thr313Ala) as well as in the ligand-binding site (Gln42Asn, Gly219Ser, Ala222Ser) either in their apo form or in complex with various hydantoin ligands (Table 3.6).

In contrast to the rest of the Mhp1 mutants, Ile41Phe yielded crystals of cubic shape and thin plates or squares were obtained instead of the usual needle-shaped Mhp1 crystals. These cubic-shaped crystals had very low resolution diffraction, thus no data were collected. For Gly219Ser very thin and fragile short needles overlapping each other prevented successful harvesting for X-ray crystallography. This was also the case for Gln42Asn, despite an increase in needle length.

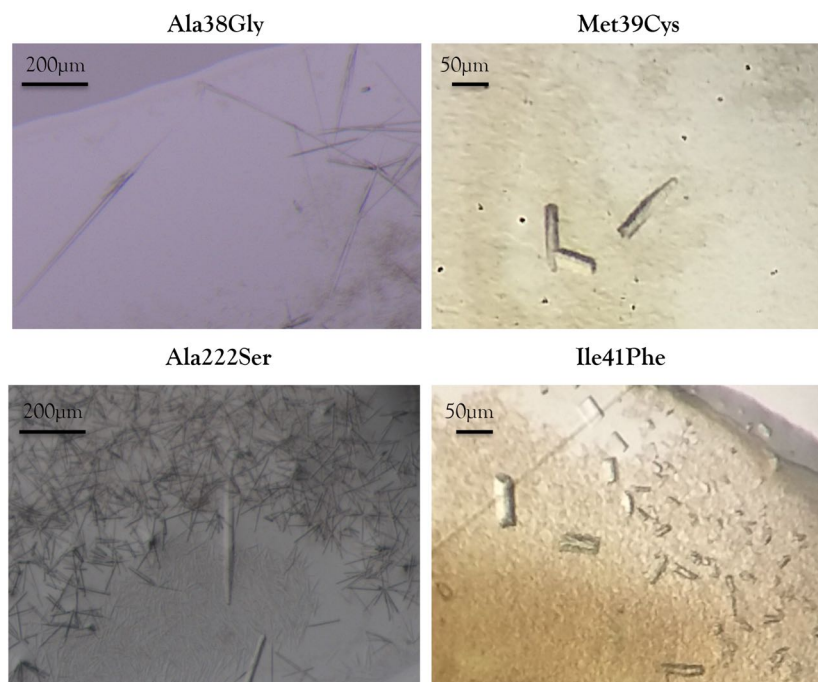


Figure 3.25: Crystals from Mhp1 mutants a) Ala38Gly, b) Met39Cys, c) Ile41Phe, d) Ala222Ser. Mhp1 crystals are long, thin and needle-shaped. Ile41Phe is the only mutant forming small blocks. The gradient from showers of small crystals to bigger and separated ones appears for all mutants. Crystal pictures were taken in different microscopes.

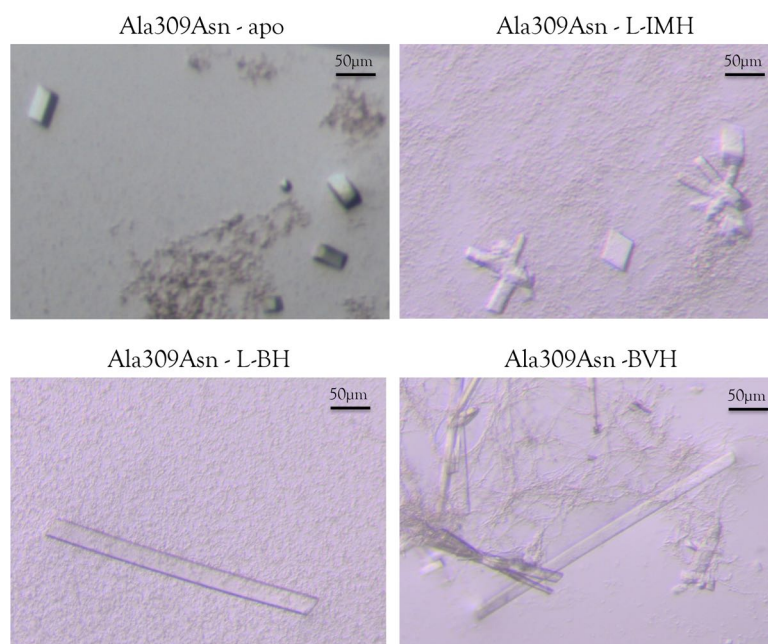


Figure 3.26: Crystallisation of Ala309Asn in orthorhombic conditions. Block-shaped crystals formed without co-crystallisation. In the presence of L-IMH, block-shaped crystals also formed. Co-crystallisation in the presence of L-BH and BVH ligands, formed rod-shaped crystals. The exact conditions are the following: **Ala309Asn - no co-crystallisation** 100 mM sodium phosphate pH 7, 150 mM NaCl, 29% v/v PEG₃₀₀, **Ala309Asn - L-BH** 100 mM sodium phosphate pH 7, 50 mM NaCl, 27% v/v PEG₃₀₀, **Ala309Asn - L-IMH** 100 mM sodium phosphate pH 7, 150 mM NaCl, 31% v/v PEG₃₀₀, **Ala309Asn - BVH** 100 mM sodium phosphate pH 7, 150 mM NaCl, 29% v/v PEG₃₀₀, ration 1µl:1µl.

Crystals of the Ala309Asn mutant in the orthorhombic crystal form conditions (100 mM Sodium phosphate pH7, 50-200 mM NaCl, 27-25% v/v PEG₃₀₀) gave rise to a crystals in a new block shape (Figure 3.26) compared to the rest of the Mhp1 mutants giving needle-shaped or rod-shaped crystals (Figure 3.25). Co-crystallisation of these mutants with the ligand *L*-IMH gave crystals of similar shape to the apo crystals. On the other hand, the co-crystallisation with either *L*-BH or BVH ligands yielded rod-shaped crystals which were longer and wider (300-400 μ m) compared to the rest of the Mhp1 mutants.

Table 3.6: Summary of crystals obtained for Mhp1 variants in outward crystal conditions.

Mhp1 Mutation	Ligand	Crystals obtained	Diffraction (\AA)
wild-type in DDM	yes	No	-
wild-type in NM*	apo	Needles	3.9 \AA
Sodium binding site			
Ala38Gly	apo	Needles	3.19 \AA
	<i>L</i> -BH	Needles	6 \AA
	<i>L</i> -IMH	Needle-shaped, long	6 \AA
	BVH	Long needle	8 \AA
Met39Cys	<i>L</i> -BH	Needles	3.29 \AA
Ile41Phe	apo	Small squares	weak diffraction
Ala309Asn	apo	Needles and blocks	weak diffraction
	<i>L</i> -IMH	Blocks	very weak diffraction
	<i>L</i> -BH	Needles	7 \AA
	BVH	Needles	7 \AA
Thr313Ala	apo	Needles	10 \AA
Ligand-binding site			
Gln42Asn	apo	Very thin needles	No diffraction
Gly219Ser	apo	Very thin needles	No diffraction
Ala222Ser	apo	Needle-shape	3.89 \AA
	<i>L</i> -BH	Needle shape	3.39 \AA
	<i>L</i> -IMH	Needle shape	3.91 \AA

* All Mhp1 mutants were purified in NM detergent

Crystal fragments of mutants that were harvested and flash-cooled in liquid nitrogen were screened at synchrotrons DLS (Didcot, UK), ESRF (European synchrotron radiation facility, Grenoble, France) and PETRAIII (DESY, Hamburg, DE) in various beamlines. Data collection from various crystals resulted in diffraction ranging from 20-3.3 Å. The diffraction was very poor in most of the screened crystals with split spots and/or multiple overlapping lattices. However, data collection for the mutants Ala38Gly, Ala222Ser and Met39Cys at a reasonable resolution was possible. The solved structures from those data sets collected are presented in the following sections.

3.3.2 Reproduction and optimisation of previously published crystallisation conditions towards an inward-form

Functional assays on Mhp1 mutants Ala309Asn and Thr313Ala have shown (Figure 3.23) that these two mutations in the sodium-binding site adopt an low-affinity inward-open conformation. The only Mhp1 structure solved in the inward-open conformation used more basic crystallisation condition (Table 3.5: Hexagonal conditions: 100 mM Bicine-NaOH pH9, 100 mM NaCl, 24-28% v/v PEG₃₀₀, ratio 1.5 µl:1.5 µl, at 4° C, yielding a hexagonal crystal lattice in space group P6₁ and crystals of hexagonal morphology (Shimamura et al. 2010).

Previous tryptophan fluorescence assays of a Gln42Asn mutant suggested it may adopt an inward conformation. However, Polyakova (2015) showed that this mutant gave rise to crystals of the usual needle-shape morphology. The protein structure was also found to be in the outward form. The protein had been purified in high sodium conditions. Because of this, it even when this protein was transferred to low sodium conditions, the outward form was present. It is possible this was an artefact arising during purification. Therefore, in order to avoid this the Mhp1 mutants Ala309Asn and Thr313Ala were purified in high sodium/no potassium and in no sodium/high potassium conditions (Section 3.23). By substituting sodium salt with the equivalent concentration of potassium salt, the ionic strength of the crystallisation mother liquor were preserved. The pH of the buffer Bicine was adjusted with NaOH or KOH accord-

ingly. For each of these, they were also crystallised under the hexagonal or the orthorhombic conditions. The crystallisation screens carried out at 4° C did not produce crystals, whereas those which were left to incubate at 18° C did thus the future crystallisation was carried out only at 18° C even for the hexagonal crystallisation conditions.

Crystallisation of Ala309Asn mutant in hexagonal conditions

Crystals of Ala309Asn in a hexagonal crystal form were successfully produced, yielding hexagonal tube-shaped crystals both in presence of sodium and potassium hexagonal crystallisation conditions (Figure 3.27). Also, needle-shaped crystals (900 µm) similar to the crystals of the previously reported structures were formed in the same drops as the hexagonal crystals (50 µm). The crystals appeared after one day and grew to full size within a week. Cryo-protectant solution was not added to the crystals prior to data collection because crystals were growing in over 30% PEG₃₀₀ which was considered enough to provide cryo-protection alone. These were directly flash-cooled in liquid nitrogen.

This alteration of the crystallisation conditions to more basic crystallisation conditions did improve the ability of the mutant Ala309Asn to crystallise in the hexagonal space group form (see below), and gave rise to reproducible crystals of visible hexagonal morphology within three days at 18° C. Surprisingly, hexagonal crystals of Ala309Asn were formed in both presence of sodium and potassium, leading to the presumption that the salt might not be the crucial variable affecting the crystal morphology.

However, the purification in complete absence of sodium and presence of potassium did not yield crystals for the Ala309Asn mutant. Wild-type Mhp1 in presence of potassium does not yield crystals either. Tryptophan fluorescence data of wild-type Mhp1 shows that the ligand binding affinity is reduced. Tryptophan fluorescence for these mutants are needed to investigate whether the ligand binding affinity is diminished as well as the in wild-type Mhp1 (in presence of potassium Figure 3.22). CD of the mutant Ala309Asn in the presence and absence

of sodium showed that there is not a big change in the secondary structure of this mutant due to the presence of potassium.

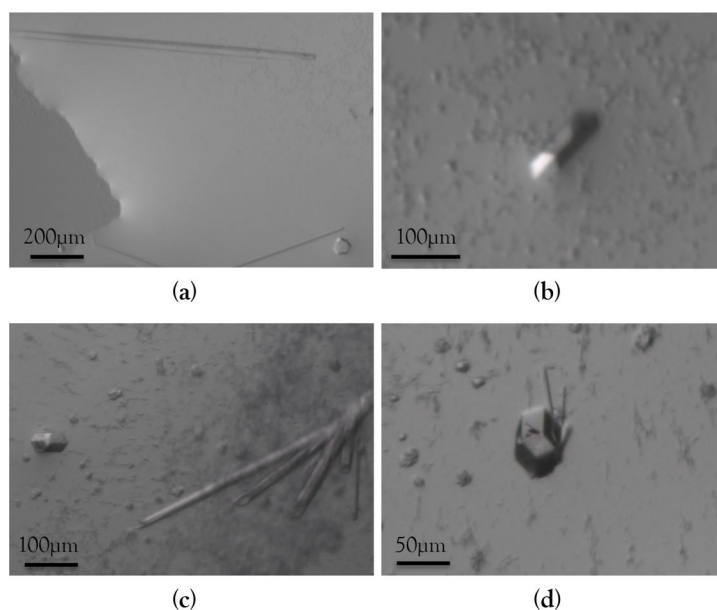


Figure 3.27: Mhp1 mutant Ala309Asn crystals obtained under hexagonal conditions in both presence and absence of sodium. Long needle rod-shaped crystals were formed as in the orthorhombic conditions and also well-shaped hexagonal tubes. **a)** 100 mM Bicine-NaOH pH 9, 50 mM NaCl, 30% v/v PEG₃₀₀, **b)** 100 mM Bicine-NaOH pH 9, 150 mM NaCl, 32% v/v PEG₃₀₀, **c), d)** 100 mM Bicine-KOH pH 9, 120 mM KCl, 30% v/v PEG₃₀₀.

Table 3.7: Crystallisation of Ala309Asn Mhp1 mutant in hexagonal conditions

Crystallisation conditions	Crystals obtained (apo or with ligand)	Crystal form	Diffraction (Å)
Purification in presence of Na			
Bicine-NaOH, pH 9	apo	Needles	14 Å
	apo	Hexagonal	12 Å
Bicine-KOH, pH 9	apo	Needles shape	8.6 Å, P622
	apo	Hexagonal	10 Å P622
	L-BH	Hexagonal	Very weak
Purification in presence of K			
Bicine-NaOH, pH9	no crystals formed		
Bicine-KOH, pH9	no crystals formed		

Data collection from flash-cooled crystals was performed at 100 K at a wavelength of 0.9677 Å. X-ray diffraction data were collected on beamline MASSIF-3 (ID30A-3) of the ESRF in brackets, and use ESRF here] using an Eiger-4M detector. Image data were autoprocessed during beamtime, but further processed post-beamtime using the xdsapp (Kabsch 2010). Hexagonal crystals diffracted to 8.6 Å with cell dimensions $a=b=146.42$ Å, $c=96.49$ Å, $\alpha=\beta=90^\circ$, $\gamma=120^\circ$, in putative space group P622. However, the resolution was not high enough to continue with molecular replacement and structure solution.

Co-crystallisation with hydantoin ligands yielded hexagonal crystals which also diffracted to lower resolution. Post-crystallisation optimisation is needed in the future to obtain better diffracting crystals. For example, Polyakova (2015) found that dehydration of crystals using the humidity controller HC1 device (Sanchez-Weatherby et al. 2009) improved the diffraction quality. The additive 15-crown-5 ether would be a potential useful modification to the crystallisation conditions, since it has been demonstrated that crown-ethers can promote crystallisation by stabilising inter-molecular interactions (Lee et al. 2014).

In the hexagonal condition crystallisation drops of the Ala309Asn mutant (purified in sodium), small crystals of rhombohedral morphology appeared (Figure 3.28) after a period of one month. These diffracted up to 2.5 Å resolution and belong to space group H3, with unit cell dimensions $a=b=145.54$, $c=514.6$ (Å), $\alpha=\beta=90^\circ$, $\gamma=120^\circ$. After no solution could be found with any Mhp1 model at this high resolution, suspicions were reused that these crystals could be from a contaminant.

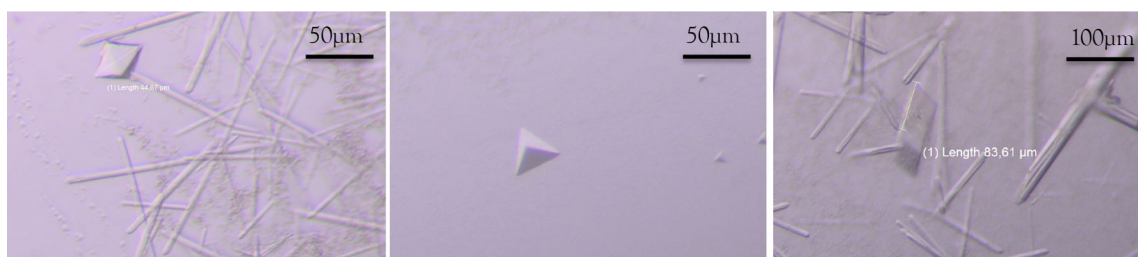


Figure 3.28: Additional crystal morphologies appeared in crystallisation drops of Ala309Asn under hexagonal conditions. Crystals were product of contaminant.

The common contaminant AcrB contamination showed an exact match for the unit cell and visible crystal morphology. Molecular replacement using AcrB confirmed that these crystals were AcrB. Acriflavine resistance protein B (AcrB), multidrug efflux pump (Edward et al. 2003), is a common contaminant of membrane proteins expressed in *E.coli* and subsequently purified by immobilised metal affinity chromatography (IMAC), due to a rich histidine cluster at the C-terminus that binds to the column (Veesler et al. 2008). It has a molecular mass of 114 kDa but it has been reported to migrate at 110 kDa (Glover et al. 2011). Although there is no obvious band corresponding to AcrB at approximately 110 kDa, this does not mean that AcrB is not present in the sample (Veesler et al. 2008, Glover et al. 2011). Thus, the *E.coli* AcrB was crystallised in previously unreported conditions according to (Veesler et al. 2008) using PEG 300 as the precipitating agent in basic buffer conditions 100 mM Bicine pH 9 (NaOH or KOH). In the present case, estimated AcrB concentration in Mhp1-Ala309Asn purified sample was about 0.1 mg/ml. In conclusion, AcrB can be crystallised from very low concentrations and is a major risk in membrane-protein crystallisation when overexpression is carried out in *E. coli* and purification involves an IMAC step.

Crystallisation of Thr313Ala mutant in hexagonal conditions

The Thr313Ala mutant was crystallised using the the orthorhombic and, to obtain the inward form, the hexagonal conditions as well. In contrast to Ala309Asn crystals, the Thr313Ala mutant yielded only the usual needle-shaped crystals and not hexagonal crystals. These long needle-shaped crystals of Thr313Ala were considerably thinner than the crystals obtained for both wild-type Mhp1 and the rest of the mutants presented in this thesis.

The Thr313Ala mutant purified in presence of potassium also crystallised as needle-shaped crystals. The cation also seems not to affect the crystal morphology, as in the case of Ala309Asn. Crystals were very fragile and difficult to harvest. This fragility is a likely reason for the poor quality of the diffraction obtained from those crystals. Co-crystallisation was also tried with

the hydantoin ligands, however, the ligands prevent crystal formation. Fragments of harvested crystals were flash-cooled in liquid nitrogen.

Table 3.8: Crystals of Thr313Ala in hexagonal conditions

Crystallisation conditions	Crystals obtained (apo or with ligand)	Crystal form	Diffraction (Å)
Purification and crystallisation in presence of Na			
Bicine-NaOH, pH 9	apo	needles	8 Å
Bicine-KOH, pH 9	apo	needles	20 Å
Purification and crystallisation in presence of K			
Bicine-NaOH, pH 9	apo	very thin needles	
Bicine-KOH, pH 9	apo	needles	20 Å

Data were collected on beamlines MASSIF-3 of ESRF and on P14 of PETRAIII. However, no usable diffraction data were collected from these crystals as they diffracted to too low a resolution. In many cases, multiple lattices were obtained with resolution limits not exceeding 8 Å.

3.4 Mhp1 mutant structural studies by X-ray crystallography

3.4.1 X-ray crystal structure of Mhp1 Ala38Gly mutant

Residue Ala 38 is one of the residues which directly coordinates the sodium ion (Weyand et al. 2008, Simmons et al. 2014). The mutation Ala38Gly was created based on the other family members of the NCS-1 family for which this residue was glycine (as in PuI and CodB) or serine (yeast transporters). The main chain carbonyl of residue 38 could be accommodated in the Mhp1 reported crystal structures without any unfavourable interactions and it is proposed to still coordinate the sodium ion. Therefore, the mutation Ala38Gly in the sodium binding site was unlikely to have any impact on the Mhp1 mechanism since both alanine and glycine residues are found in this position in homologues.

Crystals of Ala38Gly mutant (Figure 3.29) were obtained using the orthorhombic crystallisation conditions (Table 3.5). Needle-shaped crystals of Ala38Gly appeared in one day. Systematic crystal screening with X-ray diffraction revealed that the older the crystal is, the higher the resolution it diffracts to. The crystal from which the data were collected was 9 months old. During this time, being stored in a ventilated crystal tray incubator, it is very likely that the droplet was slowly becoming dehydrated, therefore giving rise to a similar effect as during controlled dehydration. Crystals were harvested and flash-cooled by direct plunging into liquid nitrogen without adding cryo-protectant buffer.

The X-ray diffraction data were collected at 100 K at a wavelength of 0.98 Å on beamline ID29 at the ESRF using detector Pilatus-6M-F. Two datasets were collected from two different positions along the same crystal to avoid radiation damage. The detector-to-sample distance was 614.23 mm, producing a possible resolution of 2.99 Å at the edge and 2.13 Å in the corner.

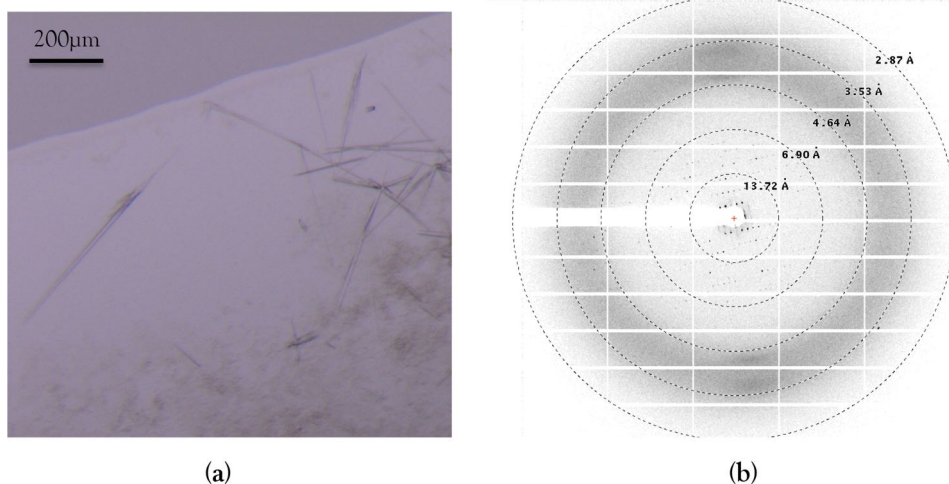


Figure 3.29: Needle shape crystals from Ala38Gly-apo and the corresponding diffraction pattern. (a) Needle shape crystals from Ala38Gly-apo mutant obtained in 100 mM sodium phosphate pH 7, 50 mM NaCl, 32% v/v PEG₃₀₀ crystallisation conditions. (b) Diffraction pattern of the Ala38Gly-apo crystal.

The diffraction patterns of mutant Ala38Gly (Figure 3.29 b) were re-processed post-beamtime with XDS (Kabsch 2010) excluding the ice rings (Thorn et al. 2017) at resolutions 2.4 Å, 3.4 Å, 3.6 Å, 3.8 Å. A ring around the beamstop was also excluded by cutting the low resolution limit at 37 Å (Figure 3.30).

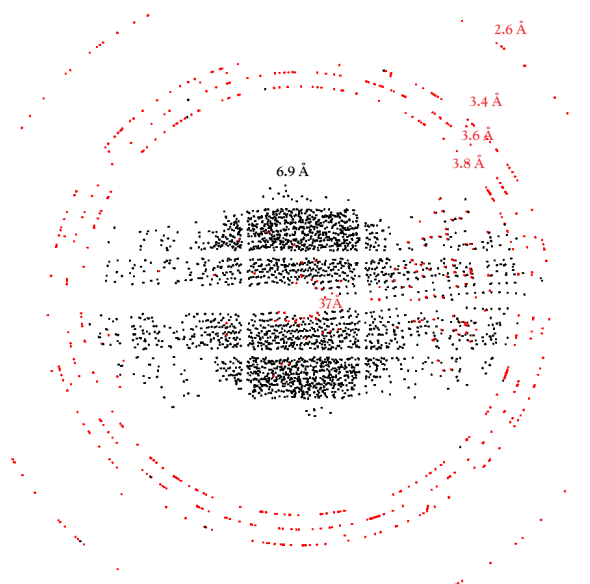


Figure 3.30: Anisotropic data of Ala38Gly-apo after indexing (IDXREF) step in XDS processing. Diffraction data were highly anisotropic with 6.9 Å and 3.6 Å resolution limits in different directions. Ice rings are depicted here in red ring an higher resolution and a detergent ring also in red is observed at 37 Å.

Pointless (Evans 2006) was used to merge the two datasets. Data were determined to be in space group $P2_12_12$ and the unit cell dimensions were refined to the values $a = 75.3$, $b = 107.3$, $c = 114.3$ Å, $\alpha = \beta = \gamma = 90^\circ$. The unit cell parameters were similar to the previous reported crystal structures therefore the same R_{free} were kept. Based on the previous crystallographic studies, wild-type Mhp1 and its mutants are in space group $P2_12_12_1$. The program initially did not recognise all the screw axes. The screw axes are calculated based on the systematic absences. In case that some data are missing (being masked due to the beamstop), or not recorded due to anisotropy, the software can find no evidence of screw axes and it gives a space group missing one or more screw axes e.g. $P2_12_12$. Thus, the space group was changed to the correct one using POINTLESS. The diffraction data were highly anisotropic (Figure 3.30). Therefore, the merged data from the two datasets were submitted to the STARANISO Server to define the anisotropic diffraction cut-off based on locally-averaged value of $I/\sigma(I)$ rather than its spherical average (French & Wilson 1978, Karplus & Diederichs 2012). An isotropic diffraction cut-off on anisotropic data results in losing the high-resolution data, while keeping unwanted noise in the weakly diffraction directions.

The structure was solved by molecular replacement with MOLREP (Vagin & Teplyakov 2010, Lebedev et al. 2008). From the three different published conformations of the Mhp1 protein; outward-open (2JLN), occluded with various ligands (4D1A (L-IMH), 4D1B (L-BH), 4D1C (BVH), 4D1D (L-NMH)) and inward-open (2X79), only the outward-open and the inward-open conformations were tested as search models because no ligands were added in the crystallisation mother liquor. The bound ions and metals of those models were removed prior to using them in molecular replacement. The TFZ score from the molecular replacement was 13.8 which indicates a good structure solution. The best initial R-factors were obtained from the outward-open structure ($R_{work}/R_{free} = 28$ and 30%), while R factors using the inward form were very high (52 and 52%), an indication that the Ala38Gly-*apo* adopted predominantly an outward-facing conformation in the crystal. The resulting solutions were submitted initially to rigid-body fitted model refinement and later with more degrees of freedom.

The outward-open model was further refined using *refmac5* (Murshudov et al. 2011) which gave R-factors 24 and 29 %. At this resolution limit is better to consider fewer parameters during refinement since enough information is not provided by those data to support all the restraints. Refinement was run using Jelly Body restraints that kept the R-factor gap reasonable. After manual model rebuilding and further jelly-body refinement the resulting statistics are reasonable for crystals of a membrane protein (Table 3.9).

Ala38Gly followed the same crystal packing as the outward-open structure (PDB code 2JLN). The Ala38Gly molecule forms interactions with one symmetry mate in the outer part of the molecule (outward-facing), and one in the inner part (outward-facing) of the molecule (yellow circles in Figure 3.31).

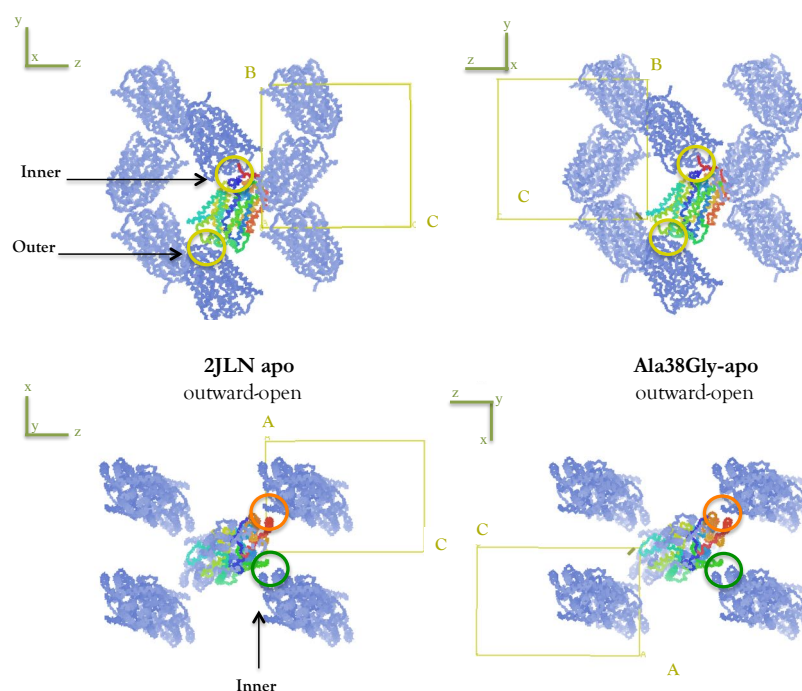


Figure 3.31: Crystal packing of Ala38Gly-apo structure. Picture shows the crystal packing of Mhp1 in outward-open conformation (PDB code 2JLN) (rainbow colours, Ca- backbone) and the crystal packing of Ala38Gly-apo (rainbow colours, Ca- backbone) determined also in outward-open conformation. The yellow rectangular represents the unit cell. The yellow circles display the interactions of Mhp1 with the symmetric mates in the same chain, while the orange and green circles display the interactions among residues of symmetric mates from neighbouring chains. Picture was prepared by COOT (Emsley & Cowtan 2004).

Molecules forming head-to-tail interactions, following a pattern like zig-zag, where the chains are running in the direction of the *b*-axis. The residues that are involved in these interactions are Arg 10, Ser 11, Arg 21, Arg 332, Thr335, Lys 337, Arg 396, Arg 461, Arg 469 and the Glu 280, Glu289, Met 200, Asp 191. In the inner part of the molecule additional crystal contacts are made tail-to-tail between Mhp1 and two symmetry mates from neighbouring chains in the *a*-plane and *c*-plane (orange and green circles Figure 3.31), involving the residues Trp 404, Lys450, Trp451, Trp447 and Asp 237, Glu 243, Lys 247, Arg 251. Both interactions head-to-tail and tail-to-tail were observed in outward-open conformation of wild-type Mhp1 (PDB code 2JLN) structure.

Table 3.9: Data collection and refinement statistics for the structure of Ala38Gly-apo Mhp1 variant. For each appropriate column, the number in brackets represents the information for the outer shell only.

Mhp1-A38G-apo	
Data collection	ESRF, ID29
Wavelength (keV/Å)	12.666/ 0.98
Resolution (Å)	45.46 - 3.19 (3.54 - 3.19)
Space group	P 2 ₁ 2 ₁ 2 ₁
Unit cell dimensions (Å, °)	a = 75.3, b = 106.9, c = 114.0, $\alpha = \beta = \gamma = 90$
Multiplicity	11.9 (8.5)
Completeness	
- spherical (%)	59.4 (11.2)
- ellipsoidal (%)	92.3 (72.3)
$\langle I/\sigma(I) \rangle$	6.1 (1.1)
Rmerge (%)	0.278 (1.975)
Rmeas (%)	0.292 (2.099)
Rp.i.m. (%)	0.086 (0.692)
CC _{1/2}	0.997 (0.541)
Refinement statistics	
Measured reflections	111697 (4022)
Unique reflections	9418 (471)
R _{work} (%)	23.48 (28.00)
R _{free} (%)	28.64 (30.30)
R.M.S.D.	
- bond (Å)	0.006
- angles (°)	1.539
Ramachandran	
- outliers (%)	2.17
- favoured (%)	85.03
Rotamer outliers (%)	3.49
Average B factors, all atoms (Å ²)	54.0

The crystal structure of Ala38Gly-apo solved at 3.19 Å was informative enough to distinguish that it adopted an outward-facing conformation as it was expected due to ligand absence. In Section 1.4.2 it was discussed that TMH 10 moves towards occluding the ligand to change the conformation from outward-facing to outward-occluded. A cross-refinement of the final refined Ala38Gly-apo model against the structure factors of the occluded conformation (PDB code 4D1B) was run in order to confirm the Ala38Gly-apo conformation. Figure 3.32 displays the superimposition of the TMH 10 in the final refined model (Ala38Gly-apo in outward-open structure, green bonds) and in a model of the outward-occluded structure (PDB code 4D1B, magenta bonds). Cross-refinement resulted in positive difference density for the TMH 10 of Ala38Gly-apo and not for the TMH 10 of a closed conformation (4D1B). TMH 11 also has similar behaviour to TMH 10. Thus, Ala38Gly-apo adopts an outward-open conformation.

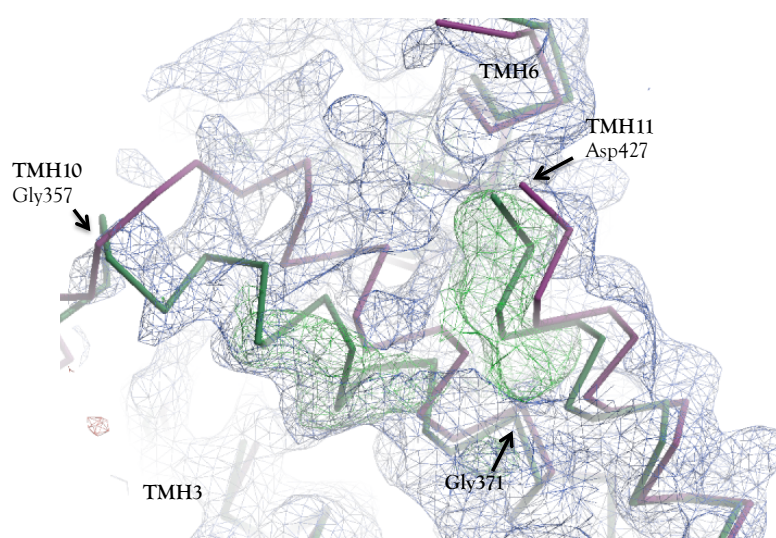


Figure 3.32: Cross-refinement to confirm the conformation of the Ala38Gly-apo state showing a segment of the external thin gate TMH 10. The $2mF_o-dF_c$ electron density is in blue, contoured at 1 rmsd for the Ala38Gly outward open structure (green bonds). The green positive F_o-F_c density at 3 rmsd appears after cross-refining the model to the outward occluded structure factors, the corresponding model for which is shown in magenta bonds. All the positive density follows the green structure, showing that this structure is outward-open. Picture were prepared by COOT (Emsley & Cowtan 2004) and rendered by Raster3D (Merritt & Bacon 1997).

Interestingly, in an overview of the Ala38Gly in apo state positive difference electron density was observed (green mesh in Figure 3.33) in a more extended region in the core of the protein. Around the unwound segment of the TMH 1 and the neighbouring TMH8 is the location

where the sodium binding site is accommodated. The positive density might be a hint that the TMH 1 tries to fold itself back to a complete α -helix possibly due to the ligand absence. However, the data do not have high enough resolution to investigate further. Several rounds of modelling and refinement were not adequate to fit the model to the data in a better way.

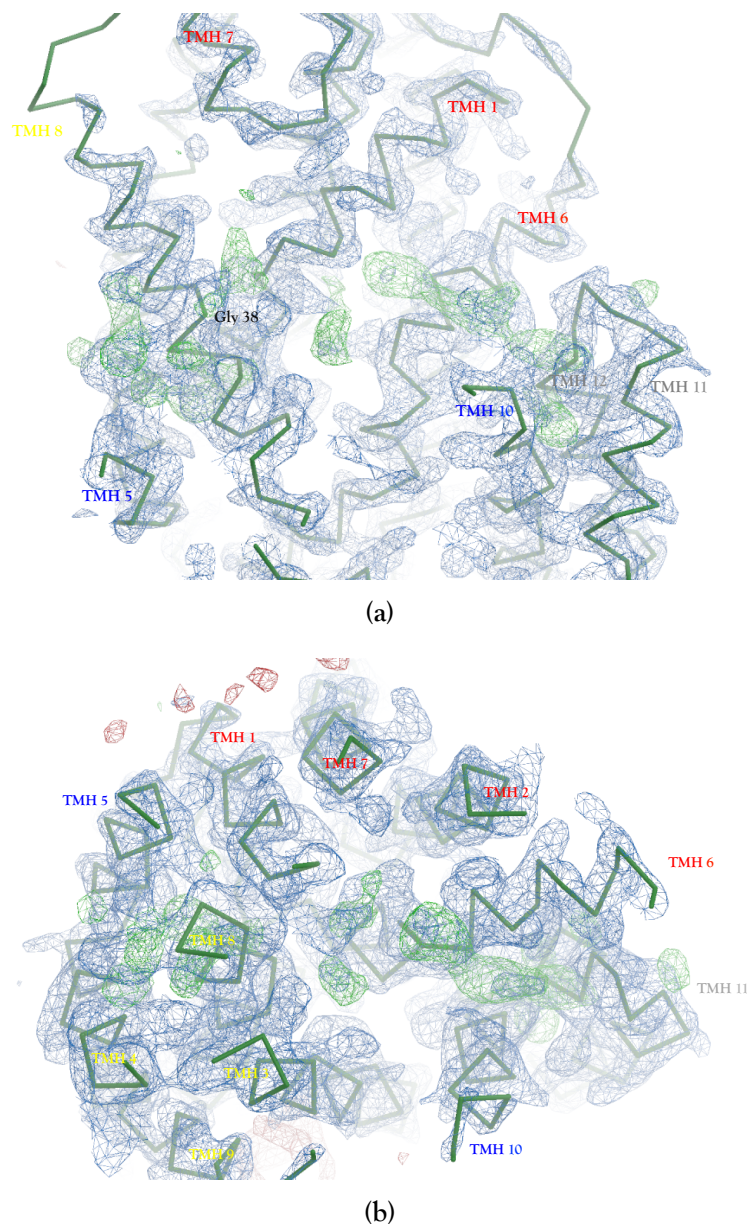


Figure 3.33: The structure of Ala38Gly in apo state. The figure displays the final refined model of Mhp1 mutant Ala38Gly a Ca-backbone representation in green colour. $2mF_o-dF_c$ map as blue mesh and positive difference density as green mesh in the core of the protein. Picture was prepared by COOT (Emsley & Cowtan 2004) and rendered by Raster3D (Merritt & Bacon 1997).

Free energies for binding of Na⁺ in Mhp1 wild-type and its mutants were calculated by Michelle Sahai and Peter Henderson using molecular dynamics simulations. Surprisingly, Ala38Gly appears to have lost its binding capacity for Na⁺ while remaining able to achieve the outward-facing conformation just as easily as wild-type from the NEM-MS data (Figure 3.34). Thus, these MD observations as well as NEM-labelling mass spectrometry appear to agree with the crystal structure of Ala38Gly solved here in an outward-open conformation.

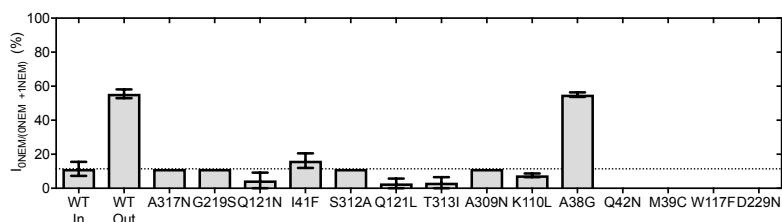


Figure 3.34: NEM-Mass spectrometry measurements in Mhp1 variants in DDM. Most mutations diminish the proportion of outward-facing conformation of Mhp1 in solution, except for the mutant Ala38Gly. (Reproduced here with kindly permission of Sahai and Henderson, unpublished data.)

The binding ability of *L*-BH to the Ala38Gly and *L*-IMH uptake assays were previously carried out only in DDM detergent (Jackson 2012). The Ala38Gly mutation had little impact on *L*-BH binding in the presence or absence of sodium in DDM, showed by the fluorescence changes promoted by *L*-BH in the steady-state spectrophotofluorimetry measurements. This is presumably because the position of the carbonyl groups in the peptide chain that engage with the cation was unaltered by this residue change. However, there was a reduction in the level of *L*-IMH uptake, approximately 20% lower than the corresponding wild-type (Jackson 2012). This reduction was unexpected due to the *L*-BH binding results being comparable to the wild-type values. These contradictory results are difficult to rationalise as the residue Gly38 was predicted to be accommodated in Mhp1 in a structurally favourable manner and the main chain is still able to coordinate the sodium ion. These assays need to be conducted in presence of NM detergent to be comparable with the crystal structure and to investigate whether this outward form is the real conformation in solution or whether it is promoted during crystal formation.

3.4.2 X-ray crystal structure of the Mhp1 mutant Met39Cys in complex with L-BH

In the intact sodium-binding site of Mhp1 the residues that directly coordinate the sodium are Ala 38 (TMH 1), Ile 41 (TMH 1), Ala 309(TMH 8), Ser 312(TMh 8) Thr 313(TMh 8) (Weyand et al. 2008, Shimamura et al. 2010, Simmons et al. 2014)) (Figure 3.1). The residue Met 39 (TMH 1) neither coordinates the sodium nor the ligand. However, Met 39 forms a hydrogen bond between its main chain carbonyl and the hydroxyl side chain of the Thr 313 residue. This interaction between Met 39 (TMH 1) and Thr 313 (TMH 8) may be important in orienting helix 8 (TMH 8) and the extended peptide region of discontinuous helix 1 (TMH 1). In addition, the side chain of Met 39 is exposed on the surface of the ligand-binding cavity where it may interact with the ligand as it approaches the ligand-binding site (Weyand et al. 2011). Finally, Met 39 is also in close proximity to the Ala 38 and Ile 41 sodium-binding site residues. To assess the role of Met 39, this was mutated to cysteine, a shorter residue, found in this position among some family members i.e. Pucl (Weyand et al. 2008).

Crystallisation of the Met39Cys mutant resulted in needle-shaped crystals. However, these crystals were very fragile and melted some days that they appeared. They also melted a few minutes after the lid of the crystallisation well had been opened for harvesting the crystals. Thus, harvesting had to be very fast and not many crystals survived. Crystals were obtained for Met39Cys only in complex with L-BH in orthorhombic conditions. Three datasets were collected for this mutant from three different crystals at Diamond Light Source (UK) at beamline I24. The anisotropic diffraction data of this mutant were re-processed post-beamtime with XDS as described for the Mhp1 mutant Ala38Gly-*apo* crystal structure in Section 3.4.1. The structure of the mutant Met39Cys in complex with L-BH presented here was determined from crystal 1, at a resolution of 3.29 Å and solved in space group $P2_12_12_1$ with unit cell dimensions $a = 90.0$, $b = 106.6$, $c = 112.9$ and $\alpha = \beta = \gamma = 90^\circ$ (Table 3.10). Crystal 3 came from the same drop as the crystal 1 with different unit cell dimensions. The occluded model with L-BH structure (PDB code 4D1B) was used as search model during molecular replacement and the

initial R factors were $R_{work}/R_{free} = 28.4/29.0$ % while molecular replacement with the outward-facing form gave higher R factors ($R_{work}/R_{free} 41/43$ %).

Table 3.10: Data collection and refinement statistics for the structure of Met39Cys in complex with L-BH Mhp1 variant. For each appropriate column, the number in brackets represents the information for the outer shell only.

Met39Cys-L-BH			
Dataset	Crystal 1	Crystal 2	Crystal 3
Data collection	DLS, I24	DLS, I24	DLS, I24
Wavelength (Å)	0.96861	0.96861	0.96861
Space group	P 2 ₁ 2 ₁ 2 ₁	P 2 ₁ 2 ₁ 2 ₁	P 2 ₁ 2 ₁ 2 ₁
Resolution (Å)	47.83 - 3.29 (3.67-3.29)	48.98-3.22 (3.76-3.23)	45.74-3.18 (3.67 - 3.18)
Unit cell dimensions a, b, c (Å), $\alpha = \beta = \gamma$ (°)	90.0, 106.6, 112.9 90	90.0 106.7 110.2 90	83.8 101.4 105.8 90
Completeness - spherical (%) - ellipsoidal (%)	37.9 (6.8) 90.8 (72.4)	30.1 (4.2) 89.9 (65.1)	33.2 (4.8) 89.0 (60.4)
Multiplicity	6.1 (6.0)	12.0 (10.0)	11.8 (9.9)
$\langle I/\sigma(I) \rangle$	10.9 (1.7)	8.0 (1.7)	7.2 (1.8)
Rmerge (%)	0.075 (1.2)	0.146 (1.715)	0.232 (2.204)
Rmeas (%)	0.083 (1.322)	0.153 (1.807)	0.244 (2.320)
Rp.i.m. (%)	0.035 (0.533)	0.047 (0.556)	0.075 (0.710)
CC _{1/2}	1.000 (0.541)	0.998 (0.528)	0.997 (0.540)
Refinement statistics			
Measured reflections	39262 (1943)	63689 (2647)	61263 (2557)
Unique reflections	6450 (323)	5303 (265)	5188 (259)
R _{work} (%)	24.10 (28.40)	28.58 (32)	27.43 (31)
R _{free} (%)	24.77 (29)	31.48 (33)	32.66 (37)
R.M.S.D. - bonds (Å) - angles (°)	0.007 1.597	0.007 1.570	0.003 1.303
Ramachandran - outliers (%) - favoured (%)	2.20 75.99	3.30 73.35	0.44 90.97
Rotamer outliers (%)	2.18	6.81	3.54
Average B factors, all atoms (Å ²)	118.0	179.0	101.0

Crystal packing of Met39Cys in complex with *L*-BH (Structure from Crystal 1) follows the packing of outward-occluded structure (PDB code 4D1B). Mhp1 interacts with symmetry mates from the same chain and not from the neighbouring as in the outward-open packing (Figure 3.35). This mutant has bigger solvent channels among the parallel chains and it is not as well-packed as the 4D1B structure. However it uses the same residues to form crystal packing interactions as the occluded structure. The residues that are involved in these interactions are Arg 10, Ser 11, Arg 21, Arg 332, Thr335, Lys 337, Arg 396, Arg 461, Arg 469 and the Glu 280, Glu289, Met 200, Asp 191 as the crystal packing here follows the main chain packing of the outward-open structure (PDB code 2JLN).

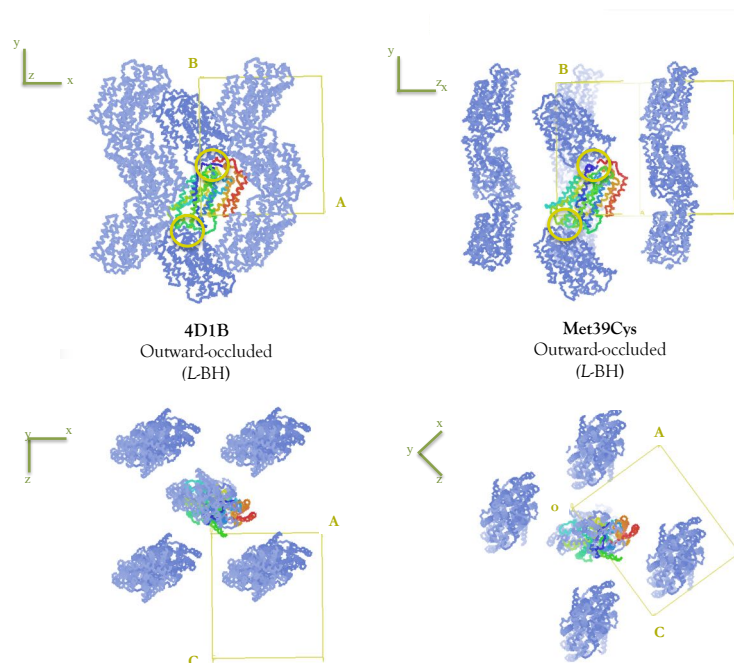


Figure 3.35: Crystal packing of Met39C-LBH structure Picture shows the crystal packing of Mhp1 in outward-occluded conformation (PDB code 4D1B with *L*-BH bound) (rainbow colours, Ca- backbone) and the crystal packing of Met39Cys-*L*-BH bound (Crystal 1) (rainbow colours, Ca- backbone) determined also in outward-occluded conformation. The yellow rectangular represents the unit cell. The yellow circles display the interactions of Mhp1 with the symmetric mates in the same chain. Picture was prepared by COOT (Emsley & Cowtan 2004).

When replacing the Met 39 with Cys 39 in the model the shorter side chain is completely covered by the electron density. In the initial stages of refinement, positive difference electron density in the $F_o - F_c$ map was clearly observed in the ligand-binding site between Trp 117 and

Trp 220. The hydantoin ligand *L*-BH was placed into the binding site of the structure and fitted well with the positive density covering both the hydantoin and the benzyl moieties (green mesh Figure 3.36). The ligand *L*-BH binds to the structure obtained from Crystal 3 in a similar way to the structure of the Crystal 1 described above.

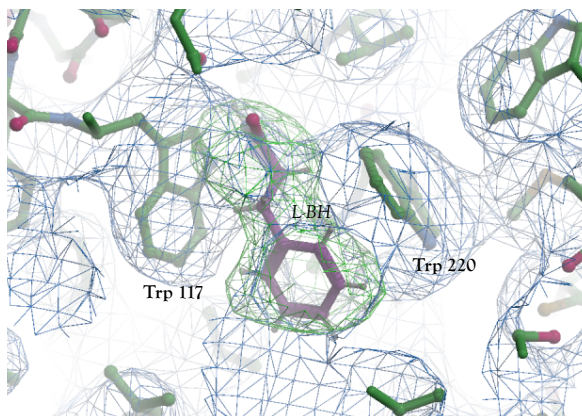


Figure 3.36: The ligand-binding site of the crystal structure of the Met39Cys in complex with *L*-BH (Crystal 1). The 2mFo-dFc electron density map (blue mesh, contoured at 1.0 σ) of the Met39Cys in complex with *L*-BH (green bonds). Positive difference density in the Fo-Fc map (green mesh, contoured at 3.0 σ) confirming the position of *L*-BH (magenta colour). Picture was prepared by COOT (Emsley & Cowtan 2004) and rendered by Raster3D (Merritt & Bacon 1997).

The structure obtained from Crystal 2 was determined at a resolution of 3.23 Å and solved in the same space group and similar unit cell dimensions as Crystal 1 (Table 3.10). However, there was no positive difference density to indicate the existence of the ligand. Cross-refinement against the outward-facing conformation (PDB code 2JLN) yielded negative difference density for a segment of the TMH 10. Thus, for this crystal, although there is no positive density for the ligand, the structure is present in an occluded conformation (Figure 3.37).

Met39Cys was co-crystallised with the four hydantoin ligands (Section 2.2.5). Crystals formed only in the presence of *L*-BH hydantoin ligand. Three structures were determined crystallographically all adopting an outward-occluded conformation. However, for Crystal 2 there is no evidence of positive density for the ligand in the binding site.

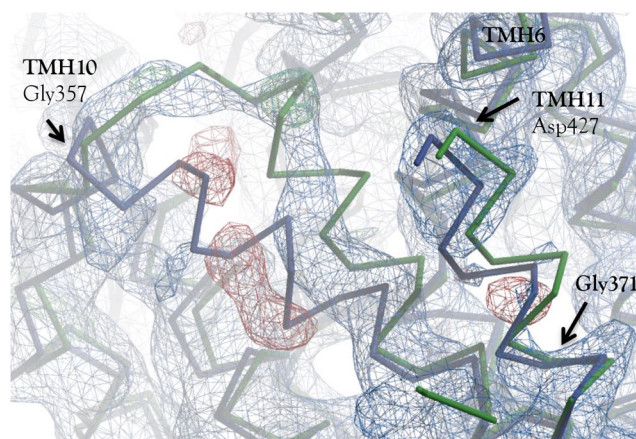


Figure 3.37: Cross refinement of the Met39Cys, Crystal 2 to confirm its conformation in the absence of ligand. The $2mF_o-dF_c$ electron density is in blue, contoured at 1 rmsd for the crystal 2 of Met39Cys structure (green bonds). The red negative F_o-F_c density at 3 rmsd appears after cross-refining the model to the outward-facing structure factors (blue bonds). This negative density for segment of the TMH 10 in blue structure (outward-open, PDB code 2JLN), shows that this structure is outward-occluded conformation. Picture was prepared by COOT (Emsley & Cowtan 2004) and rendered by Raster3D (Merritt & Bacon 1997).

It is unclear why this structure has an occluded state in the absence of the ligand. In the co-crystallisation mixture of crystal 2 1 mg *L*-BH was used compared to 1.5 mg, but this cannot explain the occluded state. The structure of crystal 2 follows the same crystal packing as the Crystal 1. There is no crystal contact clash that could prevent the structure from adopting an outward-open conformation. Spectrophotofluorimetry assay of Met39Cys (Figure 3.21b) shows that its ligand binding ability is reduced by the mutation.

It has been discussed (Section 3.2.2) that Met 39 does not interact with the ligand directly but it might interact while it approaches the binding site. The shorter side chain of Cys 39 might interact with the ligand less strongly than with the Met 39 while approaching the ligand binding site. It is possible that the segment of TMH 10 has moved to the occluded conformation but the ligand, due to the lower strong interaction with Cys 39, does not manage to continue reaching the binding site. Could this occluded structure found in one of three structures of Met39Cys be the reason for the less binding affinity? The possibilities checked above cannot be rationalised to explain this empty-occluded state of the mutant and a conclusion cannot be made for this empty-occluded structure.

3.4.3 X-ray crystal structures of Mhp1 mutant Ala222Ser

The residue Ala 222 is located close to the Mhp1 ligand-binding site but its main chain cannot form hydrogen bonds with the hydantoin moieties of *L*-BH or *L*-IMH based on the reported structures. The alanine was mutated to serine because this is typically found in position 222 in many NCS-1 family bacterial and yeast members (Weyand et al. 2008, 2011). The side chain of serine can be accommodated in place of alanine without unfavourable interactions and is not proposed to form any additional interactions with the bound ligand based on the reported structures. Therefore, this mutant was expected, based on the structure of 4D1B, to have no impact on ligand binding. Unexpectedly, biochemically there was a difference in behaviour Ala222Ser ligand binding ability. Tryptophan fluorescence quenching assay of Ala222Ser showed that this mutation, compared to the wild-type Mhp1, reduces the *L*-BH binding ability the most of the mutants studied during this thesis.

Crystals were obtained for this mutant using the orthorhombic crystallisation conditions and needle-shaped crystals formed overnight at 18° C in both the apo state as well as in complex with *L*-BH and *L*-IMH. Good quality diffraction data were collected at ERSF for the Ala222Ser mutant in the apo form and in complex with *L*-BH and *L*-IMH.

Table 3.11: Data collection and refinement statistics for the structure of Ala222Ser Mhp1 variant. For each appropriate column, the number in brackets represents the information for the outer shell only.

	Ala222Ser apo	Ala222Ser L-BH	Ala222Ser L-IMH
Data collection	ESRF, ID30A-3	ESRF, ID30A-3	ESRF, ID30A-3
Wavelength (Å)	0.9677	0.9677	0.9677
Space group	P 2 ₁ 2 ₁ 2 ₁	P 2 ₁ 2 ₁ 2 ₁	P 2 ₁ 2 ₁ 2 ₁
Resolution (Å)	33.59 - 3.89 4.27 - 3.89	40.34 - 3.39 3.80 - 3.39	46.33 - 3.91 4.5 - 3.9
Unit cell dimensions			
a, b, c (Å)	85.8 99.7 107.2	82.7 95.8 105.4	89.9 106.9 108.1
$\alpha=\beta=\gamma$ (°)	90	90	90
Completeness			
- spherical(%)	55.5 (12.3)	42.23 (7.3)	51.5 (10.2)
- ellipsoidal (%)	82.4 (38.2)	87.9 (68.4)	81.9 (50.5)
Multiplicity	5 (5.2)	4.6 (4.4)	3.5 (2.0)
$\langle I/\sigma(I) \rangle$	9.1 (1.4)	9.8 (1.3)	11.3 (4.1)
Rmerge	0.086 (1.215)	0.080 (1.346)	0.034 (0.116)
Rmeas	0.097 (1.342)	0.090 (1.520)	0.040 (0.151)
Rp.i.m.	0.62 (8.02)	0.999 (0.364)	0.020 (0.096)
CC _{1/2}	0.999 (0.556)	0.997 (0.641)	1.0 (0.984)
Refinement statistics			
Measured reflections	24746 (1345)	23778 (1114)	17763 (723)
Unique reflections	4901 (258)	5115 (256)	5070 (362)
R _{work} (%)	25.46 (29)	27.03 (32)	24.44 (31)
R _{free} (%)	34.45 (36)	31.88 (35)	32.35 (36)
R.M.S.D.			
- lengths (Å)	0.006	0.004	0.006
- angles (°)	1.415	1.336	1.455
Ramachandran			
- outliers (%)	0.87	0.22	0.88
- favoured (%)	88.29	88.55	83.26
Rotamer outliers (%)	5.09	1.90	3.80
Average B factors, all atoms (Å ²)	104.0	132.0	133.0

X-ray crystal structures of Mhp1 mutant Ala222Ser in apo state

The structure of Ala222Ser in the apo state was determined at a resolution of 3.8 Å (Table 3.11) and the structure was solved in space group $P2_12_12_1$ with unit cell dimensions $a = 85.8$, $b = 99.7$, $c = 107.2$, $\alpha = \beta = \gamma = 90^\circ$. The X-ray diffraction data were collected at 100 K at a wavelength of 0.98 Å on beamline ID30A-3 at the ESRF using a Pilatus-6M-F detector. Processing of the anisotropic data was conducted similar to previous structures of Ala38Gly-apo and Met39Cyc-LBH. The search model for the successful molecular replacement was the outward-open conformation of Mhp1 (PDB code 2JLN), which resulted in the lowest initial R-factors ($R_{work}/R_{free} = 29$ and 36 %).

Positive difference density appeared at the early stages of refinement for the sodium in its binding site (Figure 3.38 a). Figure 3.38 b displays the superimposition of the TMH 10 in the final refined model (Ala222Ser-apo in outward-open structure, green bonds) and in a model of the outward-occluded structure (PDB code 4D1B, magenta bonds). Cross-refinement resulted in positive difference density for the TMH 10 of Ala222Ser-apo and not for the TMH 10 of a closed conformation (4D1B). Thus, Ala222Ser-apo adopts an outward-open conformation.

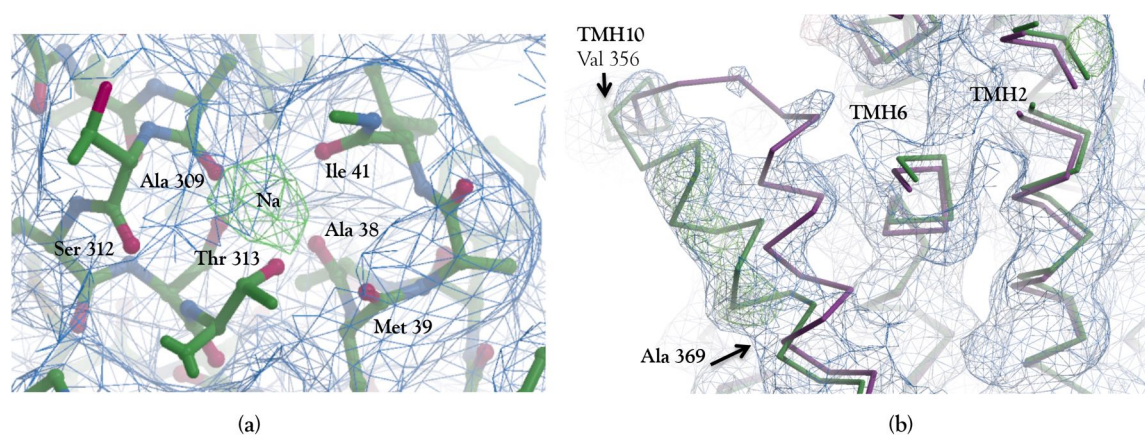


Figure 3.38: Electron density map of the crystal structure Ala222Ser in the apo state. (a) Sodium-binding site. 2mFo-dFc mesh is in blue and the Fo-Fc map shows positive density (green map) for the existence of sodium. **(b) Position of TMH 10 segment to confirm the Ala222Ser-apo conformation.** The green positive density follows the TMH 10 of the Ala222Ser-apo (green bonds), and not the outward-occluded structure (magenta bonds). Picture was prepared by COOT (Emsley & Cowtan 2004) and rendered by Raster3D (Merritt & Bacon 1997).

X-ray crystal structure of Ala222Ser in complex with L-BH

The crystal structure of the Ala222Ser mutant in complex with L-BH was determined at a resolution of 3.39 Å at the beamline ID30A-3 at ESRF and solved in space group $P2_12_12_1$ with unit cell dimensions $a = 82.7$ Å, $b = 95.8$ Å, $c = 105.4$ Å $\alpha = \beta = \gamma = 90^\circ$. The structure was solved by molecular replacement using the occluded structure in complex with L-BH (PDB code 4D1B).

Statistics of the data collection are listed in the Table 3.11. The electron density map shows positive density in the ligand-binding site indicating that the ligand L-BH is bound between the Trp220 and Trp117 as expected (Figure 3.39). Refinement after addition of the ligand L-BH showed the ligand might form extra hydrogen bond interactions with the mutated residue Ser 222.

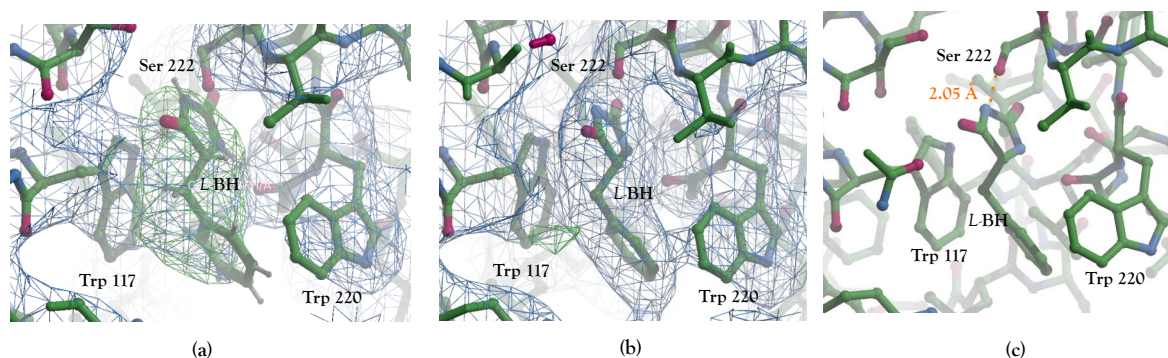


Figure 3.39: The electron density map of ligand binding site in the crystal structure Ala222Ser in complex with L-BH. (a) $2mF_o-dF_c$ is in blue and the F_o-F_c give positive density (green mesh) for the existence of L-BH. (b) After final refinement ligand obtained a better position. (c) The extra hydrogen bond forming with the Ser 222 residue (orange dash line). Picture was prepared by COOT (Emsley & Cowtan 2004) and rendered by Raster3D (Merritt & Bacon 1997).

The Ala222Ser mutant was predicted not to have any impact on the ligand binding of Mhp1. Ala 222 is located close to the ligand binding site and the mutated Ser 222, based on the reported wild-type occluded structures (Simmons et al. 2014), showed to be accommodated without any unfavourable interactions and without any additional interactions with the bound ligand. This prediction is in conflict with the tryptophan fluorescence assay where the ligand

binding affinity is significantly reduced in case of Ala222Ser. Besides this, the crystal structure determined here showed that the Ser 222 forms hydrogen bonds with the *L*-BH ligand (Figure 3.39 c). The green density might indicate that *L*-BH would be arranged in a better position where the Trp 117 can form π -stacking interaction with the hydantoin moiety of *L*-BH as it was observed in the 4D1B outward-occluded state. Higher resolution diffraction structure will elucidate the better position of the ligand in the Ala222Ser in complex with *L*-BH.

X-ray crystal structure of Ala222Ser in complex with L-IMH

Mhp1 mutation Ala222Ser was crystallised also in complex with *L*-IMH and the structure was determined at a resolution of 3.39 Å and solved in space group $P2_12_12_1$ with unit cell dimensions $a=82.7$ Å, $b=95.8$ Å, $c=105.4$ Å $\alpha = \beta = \gamma = 90^\circ$ (Table 3.11). The X-ray diffraction data were collected at 100 K at a wavelength of 0.979147 Å on beamline ID29 at the ESRF using detector Pilatus-6M-F. Processing of the anisotropic data was conducted as for Ala38Gly and Met39Cys. The search model for the successful molecular replacement was the outward-occluded structure in complex with *L*-BH (PDB code 4D1B), which resulted in the lowest initial R-factors ($R_{work}/R_{free} = 31$ and 36 %).

In the hydantoin ligand binding site, positive difference electron density in the Fo-Fc map was seen between Trp 117 and Trp 220. *L*-IMH, was placed in the same binding mode as in the structure 4D1A (Simmons et al. 2014). However, the electron density covered only a bit of the hydantoin moiety and a bit of the indole-ring (Figure 3.40). After refinement of the ligand in several poses in the ligand binding site new small amounts of positive density appeared next to the selected position. This might suggest that the ligand could be exhibiting flexibility and *L*-IMH might adopt several conformations.

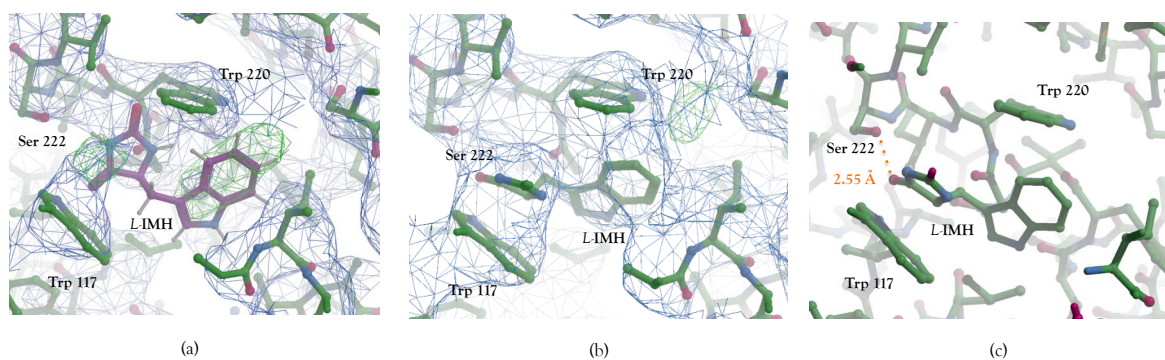


Figure 3.40: The electron density map of ligand-binding site from the Ala222Ser in complex with *L-IMH*. $2mF_o-dF_c$ map is in blue and the F_o-F_c give discontinuous positive difference density (green map) for the existence of *L-IMH* (magenta). Picture was prepared by COOT (Emsley & Cowtan 2004) and rendered by Raster3D (Merritt & Bacon 1997).

L-IMH ligand bound in the the binding site of Ala222Ser in the same way as the *L-IMH* in the wild type Mhp1 (PDB code 4D1A) with its hydantoin forming π -stacking interactions with the indole ring of Trp 117. The Ser 222 contrary to the predictions forms hydrogen bond 2.55 Å distance with the *L-IMH*. Previous biochemical studies of *L-IMH* uptake assays in Ala222Ser purified in DDM detergent showed only that the uptake of the ligand was moderately affected.

In summary, Ala222Ser was determined structurally in apo state and bound with *L-BH*, and bound with *L-IMH* ligands without big structural changes and adopting an outward-occluded conformation as it is expected for bound structures of Mhp1. It is unclear the role of this mutation in the ligand binding affinity. In contrary to the predictions, the Ser 222 formed interactions with the ligands *L-BH* and *L-IMH* based on the structures determined during this thesis. Also, based on tryptophan fluorescence assay, again in contrary to the predictions, Ala222Ser significantly reduced *L-BH* binding affinity. However, the *L-IMH* uptake assays previously studied, are in an agreement with the prediction, since this mutation had a moderate impact observed on the uptake assay (Jackson 2012). These results make it difficult to elucidate the ligand binding mechanism of Ala222Ser. In conclusion, Ala222Ser is a very interesting mutation of Mhp1. In contrast to the predictions the mutant effect the behaviour of this mutant.

3.4.4 Data processing of Ala309Asn

The protein mutant Ala309Asn was subjected to the previously published crystallisation conditions for the hexagonal crystal form (Table 3.5) in order to examine whether any structural changes could be related to the result of the functional assays.

Mhp1 mutation Ala309Asn indeed gave rise to hexagonal crystals (Figure 3.27) both in morphology and crystal lattice with a space group (Table 3.12) similar to the inward-open conformation of Mhp1 using the hexagonal crystallisation conditions (Table 3.5). Although the extensive crystal optimisation, resolution diffraction was not exceeded the 8 Å. As a result crystal structures from those mutants were not solved. However, the fact that Ala309Asn crystallised in P622 space group is a very promising result indicating that this mutant will reveal an alternative conformation of the Mhp1 protein.

3.5 Discussion

Membrane protein crystals are notorious for being fragile and having weak diffraction. This was the case for the Mhp1 mutant crystals presented in the current thesis. Crystal quality sometimes varied considerably, even between crystals from the same drop. As a result, a large number of crystals had to be screened at the synchrotron before data could be collected. Crystals that did diffract beyond 5 Å were highly anisotropic. The very long needles in case of Ala38Gly would break upon attempting to extract them from the droplet into smaller fragments. Other crystals would start bending or even dissolving as soon as the crystallisation droplet was interfered with, as in the case of Met39Cys. Many Mhp1 mutants, especially the Ala222Ser, had many droplets with a lot of precipitant and the crystals would stick to the precipitant, making it difficult to harvest even a fragment clean of precipitant. The precipitant contributes to high background in the diffraction pattern. As far as the mutants Gly219Ser

and Gln42Asn were concerned, many tiny needles were formed, making these very difficult to harvest and giving negligible diffraction. Ala309Asn mutant gave rise to rod-shape crystals as well as to hexagonal crystals using different crystallisation conditions, while for the Thr313Ala only needle-shaped crystals were observed. Although, extensive crystal optimisation was carried out the resolution was not high enough for structure solution (Table 3.6). Notable, all the Mhp1 mutants presented in this thesis, was only ever obtained using the streaking method (Figure 3.24). CD spectroscopy was found to be useful in the crystallisation prediction of Mhp1 mutants. It was observed that Mhp1 mutants that had estimated T_m 's lower than 60° C did not yielded diffracting crystals (Table 3.13). Even though most of the T_m 's are estimated and not calculated for the reasons explained earlier (Section 3.2.1), T_m could be a good indicator of the crystallisability of Mhp1 mutants.

The crystallographic studies of the Mhp1 single point mutations in the sodium- and ligand-binding site revealed various new structures of Mhp1 mutants in the apo state and in complex with various ligands. Crystal structures of the mutations in the sodium-binding site with higher resolution diffraction were obtained only for the Ala38Gly in apo state and Met39Cys in complex with *L*-BH. Of the ligand-binding site mutants the Ala222Ser mutation was crystallised in the apo state and in complex with the ligands *L*-BH and *L*-IMH. Overall, none of the above mutations produced any significant conformational change. The resolution of the data was high enough to resolve the overall global conformation of each protein variant. Subtle local changes at the binding sites of the mutations were not able to be detected at this resolution, including that of the mutation itself. However, the movement of TMH 10, which acts as the thin extracellular gate, was detectable. Thus, a classification as to whether the structure had adopted an outward-facing or occluded conformation was possible. The mutants Ala38Gly-apo and Ala222Ser-apo adopted an outward-open conformation, while the Met39Cys-*L*-BH, Ala222Ser-*L*-BH and Ala222Ser-*L*-IMH an outward-occluded conformation (Table 3.12). The crystal packing of Ala38Gly-apo in outward-open form followed the crystal packing of the wild-type Mhp1 (PDB code 2JLN) (Figure 3.31). However, the Ala222Ser-apo even though it was solved in outward-open conformation, its crystal packing was similar to the outward-occluded

wild-type Mhp1 (PDB code 4D1B) (Figure 3.35). Crystal packing of the mutants Met39Cys in complex with *L*-BH and Ala222Ser in complex with *L*-BH and with *L*-IMH exhibit the same crystal packing as outward-occluded structures of the wild-type Mhp1 (Figure 3.35).

Table 3.12: Summary of Mhp1 mutant crystal structures obtained

Mhp1 variant	Crystal morphology	Lattice type	Space group	Cell dimensions a, b, c (Å) α, β, γ (°)	Resolution (Å)	Conformation
Ala38Gly apo	needles	Orthorhombic	P2 ₁ 2 ₁ 2 ₁	75.3, 106.9, 114.0 $\alpha=\beta=\gamma=90$	3.19	Outward open
Met39Cys <i>L</i> -BH	needles	Orthorhombic	P2 ₁ 2 ₁ 2 ₁	90.0 106.6 112.9 $\alpha=\beta=\gamma=90$	3.29	Outward occluded
Ala222Ser apo	needles	Orthorhombic	P2 ₁ 2 ₁ 2 ₁	85.8 99.7 107.2 $\alpha=\beta=\gamma=90$	3.89	Outward open
Ala222Ser <i>L</i> -BH	needles	Orthorhombic	P2 ₁ 2 ₁ 2 ₁	82.7 95.8 105.4 $\alpha=\beta=\gamma=90$	3.39	Outward occluded
Ala222Ser <i>L</i> -IMH	needles	Orthorhombic	P2 ₁ 2 ₁ 2 ₁	89.9 106.9 108.1 $\alpha=\beta=\gamma=90$	3.91	Outward occluded
Ala309Asn apo	hexagonal rods	Hexagonal	P622	164.4 164.4 96.4 $\alpha=\beta=90, \gamma=120$	8	Unknown

Mutations chosen were based on conserved residues found in homologues. Therefore the mutations are likely to still permit function of the protein unless coupled to a second mutation elsewhere in the sequence. Previous biochemical and biophysical studies of Mhp1 mutations of residues in the sodium and ligand binding sites have either severely impaired the ligand binding and/or ligand transport (Gln 42, Trp 117, Gln 121, Gly 219, Trp 220 or Asn 318), or did not have a dramatic effect (Met 39, Ile 41, Gln 153, Ala 222 or Asn 314). Interestingly, the mutations in the ligand binding site Ala 317 as well as the sodium binding mutations Ser 312 and Thr 313 removed the sodium-dependence of ligand binding and the mutation Ala309Asn (also in the sodium binding site) exhibited a sodium-independent high ligand binding affinity.

For example the mutation Ala38Gly, purified and crystallised in NM, crystallographically did not show any significant conformational change in the binding site (Section 3.4.1) and the

protein adopted an outward-open conformation. The residue in position 38 coordinates the sodium based on the carbonyl oxygen and not through the side chain group. Instead of mutating alanine to glycine, which is a small modification another residue should be chosen. However, the NEM-MS studies of Ala38Gly purified in DDM (Figure 3.34) show different behaviour in solution compare to the other Mhp1 variants in solution. Ala38Gly-DDM was the only Mhp1 variant in outward-facing conformation. Thus, more research on this mutant needed to investigate why this protein is outward in solution. The fact that Ala38Gly-apo crystallised in outward-facing conformation is not enough to confirm the conformation because Mhp1 variants have shown a tendency of crystallising in this conformation even if in solution they predominantly adopt an inward facing state.

Table 3.12 lists the 3D structures of wild-type Mhp1 and its variants that have been solved as an outcome from the current thesis. The majority of the Mhp1 structures adopt an outward-facing or an outward-occluded conformations and only one structure revealed the Mhp1 in an inward-facing conformation (Shimamura et al. 2010). This means that inward-facing conformation is difficult to obtain with techniques that have been used so far. Calabrese et al. (2017) in mass spectrometry experiments (Section 1.4.3) have shown that inward-facing is the predominant conformation of wild-type Mhp1 in solution and the co-addition of sodium and *L*-BH is needed to change the equilibrium to an outward-facing conformation. All these lead to the hypothesis that it might be the crystal packing during crystallisation procedure that force the protein to obtain an outward conformation.

In summary, structural characterisation is of high importance to be comparable with biochemical studies in order to investigate the role of Mhp1 mutants in the ligand binding mechanism. Mhp1 mutations, none of which are on the surface, cause changes in the ligand binding affinity based on the tryptophan fluorescence assays, and in some cases in the crystal packing as well. Are those changes in fact changing the structure into different conformation which are hid-

den due to the crystal packing on the crystals? Solution based experiments such as NEM-MS (Section 1.4.3) will shed light on the conformation of those mutants purified in NM detergent.

Table 3.13: List of estimated melting points (T_m) obtained from CD thermal melts of the Mhp1 mutants purified in NM.

Mhp1 Mutation	Melting Temperature T _m ° C	Crystals	Diffraction (Å)
Wild type in DDM	57.8	no	-
Wild type in NM*	42.7 and 74.8	yes	3.9
Sodium binding site			
Ala38Gly	75	yes	3.19
Met39Cys	61.2	yes	3.29
Ile41Phe	60.8	yes	weak
Ala309Asn+	74.7	yes	8
Ala309Asn**	60.1	no	-
Thr313Ala+	62.9	yes	10
Thr313Ala**	70.1	yes	10
Ligand binding site			
Gln42Asn	52.8	yes	weak
Gly219Ser+	53.9	yes	weak
Ala222Ser	73.9	yes	3.4-3.9

* WT-NM: Two T_ms for each transition

**Mutants purified in absence of sodium and presence of potassium

+Calculated T_m values

Mhp1 mutants are purified in NM detergent and in presence of sodium.

Chapter 4

Mhp1 variants in complex with detergent, a solution based study

In order to facilitate the transportation of hydantoin compounds across the cell membrane Mhp1 utilises an alternating access mechanism. This is a highly dynamic process. X-ray crystallography, although a powerful technique to decipher the 3D structure of a protein in high atomic resolution, can provide only limited information regarding the dynamic especially where large conformational change is expected. Three conformational states of Mhp1 have been identified by X-ray crystallography, the outward-open, the outward-occluded and the inward-open. The ultimate aim of this project is to capture Mhp1 in all intermediate states using single-point mutation on the sodium and binding sites.

Although functional assays of specific mutations revealed that they might adopt an inward conformation, alternative conformations or intermediate states of the already known conformations are often limited due to crystal packing effects. In addition, some conformational changes cannot be accommodated by a crystal lattice (Deller et al. 2016). Therefore, a complementary technique to X-ray crystallography is needed to study this highly dynamic process of the alternating mechanism.

Small-angle X-ray scattering (SAXS) was used in this project, coupled with size exclusion chromatography to obtain information on Mhp1 variants in complex with detergent (PDC) to understand the effects on shape and properties of Mhp1 in the presence of various detergents in Mhp1 ligand binding affinity (Table 3.2, Section 3.2.2). In addition, Mhp1 has also been shown to exhibit oligomerisation in solution different detergents. The determination whether different oligomers were linked to crystallisation outcomes was aimed.

4.1 Structural studies of wild type Mhp1 in solution

The ultimate goal of this project is to understand structurally and functionally the individual steps of the transport cycle of the alternating access mechanism of Mhp1. Previous work by our collaborators, using NEM-MS experiments (Calabrese et al. 2017), gave important insights into the different topological states of Mhp1 in DDM detergent (WT-DDM). Those data showed that WT-DDM in solution adopts predominantly an inward-facing conformation (Section 1.4.3). Mhp1 remains in the inward-facing state in the presence either of sodium or *L*-BH. However, the simultaneous addition of sodium and hydantoin ligand *L*-BH shifts the WT-DDM conformation from inward-facing to outward-facing form in a concentration-dependent manner (Figure 1.13).

Early in Mhp1 crystallographic studies it was clear that wild-type Mhp1 purified in DDM (WT-DDM) detergent did not yield crystals. An extra step of detergent exchange to a shorter one, NM, was mandatory for crystal formation (Weyand et al. 2006, Simmons et al. 2014), although WT-NM was impaired in activity (Polyakova 2015). Crystal structures from wild-type Mhp1 purified in NM (WT-NM) detergent and several Mhp1 mutants also purified in NM have been previously solved (Polyakova 2015) revealing that they had all adopt an outward conformation (Table 1.2). Even the Mhp1 mutants that had been functionally predicted (Jackson 2012) to adopt an inward-facing conformation were only crystallised in an outward conformation

(Polyakova 2015) (Table 1.2).

These observations gave rise to the hypotheses that NM detergent might drive the protein into an outward conformation. Alternatively, the outward conformation may simply have a high crystallisation propensity (Polyakova 2015). Therefore, was decided the investigation of Mhp1 purified in both DDM and NM detergents (WT-DDM and WT-NM) using small angle X-ray scattering to determine whether they could provide insights into the different Mhp1 behaviour in NM and DDM. SEC-SAXS experiments were carried out to differences in the overall PDC shape and properties in different detergents. In addition, the effect of salt and hydantoin on Mhp1's oligomeric state was also explored.

4.1.1 SEC-SAXS studies of wild-type Mhp1 in complex with NM detergent

SEC-SAXS experiments were first performed at the biological small-angle X-ray scattering beamline BL4-2 at Stanford Synchrotron Radiation facility-SSRL (CA, USA) (Section 2.7.2). WT-NM was purified as described previously for crystallisation purposes (Section 2.2). WT-NM crystallises in an outward-open conformation and exhibits lower ligand binding affinity to the LBH compared to the WT-DDM (Polyakova 2015). To test whether WT-NM remains in an outward-facing conformation in solution, SEC-SAXS experiments were carried out.

Calculated scattering plots (Figure 4.1) suggest any differences will be very subtle, but the experiment was carried out to test whether they could be resolved. SEC-SAXS were carried out for the apo protein in presence of high sodium and high ligand concentrations to test whether any conformational changes occur upon binding in solution as would be expected based on NEM-MS observations for WT-DDM Calabrese et al. (2017). SEC-SAXS experiments were also conducted in absence of sodium and presence of potassium in order to probe the effects of potassium in Mhp1.

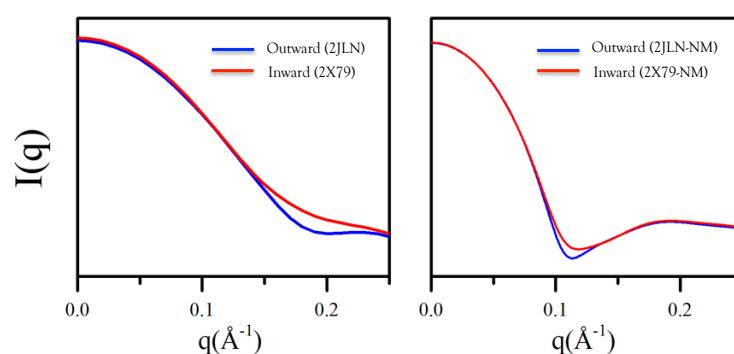


Figure 4.1: Calculated scattering curve of Mhp1 in absence and presence of NM detergent **Left:** The calculated scattering curve of Mhp1 using the outward-open conformation (blue line PDB code 2JLN) and the inward-open conformation (red line, PDB code 2X79), **Right:** The same calculated scattering curves, but in the presence of NM micelles.

In Figure 4.2 the elution profiles from the SEC-SAXS runs of WT-NM are displayed. WT-NM eluted as a single peak in NM buffer, while in the presence of salt and *L*-BH multiple peaks were observed. The single peak observed for WT-NM (Peak I) at 0.9 ml has an R_g of 91-100 Å and D_{max} of 300-345 Å. This is much larger than would be expected for the Mhp1 monomer even with the micelle accounted for and is most consistent with a trimeric state. Interestingly, upon addition of 1 M NaCl and 2 mM *L*-BH the WT-NM eluted in two peaks, one minor peak (Peak I) similar to the peak of apo WT-NM and a second major peak eluting later at 1.25 ml (Peak II). The physical parameters obtained from SAXS analysis again suggested a trimer for peak I, but a dimer for peak II. The third peak (Peak m) in this run is empty micelles, plus potential proteolysis fragments of Mhp1. Surprisingly, in the presence of potassium and *L*-BH ligand, the Mhp1 major peak elutes much later at 1.9 ml (Peak IV) and has R_g and D_{max} parameters consistent with a monomeric form. The minor peak at 1.25 ml (Peak II) of WT-NM in potassium and *L*-BH corresponds to a dimer. The physical parameters obtained by SAXS calculations R_g and D_{max} are summarised in Table 4.1. SAXS processing and analysis had been conducted by Mr. Yunyun Gao Ph.D. student in the same research group as a part of his doctoral thesis.

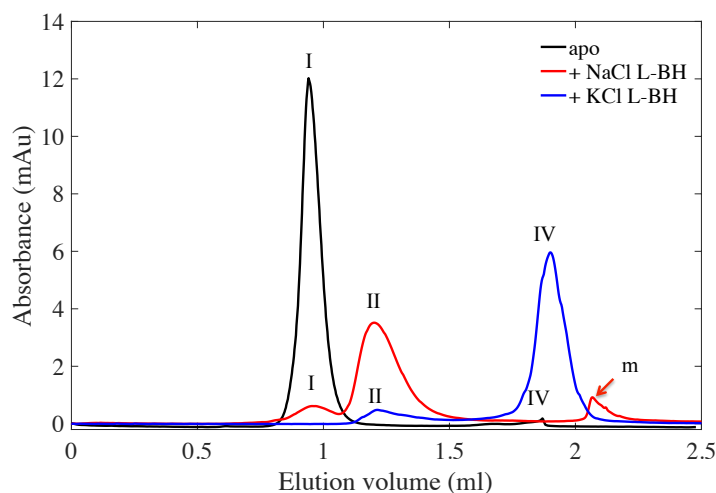


Figure 4.2: Elution profiles from the SEC-SAXS runs of the wild-type Mhp1 in complex with NM detergent. Wild-type Mhp1 in NM micelles (blank line), in NM micelles and presence of 1 M NaCl and 2 mM L-BH (red line), in NM micelles and presence of 1 M KCl and 2 mM L-BH (blue line). Peaks are named in order of appearance to facilitate comparing them across different runs.

Table 4.1: Summary of SEC-SAXS parameters of the wild-type Mhp1 purified in NM detergent

Wild-type Mhp1-NM complex				
Buffer conditions	Elution volume (ml)	R _g (Å)	D _{max} (Å)	Oligomeric state
apo	Peak I: 0.94 ml	91-100 Å	300-345 Å	Trimer
+ 1 M Na, 2 mM L-BH*	Peak I: 0.9 ml Peak II: 1.25 ml more isotropic on average	110 Å 57 Å	338 Å 221 Å	Trimer isotropic Dimer
+ 1 M K, 2 mM L-BH**	Peak II: 1.25 ml even more isotropic Peak IV: 1.9 ml	118 Å 35 Å	322 Å 100 Å	Dimer Monomer

*Buffers compositions see Appendix A.2

The appearance of trimers of apo WT-NM after the size-exclusion chromatography indicates in NM that Mhp1 oligomerises in solution. SAXS modelling (Gao Thesis) suggests that these oligomers are not in the plane of the membrane but are rather "head-to-tail" oligomers. The dimensions are reminiscent of the crystal packing arrangements of Mhp1 molecules and led us to ask whether the oligomer state observed in solution could provide a guide to help steer

crystallisation form. With standard SAXS analysis it was not possible to determine whether the Mhp1 was inward or outward facing. However, Mr Gao has developed new analysis approaches that suggest this differentiation may be possible. This will be presented in his thesis.

4.1.2 Oligomerisation of Mhp1 in crystal packing based on reported Mhp1 structures

In this thesis the changes in oligomerisation state in different conditions and their relation to crystal form were further explored. Mhp1 crystals are obtained using the *in surfo* crystallisation method (Section 3.3). The contacts between the Mhp1 molecules in the crystal results in a type II crystal lattice packing (Section 1.5.3). Two crystal lattice types have been observed for Mhp1. Orthorhombic ($P2_12_12_1$) packing is observed in outward-open and -occluded conformations (Figure 4.3), and a hexagonal (P6) crystal lattice in the inward-open conformation (Figure 4.4). The Mhp1 molecules in the orthorhombic lattice ($P2_12_12_1$) are form interactions following a zig-zag pattern where the molecules running in the direction of the *b*-axis, head-to-tail. The residues that are involved in the intermolecular interactions are Arg 10, Ser 11, Arg 21, Arg 332, Thr335, Lys 337, Arg 396, Arg 461, Arg 469 and the Glu 280, Glu289, Met 200, Asp 191. Additional crystal contacts are made between Mhp1 molecules from neighbouring chains in the *a*-plane and *c*-plane, tail-to-tail, involving the following residues Trp 404, Lys450, Trp451, Trp447 and Asp 237, Glu 243, Lys 247, Arg 251.

As a result, in the crystal packing of Mhp1 in the outward conformation three different trimers can be defined. A "linear-trimer" where Mhp1 forms head-to-tail interactions (Figure 4.3 a) and two "cross-trimers" interacting with two neighbouring chains (Figure 4.3 b and c).

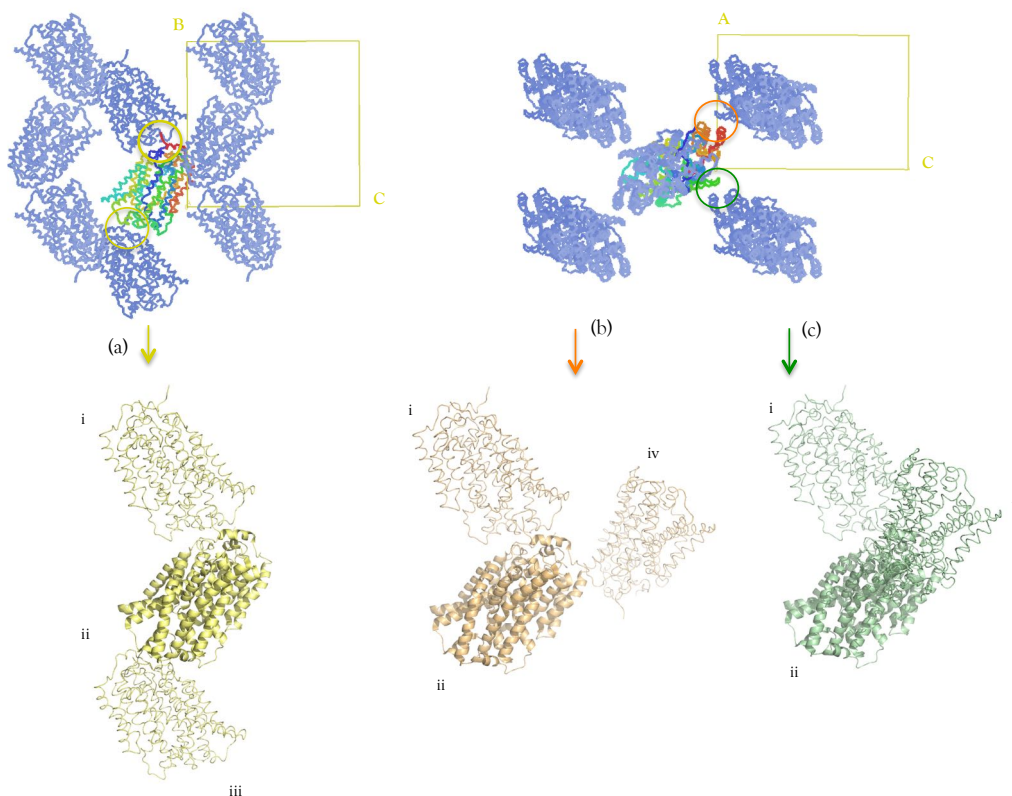


Figure 4.3: Crystal packing of Mhp1 crystallised in outward-facing conformation ($P2_12_12_1$). (a) **Linear-trimer** Crystal contacts of Mhp1 with symmetry molecules in the same chain are observed as head-to-tail. (b) and (c) **Cross-trimers** Mhp1 forms head-to-head interactions with molecules from the neighbouring chains D and E. Mhp1 is displayed here as cartoon representation and the symmetry molecules in ca-backbone. Mhp1 PDB code 2JLN was used to prepare this picture using PyMOL Molecular Graphics System, Schrödinger, LLC.

The second oligomer can be found in the crystal packing of Mhp1 of the inward-facing conformation (P6). Here, Mhp1 packs in a hexagonal lattice crystal. The molecules form a head-to-tail interaction (Figure 4.4 b). Residues that are involved in the crystal contacts are on the head the Glu 280, Glu 289, MSE 200, Glu 196-Asp 191 and Leu 277, Val 278, while in the tail the residues Arg 332, Arg 10, Arg 405 and Lys 398.

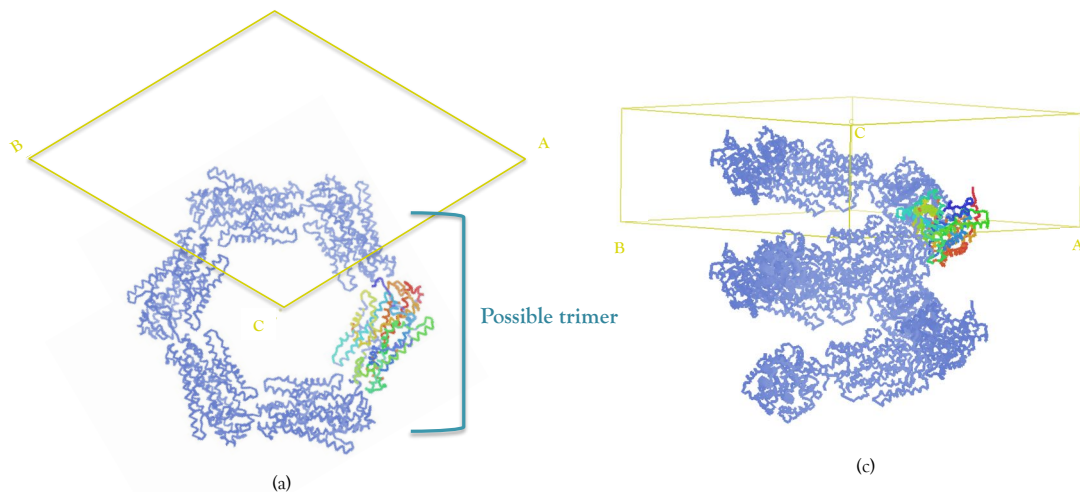


Figure 4.4: Crystal packing of Mhp1 crystallised in inward-facing conformation (P6). (a) The crystal packing along *c*. The Mhp1 molecule in rainbow colour and its symmetry molecules in light blue. The yellow rectangular is the unit cell. (b) The crystal packing along the diagonal of *a* and *b*. The PDB code 2X79 was used to prepare this picture, using coot (Emsley & Cowtan 2004) and PyMOL Molecular Graphics System, Schrödinger, LLC.

In summary, in solution scattering studies (SEC-SAXS) of wild-type Mhp1 purified in NM (WT-NM) small oligomers are observed that are reminiscent of the Mhp1 crystal packing arrangements in different space groups. In presence of the substrates, sodium and *L*-BH, the trimers break down to form dimers, while in the absence of sodium and presence of potassium monomers are obtained. Do these oligomers reflect the very early stages of crystallisation? And can the type of oligomer and crystal habit be steered by altering the solution conditions?

4.1.3 SEC-SAXS studies of wild-type Mhp1 in complex with DDM detergent

To further investigate these questions, wild-type Mhp1 purified in DDM (WT-DDM) was also examined. Based on the NEM-MS experiments, this adopts a predominately inward-facing conformation in solution (Calabrese et al. 2017).

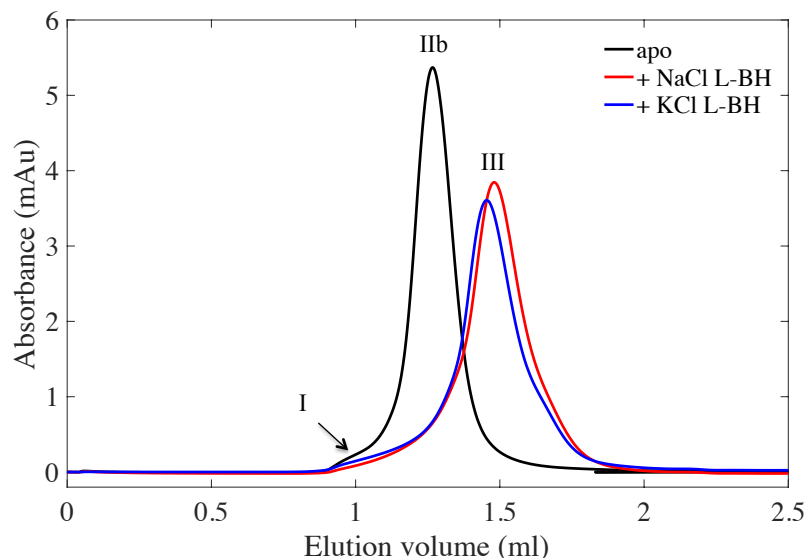


Figure 4.5: Elution profiles from the SEC-SAXS runs of the wild-type Mhp1 in DDM. Apo wild-type Mhp1 in DDM micelles (black line), in DDM micelles and in presence of 1 M NaCl and 2 mM L-BH (red line), in 1 M KCl and 2 mM L-BH (blue line).

SEC-SAXS experiments were performed at the biological small-angle X-ray scattering beamline BM29 at the ESRF using double protein concentration (Section 2.7.2). SEC runs of WT-DDM (Figure 4.5) showed that WT-DDM eluted later than WT-NM at 1.27 ml (Peak IIb) corresponding to a dimer, similar to the elution volume of the WT-NM dimer in the presence of sodium and L-BH (Peak II). Upon the addition of sodium and L-BH the WT-DDM elution shifted to 1.48 ml (Peak III) and to 1.45 ml (Peak III) in the presence of potassium. Although these elute later than apo WT-DDM, SAXS suggests a dimer. No evidence of a strong trimer population is observed. The lack of this higher order oligomer may be related to the lack of crystals obtained from Mhp1 in DDM. The dimer might be insufficient to start nucleation and subsequent crystal formation. The addition of substrate also had a different effect to WT-NM. WT-DDM did elute later in the presence of ligands, but there was no major difference between sodium or potassium.

Table 4.2: Summary of SEC-SAXS parameters of the wild-type Mhp1 purified in DDM detergent

Wild-type Mhp1-DDM complex				
Buffer conditions	Elution volume (ml)	R _g (Å)	D _{max} (Å)	Oligomeric state
apo	Peak IIb: 1.27 ml	58.8-42.8 Å	200 Å	Dimer +
+ 1 M NaCl, 2 mM L-BH	Peak III: 1.48 ml	53.5-40.3 Å	161 Å	interestingly have similar R _g yet different D _{max}
+ 1 M KCl, 2 mM L-BH	Peak III: 1.45 ml	57.8-43.5 Å	178 Å	interestingly have different D _{max}

+with different amount of detergents attached

*Buffers compositions see Appendix A.2

These data clearly show that both detergent and ligands have major effects on the oligomerisation state of Mhp1. The longer detergent, DDM, gave a smaller oligomer. Mhp1 has maximum distance in the membrane plane of 50 Å and perpendicular to the membrane of 75 Å as measured in Coot using the maximum distance tool. From other work the thickness of NM (9C) micelle can be estimated as 27.5 Å by extrapolating the experimentally determined values of DDM (12C) 34-35 Å and DM (10) 29-30.3 Å maltoside detergents (Lipfert et al. 2007). It is possible less residues are accessible in the DDM to form crystal contacts and this is why no higher order oligomers are seen.

In addition, the effect of sodium concentration was further investigated using SEC-SAXS for the wild-type Mhp1 in DDM detergent. The addition of sodium in different concentrations did not change the oligomer distribution, protein eluted similar to Peak IIb (Figure 4.5) where wild-type Mhp1 in DDM eluted (apo state). The parameters derived from SAXS also suggest all peaks are dimer states with varying compactness (Figure 4.6). Only the co-addition of sodium and L-BH resulted in a large shift in oligomeric distribution (Peak III, Figure 4.6 and/or Figure 4.5). In order to mimic the ionic strength sodium was replaced with choline. The addition of choline-chloride had no effect regarding of the presence of absence of L-BH substrate (Figure 4.6 b).

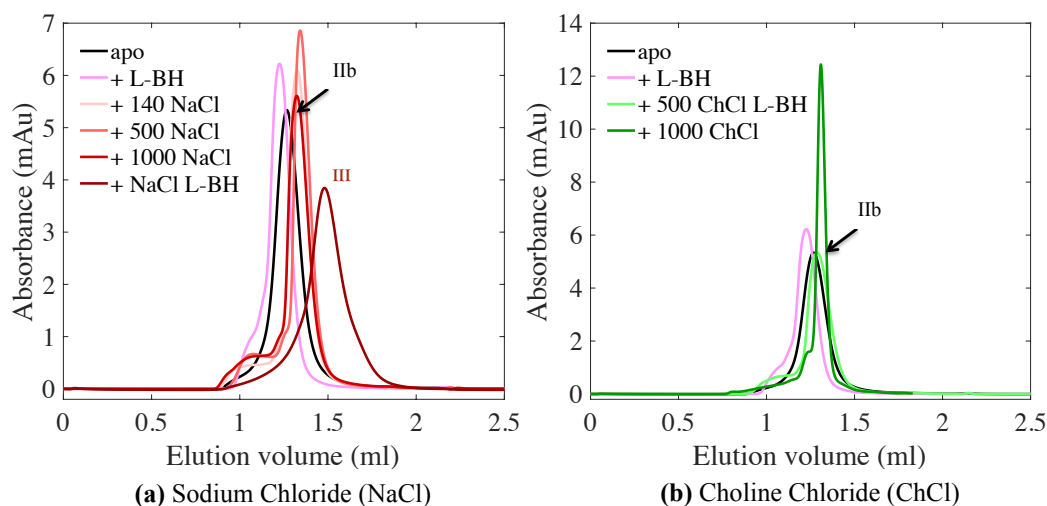


Figure 4.6: Elution profiles from the SEC-SAXS runs of the WT-DDM in various salt concentrations. (a) **Sodium Chloride (NaCl):** Wild-type Mhp1 in DDM micelles (blank line), in DDM micelles and 2 mM L-BH (pink line), in presence of various NaCl concentrations in red shades, in presence of 1 M NaCl and 2 mM L-BH (dark red line), (b) **Choline Chloride (ChCl):** Wild-type Mhp1 in DDM micelles (blank line), in DDM micelles and 2 mM L-BH (pink line), in presence of 500 mM ChCl and 2 mM L-BH (light green line) and in presence of 1 M ChCl (dark red green).

4.2 Structural studies of Mhp1 mutants in solution

4.2.1 SEC-SAXS of Mhp1 mutants adopting an outward conformation in crystals

The behaviour of Mhp1 mutants in solution were also explored. Mhp1 mutants purified in NM were examined in solution by SEC-SAXS studies carried out in SSRL as described in Section 2.7.2. In apo NM buffer the mutants Met39Cys and Ala222Ser owed very similar behaviour to WT-NM in the absence of ligands, peak eluting at 0.9 ml (Peak I) consistent with a trimer. Ala222Ser shows also a small population of a dimer (Peak IIo). Consistent with the SEC-SAXS these mutants crystallised in an outward-open form and orthorhombic space group. The crystal structures of both Met39Cys (only holo structure determined) and Ala222Ser (holo and apo structures determined) show the outward occluded form and a crystal packing with only the linear trimer present.

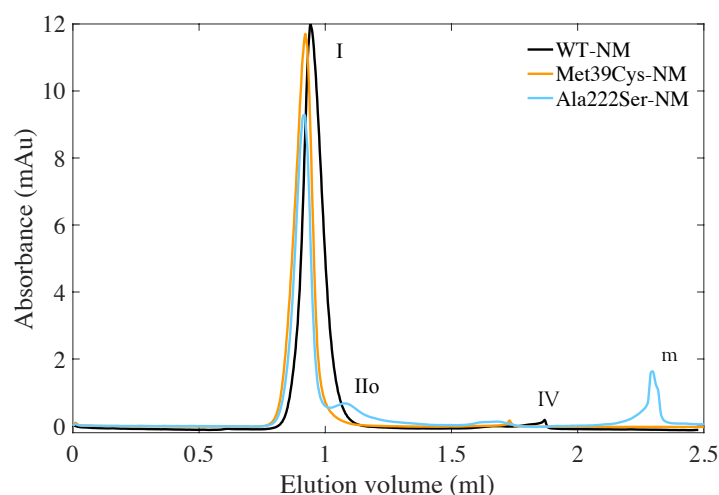


Figure 4.7: Elution profiles from the SEC-SAXS runs of the Mhp1 mutants Met39Cys and Ala222Ser in NM detergent. Wild-type Mhp1 in NM detergent (black line), Met39Cys in NM detergent (orange line) and Ala222Ser in NM detergent (light blue).

Table 4.3: Summary of SEC-SAXS parameters of the Mhp1 mutants Met39Cys and Ala222Ser purified in NM.

Mhp1 mutant	Elution volume (ml)	Rg (Å)	Dmax (Å)	Oligomeric state
Met39Cys-NM	Peak I: 0.9 ml	100 Å	300 Å	Trimer
Ala222Ser-NM	Peak I: 0.9 ml Peak IIo: 1.2 ml	109 Å	308 Å	Trimer

*Buffers compositions see Appendix A.2

The crystal structures of Mhp1 mutants purified in NM detergent solved during the current project presented similar crystal packing to the wild-type Mhp1 structures purified also in NM. More specific, the Mhp1 mutant crystallised with bound ligand (Section 3.4.2 for Met39Cys-L-BH and Section 3.4.3 for Ala222Ser-L-BH and Ala222Ser-L-IMH) showed that the protein molecules in the crystal packing forming chains following the zig-zag pattern of Mhp1 wild-type outward-occluded crystal structure with PDB code 4D1B (Figure 3.35), with head-to-tail interactions using similar involving residues. The Ala38Gly-apo crystallised in apo state (Section 3.4.1) exhibits the additional crystal contacts of Mhp1 wild-type outward-open crystal structure with PDB code 2JLN with two neighbouring chains forming head-to-head interactions.

Notably, the mutant Ala222Ser in apo state (Section 3.4.3) formed only the zig-zag pattern in the crystal lattice.

4.2.2 SEC-SAXS of Mhp1 mutants proposed to occupy an inward conformation

Ala309Asn and Thr313Ala adopt an inward facing conformation, as discussed in Section 3.2.4. While crystals of both Ala309Asn and Thr313Ala in NM were obtained in this project, the diffraction quality was very poor. The Thr313Ala data could not be indexed, however, the 8 Å Ala309Asn data could be indexed as P622, although the data were not good enough for map calculation.

The main chain carbonyl of Ala 309 is predicted to be involved in the sodium coordination in the outward-facing state and in the ligand-bound states according to the reported crystal structures (outward-open: 2JLN, outward-occluded *L*-BH bound: 4D1B, *L*-IMH bound: 4D1A). Typically this position has a small chain amino acid among the NCS-1 family homologues, although in some of the yeast transporters aspartate is found in this position. The mutation Ala309Asn was created and the side chain of Asn 309 is predicted to be accommodated in the Mhp1 structure without any unfavourable interactions, while its main chain carbonyl is expected to coordinate the sodium as for the original residue Ala 309. However, an additional hydrogen bond could form between the side chain carboxamide of Asn309 (TMH 8) and the main chain carbonyl of Ile 41 (TMH 1) (3.9 Å) which may stabilise the sodium-binding site.

The hydroxyl side chain of Thr 313 is proposed to coordinate the sodium ion as well as forming a hydrogen bond with the main chain carbonyl of Met 39 in the outward-facing open (PDB code 2JLN) and outward-occluded (PDB code 2JLN) wild-type Mhp1 crystal structures. This interaction with Met 39 may be important in orienting TMH 8 and the extended peptide region of discontinuous TMH 1.

SEC-SAXS of Mhp1 mutants Ala309Asn and Thr313Asn

SEC-SAXS experiments of both Mhp1 mutants Ala309Asn, and Thr313Ala in NM detergent were performed in BM29 beamline at ESRF, double protein concentration was used for better SAXS signal (Section 2.7.2) compared to the SEC-SAXS experiments of wild-type Mhp1 in SSRL (Section 4.1.1). Experiments showed a markedly different behaviour of these mutants over the WT-NM, and the mutants Met39Cys-NM and Ala222Ser-NM carried out at SSRL at 5 mg/ml final protein concentration.

In the NM buffer (Tris buffer: Appendix A.2), which is similar to that which yields orthorhombic crystals (Section 3.3), both Mhp1 mutants Ala309Asn-apo (Figure 4.8a, Table 4.4) and Thr313Ala-apo (Figure 4.9a and Table 4.5) elute with a major peak at 1.24 ml (Peak II) and a minor peak at 1.03 ml (Peak Ib). Upon addition of either choline chloride, sodium chloride and L-BH or potassium chloride and L-BH the major peak of each mutant shifts to 1.43 ml (Peak III), suggesting this shift is purely due to altered ionic strength. In buffer conditions similar to those which yielded the hexagonal crystals of Ala309Asn (Bicine pH 9.0 vs Tris pH 8.0, Appendix A.2) very similar behaviour is observed upon the addition of salts and/or L-BH ligand (Figures 4.8b and 4.9b), suggesting that the change in oligomer structure is not linked to a change in pH or buffer type.

However, for Thr313Ala, under "hexagonal" buffer conditions (Bicine buffer, Appendix A.2), but in the presence of potassium and L-BH, although the elution volume of the major peak is that same as that for sodium and L-BH, the SAXS analysis indicates that the mutant is monomeric in the presence of potassium and dimeric in the presence of sodium. This suggests that the dimer observed under sodium conditions must be relatively compact to elute at the same volume as the potassium-monomer.

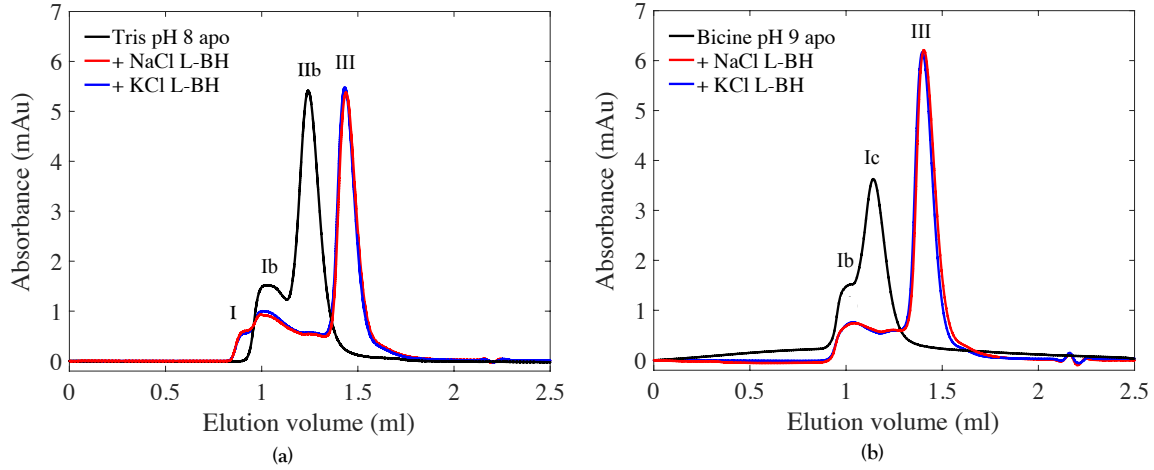


Figure 4.8: Elution profiles from the SEC-SAXS runs of the Mhp1 mutant Ala309Asn in NM detergent. (a) Tris buffer, (b) Bicine buffer of Mhp1 Ala309Asn mutant in NM micelles (blank line), in NM micelles and presence of 1 M NaCl and 2 mM L-BH (red line), and presence of 1 M KCl and 2 mM L-BH (blue line).

Table 4.4: Ala309Asn in NM detergent in Tris and Bicine buffers.

Buffer conditions	Elution volume (ml)	Rg (Å)	Dmax (Å)	Oligomeric state
Ala309Asn-NM (Tris buffer pH 8.0) +				
Tris pH 8.0 (apo)	Peak Ib: 1.03 ml	n/a	n/a	n/a
	Peak II: 1.24 ml	n/a	n/a	n/a
+ 1 M NaCl, 2 mM L-BH	Peak I: 0.99 ml	n/a	n/a	n/a
	Peak Ib: 1.03 ml	n/a	n/a	n/a
	Peak III: 1.43 ml	n/a	n/a	n/a
+ 1 M KCl, 2 mM L-BH	Peak I: 0.99 ml	n/a	n/a	n/a
	Peak Ib: 1.03 ml	n/a	n/a	n/a
	Peak III: 1.43 ml	n/a	n/a	n/a
Ala309Asn-NM (Bicine buffer pH 9.0, hexagonal conditions)				
Bicine pH 9.0 (apo)	Peak Ib: 1.03 ml	122.9 Å	440 Å	Trimer
	Peak Ic: 1.14 ml	84.5 Å	326 Å	Trimer
+ 1 M NaCl, 2 mM L-BH	Peak Ib: 1.03 ml	96.9 Å	373 Å	Trimer
	Peak III: 1.40 ml	47.5 Å	182 Å	Dimer
+ 1 M KCl, 2 mM L-BH	Peak Ib: 1.03 ml	106.2 Å	380 Å	Trimer
	Peak III: 1.40 ml	42.4 Å	184 Å	Dimer

*Buffers compositions see Appendix A.2

+SAXS data were not clear to give conclusive Rg and Dmax analysis

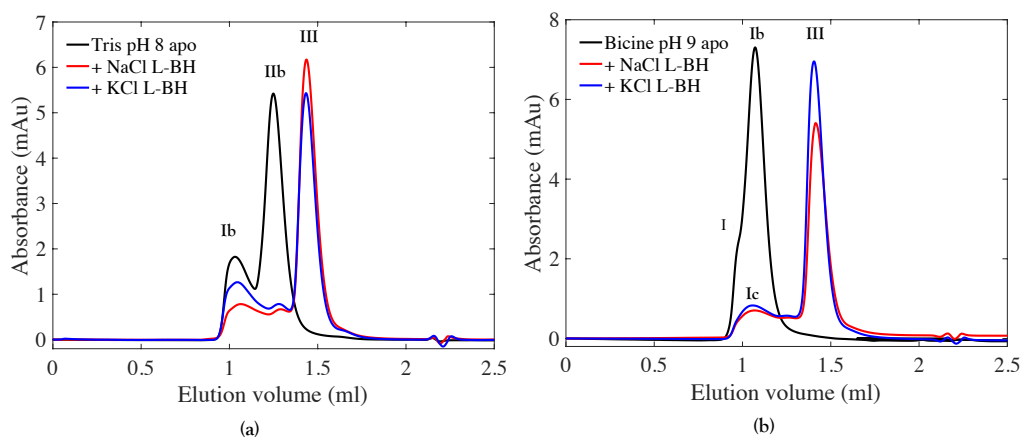


Figure 4.9: Elution profiles from the SEC-SAXS runs of the Mhp1 mutant Thr313Ala in NM detergent. (a) Tris buffer, (b) Bicine buffer of Mhp1 Thr313Ala mutant in NM micelles (blank line), in NM micelles and presence of 1 M NaCl and 2 mM L-BH (red line), and presence of 1 M KCl and 2 mM L-BH (blue line).

Table 4.5: Thr313Ala in NM detergent in Tris and Bicine buffers.

Buffer conditions	Elution volume (ml)	Rg (Å)	Dmax (Å)	Oligomeric state
Thr313Ala-NM (Tris buffer pH 8.0) +				
Tris pH 8.0 (apo)	Peak Ib: 1.03 ml	n/a	n/a	n/a
	Peak II: 1.24 ml	n/a	n/a	n/a
+ 1 M NaCl, 2 mM L-BH	Peak Ib: 1.03 ml	n/a	n/a	n/a
	Peak III: 1.43 ml	n/a	n/a	n/a
+ 1 M KCl, 2 mM L-BH	Peak Ib: 1.03 ml	n/a	n/a	n/a
	Peak III: 1.43 ml	n/a	n/a	n/a
Thr313Ala-NM (Bicine buffer pH 9.0, hexagonal conditions)				
Bicine pH 9.0 (apo)	Peak I: 0.97 ml	93.5 Å	350 Å	Trimer
	Peak Ib: 1.07 ml	64.5 Å	300 Å	Dimer (elongated)
+ 1 M NaCl, 2 mM L-BH	Peak Ic: 1.13 ml	92.2 Å	320 Å	Trimer
	Peak III: 1.41 ml	55.4 Å	223 Å	Dimer (II or due to overlap with trimer)
+ 1 M KCl, 2 mM L-BH	Peak Ic: 1.12 ml	94.7 Å	332 Å	Trimer
	Peak III: 1.40 ml	35.8 Å	109 Å	Monomer

*Buffers compositions see Appendix A.2

+SAXS data were not clear to give conclusive Rg and Dmax analysis

In a more detailed view of the predicted inward Mhp1 mutant Ala309Asn a very interesting behaviour was observed. A comparison of the elution profiles of Ala309Asn-NM and the elution profiles of the WT-NM and WT-DDM (Figure 4.10) showed that the major peak of Ala309Asn-NM in Tris buffer the Peak IIb (pink line) is eluted similar to Peak IIb of WT-DDM (black line), while in Bicine buffer this major peak eluted faster Peak Ic (magenta line) towards the Peak I of WT-NM elution profile (grey line). Based on SEC-SAXS analysis the peaks towards Peak I have a trimeric form while towards Peak IIb dimeric form (Table 4.6). This observation aligns with the crystallisability of Mhp1 where crystals obtained only in trimeric form. To sum up, Mhp1 might adopts inward conformation when the predicted Mhp1 mutants are crystallised in the hexagonal crystal conditions (Bicine pH 9) and having clear elution profile of trimeric form.

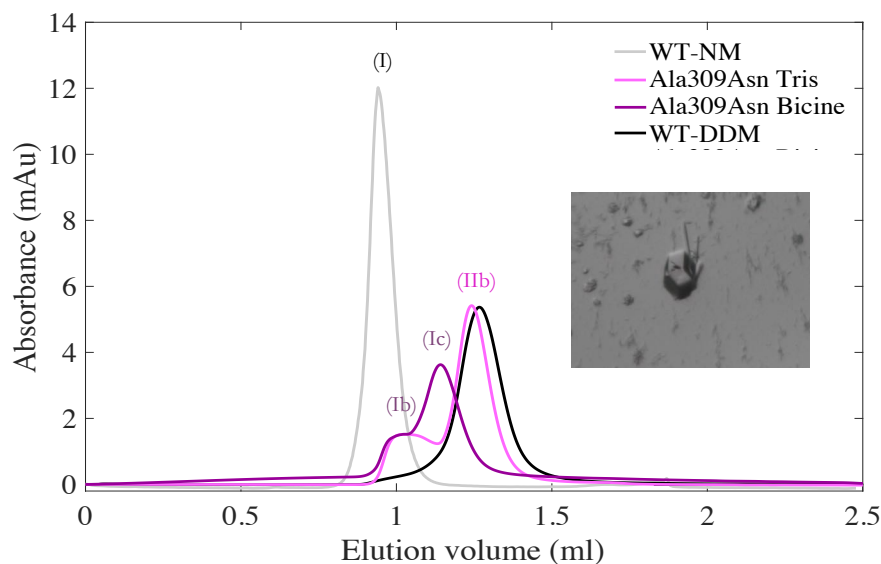


Figure 4.10: Comparison of the elution profiles from the SEC-SAXS runs of the Mhp1 mutant Ala309Asn in NM detergent in orthogonal (Tris buffer, pH 8) and hexagonal (Bicine buffer, pH 9) conditions with the elution profiles of the wild-type Mhp1 in NM and DDM detergent. Wild-type Mhp1 in NM detergent Tris buffer, pH 8 (grey line), wild-type Mhp1 in DDM detergent Tris buffer, pH 8 (black line), Ala309Asn in NM detergent Tris buffer, pH 8 (pinkline), and Ala309Asn in NM detergent Bicine buffer, pH 9 (magenta-line). Zoom in picture of the Ala309Asn-NM hexagonal crystal obtained in Bicine hexagonal conditions (Section 3.3.2, Figure 3.27).

Table 4.6: Comparison of Mhp1 wild-type in NM and DDM detergents (Tris buffer) with the Mhp1 mutant Ala309Asn in NM detergent in Tris and Bicine buffers.

Buffer conditions	Elution volume (ml)	Rg (Å)	Dmax (Å)	Oligomeric state
WT-NM (apo, Tris)	Peak I: 0.94 ml	91-100 Å	300-345 Å	Trimer
Ala309Asn-NM (apo, Tris)	Peak Ib: 1.03 ml	n/a	n/a	n/a
	Peak II: 1.24 ml	n/a	n/a	n/a
Ala309Asn-NM (apo, Bicine)	Peak Ib: 1.03 ml	122.9 Å	440 Å	Trimer
	Peak Ic: 1.14 ml	84.5 Å	326 Å	Trimer
WT-DDM (apo, Tris)	Peak IIb: 1.27 ml	58.8-42.8 Å	200 Å	Dimer

*Buffers compositions see Appendix A.2

+SAXS data were not clear to give conclusive Rg and Dmax analysis

4.3 Discussion

The work presented in this chapter shows that SEC-SAXS is a useful tool to investigate the changes in solution behaviour (oligomerisation and polydispersity) of membrane protein Mhp1. In this project it was not possible to use the SAXS data directly to distinguish outward and inward facing forms as was planned initially. Although new analysis approaches developed by Yunyun Gao have made advances in this area. However, it was clearly possible to identify different oligomeric populations upon the addition of salt and ligand. Interesting, these appeared to be predictive of the ultimate crystal form and packing obtained.

In conclusion, both the predicted inward facing mutants Ala309Asn and Thr313Ala purified in NM have similar behaviour that is distinct from WT-NM and the outward-facing mutants Ala222Ser and Met39Cys. These mutants also show a more polydisperse distribution of monomers, dimers and trimers in contrast to the clean single peak observed for WT-NM, Ala222Ser and Met39Cys. This may explain why high quality crystals of these variants could not be obtained. Moreover, based on this research we suggest that in order to obtain the hexagonal crystal form of Mhp1 leading to inward conformations two indications are crucial:

hexagonal buffer conditions (Bicine pH 9, Appendix 2) as well as SEC elution profile shifted to trimeric form as WT-NM elutes (Figure 4.10). This means, that SEC-SAXS can be used to determine the optimal solution conditions to favour trapping of different Mhp1 conformations in the crystalline state for structure analysis.

Chapter 5

LeuT

Structural and functional studies of homologue structures bring numerous advantages to understanding the alternating mechanism of secondary active transporters. A second membrane protein studied during this thesis, the bacterial Leucine transporter (LeuT), from *Aquifex aeolicus*, a bacterial homologue of the neurotransmitter sodium symporter (NSS) family (Section 1.3). Our interest was to study the LeuT mechanism using time-resolved X-ray crystallography. To achieve this goal the biological function needs to be triggered in the crystal rapidly and uniformly at room temperature (Schmidt et al. 2005, Neutze & Moffat 2012, Šrajer & Schmidt 2017). There are many ways to initiate a reaction in protein crystals such as light-initiated reactions, photolabile caged compounds, temperature jump, pH jump, and diffusion (Levantino et al. 2015). After the initiation of the reaction at a specific time, X-rays are used to probe the intermediates in real time and at room temperature at a series of time delays.

A LeuT variant was designed in which Leu400Cys-Lys288Ala-Phe320Cys, triple-mutant LeuT (LeuT-SS). Residues 320 (EL-4b: extracellular loop 4b) and 400 (TMH 10) were mutated to cysteines (Figure 5.5) for the future creation of a disulphide bond. The Lys288Ala mutation enhances expression and transport activity of LeuT. To ensure the protein adopts an inward conformation so that the cysteines come into proximity the LeuT-SS needs to be handled in the complete absence of both sodium and its ligand leucine. The disulphide bond (SS-bond) is

proposed to lock the transporter in an inactive conformation unable to bind the ligand (Prof. Stockner, personal communication). By the addition of a reducing agent or photolysis using laser light or X-rays the disulphide bond can be broken, allowing the reaction to start. Several challenges must be overcome at different stages: successful cloning of the LeuT-SS, expression, purification, disulphide bond formation and crystallisation.

5.1 Protein Purification of wild-type LeuT (LeuT-WT)

5.1.1 Purification wild-type LeuT

Optimisation of the purification of the wild-type LeuT (LeuT-WT) was a mandatory prior to the triple mutant LeuT (LeuT-SS) work. LeuT-WT was over-expressed at the Medical University of Vienna by our collaborator Dr. Azmat Sohail, as described in Section 2.3.1, and purified (by the author) *via* affinity chromatography based on previously established protocols (Section 2.3). Solubilisation and purification was performed using DDM (Sohail et al. 2016). However, for structural studies and especially crystallisation trials, further purification steps are needed. Firstly, the His₈-tag was removed by thrombin digestion reaction (Section 2.3.4), since its high flexibility might prevent crystal formation. Secondly, an extra mandatory step for crystal formation was the exchange of DDM detergent to β -OG (n-octyl- β -D-glucopyranoside) using size-exclusion chromatography as the last step of purification to achieve the detergent exchange (Section 2.3.5). The protein purity was determined by SDS-PAGE gel electrophoresis under denaturing conditions. Samples from all the purification steps were kept and are displayed in the Figures 5.1 and 5.3.

Size exclusion chromatography was performed in order to exchange the DDM to β -OG detergent. An attempt to exchange the detergent earlier during the first affinity purification (as in the Mhp1 protocol) led to precipitation of the protein. Thus, for LeuT the final size-exclusion

chromatography was the only step in which detergent was exchanged, yielding a pure and stable protein solution. The elution profile (Figure 5.2) indicates the existence of oligomers. Only fractions from the first, major, peak were collected, and concentrated (to approximately 7 mg/ml).

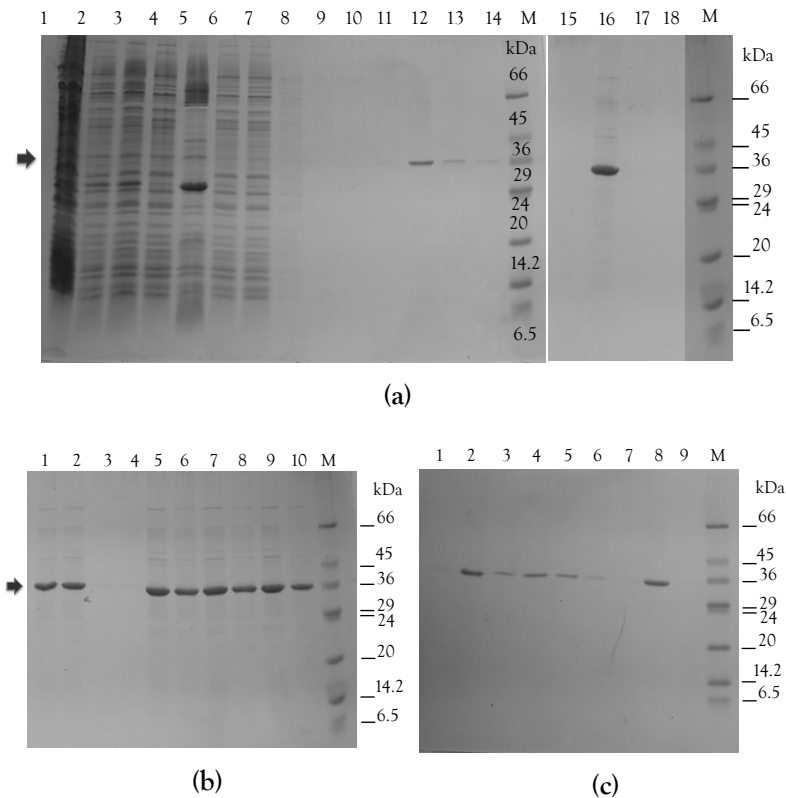


Figure 5.1: SDS-PAGE of wild-type LeuT purification steps in DDM. (a) Affinity purification in DDM (cobalt resin): (1) thaw membrane prep, (2) membranes after homogenisation, (3) membranes after solubilisation (2hrs), (4) supernatant after ultra-centrifugation, (5) insoluble pellet after ultra-centrifugation, (6) unbound flowthrough 1, (7) unbound flowthrough 2, (8) after wash with 0 mM imidazole, (9) after wash with 5 mM imidazole, (10) after first wash with 10 mM imidazole, (11) after wash with 20 mM imidazole, (12) elution 1st CV, (13) elution 2nd CV, (14) elution 3rd CV, (M) molecular weight marker, (15) flowthrough of concentration after elution in 16, (16) concentration after elution (17) elution flowthrough (cleaning column) 1 CV (18) elution flowthrough (cleaning column) 2 CV, **(b) Desalting step and thrombin digestion in DDM:** (1) after desalting-1, (2) after desalting-2*, (3) flowthrough after desalting-1*, (4) flowthrough after desalting-2*, (5) pre-cleavage reaction mixture-1* $t=0$, (6) pre-cleavage reaction mixture-2* $t=0$, (7) post-Cleavage reaction mixture-1* 3 hrs, (8) post-Cleavage reaction mixture-2* 3 hrs, (9) after cleavage-1* O/N, (10) after cleavage-2* O/N, (M) molecular weight marker, **(c) Affinity chromatography with benzamidine column and cobalt resin:** (1) benzamidine step sample application, (2) after benzamidine step, (3) benzamidine flowthrough, (4) after second affinity with cobalt $t=0$ (5) after second affinity with cobalt total, (6) flowthrough of second affinity with cobalt, (7) cleaning cobalt affinity resin with 1 M imidazole, (8) concentration after second affinity cobalt, (9) flowthrough during concentration from (8), (M) molecular weight marker. The arrows indicate the position of LeuT. *sample 1 and sample 2.

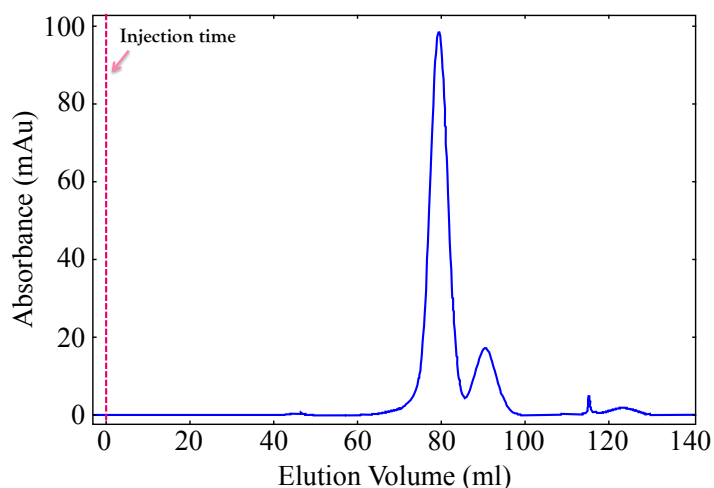


Figure 5.2: Size exclusion chromatography profile of wild-type LeuT in β -OG detergent.

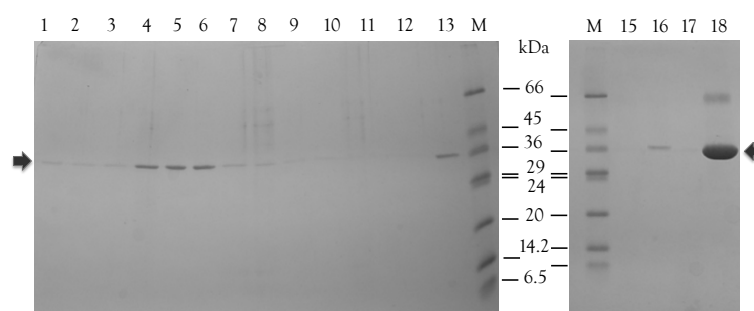


Figure 5.3: SDS-PAGE gel of wild-type LeuT size exclusion chromatography in β -OG detergent. (1) Fraction 90, (2) Fraction 133, (3) Fraction 143, (4) Fraction 148, (5) Fraction 158, (6) Fraction 168, (7) Fraction 176, (8) Fraction 178, (9) Fraction 182, (10) Fraction 193, (11) Fraction 230, (12) Fraction 248, (13) Fraction 258, (14) all fractions, (M) molecular weight marker, (15) after second wash with 10 mM imidazole** from gel Figure 5.1a, (16) all elution fractions from gel filtration column. Figure 5.1a, (17) empty, (18) concentrated after size exclusion for crystallisation.

5.1.2 Crystallisation of wild-type LeuT and initial crystallographic data

Attempts to crystallise purified LeuT variants (wild-type and mutants) shipped frozen from Vienna did not yield any crystals. In contrast, freshly prepared protein from both fresh membranes and frozen membranes, yielded usable crystals (Figure 5.4a). The purification and crystallisation experiments were reproducible. To conclude, wild-type LeuT was only crystallised from freshly purified protein solutions.

Fresh wild-type LeuT after size-exclusion chromatography and concentration (Section 5.1.1), was subjected to crystallisation trials based on previously used conditions (Yamashita et al. 2005, Malinauskaite et al. 2016) in sitting drop and hanging drop configuration and incubated at 18° C. Crystals appeared in one day only in Hepes conditions (Yamashita et al. 2005). A cryo-protectant solution was added (Section 2.3.6) prior to flash-cooling in liquid nitrogen. In Figure 5.4a crystals of wild-type LeuT are displayed. The crystals grew very fast and in the period of one week they overlapped each other.

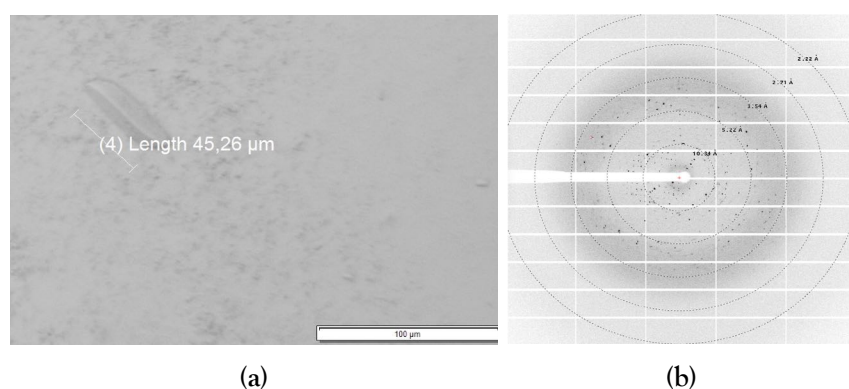


Figure 5.4: Initial crystallisation and diffraction of wild-type LeuT. (a) Wild-type LeuT crystals size of 40-45μm, (b) Diffraction pattern obtained from a wild-type LeuT crystal at 3.5 Å.

X-ray diffraction data were collected at 100 K at a wavelength of 0.97 Å on beamline ID23-1 at the ESRF using a Pilatus-6M-F detector. The detector-to-sample distance was 401.65 mm, producing a possible resolution of 2.27 Å at the edge and 2.04 Å in the corner. Processing was carried out using XDS (Kabsch 2010) and the good batches from the two datasets were used in the CCP4 suite programs for space group determination using POINTLESS and AIMLESS. The diffraction patterns of LeuT-WT were re-processed post-beamtime with XDS (Kabsch 2010) and determined to be in space group C 1 2 1. The unit cell dimensions were refined to the values $a = 86.0$, $b = 86.6$, $c = 80.4$ Å $\alpha = 90.0$, $\beta = 95.3$, $\gamma = 90.0$ ° (Table 5.1). The structure was solved by molecular replacement using the LeuT structure with PDB code 2A65 (Yamashita et al. 2005) as a search model. The bound ions, metals and ligands of the model were removed from the model prior to molecular replacement. The resulting solutions were

submitted to rigid-body refinement. Initial R factors were 25% / 29% (R_{work}/R_{free}). After refinement with jelly body restraints the R factors remained at 25% / 28% (R_{work}/R_{free}).

Table 5.1: Data collection Statistics for the structure of wild-type LeuT. For each appropriate column, the number in brackets represents the information for the outer shell only

wild-type LeuT	
Data collection	ESRF, ID23-1
Wavelength (keV, Å)	12.750, 0.97
Space group	C 1 2 1
Resolution (Å)	47.00 - 2.45 (2.55 - 2.45)
Unit cell dimensions (Å, °)	a = 86.0, b = 86.6, c = 80.4, α = 90.00, β = 95.3, γ = 90.00
Multiplicity	4.4 (4.3)
Completeness (%)	97.9 (98.8)
$\langle I/\sigma(I) \rangle$	6.5 (0.5)
Rmerge	0.102 (1.783)
Rmeas	0.127 (2.238)
Rp.i.m.	0.074 (1.334)
CC _{1/2}	0.999 (0.384)
Refinement statistics	
Measured reflections	92481 (10363)
No. of unique reflections	21208 (2404)
R_{work} (%)	24.91 (32.64)
R_{free} (%)	29.25 (32.67)
R.M.S.D.	
- bonds (Å)	0.006
- angles (°)	1.415
Ramachandran	
- outliers (%)	0.59
- favoured (%)	92.28
Rotamer outliers (%)	0.97
Average B factors, all atoms (Å ²)	104.0

5.2 Triple-mutant LeuT (LeuT-SS) purification and cross-linking attempts

To study the flexibility and allostery of the LeuT transporter (Section 1.3), and more specifically the relative placement and orientation of the transmembrane helices, cysteine residues were introduced using site-directed mutagenesis at specific locations of the LeuT mutant K288A at position 400 in TMH 10 and at position 320 (EL-4b: extracellular loop 4b) (LeuT-SS: Leu400Cys-Phe320Cys-Lys288Ala).

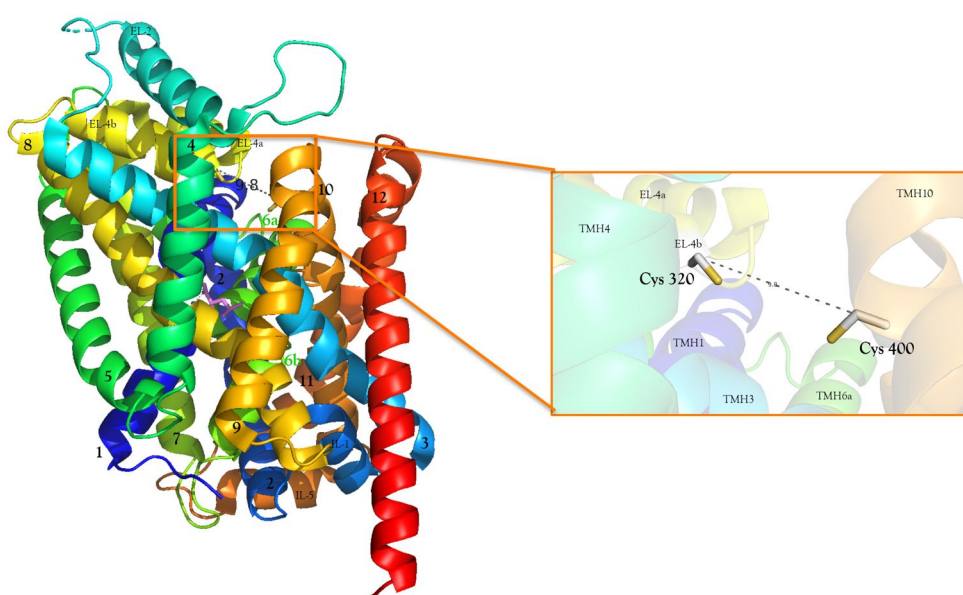


Figure 5.5: Graphical representation of triple mutant LeuT S-S with the mutated cysteine residues. Protein is displayed in cartoon representation coloured from N- to C-terminus from blue to red. The ligand Leucine is in ball and sticks representation coloured purple. The mutated cysteines 320 (EL-4b: extracellular loop 4b) and 400 (TMH 10) are in stick representation and the thiol group is coloured orange. The distance between their $C\beta$ atoms are depicted in dash line 9.8 Å. Picture was prepared using the wild-type LeuT (PDB ID: 2A65) by PyMOL Molecular Graphics System, Schrödinger, LLC.

5.2.1 Expression and membrane preparation of the triple-mutant LeuT (LeuT-SS)

LeuT-SS was expressed as a His₈-fusion protein and membranes were prepared in Vienna, flash frozen and shipped to Hamburg by Mr. Jawad Khan. For the purification of the triple LeuT

mutants the same procedure was followed as for the wild-type LeuT with the only difference being that a pre-packed cobalt column was used instead of free resin (Section 2.4.2).

5.2.2 Disulphide bond formation on LeuT transporter

Disulphide bonds (SS-bonds) are covalent bonds between the sulphydryl groups of cysteine residues in close proximity ($C\alpha$ -carbons max distance 7 Å and/or $C\beta$ carbons \leq 5.5 Å (Katz & Kossiakoff 1986, Masip et al. 2004). They are appealing candidates in protein engineering efforts because disulphide bonds increase conformational stability and also can probe conformational movements, spatial relationships and interactions within and between molecules. By trapping structural fluctuations with targeted cross-linking, specific ligand-induced changes in the structure can also be detected (Hastrup et al. 2001, Takatsuka et al. 2010). SS-bonds provide valuable information regarding topology, conformation and structural rearrangements of the transmembrane helices in various membrane proteins (Falke & Koshland 1987, Jiang & Fillingame 1998, Loo & Clarke 2000, Moore & Fillingame 2008).

The cross-linking of the LeuT-SS was examined *in vitro*, using an oxidising agent to drive SS-bond formation (Kadokura et al. 2003, Kadokura & Beckwith 2009). Copper phenanthroline was used in this case (Section 2.4.3). To detect the formation of disulphide bonds several methods can be used. Cross-linking affects the migration of the protein on SDS-PAGE, even when it occurs within an oligomer (Bowman & Owen-Hughes 2012). This can also ascertain whether the disulphide bond is intra-molecular or between different oligomers. HPLC gel filtration before and after quantitative formation of disulphide bond can also indicate the effect of oligomeric state.

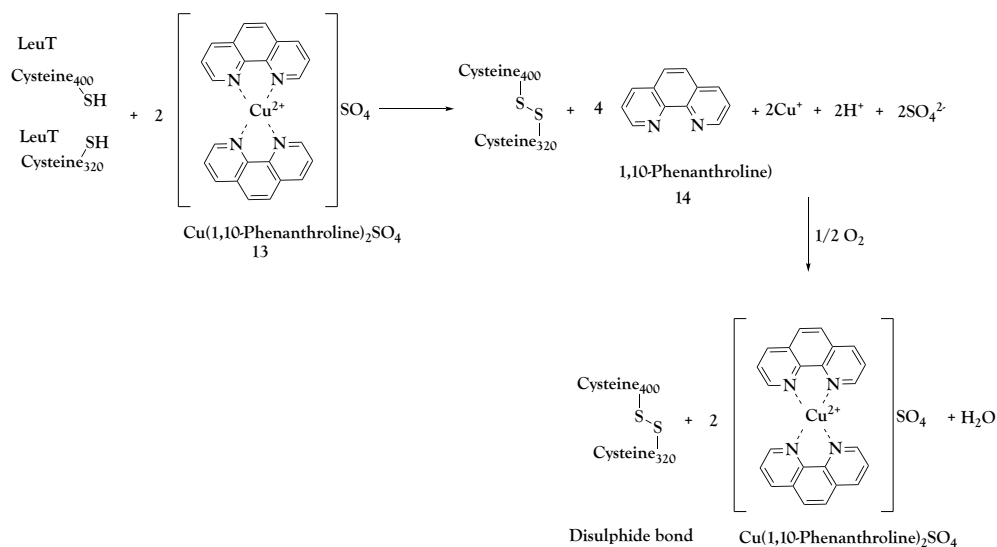


Figure 5.6: Scheme of cross-linking disulphide bond formation using the catalyst copper-phenanthroline.

SS-bond formation can also be followed using DNTB (5,5'-Dithio-bis-(2-nitrobenzoic acid) **15** or Ellman's reagent assay (Ellman 1959). The double bond of DNTB is reduced by free thiols. The reaction products are a mixed disulphide-protein and a yellow coloured product 5 TNB²⁻ (-Thio-2-NitroBenzoic acid) **16** (Figure 5.7). The amount of TNB generated correlates with the thiol content and can be measured spectrophotometrically. To measure the concentration of free thiol groups, the product TNB was quantified using UV-Vis absorption spectrophotometer at 412 nm either using a cysteine Standard or molar absorptivity (TNB molar extinction coefficient is 14.150 M⁻¹ cm⁻¹ (Riddles et al. 1983)).

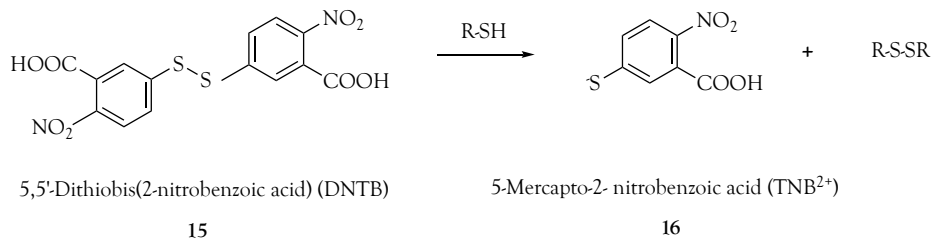


Figure 5.7: Scheme of DNTB reaction with thiol compound. Reduction of Ellman's reagent (DNTB) into its products TNB²⁻ and disulphide-bonded protein.

5.2.3 Cysteine cross-linking on membranes

The formation of the SS-bond was attempted prior to crystallisation of the LeuT-SS to ensure the inward-facing form was crystallised. An established protocol for the SS-bond formation of LeuT was not available. Therefore, the creation of this bond was examined in membranes and in pure protein in detergent, as described in Section 2.4.3. Cross-linking was initiated by the addition of the oxidant catalyst copper-phenanthroline to membrane preparations with 1-2 mg/ml protein concentration (measured by the Schaffner-Weissmann protein concentration assay, 1973) with different incubation times. Reactions were quenched with 5 mM EDTA to chelate Cu(II) and 100 mM N-ethyl-maleimide (NEM) to block any remaining free sulphhydryl groups at different incubation times at room temperature and at 4° C to investigate the optimal cross-linking conditions. SDS-PAGE electrophoresis analysis was carried out for samples from all the reactions. Disulphide bond formation can be only reversed by reducing agents. Therefore, samples were prepared with and without the addition of a reducing agent (10 mM β -ME) as a control (Figure 5.8).

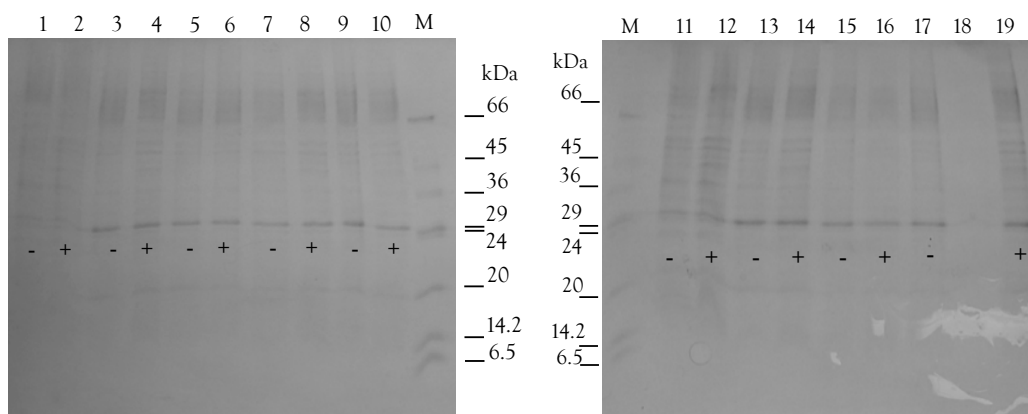


Figure 5.8: Comparing triple-mutant LeuT mobility in SDS-PAGE under reducing and non reducing conditions after cross-linking treatment on membranes. After quenching the reaction at different times with EDTA and NEM, samples were run in parallel with (marked with +) and without reducing agent (marked with -). (a) (1) homogenised membranes, no β -ME, (2) homogenised membranes, with β -ME, (3) 50 μ M:100 μ M RT, no β -ME, (4) 50 μ M:100 μ M RT, yes β -ME, (5) 50 μ M:100 μ M 4° C, no β -ME, (6) 50 μ M:100 μ M 4° C Yes β -ME, (7) 200 μ M:400 μ M RT, no β -ME, (8) 200 μ M:400 μ M RT, Yes β -ME, (9) 200 μ M:400 μ M 4° C, no β -ME, (10) 200 μ M:400 μ M 4° C, yes β -ME, (M) molecular weight marker, (11) homogenised membranes, no β -ME, (12) homogenised membranes, yes β -ME, (13) 100 μ M: 250 μ M RT, no β -ME, (14) 100 μ M: 250 μ M RT, yes β -ME, (15) 100 μ M: 250 μ M 4° C, no β -ME, (16) 100 μ M: 250 μ M 4° C, yes β -ME, (17) 1 mM:2.5 mM RT, no β -ME, (18) empty, (19) 1 mM:2.5 mM, yes β -ME. RT: room temperature.

The disulphide bond formation after the cross-linking treatment was examined by SDS-PAGE gel using SDS sample buffer lacking reducing agent (Section 2.4.3). Protein containing disulphide bonds is expected to exhibit higher mobility in non-reducing conditions because the presence of disulphide bonds will make the protein more compact. The SDS-PAGE gels in Figure 5.8 show a major band at the same migration distance in both in the presence and absence of reducing agent. However, no band is present at the expected size for the LeuT-SS in the presence of reducing agent, and indeed, no shift in the bands is seen with and without reducing agent. This strongly suggests this major band is not LeuT-SS, instead this may be the strong band seen in the membrane pellet before affinity purification (Figure 5.1a, lane 5). As no LeuT could be observed on the SDS-PAGE gel no conclusions could be drawn about the degree of cross-linking under the various conditions tested (Figure 5.8). Therefore cross-linking conditions based on Radchenko et al. (2016) were used and the LeuT-SS purified for further analysis.

5.2.4 Small-scale purification of wild-type LeuT and triple-mutant LeuT after cross-linking on membranes

Frozen aliquots of membrane preparations for the wild-type LeuT (LeuT-WT) and the LeuT-SS were treated under the same cross-linking conditions (with 200 μ M:400 μ M CuP on ice) in parallel. Wild-type LeuT was used as a negative control since it does not contain any cysteines. After cross-linking on membranes, LeuT was solubilised in DDM and the first affinity was run. In the solubilisation mixture after the cross-linking treatment a darker colour was observed compared to the non-cross linked protein. White fibres were also observed in both reactions (wild-type LeuT and triple-mutant LeuT) during the solubilisation step. These white fibres were still visible in the the supernatant after ultra-centrifugation, as well as in the insoluble pellet. The cross-linked LeuT-SS was obtained in only very low yield. This suggests that LeuT-SS did not survive the cross-linking treatment (oxidation treatment) on the membranes and so cross-linked trials should be done on pure proteins instead.

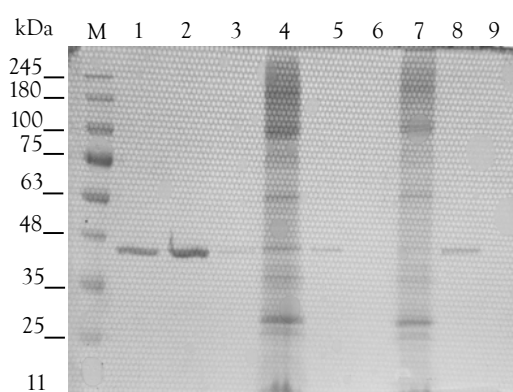


Figure 5.9: SDS-PAGE gel of the wild-type LeuT and triple-mutant LeuT after cross-linking treatment on membranes. The SDS-PAGE was loaded as follows and stained with Coomassie Blue: (M) Molecular weight marker, (1) wild-type LeuT first elution, (2) wild-type LeuT second elution, (3) wild-type LeuT third elution, (4) wild-type LeuT solubilised membrane, (5) wild-type LeuT cobalt resin after elution, (6) Triple-mutant LeuT-SS cobalt resin after elution, (7) triple-mutant LeuT-SS solubilised membrane, (8) triple-mutant LeuT-SS second elution, (9) triple-mutant LeuT-SS third elution.

Both purified wild-type LeuT (LeuT-WT) and triple-mutant LeuT (LeuT-SS) were cross-linked by incubation in copper-phenanthroline for 30 minutes on ice. Then remaining free sulphhydryl groups were quantified using Ellman's reagent in the presence of EDTA to inactivate the cop-

per phenanthroline (Ellman et al. 1958)) (Sections 5.2.2. The product TNB^{2-} from the reaction of DNTB with the free thiols of the non-bonded cysteines is detected at 412 nm using an UV-Visible spectrophotometer (Section 2.4.4). The quantification of the free thiol groups using Ellman's reagent was difficult. Protein concentration for both wild-type LeuT and triple mutant LeuT was very low there was insufficient material to perform both the protein assay and the controls. Higher protein yield is needed, to perform the needed series of experiment for the cross-linked and non-cross-linked protein.

5.3 Discussion

LeuT is able to crystallise only from freshly purified protein at 4° C. The purification had to be done quickly, with no long delays. Good quality crystals were obtained in the published conditions. For the LeuT-SS, many obstacles still need to be overcome to obtain pure, stable protein in high yields and to determine the optimal conditions for purification in potassium conditions. 24 L of LeuT-WT culture usually gave 100 µl pure protein at 7 mg/ml but for the LeuT-SS, from the same culture volume, after cross-linking treatment only 50 µl of 0.12 mg/ml final protein were obtained, while for the non-cross-linked triple mutant-SS only 50 µl of 0.45 mg/ml of pure protein. If higher yields cannot be obtained, one possibility would be to scale up the starting culture using a fermenter.

The experiments presented here have shown that the formation of the disulphide bond by cross-linking with copper phenanthroline in membranes results in loss of LeuT protein. Therefore cross-linking of purified proteins is likely to be needed and first investigations of this have been carried out. The need for further experiments for this very promising project is evident. Only more extensive research will allow us to choose the optimum conditions for LeuT variant cross-linking prior to crystallisation.

Chapter 6

Conclusions and future outlook

Secondary active transmembrane transports are responsible for the transportation of important solutes across the cell membrane utilising the free energy stored in an ionic gradient. These transporters have a similar structural fold, the LeuT-fold, and are believed to share the same transport mechanism, the alternating access mechanism. In this mechanism, the transporter is open to one side of the membrane to bind ligand, it then closes and opens to the opposite side of the membrane to release the ligand. Mhp1 and LeuT are two secondary active transporters examined during this thesis as model systems to study the transport mechanism, both functionally and structurally.

To date, three conformational states have been identified crystallographically for Mhp1: the outward-open, outward-occluded and inward-open states (Weyand et al. 2006, Shimamura et al. 2010). This thesis describes our attempts to capture Mhp1 in additional conformational states (representing intermediate states of the alternating access mechanism) using various Mhp1 mutants. Previous functional studies (Jackson 2012) of Mhp1 mutants have shown specific mutations to affect the ligand binding affinity and thus potentially adopt a different conformation. Five new crystal structures of Mhp1 mutants were determined by X-ray crystallography during this thesis in both apo state and bound with hydantoin ligands. The structures Ala38Gly-apo and Ala222Ser-apo were found in the outward-open conformation, while the

Met39Cys-*L*-BH, Ala222Ser-*L*-BH and Ala222Ser-*L*-IMH adopted an outward-occluded conformation. Two further mutants Ala309Asn and Thr313Ala, predicted based on biochemical studies to adopt an inward facing conformation yielded either no (Thr313Ala) or very poorly diffracting crystals (Ala309Asn). Interestingly, the low resolution diffraction obtained for Ala309Asn indicated a hexagonal packing, which has previously only been observed for wild type Mhp1 in an inward-facing conformation. Further optimisation of the crystallisation of this mutant may enable this structure to eventually be solved. Thus, the inward-facing states remain the most difficult structures to obtain. In order to obtain higher resolution crystallisation conditions in lipidic cubic phase or lipid sponge phase could be tested (Caffrey 2009, Wöhri et al. 2008).

Mhp1 purified in DDM detergent does not form crystals. In NM detergent, Mhp1 can be crystallised, but based on tryptophan fluorescence assays the ligand binding activity is reduced. Initial SAXS studies suggested that there were some changes in Mhp1 in the presence of different detergents (Polyakova 2015). SAXS is a useful and effective tool to characterise protein structure in solution prior to crystallisation and to characterise protein-protein interactions in solution in order to determine crystallisation conditions (Bonneté et al. 2004, Budayova et al. 1999, Ducruix et al. 1996, Narayanan & Liu 2003, Veessler et al. 1996). Especially in case of membrane proteins, this information is useful to understand the crystallisation propensity of the protein in combination with the detergent packing around the protein molecules in crystallisation procedure. In this project SEC-SAXS experiments showed that wild type Mhp1 in NM is predominantly present as a trimeric oligomer, whereas in DDM dimers are observed. The effect of salt and *L*-BH substrate on the oligomerisation of Mhp1 was also explored. SEC-SAXS data showed that the ligands and presence of sodium or potassium also have major effects on the oligomerisation state of Mhp1. In potassium predominantly monomers of WT-NM are obtained, possibly explaining why crystals are not obtained in potassium-based conditions.

The oligomerisation state of Mhp1 mutants was also explored using SEC-SAXS. Mhp1 mutants, Ala222Ser and Met39Cys, showed very similar behaviour to WT-NM, consistent with the crystallographic and biochemical studies. However, the Ala309Asn and Thr313Ala variants showed a distinct distribution of monomers, dimers and trimers that might explain why high quality crystals could not be obtained. These attempts to investigate the crystallisation propensity and detergent packing of Mhp1 variants using SEC-SAXS experiments are at an early stage, but are promising and worthy of further study.

It is difficult to assess the degree of the detergent exchange that is achieved by exchanging the detergent on the Ni-NTA affinity column during the purification from DDM to NM. The final Mhp1 protein-detergent complex that crystallises is likely to consist of a mixture of the two detergents. It is possible that this helps with crystal packing, but it is equally possible that even better crystals could be obtained with a purer protein-detergent complex. For a better comparison of Mhp1's properties in complex with different detergents solubilisation and full purification in the different detergents could be tried. Future experiments of SEC-SAXS also could be usefully coupled with light scattering (MALLS) and reflective index (RI) to better investigate the detergent composition prior to crystallisation.

Another major difficulty in the analysis of transmembrane transporters is that physical studies of protein structure while protein is in the membrane are difficult to perform (Seddon et al. 2004). On the other hand studies of proteins solubilised in detergent environments raise questions as to whether the detergent has caused alterations in the structure being observed. Thus, new approaches that are equally applicable in membranes and detergents are needed. One possibility is to reconstitute the purified Mhp1 in detergent into nanodiscs as these provide a more native-like lipid environment for integral membrane proteins (Bayburt & Sligar 2010, Denisov & Sligar 2016). These could be used for SEC-SAXS studies or even single particle cryo-electron microscopy. Prior to structural studies it is also advisable to use tryptophan flu-

orescence to monitor the ligand binding activity of Mhp1 reconstituted into nanodiscs.

As far as the time-resolved X-ray crystallography experiments of LeuT transporters many obstacles need to be overcome. Wild type LeuT crystals were successfully obtained, but only from freshly purified protein. The triple mutant with SS-bond crosslinking was expressed and purified, however both the cross-linking and crystallisation conditions need to be optimised.

Bibliography

- Abramson, J. & Wright, E. M. (2009), 'Structure and function of na⁺-symporters with inverted repeats', *Current opinion in structural biology* **19**(4), 425–432.
- Adelman, J. L., Dale, A. L., Zwier, M. C., Bhatt, D., Chong, L. T., Zuckerman, D. M. & Grabe, M. (2011), 'Simulations of the alternating access mechanism of the sodium symporter mhp1', *Biophysical journal* **101**(10), 2399–2407.
- Ataka, M. (1993), 'Protein crystal growth: an approach based on phase diagram determination', *Phase Transitions: A Multinational Journal* **45**(2-3), 205–219.
- Auer, M., Kim, M. J., Lemieux, M. J., Villa, A., Song, J., Li, X.-D. & Wang, D.-N. (2001), 'High-yield expression and functional analysis of escherichia coli glycerol-3-phosphate transporter', *Biochemistry* **40**(22), 6628–6635.
- Bayburt, T. H. & Sligar, S. G. (2010), 'Membrane protein assembly into nanodiscs', *FEBS letters* **584**(9), 1721–1727.
- Bergfors, T. (1999), 'Protein samples', *Protein Crystallization: A Laboratory Manual* pp. 17–25.
- Bergfors, T. (2003), 'Seeds to crystals', *Journal of structural biology* **142**(1), 66–76.
- Berthaud, A., Manzi, J., Pérez, J. & Mangenot, S. (2012), 'Modeling detergent organization around aquaporin-0 using small-angle x-ray scattering', *Journal of the American Chemical Society* **134**(24), 10080–10088.
- Birch, J., Axford, D., Foadi, J., Meyer, A., Eckardt, A., Thielmann, Y. & Moraes, I. (2018), 'The fine art of integral membrane protein crystallisation', *Methods* .

- Bonneté, F., Ferté, N., Astier, J. & Veessler, S. (2004), Protein crystallization: Contribution of small angle x-ray scattering (saxs), in 'Journal de Physique IV (Proceedings)', Vol. 118, EDP sciences, pp. 3–13.
- Boudker, O. & Verdon, G. (2010), 'Structural perspectives on secondary active transporters', *Trends in pharmacological sciences* **31**(9), 418–426.
- Bowman, A. & Owen-Hughes, T. (2012), Sulfhydryl-reactive site-directed cross-linking as a method for probing the tetrameric structure of histones h3 and h4, in 'Chromatin Remodeling', Springer, pp. 373–387.
- Bröer, S. & Palacin, M. (2011), 'The role of amino acid transporters in inherited and acquired diseases', *Biochemical Journal* **436**(2), 193–211.
- Budayova, M., Bonneté, F., Tardieu, A. & Vachette, P. (1999), 'Interactions in solution of a large oligomeric protein', *Journal of crystal growth* **196**(2-4), 210–219.
- Bulheller, B. M., Rodger, A. & Hirst, J. D. (2007), 'Circular and linear dichroism of proteins', *Physical Chemistry Chemical Physics* **9**(17), 2020–2035.
- Caffrey, M. (2008), 'On the mechanism of membrane protein crystallization in lipidic mesophases', *Crystal Growth and Design* **8**(12), 4244–4254.
- Caffrey, M. (2009), 'Crystallizing membrane proteins for structure determination: use of lipidic mesophases', *Annual review of biophysics* **38**, 29–51.
- Caffrey, M., Li, D. & Dukupati, A. (2012), 'Membrane protein structure determination using crystallography and lipidic mesophases: recent advances and successes', *Biochemistry* **51**(32), 6266–6288.
- Caffrey, M. & Porter, C. (2010), 'Crystallizing membrane proteins for structure determination using lipidic mesophases', *JoVE (Journal of Visualized Experiments)* (45), e1712.
- Calabrese, A. N., Jackson, S. M., Jones, L. N., Beckstein, O., Heinkel, F., Gsponer, J., Sharples, D., Sans, M., Kokkinidou, M., Pearson, A. R. et al. (2017), 'Topological dissection of the

- membrane transport protein mhp1 derived from cysteine accessibility and mass spectrometry', *Analytical chemistry* **89**(17), 8844–8852.
- Carpenter, E. P., Beis, K., Cameron, A. D. & Iwata, S. (2008), 'Overcoming the challenges of membrane protein crystallography', *Current opinion in structural biology* **18**(5), 581–586.
- Chayen, N. E. (1998), 'Comparative studies of protein crystallization by vapour-diffusion and microbatch techniques', *Acta Crystallographica Section D: Biological Crystallography* **54**(1), 8–15.
- Chen, Y. & Barkley, M. D. (1998), 'Toward understanding tryptophan fluorescence in proteins', *Biochemistry* **37**(28), 9976–9982.
- Cherezov, V., Yamashita, E., Liu, W., Zhahnina, M., Cramer, W. & Caffrey, M. (2006), 'In meso structure of the cobalamin transporter, btub, at 1.95 Å resolution', *Journal of molecular biology* **364**(4), 716–734.
- Clemente-Jiménez, J. M., Martínez-Rodríguez, S., Rodríguez-Vico, F. & Heras-Vázquez, F. J. (2008), 'Optically pure α -amino acids production by the "hydantoinase process."', *Recent Pat Biotechnol* **2**(1), 35–46.
- Deller, M. C., Kong, L. & Rupp, B. (2016), 'Protein stability: a crystallographer's perspective', *Acta Crystallographica Section F: Structural Biology Communications* **72**(2), 72–95.
- Delmar, J. A., Bolla, J. R., Su, C.-C. & Edward, W. Y. (2015), Crystallization of membrane proteins by vapor diffusion, in 'Methods in enzymology', Vol. 557, Elsevier, pp. 363–392.
- Denisov, I. G. & Sligar, S. G. (2016), 'Nanodiscs for structural and functional studies of membrane proteins', *Nature structural & molecular biology* **23**(6), 481.
- Diallinas, G. (2008), 'An almost-complete movie', *Science* **322**(5908), 1644–1645.
- Drew, D., Fröderberg, L., Baars, L. & de Gier, J.-W. L. (2003), 'Assembly and overexpression of membrane proteins in escherichia coli', *Biochimica et Biophysica Acta (BBA)-Biomembranes* **1610**(1), 3–10.

- Ducruix, A. & Giegé, R. (1999), *Crystallization of nucleic acids and proteins: a practical approach*, number 210, Practical Approach Series.
- Ducruix, A., Guilloteau, J. P., Riès-Kautt, M. & Tardieu, A. (1996), 'Protein interactions as seen by solution x-ray scattering prior to crystallogenesis', *Journal of Crystal Growth* **168**(1-4), 28-39.
- Edward, W. Y., Aires, J. R. & Nikaido, H. (2003), 'Acrb multidrug efflux pump of escherichia coli: composite substrate-binding cavity of exceptional flexibility generates its extremely wide substrate specificity', *Journal of bacteriology* **185**(19), 5657-5664.
- Ellman, G. L. (1959), 'Tissue sulfhydryl groups', *Archives of biochemistry and biophysics* **82**(1), 70-77.
- Ellman, G. L. et al. (1958), 'A colorimetric method for determining low concentrations of mercaptans.', *Archives of Biochemistry* **74**, 443-450.
- Emsley, P. & Cowtan, K. (2004), 'Coot: model-building tools for molecular graphics', *Acta Crystallographica Section D: Biological Crystallography* **60**(12), 2126-2132.
- Eshaghi, S., Hedrén, M., Nasser, M. I. A., Hammarberg, T., Thornell, A. & Nordlund, P. (2005), 'An efficient strategy for high-throughput expression screening of recombinant integral membrane proteins', *Protein Science* **14**(3), 676-683.
- Evans, P. (2006), 'Scaling and assessment of data quality', *Acta Crystallographica Section D: Biological Crystallography* **62**(1), 72-82.
- Faham, S. & Bowie, J. U. (2002), 'Bicelle crystallization: a new method for crystallizing membrane proteins yields a monomeric bacteriorhodopsin structure', *Journal of molecular biology* **316**(1), 1-6.
- Faham, S., Watanabe, A., Besserer, G. M., Cascio, D., Specht, A., Hirayama, B. A., Wright, E. M. & Abramson, J. (2008), 'The crystal structure of a sodium galactose transporter reveals mechanistic insights into na⁺/sugar symport', *Science* **321**(5890), 810-814.

- Falke, J. J. & Koshland, D. E. (1987), 'Global flexibility in a sensory receptor: a site-directed cross-linking approach', *Science* **237**(4822), 1596–1600.
- Fang, Y., Jayaram, H., Shane, T., Kolmakova-Partensky, L., Wu, F., Williams, C., Xiong, Y. & Miller, C. (2009), 'Structure of a prokaryotic virtual proton pump at 3.2 Å resolution', *Nature* **460**(7258), 1040.
- Forrest, L. R., Krämer, R. & Ziegler, C. (2011), 'The structural basis of secondary active transport mechanisms', *Biochimica et Biophysica Acta (BBA)-Bioenergetics* **1807**(2), 167–188.
- Forrest, L. R. & Rudnick, G. (2009), 'The rocking bundle: a mechanism for ion-coupled solute flux by symmetrical transporters', *Physiology* **24**(6), 377–386.
- Forsythe, E. L., Maxwell, D. L. & Pusey, M. (2002), 'Vapor diffusion, nucleation rates and the reservoir to crystallization volume ratio', *Acta Crystallographica Section D: Biological Crystallography* **58**(10), 1601–1605.
- French, S. & Wilson, K. (1978), 'On the treatment of negative intensity observations', *Acta Crystallographica Section A: Crystal Physics, Diffraction, Theoretical and General Crystallography* **34**(4), 517–525.
- Gadsby, D. C. (2009), 'Ion channels versus ion pumps: the principal difference, in principle', *Nature reviews Molecular cell biology* **10**(5), 344.
- Gao, X., Lu, F., Zhou, L., Dang, S., Sun, L., Li, X., Wang, J. & Shi, Y. (2009), 'Structure and mechanism of an amino acid antiporter', *Science* **324**(5934), 1565–1568.
- Garavito, R. M. & Ferguson-Miller, S. (2001), 'Detergents as tools in membrane biochemistry', *Journal of Biological Chemistry* **276**(35), 32403–32406.
- García-Ruiz, J. M. (2003), Counterdiffusion methods for macromolecular crystallization, in 'Methods in Enzymology', Vol. 368, Elsevier, pp. 130–154.
- Garman, E. (2003), "cool"crystals: macromolecular cryocrystallography and radiation damage', *Current opinion in structural biology* **13**(5), 545–551.

- Gether, U., Andersen, P. H., Larsson, O. M. & Schousboe, A. (2006), 'Neurotransmitter transporters: molecular function of important drug targets', *Trends in pharmacological sciences* 27(7), 375–383.
- Glover, C. A., Postis, V. L., Charalambous, K., Tzokov, S. B., Booth, W. I., Deacon, S. E., Wallace, B., Baldwin, S. A. & Bullough, P. A. (2011), 'Acrb contamination in 2-d crystallization of membrane proteins: lessons from a sodium channel and a putative monovalent cation/proton antiporter', *Journal of structural biology* 176(3), 419–424.
- Greenfield, N. J. (2006), 'Using circular dichroism collected as a function of temperature to determine the thermodynamics of protein unfolding and binding interactions', *Nature protocols* 1(6), 2527.
- Hastrup, H., Karlin, A. & Javitch, J. A. (2001), 'Symmetrical dimer of the human dopamine transporter revealed by cross-linking cys-306 at the extracellular end of the sixth transmembrane segment', *Proceedings of the National Academy of Sciences* 98(18), 10055–10060.
- Humphrey, W., Dalke, A. & Schulten, K. (1996), 'Vmd: visual molecular dynamics', *Journal of molecular graphics* 14(1), 33–38.
- Iwata, S. (2003), *Methods and results in crystallization of membrane proteins*, Vol. 4, Internat'l University Line.
- Jackson, S. M. (2012), Elucidating the molecular mechanisms of ligand binding and transport by the Na⁺-hydantoin transport protein, Mhp1, PhD thesis, University of Leeds.
- Jackson, S. M., Patching, S. G., Ivanova, E., Simmons, K., Weyand, S., Shimamura, T., Brueckner, F., Suzuki, S., Iwata, S., Sharples, D. J. et al. (2013), 'Mhp1, the na⁺-hydantoin membrane transport protein', *Encyclopedia of biophysics* pp. 1514–1521.
- Jardetzky, O. (1966), 'Simple allosteric model for membrane pumps', *Nature* 211(5052), 969.
- Jiang, W. & Fillingame, R. H. (1998), 'Interacting helical faces of subunits a and c in the f1fo atp synthase of escherichia coli defined by disulfide cross-linking', *Proceedings of the National Academy of Sciences* 95(12), 6607–6612.

- Jung, H., Buchholz, M., Clausen, J., Nietschke, M., Revermann, A., Schmid, R. & Jung, K. (2002), 'Cait of escherichia coli, a new transporter catalyzing l-carnitine/ γ -butyrobetaine exchange', *Journal of Biological Chemistry* **277**(42), 39251–39258.
- Junge, F., Schneider, B., Reckel, S., Schwarz, D., Dötsch, V. & Bernhard, F. (2008), 'Large-scale production of functional membrane proteins', *Cellular and Molecular Life Sciences* **65**(11), 1729–1755.
- Kabsch, W. (2010), 'Xds', *Acta Crystallographica Section D: Biological Crystallography* **66**(2), 125–132.
- Kadokura, H. & Beckwith, J. (2009), 'Detecting folding intermediates of a protein as it passes through the bacterial translocation channel', *Cell* **138**(6), 1164–1173.
- Kadokura, H., Katzen, F. & Beckwith, J. (2003), 'Protein disulfide bond formation in prokaryotes', *Annual review of biochemistry* **72**(1), 111–135.
- Kaplan, R. S. & Pedersen, P. L. (1985), 'Determination of microgram quantities of protein in the presence of milligram levels of lipid with amido black 10b1', *Analytical biochemistry* **150**(1), 97–104.
- Karplus, P. A. & Diederichs, K. (2012), 'Linking crystallographic model and data quality', *Science* **336**(6084), 1030–1033.
- Katona, G., Andreasson, U., Landau, E. M., Andreasson, L.-E. & Neutze, R. (2003), 'Lipidic cubic phase crystal structure of the photosynthetic reaction centre from rhodospirillum rubrum at 2.35 Å resolution', *Journal of molecular biology* **331**(3), 681–692.
- Katz, B. & Kossiakoff, A. (1986), 'The crystallographically determined structures of atypical strained disulfides engineered into subtilisin.', *Journal of Biological Chemistry* **261**(33), 15480–15485.
- Kazmier, K., Claxton, D. P. & Mchaourab, H. S. (2017), 'Alternating access mechanisms of leucine transporters: trailblazing towards the promised energy landscapes', *Current opinion in structural biology* **45**, 100–108.

- Kazmier, K., Sharma, S., Islam, S. M., Roux, B. & Mchaourab, H. S. (2014), 'Conformational cycle and ion-coupling mechanism of the Na^+ /hydantoin transporter mhp1', *Proceedings of the National Academy of Sciences* **111**(41), 14752–14757.
- Kelly, S. M., Jess, T. J. & Price, N. C. (2005), 'How to study proteins by circular dichroism', *Biochimica et Biophysica Acta (BBA)-Proteins and Proteomics* **1751**(2), 119–139.
- Kikhney, A. G. & Svergun, D. I. (2015), 'A practical guide to small angle x-ray scattering (saxs) of flexible and intrinsically disordered proteins', *FEBS letters* **589**(19PartA), 2570–2577.
- Kowalczyk, L., Ratera, M., Paladino, A., Bartoccioni, P., Errasti-Murugarren, E., Valencia, E., Portella, G., Bial, S., Zorzano, A., Fita, I. et al. (2011), 'Molecular basis of substrate-induced permeation by an amino acid antiporter', *Proceedings of the National Academy of Sciences* **108**(10), 3935–3940.
- Krishnamurthy, H. & Gouaux, E. (2012), 'X-ray structures of leut in substrate-free outward-open and apo inward-open states', *Nature* **481**(7382), 469.
- Krishnamurthy, H., Piscitelli, C. L. & Gouaux, E. (2009), 'Unlocking the molecular secrets of sodium-coupled transporters', *Nature* **459**(7245), 347.
- Landau, E. M. & Rosenbusch, J. P. (1996), 'Lipidic cubic phases: a novel concept for the crystallization of membrane proteins', *Proceedings of the National Academy of Sciences* **93**(25), 14532–14535.
- Las Heras-Vázquez, F. J., Clemente-Jiménez, J. M., Martínez-Rodríguez, S. & Rodríguez-Vico, F. (2008), 'Hydantoin racemase: the key enzyme for the production of optically pure α -amino acids', *Modern Biocatalysis: Stereoselective and Environmentally Friendly Reactions* .
- le Maire, M., Champeil, P. & Møller, J. V. (2000), 'Interaction of membrane proteins and lipids with solubilizing detergents', *Biochimica et Biophysica Acta (BBA)-Biomembranes* **1508**(1-2), 86–111.

- Lebedev, A. A., Vagin, A. A. & Murshudov, G. N. (2008), 'Model preparation in molrep and examples of model improvement using x-ray data', *Acta Crystallographica Section D: Biological Crystallography* **64**(1), 33–39.
- Lee, A. G. (2005), 'How lipids and proteins interact in a membrane: a molecular approach', *Molecular BioSystems* **1**(3), 203–212.
- Lee, C.-C., Maestre-Reyna, M., Hsu, K.-C., Wang, H.-C., Liu, C.-I., Jeng, W.-Y., Lin, L.-L., Wood, R., Chou, C.-C., Yang, J.-M. et al. (2014), 'Crowning proteins: modulating the protein surface properties using crown ethers', *Angewandte Chemie International Edition* **53**(48), 13054–13058.
- Levantino, M., Yorke, B. A., Monteiro, D. C., Cammarata, M. & Pearson, A. R. (2015), 'Using synchrotrons and xfels for time-resolved x-ray crystallography and solution scattering experiments on biomolecules', *Current opinion in structural biology* **35**, 41–48.
- Lipfert, J., Columbus, L., Chu, V. B., Lesley, S. A. & Doniach, S. (2007), 'Size and shape of detergent micelles determined by small-angle x-ray scattering', *The journal of physical chemistry B* **111**(43), 12427–12438.
- Loll, P. J., Tretiakova, A. & Soderblom, E. (2003), 'Compatibility of detergents with the microbatch-under-oil crystallization method', *Acta Crystallographica Section D: Biological Crystallography* **59**(6), 1114–1116.
- Loo, T. W. & Clarke, D. M. (2000), 'Identification of residues within the drug-binding domain of the human multidrug resistance p-glycoprotein by cysteine-scanning mutagenesis and reaction with dibromobimane', *Journal of Biological Chemistry* **275**(50), 39272–39278.
- Ma, D., Lu, P., Yan, C., Fan, C., Yin, P., Wang, J. & Shi, Y. (2012), 'Structure and mechanism of a glutamate-gaba antiporter', *Nature* **483**(7391), 632.
- Malinauskaitė, L., Said, S., Sahin, C., Grouleff, J., Shahsavari, A., Bjerregaard, H., Noer, P., Severinsen, K., Boesen, T., Schiøtt, B. et al. (2016), 'A conserved leucine occupies the empty substrate site of LeuT in the Na⁺-free return state', *Nature communications* **7**, 11673.

- Martin, G., Rutherford, N., Henderson, P. & Walmsley, A. (1995), 'Kinetics and thermodynamics of the binding of forskolin to the galactose-h⁺ transport protein, galp, of escherichia coli', *Biochemical Journal* **308**(1), 261–268.
- Masip, L., Pan, J. L., Haldar, S., Penner-Hahn, J. E., DeLisa, M. P., Georgiou, G., Bardwell, J. C. & Collet, J.-F. (2004), 'An engineered pathway for the formation of protein disulfide bonds', *Science* **303**(5661), 1185–1189.
- McPherson, A. (1999), *Crystallization of biological macromolecules*.
- McPherson, A., Nguyen, C., Cudney, R. & Larson, S. (2011), 'The role of small molecule additives and chemical modification in protein crystallization', *Crystal Growth & Design* **11**(5), 1469–1474.
- Merritt, E. A. & Bacon, D. J. (1997), [26] raster3d: Photorealistic molecular graphics, in 'Methods in enzymology', Vol. 277, Elsevier, pp. 505–524.
- Michel, H. (1983), 'Crystallization of membrane proteins', *Trends in Biochemical Sciences* **8**(2), 56–59.
- Michel, H. (2018), *Crystallization of Membrane Proteins: 0*, CRC Press.
- Miles, A. J. & Wallace, B. A. (2016), 'Circular dichroism spectroscopy of membrane proteins', *Chemical Society Reviews* **45**(18), 4859–4872.
- Moore, K. J. & Fillingame, R. H. (2008), 'Structural interactions between transmembrane helices 4 and 5 of subunit a and the subunit c ring of escherichia coli atp synthase', *Journal of Biological Chemistry* **283**(46), 31726–31735.
- Murshudov, G. N., Skubák, P., Lebedev, A. A., Pannu, N. S., Steiner, R. A., Nicholls, R. A., Winn, M. D., Long, F. & Vagin, A. A. (2011), 'Refmac5 for the refinement of macromolecular crystal structures', *Acta Crystallographica Section D: Biological Crystallography* **67**(4), 355–367.

- Narayanan, J. & Liu, X. (2003), 'Protein interactions in undersaturated and supersaturated solutions: a study using light and x-ray scattering', *Biophysical journal* **84**(1), 523–532.
- Neutze, R. & Moffat, K. (2012), 'Time-resolved structural studies at synchrotrons and x-ray free electron lasers: opportunities and challenges', *Current opinion in structural biology* **22**(5), 651–659.
- Newby, Z. E., D O'Connell III, J., Gruswitz, F., Hays, F. A., Harries, W. E., Harwood, I. M., Ho, J. D., Lee, J. K., Savage, D. F., Miercke, L. J. et al. (2009), 'A general protocol for the crystallization of membrane proteins for x-ray structural investigation', *Nature protocols* **4**(5), 619.
- Ng, J. D., Gavira, J. A. & Garcia-Ruiz, J. M. (2003), 'Protein crystallization by capillary counterdiffusion for applied crystallographic structure determination', *Journal of structural biology* **142**(1), 218–231.
- Oliver, R. C., Lipfert, J., Fox, D. A., Lo, R. H., Doniach, S. & Columbus, L. (2013), 'Dependence of micelle size and shape on detergent alkyl chain length and head group', *PloS one* **8**(5), e62488.
- Pantazopoulou, A. & Diallinas, G. (2007), 'Fungal nucleobase transporters', *FEMS microbiology reviews* **31**(6), 657–675.
- Patching, S. G. (2011), 'Efficient syntheses of ¹³C- and ¹⁴C-labelled 5-benzyl and 5-indolylmethyl hydantoin', *Journal of Labelled Compounds and Radiopharmaceuticals* **54**(2), 110–114.
- Pernot, P., Round, A., Barrett, R., De Maria Antolinos, A., Gobbo, A., Gordon, E., Huet, J., Kieffer, J., Lentini, M., Mattenet, M. et al. (2013), 'Upgraded esrf bm29 beamline for saxs on macromolecules in solution', *Journal of synchrotron radiation* **20**(4), 660–664.
- Polyakova, A. (2015), Applying complementary structural techniques to elucidate structure-function relationships of the bacterial Na⁺-hydantoin transporter Mhp1, PhD thesis, University of Leeds.

- Privé, G. G. (2007), 'Detergents for the stabilization and crystallization of membrane proteins', *Methods* **41**(4), 388–397.
- Qutub, Y., Reviakine, I., Maxwell, C., Navarro, J., Landau, E. M. & Vekilov, P. G. (2004), 'Crystallization of transmembrane proteins in cubo: mechanisms of crystal growth and defect formation', *Journal of molecular biology* **343**(5), 1243–1254.
- Radchenko, M., Nie, R. & Lu, M. (2016), 'Disulfide cross-linking of a multidrug and toxic compound extrusion transporter impacts multidrug efflux', *Journal of Biological Chemistry* **291**(18), 9818–9826.
- Rath, A., Glibowicka, M., Nadeau, V. G., Chen, G. & Deber, C. M. (2009), 'Detergent binding explains anomalous sds-page migration of membrane proteins', *Proceedings of the National Academy of Sciences* **106**(6), 1760–1765.
- Ren, Q., Chen, K. & Paulsen, I. T. (2006), 'Transportdb: a comprehensive database resource for cytoplasmic membrane transport systems and outer membrane channels', *Nucleic acids research* **35**(suppl_1), D274–D279.
- Ren, Q. & Paulsen, I. T. (2007), 'Large-scale comparative genomic analyses of cytoplasmic membrane transport systems in prokaryotes', *Journal of molecular microbiology and biotechnology* **12**(3-4), 165–179.
- Ressl, S., van Scheltinga, A. C. T., Vorrhein, C., Ott, V. & Ziegler, C. (2009), 'Molecular basis of transport and regulation in the na⁺/betaine symporter betp', *Nature* **458**(7234), 47.
- Riddles, P. W., Blakeley, R. L. & Zerner, B. (1983), [8] reassessment of ellman's reagent, in 'Methods in enzymology', Vol. 91, Elsevier, pp. 49–60.
- Rosenbusch, J. P. (2001), 'Stability of membrane proteins: relevance for the selection of appropriate methods for high-resolution structure determinations', *Journal of structural biology* **136**(2), 144–157.
- Round, A., Felisaz, F., Fodinger, L., Gobbo, A., Huet, J., Villard, C., Blanchet, C. E., Pernot, P., McSweeney, S., Roessle, M. et al. (2015), 'Biosaxs sample changer: a robotic sample

- changer for rapid and reliable high-throughput x-ray solution scattering experiments', *Acta Crystallographica Section D: Biological Crystallography* **71**(1), 67–75.
- Saidijam, M., Bettaney, K. E., Szakonyi, G., Psakis, G., Shibayama, K., Suzuki, S., Clough, J. L., Blessie, V., Abu-Bakr, A., Baumberg, S. et al. (2005), 'Active membrane transport and receptor proteins from bacteria'.
- Saidijam, M., Psakis, G., Clough, J. L., Mueller, J., Suzuki, S., Hoyle, C. J., Palmer, S. L., Morrison, S. M., Pos, M. K., Essenberg, R. C. et al. (2003), 'Collection and characterisation of bacterial membrane proteins', *FEBS letters* **555**(1), 170–175.
- Saier Jr, M. H., Tran, C. V. & Barabote, R. D. (2006), 'Tcdb: the transporter classification database for membrane transport protein analyses and information', *Nucleic acids research* **34**(suppl_1), D181–D186.
- Saier Jr, M. H., Yen, M. R., Noto, K., Tamang, D. G. & Elkan, C. (2008), 'The transporter classification database: recent advances', *Nucleic acids research* **37**(suppl_1), D274–D278.
- Sanchez-Weatherby, J., Bowler, M. W., Huet, J., Gobbo, A., Felisaz, F., Lavault, B., Moya, R., Kadlec, J., Ravelli, R. B. & Cipriani, F. (2009), 'Improving diffraction by humidity control: a novel device compatible with x-ray beamlines', *Acta Crystallographica Section D: Biological Crystallography* **65**(12), 1237–1246.
- Schaffner, W. & Weissmann, C. (1973), 'A rapid, sensitive, and specific method for the determination of protein in dilute solution', *Analytical biochemistry* **56**(2), 502–514.
- Schmidt, M., Ihee, H., Pahl, R. & Šrajer, V. (2005), Protein-ligand interaction probed by time-resolved crystallography, in 'Protein-Ligand Interactions', Springer, pp. 115–154.
- Schnell, D. J. & Hebert, D. N. (2003), 'Protein translocons: multifunctional mediators of protein translocation across membranes', *Cell* **112**(4), 491–505.
- Schulze, S., Köster, S., Geldmacher, U., van Scheltinga, A. C. T. & Kühlbrandt, W. (2010), 'Structural basis of na⁺-independent and cooperative substrate/product antiport in cait', *Nature* **467**(7312), 233.

- Seddon, A. M., Curnow, P. & Booth, P. J. (2004), 'Membrane proteins, lipids and detergents: not just a soap opera', *Biochimica et Biophysica Acta (BBA)-Biomembranes* **1666**(1-2), 105–117.
- Segelke, B. (2005), 'Macromolecular crystallization with microfluidic free-interface diffusion', *Expert review of proteomics* **2**(2), 165–172.
- Shaffer, P. L., Goehring, A., Shankaranarayanan, A. & Gouaux, E. (2009), 'Structure and mechanism of a Na⁺-independent amino acid transporter', *Science* **325**(5943), 1010–1014.
- Shi, Y. (2013), 'Common folds and transport mechanisms of secondary active transporters', *Annual review of biophysics* **42**, 51–72.
- Shimamura, T., Weyand, S., Beckstein, O., Rutherford, N. G., Hadden, J. M., Sharples, D., Sansom, M. S., Iwata, S., Henderson, P. J. & Cameron, A. D. (2010), 'Molecular basis of alternating access membrane transport by the sodium-hydantoin transporter mhp1', *Science* **328**(5977), 470–473.
- Shimamura, T., Yajima, S., Suzuki, S., Rutherford, N. G., O'Reilly, J., Henderson, P. J. & Iwata, S. (2008), 'Crystallization of the hydantoin transporter mhp1 from microbacterium liquefaciens', *Acta Crystallographica Section F: Structural Biology and Crystallization Communications* **64**(12), 1172–1174.
- Simmons, K. J., Jackson, S. M., Brueckner, F., Patching, S. G., Beckstein, O., Ivanova, E., Geng, T., Weyand, S., Drew, D., Lanigan, J. et al. (2014), 'Molecular mechanism of ligand recognition by membrane transport protein, mhp1', *The EMBO journal* p. e201387557.
- Singh, S. K., Piscitelli, C. L., Yamashita, A. & Gouaux, E. (2008), 'A competitive inhibitor traps leuT in an open-to-out conformation', *Science* **322**(5908), 1655–1661.
- Smirnova, I., Kasho, V., Sugihara, J., Vázquez-Ibar, J. L. & Kaback, H. R. (2012), 'Role of protons in sugar binding to lacY', *Proceedings of the National Academy of Sciences* **109**(42), 16835–16840.
- Smirnova, I. N., Kasho, V. & Kaback, H. R. (2008), 'Protonation and sugar binding to lacY', *Proceedings of the National Academy of Sciences* **105**(26), 8896–8901.

- Sohail, A., Jayaraman, K., Venkatesan, S., Gotfryd, K., Daerr, M., Gether, U., Loland, C. J., Wanner, K. T., Freissmuth, M., Sitte, H. H. et al. (2016), 'The environment shapes the inner vestibule of leuT', *PLoS computational biology* **12**(11), e1005197.
- Šrajer, V. & Schmidt, M. (2017), 'Watching proteins function with time-resolved x-ray crystallography', *Journal of physics D: Applied physics* **50**(37), 373001.
- Stone, J. (1998), *An Efficient Library for Parallel Ray Tracing and Animation*, Master's thesis, Computer Science Department, University of Missouri-Rolla.
- Sukumar, P. (2012), Molecular dissection of substrate and inhibitor binding to the D-galactose-H⁺ symport protein (GalP) from *Escherichia coli*-the bacterial homologue of GLUT1, PhD thesis, University of Leeds.
- Sutton, B. J. & Sohi, M. K. (1994), Crystallization of membrane proteins for x-ray analysis, in 'Biomembrane Protocols', Springer, pp. 1-18.
- Suzuki, S. & Henderson, P. J. (2006), 'The hydantoin transport protein from microbacterium liquefaciens', *Journal of bacteriology* **188**(9), 3329-3336.
- Syldatk, C., Läufer, A., Müller, R. & Höke, H. (1990), Production of optically pure d- and l- α -amino acids by bioconversion of d, l-5-monosubstituted hydantoin derivatives, in 'Microbial Bioproducts', Springer, pp. 29-75.
- Takatsuka, Y., Chen, C. & Nikaido, H. (2010), 'Mechanism of recognition of compounds of diverse structures by the multidrug efflux pump AcrB of *Escherichia coli*', *Proceedings of the National Academy of Sciences* **107**(15), 6559-6565.
- Tang, L., Bai, L., Wang, W.-h. & Jiang, T. (2010), 'Crystal structure of the carnitine transporter and insights into the antiport mechanism', *Nature structural & molecular biology* **17**(4), 492.
- Thenmozhiyal, J. C., Wong, P. T.-H. & Chui, W.-K. (2004), 'Anticonvulsant activity of phenylmethylenehydantoins: A structure-activity relationship study', *Journal of medicinal chemistry* **47**(6), 1527-1535.

- Thorn, A., Parkhurst, J., Emsley, P., Nicholls, R. A., Vollmar, M., Evans, G. & Murshudov, G. N. (2017), 'Auspex: a graphical tool for x-ray diffraction data analysis', *Acta Crystallographica Section D: Structural Biology* **73**(9), 729–737.
- Towbin, H., Staehelin, T. & Gordon, J. (1979), 'Electrophoretic transfer of proteins from polyacrylamide gels to nitrocellulose sheets: procedure and some applications', *Proceedings of the National Academy of Sciences* **76**(9), 4350–4354.
- Vagin, A. & Teplyakov, A. (2010), 'Molecular replacement with molrep', *Acta Crystallographica Section D: Biological Crystallography* **66**(1), 22–25.
- Vaguine, A. A., Richelle, J. & Wodak, S. (1999), 'Sfcheck: a unified set of procedures for evaluating the quality of macromolecular structure-factor data and their agreement with the atomic model', *Acta Crystallographica Section D: Biological Crystallography* **55**(1), 191–205.
- Vastermark, A., Wollwage, S., Houle, M. E., Rio, R. & Saier Jr, M. H. (2014), 'Expansion of the apc superfamily of secondary carriers', *Proteins: Structure, Function, and Bioinformatics* **82**(10), 2797–2811.
- Veenstra, M., Turk, E. & Wright, E. (2002), 'A ligand-dependent conformational change of the na⁺/galactose cotransporter of vibrio parahaemolyticus, monitored by tryptophan fluorescence', *Journal of Membrane Biology* **185**(3), 249–255.
- Veesler, D., Blangy, S., Cambillau, C. & Sciara, G. (2008), 'There is a baby in the bath water: Acrb contamination is a major problem in membrane-protein crystallization', *Acta Crystallographica Section F: Structural Biology and Crystallization Communications* **64**(10), 880–885.
- Veesler, S., Lafont, S., Marcq, S., Astier, J. P. & Boistelle, R. (1996), 'Prenucleation, crystal growth and polymorphism of some proteins', *Journal of crystal growth* **168**(1-4), 124–129.
- Vergara, A., Lorber, B., Sauter, C., Giegé, R. & Zagari, A. (2005), 'Lessons from crystals grown in the advanced protein crystallisation facility for conventional crystallisation applied to structural biology', *Biophysical chemistry* **118**(2-3), 102–112.

- Wadsten, P., Wöhri, A. B., Snijder, A., Katona, G., Gardiner, A. T., Cogdell, R. J., Neutze, R. & Engström, S. (2006), 'Lipidic sponge phase crystallization of membrane proteins', *Journal of molecular biology* **364**(1), 44-53.
- Wagner, S., Bader, M. L., Drew, D. & de Gier, J.-W. (2006), 'Rationalizing membrane protein overexpression', *Trends in biotechnology* **24**(8), 364-371.
- Wallace, B. A. & Janes, R. W. (2003), 'Circular dichroism and synchrotron radiation circular dichroism spectroscopy: tools for drug discovery'.
- Wallace, B., Lees, J., Orry, A., Lobley, A. & Janes, R. W. (2003), 'Analyses of circular dichroism spectra of membrane proteins', *Protein Science* **12**(4), 875-884.
- Walmsley, A. R., Lowe, A. G. & Henderson, P. J. (1994), 'The kinetics and thermodynamics of the binding of cytochalasin b to sugar transporters', *European journal of biochemistry* **221**(1), 513-522.
- Wang, H., Elferich, J. & Gouaux, E. (2012), 'Structures of leuT in bicelles define conformation and substrate binding in a membrane-like context', *Nature structural & molecular biology* **19**(2), 212.
- Ward, A. (2000), 'The amplified expression, identification, purification, assay and properties of histidine-tagged bacterial membrane transport proteins', *Membrane Transport-a Practical Approach* .
- Watanabe, A., Choe, S., Chaptal, V., Rosenberg, J. M., Wright, E. M., Grabe, M. & Abramson, J. (2010), 'The mechanism of sodium and substrate release from the binding pocket of vsglt', *Nature* **468**(7326), 988.
- Weyand, S., Ma, P., Saidijam, M., Baldwin, J., Beckstein, O., Jackson, S., Suzuki, S., Patching, S. G., Shimamura, T., Sansom, M. S. et al. (2006), 'The nucleobase-cation-symport-1 family of membrane transport proteins', *Handbook of Metalloproteins* .
- Weyand, S., Ma, P., Saidijam, M., Baldwin, J., Beckstein, O. et al. (2010), 'The nucleobase-cation-symport-1 family of membrane transport proteins. handbook of metalloproteins'.

- Weyand, S., Shimamura, T., Beckstein, O., Sansom, M. S., Iwata, S., Henderson, P. J. & Cameron, A. D. (2011), 'The alternating access mechanism of transport as observed in the sodium-hydantoin transporter mhp1', *Journal of synchrotron radiation* **18**(1), 20–23.
- Weyand, S., Shimamura, T., Yajima, S., Suzuki, S., Mirza, O., Krusong, K., Carpenter, E. P., Rutherford, N. G., Hadden, J. M., O'reilly, J. et al. (2008), 'Structure and molecular mechanism of a nucleobase-cation-symport-1 family transporter', *Science* **322**(5902), 709–713.
- Wöhri, A. B., Johansson, L. C., Wadsten-Hindrichsen, P., Wahlgren, W. Y., Fischer, G., Horsefield, R., Katona, G., Nyblom, M., Öberg, F., Young, G. et al. (2008), 'A lipidic-sponge phase screen for membrane protein crystallization', *Structure* **16**(7), 1003–1009.
- Wong, F. H., Chen, J. S., Reddy, V., Day, J. L., Shlykov, M. A., Wakabayashi, S. T. & Saier Jr, M. H. (2012), 'The amino acid-polyamine-organocation superfamily', *Journal of molecular microbiology and biotechnology* **22**(2), 105–113.
- Wright, E. M. (2013), 'Glucose transport families slc5 and slc50', *Molecular aspects of medicine* **34**(2-3), 183–196.
- Yamashita, A., Singh, S. K., Kawate, T., Jin, Y. & Gouaux, E. (2005), 'Crystal structure of a bacterial homologue of na⁺/cl⁻-dependent neurotransmitter transporters', *Nature* **437**(7056), 215.
- Zhou, Z., Zhen, J., Karpowich, N. K., Goetz, R. M., Law, C. J., Reith, M. E. & Wang, D.-N. (2007), 'Leut-desipramine structure reveals how antidepressants block neurotransmitter reuptake', *Science* **317**(5843), 1390–1393.
- Zhou, Z., Zhen, J., Karpowich, N. K., Law, C. J., Reith, M. E. & Wang, D.-N. (2009), 'Antidepressant specificity of serotonin transporter suggested by three leut-ssri structures', *Nature structural & molecular biology* **16**(6), 652.

Appendix A

Mhp1 and LeuT buffers

A.1 Mhp1 protein purification buffers

Solubilisation buffer

20 mM Tris-HCl pH 8.0, 20 mM imidazole pH 8.0, 300 mM NaCl, 20% v/v glycerol, 1% w/v n-dodecyl- β -D-maltopyranoside (DDM) detergent

Washing buffer step 1: DDM Wash

10 mM Tris-HCl pH 8.0, 20 mM imidazole pH 8.0, 10% v/v glycerol 0.1% w/v n-dodecyl- β -D-maltopyranoside (DDM) detergent

Washing buffer step 2: NM Wash

10 mM Tris-HCl pH 8.0, 20 mM imidazole pH 8.0, 10% v/v glycerol, 0.7% w/v n-nonyl- β -D-maltopyranoside (NM) detergent

Elution step: NM Elution

10 mM Tris-HCl pH 8.0, 300 mM imidazole pH 8.0, 5% v/v glycerol, 0.7% w/v n-nonyl- β -D-maltopyranoside (NM) detergent

Storage buffer: NM Desalting

10 mM Tris-HCl pH 8.0, 2.5% v/v glycerol, 0.5% w/v n-nonyl- β -D-maltopyranoside (NM) detergent

A.2 Mhp1 size-exclusion chromatography buffers for scattering studies (SEC-SAXS)

SEC buffer of various detergents

DDM SEC buffer: 10 mM Tris-HCl pH 8.0, 2.5% v/v Glycerol, 0.05% w/v DDM

NM SEC buffer: 10 mM Tris-HCl pH 8.0, 2.5% v/v Glycerol, 0.5% w/v NM

SEC buffers in NM (Sections 4.1.1, 4.2.1, and 4.2.2)

Tris buffer or NM buffer 10 mM Tris-HCl pH 8.0, 2.5% v/v Glycerol, 0.5% w/v NM

+ **NaCl, L-BH** 10 mM Tris-HCl pH 8.0, 2.5% v/v Glycerol, 1 M NaCl, 2 mM L-BH, 0.5% w/v NM

+ **KCl, L-BH** 10 mM Tris-HCl pH 8.0, 2.5% v/v Glycerol, 1 M KCl, 2 mM L-BH, 0.5% w/v NM

SEC buffers in DDM (Section 4.1.3)

DDM-buffer 10 mM Tris-HCl pH 8.0, 2.5% v/v Glycerol, 0.05% w/v DDM

+ **NaCl, L-BH** 10 mM Tris-HCl pH 8.0, 2.5% v/v Glycerol, 1 M NaCl, 2 mM L-BH, 0.05% w/v DDM

+ **KCl, L-BH** 10 mM Tris-HCl pH 8.0, 2.5% v/v Glycerol, 1 M KCl, 2 mM L-BH, 0.05% w/v DDM

SEC buffers in hexagonal conditions in NM detergent (Section 4.2.2)

Bicine buffer or hexagonal buffer 100 mM Bicine pH 9.0, 2.5% v/v Glycerol, 0.5% w/v NM

+ **NaCl, L-BH** 100 mM Bicine pH 9.0, 2.5% v/v Glycerol, 1 M NaCl, 2 mM L-BH, 0.5% w/v NM

+ **KCl, L-BH** 100 mM Bicine pH 9.0, 2.5% v/v Glycerol, 1 M KCl, 2 mM L-BH, 0.5% w/v NM

Table A.1: Detergent concentrations during Mhp1 purification steps and desired exchange.

Detergent Name	Solubilisation	Wash buffer 1*	Exchange buffer	Elution buffer	Desalting buffer
DDM	1% w/v 19 mM	0.1% w/v 1.9 mM	0.05% w/v 0.95 mM	0.05% w/v or 0.95 mM	0.05% w/v 0.425 mM
NM			0.7% w/v 14 mM	0.7% w/v 14 mM	0.5% w/v 10 mM
	10x CMC	2.5x CMC	2.5x CMC	2.5x CMC	1.8x CMC

* Wash buffer 1 is happening on the same detergent as the solubilisation was

**During this thesis solubilisation happened only on DDM

Table A.2: Detergent used in the current thesis.

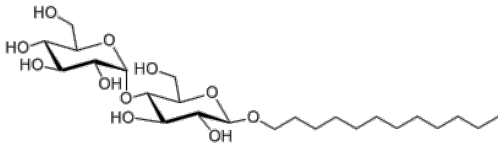
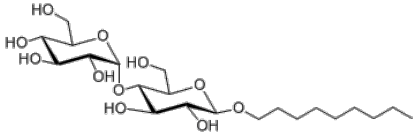
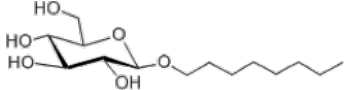
Structure	Name of detergent
	n-dodecyl- β -D-maltopyranoside (DDM)
	n-nonyl- β -D-maltopyranoside (NM)
	n-octyl- β -glucopyranoside (β -OG)

Table A.3: Characteristics of detergents used for Mhp1 and LeuT purifications.

Detergent Name	CMC (H ₂ O) (%/mM)	Aggregation Number, N1	Micelle size Mw (kDa)	Mw (Da)	dn/dc (ml/gm)	Mean Rh of micelles (nm) (6)
DDM	0.0087/0.17 (1)	80-150 78-149 (1)	65-70 (2,3) 72 (3)	510.6	0.1435	3.3±0.5
NM	0.28/6	55		468.5	0.1377	2.5±0.3
β -OG	0.53/20(5)	25(5)	30-100	296.6	0.1159	

A.3 Assays buffers

Schaffner-Weissmann protein concentration assay

Buffer SW: 1 M Tris-HCl pH 7.5, 10% w/v SDS

Solution 1: 60% v/v TCA

Solution 2: 6% v/v TCA

Elution buffer: 25 mM NaOH, 0.05 mM EDTA, 50% v/v ethanol

SDS-PAGE gel

Table A.4: SDS-PAGE stacking and running gels

	4% v/v Stacking gel pH 6.8	15% v/v Running gel pH 8.8
40% Acrylamide	1.54 ml	8.54 ml
2% Bis	0.78 ml	0.98 ml
1.5 M Tris	1.5 ml	5.62 ml
10% v/v SDS	0.1 ml	0.2 ml
H ₂ O	6.4 ml	6.96 ml
10% v/v APS	100 μ l	100 μ l
TEMED	10 μ l	10 μ l

Stain solution: methanol, acetic acid and water in a 50:10:40 v/v ratio, 0.2% w/v Coomassie Brilliant Blue R

Destaining solution: methanol, acetic acid and water in a 8:10:82 v/v ratio

Western blotting

TBST buffer: 25 mM Tris-HCl pH 7.8, 150 mM NaCl, 0.05% v/v Tween-20

SuperSignal West Pico chemiluminescent Working solution: a) peroxide solution, b) luminol/enhancer solution

Steady-state spectrophotofluorimetry

Fluorimetry buffer 1:

50 mM Tris-HCl pH 7.6, 2% v/v DMSO, 0.5% w/v NM, 0 mM NaCl, and 140 mM Cloline chloride

Fluorimetry buffer 2:

50 mM Tris-HCl pH 7.6, 2% v/v DMSO, 0.5% w/v NM, 15 mM NaCl, and 125 mM Cloline chloride

Fluorimetry buffer 3:

50 mM Tris-HCl pH 7.6, 2% v/v DMSO, 0.5% w/v NM, 140 mM NaCl, and 0 mM Cloline chloride

A.4 LeuT protein purification buffers

Protein expression

Lysis buffer:

20 mM Hepes pH 7.5, 200 mM NaCl, 1 mM EDTA, 1 mM PMSF, 0.4 mg/ml Lysozyme, 20 µg/ml DNAse-1

Membrane preparation

Membrane storage buffer:

20 mM Hepes pH 7.5, 200 mM NaCl, 1 mM PMSF, 30% v/v glycerol

Protein purification steps

DDM-Homogenisation buffer

20 mM Hepes pH 7.5, 200 mM NaCl, 1 mM PMSF, NO n-dodecyl- β -D-maltopyranoside

DDM-Solubilisation buffer

20 mM Hepes pH 7.5, 200 mM NaCl, 1 mM PMSF, 1% w/v n-dodecyl- β -D-maltopyranoside

DDM-Binding buffer

20 mM Hepes pH 7.5, 200 mM NaCl, 5 mM Imidazole, 2.5% v/v Glycerol, 0.05% n-dodecyl- β -D-maltopyranoside

DDM wash buffers with increasing imidazole concentration:

20 mM Hepes pH 7.5, 200 mM NaCl, 0 mM, 5 mM, 10 mM, 10 mM, 20 mM imidazole, 2.5% v/v glycerol 0.05% n-dodecyl- β -D-maltopyranoside

DDM-Elution buffer:

20 mM Hepes pH 7.5, 200 mM NaCl, 250 mM imidazole, 2.5% v/v glycerol, 0.05% w/v n-dodecyl- β -D-maltopyranoside

DDM-Desalting buffer

20 mM Hepes pH 7.5, 200 mM NaCl, 2.5% v/v glycerol, 0.05% w/v n-dodecyl- β -D-maltopyranoside

β -OG Exchange buffer by Gel Filtration:

20 mM Hepes pH 8.0, 190 mM NaCl, 10 mM KCl, 40 mM n-octyl- β -D-glucopyranoside (2x CMC)

His-tagged:

Second affinity purification

Binding buffer:

20 mM Hepes pH 7.5, 200 mM KCl, 5 mM imidazole, 1 mM PMSF, 0.25-0.5% w/v n-dodecyl- β -D-maltopyranoside (DDM), Na-chelator, Cobalt-TALON resin

Wash buffer:

20 mM Hepes pH 7.5, 200 mM KCl, 1 mM PMSF, 0.05% w/v n-dodecyl- β -D-maltoside (DDM) with increase of imidazole concentration 5 mM, 10 mM, 10 mM (second time), and 20 mM

Elution buffer:

20 mM Hepes pH 7.5, 200 mM KCl, 300 mM imidazole, 1 mM PMSF, 0.05% w/v n-dodecyl- β -D-maltopyranoside

Desalting buffer:

20 mM Hepes pH 7.5, 200 mM KCl, 0.05% w/v n-dodecyl- β -D-maltopyranoside

Benzamidine affinity purification

Binding buffer: 20 mM Hepes pH 7.5, 200 mM KCl, 0.05% w/v n-dodecyl- β -D-maltopyranoside

Acetic buffer: 0.05 M Glycine pH 3

Competitive buffer: 20 mM p-aminobenzamidine in binding buffer

Affinity purification with TALON cobalt resin 2

Binding buffer – Storage buffer

20 mM Hepes pH 7.5, 200 mM KCl, 0.05% w/v n-dodecyl- β -D-maltopyranoside (DDM)

Elution buffer

20 mM Hepes pH 7.5, 200 mM KCl, 1 M imidazole

Gel Filtration

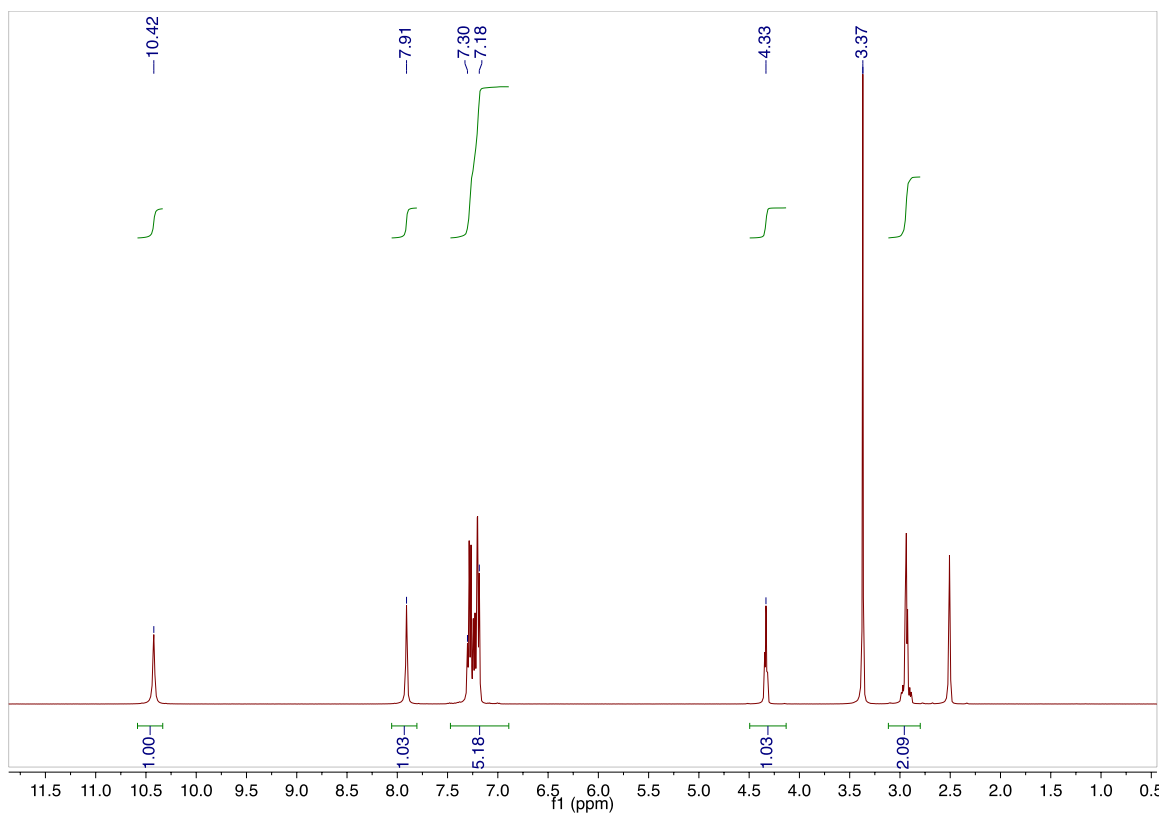
β -OG Buffer:

20 mM Hepes pH 8, 190 mM NaCl, 10 mM KCl, 40 mM n-octyl- β -glucopyranoside (β -OG).

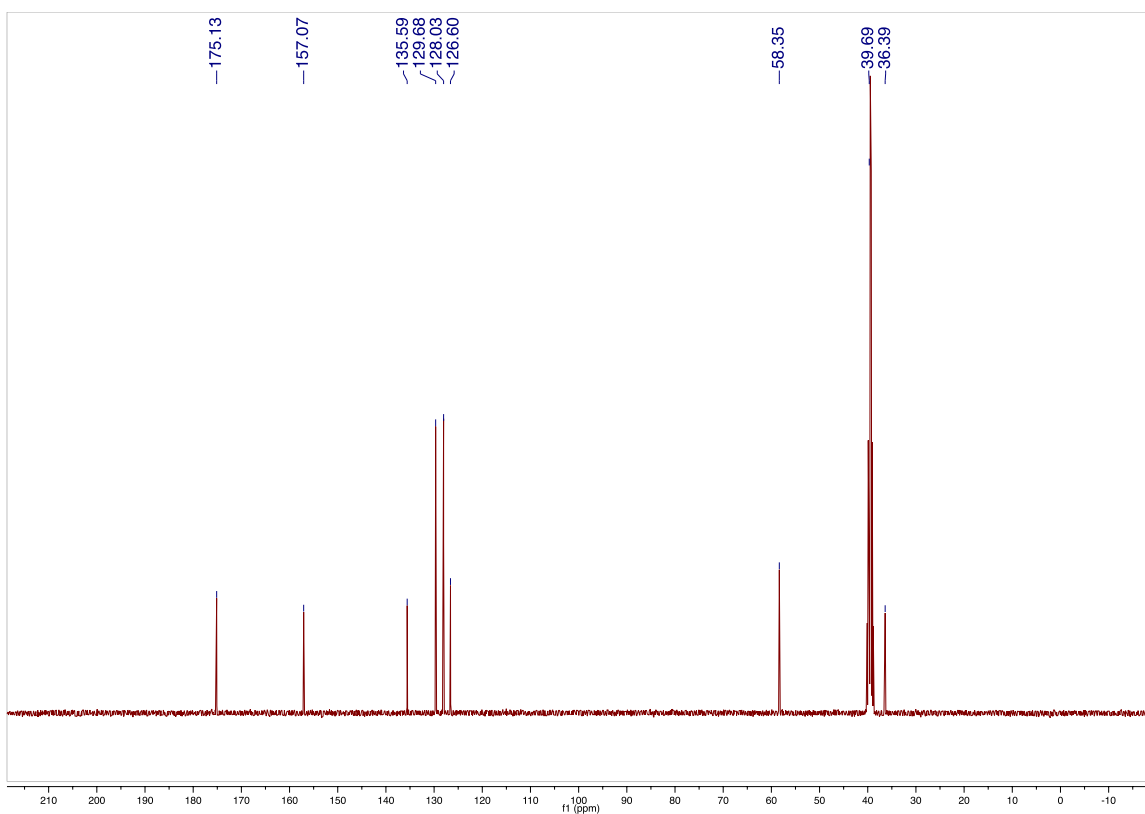
Appendix B

NMR spectra

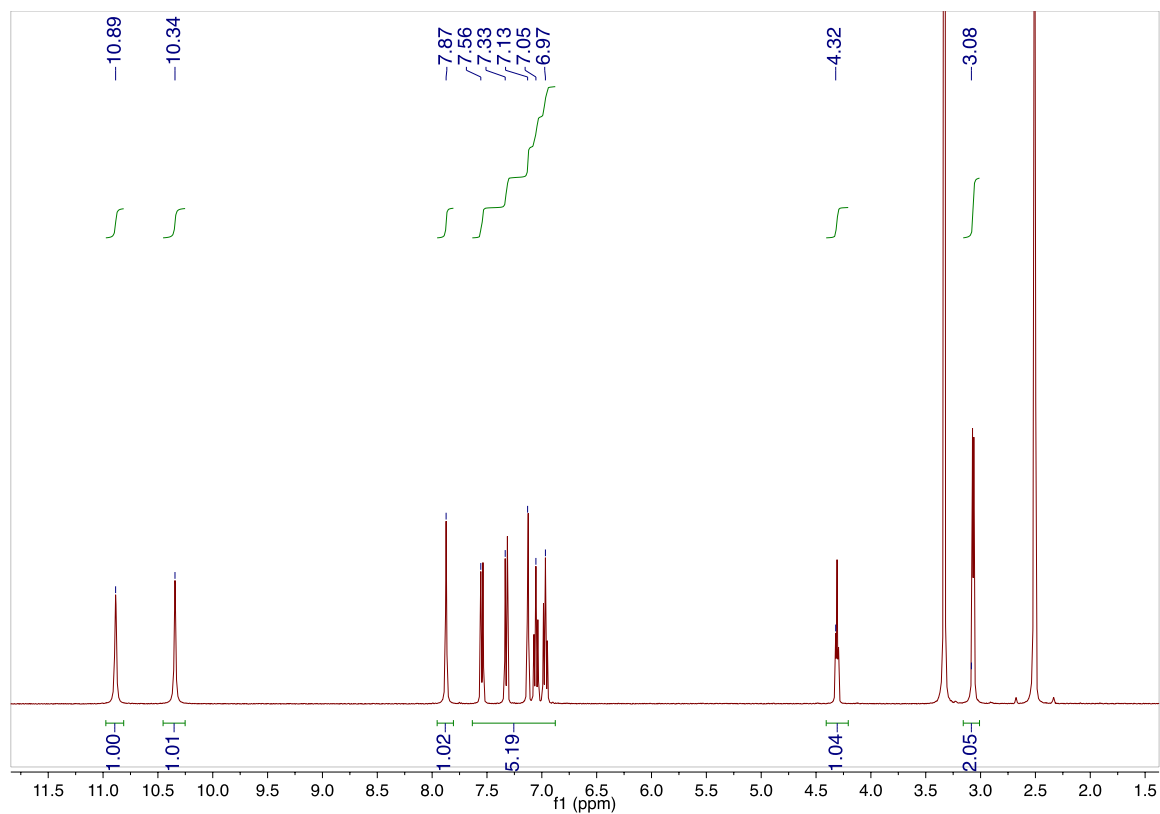
NMR spectra from the hydantoin compounds are presented below. Chemical shifts of each signal are given in ppm. The abbreviations used to describe multiplicity are: s. singlet, d. doublet, t. triplet, m. multiplet.



(a) ¹H-NMR (400 MHz, DMSO) of LBH:
 δ ppm 10.42 (s, 1H, NH), 7.91 (s, 1H, NH), 7.30-7.18 (m, 5H, ArH), 4.33 (m, 1H, CH), 2.09 (d, 2H, CH₂).

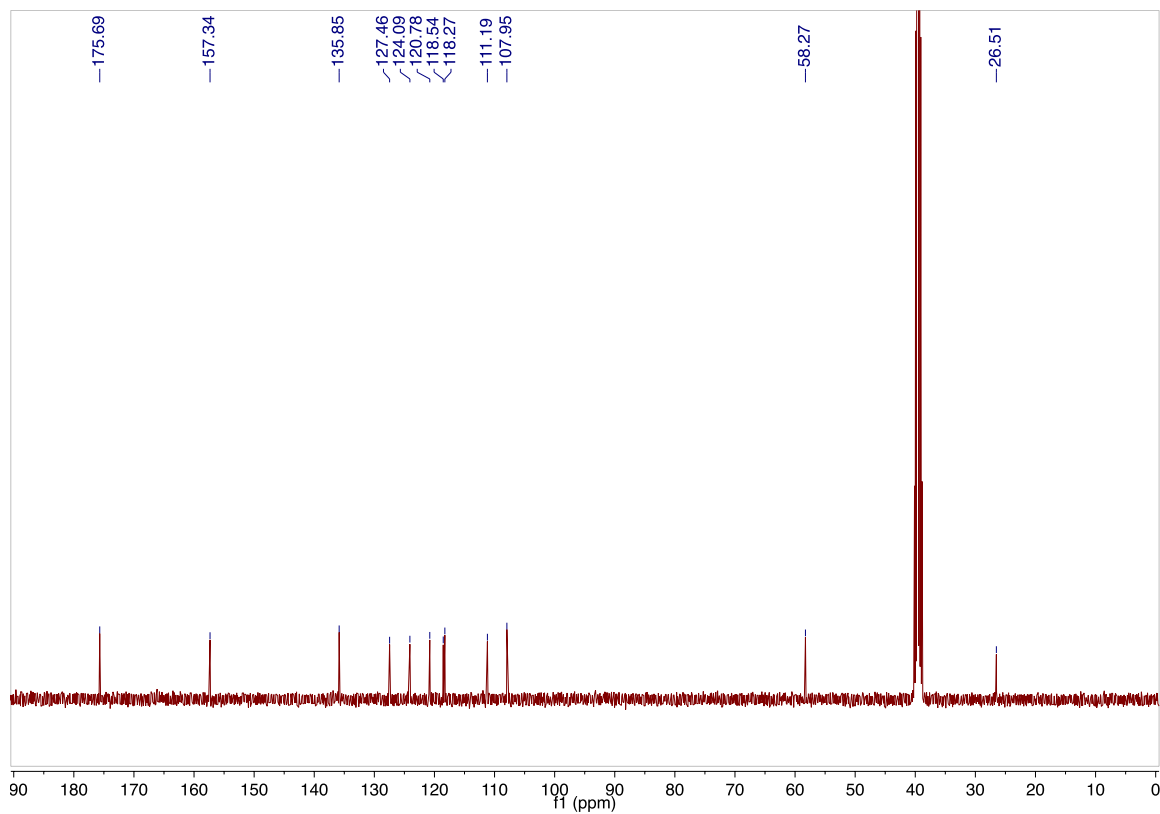


(b) ¹³C NMR (DMSO-d₆, 100 MHz) of LBH

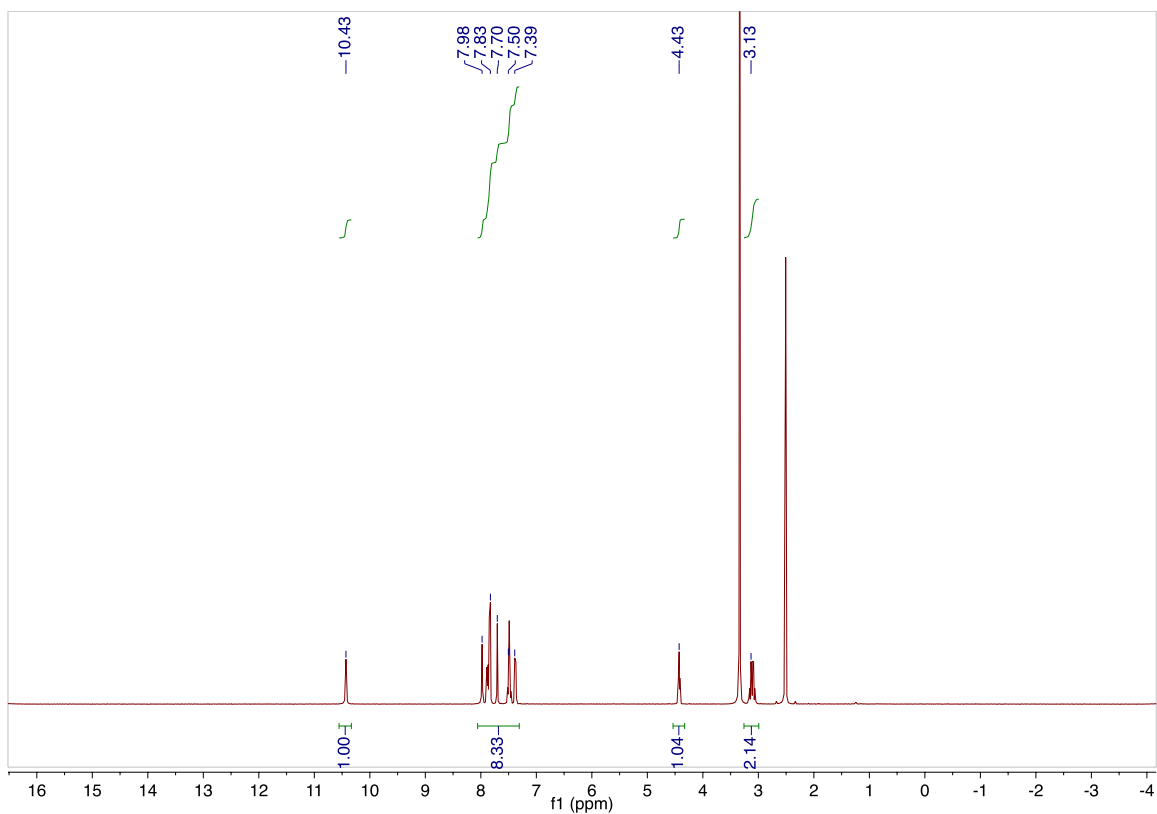


(c) ^1H -NMR (400 MHz, DMSO) of *L*-IMH:

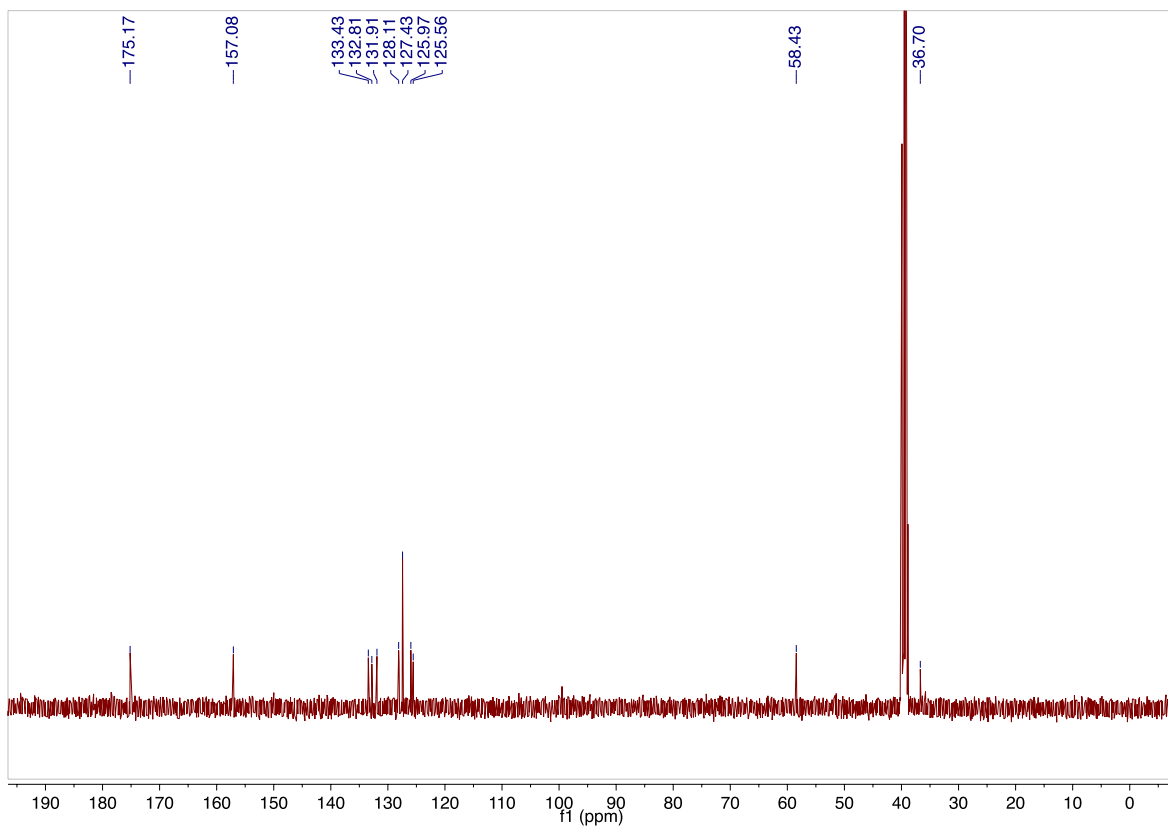
δ ppm 10.89 (s, 1H, NH), 10.34 (s, 1H, NH), 7.87 (s, 1H, NH), 7.56-6.97 (m, 5H, ArH), 4.32 (t, 1H, CH), 3.08 (d, 2H, CH_2).



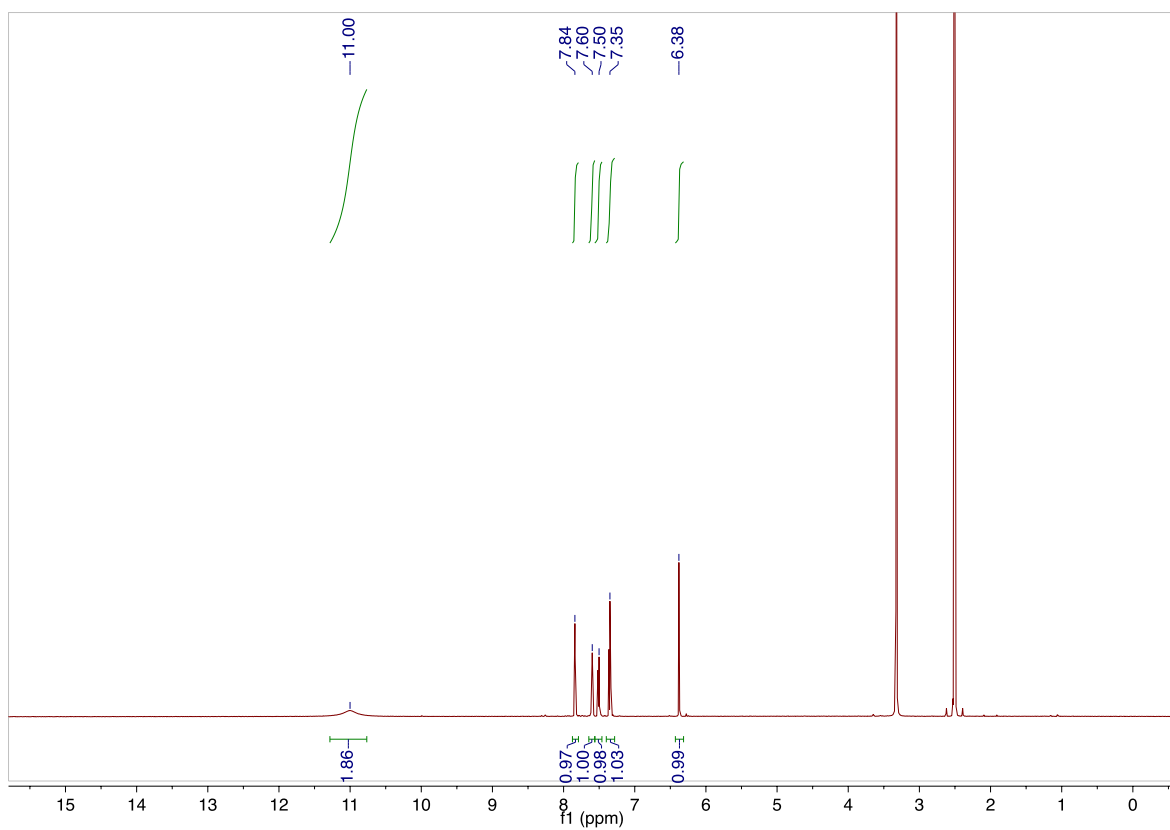
(d) ^{13}C NMR (DMSO- d_6 , 100 MHz) of *L*-IMH



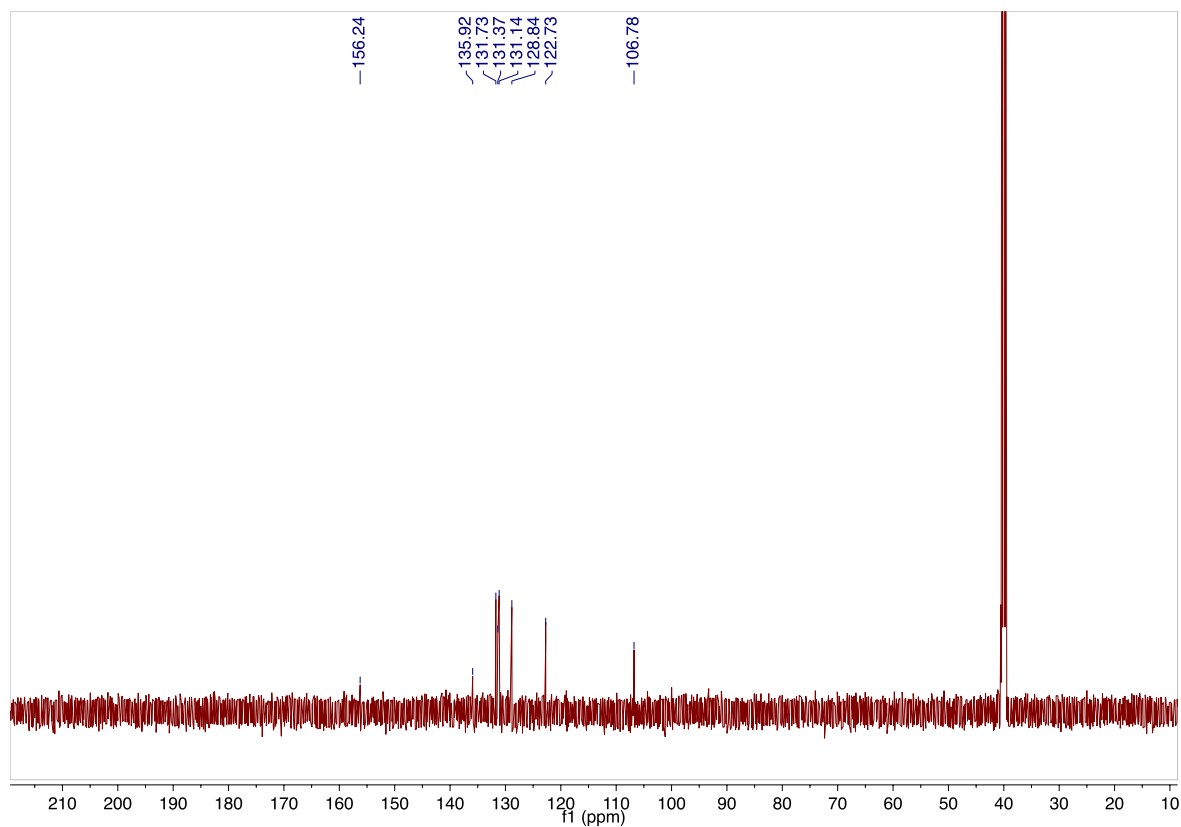
(e) ^1H -NMR (400 MHz, DMSO) of *L*-NMH:
 δ ppm 10.43 (s, 1H, NH), 7.98-7.39 (m, 5H, ArH), 4.43 (s, 1H, CH), 3.13 (m, 2H, CH₂).



(f) ^{13}C NMR (DMSO-*d*₆, 100 MHz) of *L*-NMH



(g) $^1\text{H-NMR}$ (400 MHz, DMSO) of BVH:
 δ ppm 11.02 (s, 2H, NH), 7.84-7.35 (m, 4H, ArH), 6.38 (s, 1H, CH).



(h) $^{13}\text{C NMR}$ (DMSO- d_6 , 100 MHz) of BVH

Appendix C

List of hazardous substances

The hazardous substances used in this work are listed below and marked with H(hazard) and P (precautionary) statements.

Reagent	Pictogram	Hazardous (H)/Precautions(P) statements
Acetic acid 100 %,	GHS02 GHS05	H226, H290, H314 P210, P280, P303 +P361 + P353, P305 + P351 +P338, P310
Acrylamide/Bis stock sol. (40% w/v) 29:1 (40% w/v)	GHS07 GHS08	H301, H312 + H332, H315, H317, H319, H340, H350, H361f, H372 P201, P260, P280, P301+ P330 + P331 + P310, P305 + P351 + P338, P308 + P313
Ammonium peroxodisulphate	GHS03 GHS07 GHS08	H272, H302, H315, H317, H319, H334, H335, P261, P280, P302 + P352, P305 + P351 + P338, P332 + P313, P337 + P313
cOmplete, EDTA-free protease inhibitor cocktail tablets	GHS05	H314 P260, P280, P301 + P330 + P331, P303 + P361 + P353, P304 + P340 + P310, P305 + P351 + P338 + P310
EDTA tetrasodiumsalt	GHS05 GHS07 GHS08	H302 + H332, H318, H373, P261, P270, P280, P305 + P351 + P338, P310 + P310, P305 + P351 + P338 + P310
Ethanol ≥ 99.8%	GHS02 GHS07	H225, H319 P210, P233, P305 + P351 + P338 + P310, P305 + P351 + P338 + P310
Guanidine hydrochloride ≥ 99,5%	GHS07	H302, H315, H319, P280, P302 + P352, P305 + P351 + P338 + P310, P305 + P351 + P338 + P310
Hydrochloric Acid 32%	GHS05 GHS07	H290, H314, H335 P280, P303 + P361 + P353, P304 + P340, P30 + P351+P338, P312 + P310, P305 + P351 + P338 + P310
Imidazole, Pufferan ≥99%, p.a.	GHS05 GHS07 GHS08	H302, H314, H360D P260, P280, P301 + P330 +P331, P303 + P361 + P353, P305 +P351 + P338, P308+ P313
Methanol ≥ 99.9 %, p.a. ACS, ISO	GHS02 GHS06 GHS08	H225, H301 + H311 + H331, H370 P210, P270, P280, P303 + P361 + P353, P304+ P340, P308 + P311

Table C.1: List of hazardous substances

Eidesstattliche Versicherung

Hiermit versichere ich an Eides statt, die vorliegende Dissertation selbst verfasst und keine anderen als die angegebenen Hilfsmittel benutzt zu haben. Die eingereichte schriftliche Fassung entspricht der auf dem elektronischen Speichermedium. Ich versichere, dass diese Dissertation nicht in einem früheren Promotionsverfahren eingereicht wurde.

Declaration on oath

I hereby declare, on oath, that I have written the present dissertation by my own and have not used other than the acknowledged resources and aids. The submitted written version corresponds to the version on the electronic storage medium. I hereby declare that I have not previously applied or pursued for a doctorate (Ph.D studies)

Maria C. Kokkinidou

Hamburg, July 2019

Unterschrift

